eman ta zabal zazu

UPV EHU

Design and Engineering of Artificial Metabolic Cells for Chemical Manufacturing

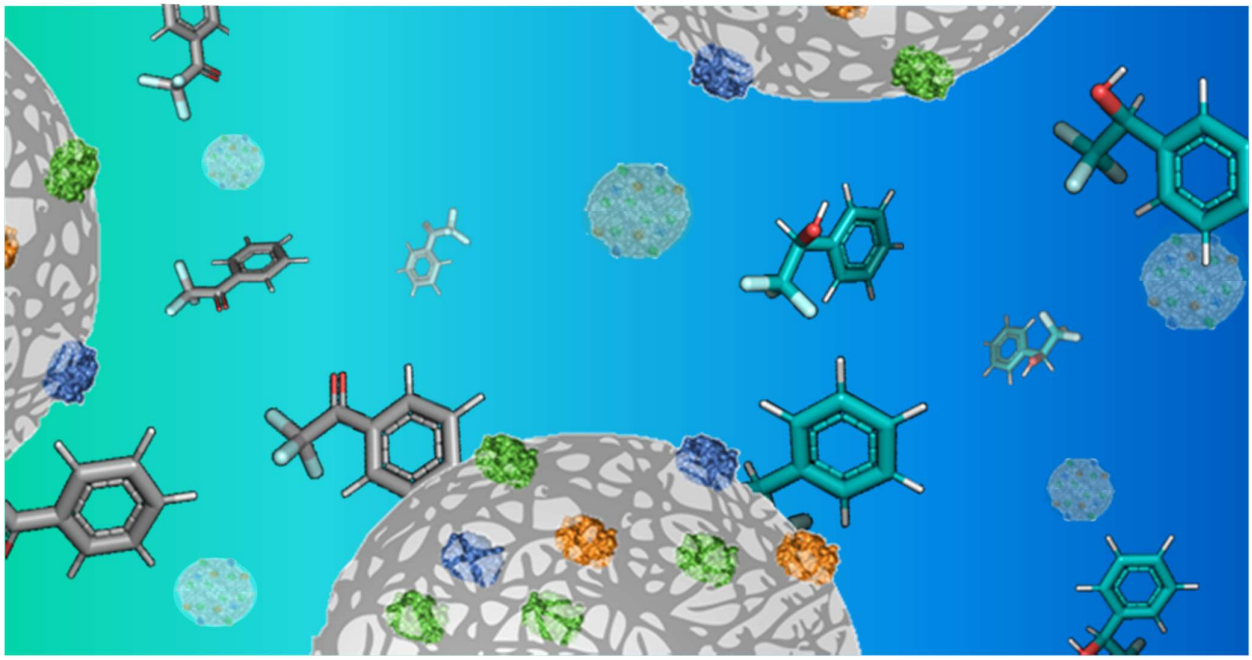

2019

Ana Isabel Benítez Mateos

Design and Engineering of Artificial Metabolic Cells for Chemical Manufacturing

to obtain the degree of PhD in
Synthetic and Industrial Chemistry
at the University of Basque Country

(UPV/EHU)

Ana Isabel Benítez Mateos

2019

Thesis Supervisor:

Dr. Fernando López Gallego

- Heterogeneous Biocatalysis Group, CIC biomaGUNE. San Sebastián (Spain).
- Heterogeneous Biocatalysis Group, Institute of Organic Chemistry and Homogeneous Catalysis (ISQCH-CSIC), Department of Organic Chemistry, University of Zaragoza. Zaragoza (Spain).

University tutor:

Prof. Dr. María Nuria Sotomayor Anduiza

- Department of Organic Chemistry, Faculty of Science and Technology, University of the Basque Country (UPV/EHU). Bilbao (Spain).

Table of contents

Abstract

Industrial biocatalysis is a smart path towards more cost-effective and sustainable chemical processes. However, there are still some drawbacks in terms of enzyme stability, molecule recycling and mass transfer matters among others that limit the progress of heterogeneous biocatalysis. In order to overcome these issues, micro-scale approaches and tailor-made designs of heterogeneous biocatalysts are needed to make more efficient the final industrial reactions. Inspired by the natural compartmentalization of metabolic pathways inside the living cells, we assembled molecular systems into artificial solid supports to build functional biomaterials called artificial metabolic cells. Based on this concept, different micro-architectures were developed for the co-immobilization of multi-enzyme systems and the expensive cofactors on solid materials. The integration of all molecules in the solid phase enabled the recycle and reuse of the heterogeneous biocatalysts, decreasing costs and waste. The scope of this strategy was expanded to engineer artificial metabolic cells based on different enzymes (dehydrogenases, oxidades, ketoreductases and ω-transaminases) with their corresponding cofactors (NADH, FAD^+, NADPH and PLP). Parallely, we developed several techniques to aid and guide the design process of these heterogeneous biocatalysts. Firstly, a synthetic-biological platform was developed to easily screen different materials and binding chemistries for the protein immobilization. Secondly, fluorescence microscopy was applied to analyze the distribution of enzymes and cofactors onto the porous microparticles at single-particle level and with spatio-temporal resolution. Finally, artificial metabolic cells were successfully tested in continuous flow reactions for the asymmetric synthesis of several chiral amines and alcohols.

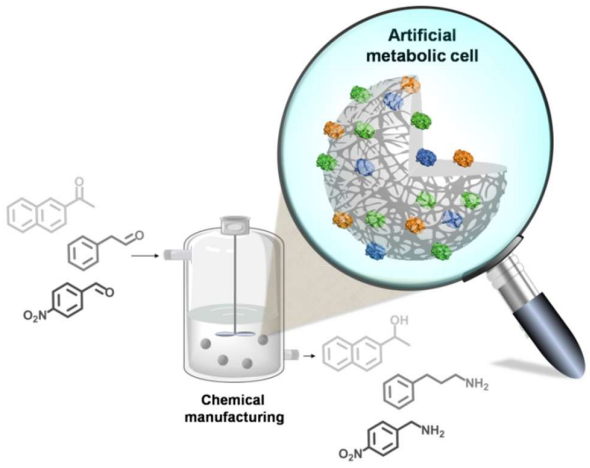

Resumen

En los dos últimos siglos tras la revolución industrial, el cambio de nuestro modelo socio-económico ha incrementado exponencialmente la demanda de productos químicos para diferentes fines como agricultura, biomedicina y construcción. El uso del petróleo en la industria ha sido (y sigue siendo) el epicentro para satisfacer las necesidades de nuestra sociedad. Sin embargo, el aumento del consumo de combustibles fósiles ha provocado una aceleración en la degradación de nuestro medio ambiente. La biocatálisis ha surgido como una herramienta eficaz para combatir el desgaste de nuestro planeta a la vez que permite el avance tecnológico de forma sostenible hacia un modelo bioeconómico.

La biocatálisis consiste en el uso de enzimas como catalizadores de reacciones químicas que permite la obtención de productos de interés. Estas proteínas se encuentran de forma natural en las células de todos los seres vivos llevando a cabo reacciones metabólicas que permiten el progreso de la vida. Además de los biocatalizadores enzimáticos, existen catalizadores no biológicos que realizan funciones equivalentes. Sin embargo, las enzimas presentan una serie de características que les hacen catalizadores únicos: presentan una excelente capacidad catalítica y una amplia selectividad química. Además, las enzimas trabajan a condiciones fisiológicas de pH y temperatura debido a su evolución natural en el interior de las células. Otra de sus características más destacables es la capacidad de producir compuestos enantioméricamente puros, que es fundamental para la fabricación de productos farmacéuticos.

Los procesos biocatalíticos pueden realizarse fundamentalmente con células que contienen las enzimas en su interior o con enzimas purificadas. La biocatálisis con células es más utilizada en procesos que necesitan cofactores, ya que éstas los contienen de forma natural mientras que la suplementación con cofactores exógenos supone un alto coste económico. Pero las limitaciones en el transporte de sustratos y productos desde y hacia el interior celular, junto a la laboriosa purificación del producto final, hacen que este método sea menos eficiente. Por otro lado, las enzimas pueden ser expresadas *in vivo* y posteriormente purificadas para su uso como biocatalizadores aislados. Aunque los procesos *downstream* son más livianos en este caso, las enzimas pueden presentar una baja estabilidad y/o actividad al encontrarse desprotegidas fuera de su ambiente natural.

Durante las últimas décadas, las estrategias de ingeniería de proteínas, la inmovilización de enzimas purificadas y el descubrimiento de nuevas enzimas han permitido el acceso a una amplia gama de estrategias para el desarrollo de nuevos biocatalizadores. Las técnicas computacionales y genéticas para el diseño de enzimas han abierto las puertas a diversas variantes de la misma enzima con propiedades mejoradas. Así mismo, la inmovilización de enzimas en soportes sólidos (biocatalizadores heterogéneos) ha sido crucial para poder reciclar el biocatalizador y aumentar su estabilidad durante el proceso de reacción. Sin embargo, los biocatalizadores heterogéneos siguen presentando problemas de estabilidad, limitación de reusos y baja eficiencia que se agravan a nivel industrial. En este contexto, es importante que el proceso biocatalítico sea robusto, sostenible y económico para asegurar su éxito.

El enfoque que se plantea en esta tesis doctoral para abordar estas cuestiones es el diseño de biocatalizadores heterogéneos autosuficientes mimetizando a las células naturales. Inspirados en la distribución espacial de las rutas metabólicas intracelulares, se han desarrollado estructuras micrométricas llamadas células artificiales metabólicas que pueden sintetizar productos químicos de forma más eficiente a nivel industrial.

En primer lugar, se ha estudiado la estrategia para la inmovilización de proteínas en soportes sólidos. Tradicionalmente, los biocatalizadores heterogéneos han sido desarrollados probando de forma empírica la inmovilización de una enzima en diferentes soportes. Este proceso puede durar semanas hasta encontrar el soporte adecuado con la química de unión correcta para unir la enzima al soporte de forma orientada, funcional y estable. En el primer capítulo experimental (capítulo 3) de esta tesis se describe una nueva metodología con la que se podrían examinar diferentes tipos de inmovilización de enzimas en diferentes materiales en unas horas. En estos estudios se ha utilizado principalmente la proteína verde fluorescente (sGFP) como modelo debido a su fácil detección. Para controlar la orientación de la proteína cuando ésta se inmoviliza, se ha desarrollado un kit de cuatro plásmidos que codifican para la sGFP etiquetada con diferentes polipéptidos (poly-(6x)His, poly-(6x)Cys, poly-(6x)Lys) y sin etiquetar.

Sin embargo, la expresión y purificación de las enzimas es otro proceso que conlleva diversos protocolos consumiendo a su vez tiempo y recursos. Para solventar este problema, hemos aplicado una estrategia de biología sintética que utiliza

extractos celulares aislados para producir proteínas *in vitro* de forma más rápida y sencilla. Este método conocido como *cell-free protein synthesis* (CFPS) se basa en extraer de la célula toda la maquinaria transcripcional y traduccional necesaria para poder llevar a cabo la síntesis de proteínas en sólo unas horas. Además, estos extractos celulares se pueden almacenar por largos periodos de tiempo conservando su funcionalidad, se pueden transportar en recipientes pequeños y además pueden expresar proteínas que *in vivo* no es posible producir.

La combinación de estos tres elementos, ADN, soportes materiales y extractos celulares da lugar a la síntesis *in vitro* e inmovilización de proteínas en un solo paso (CFPS-i). Éste método se puede realizar en un microtubo o en una placa multipocillos para obtener la proteína de interés unida de forma orientada a diferentes soportes mediante diferentes químicas de inmovilización. En concreto, en este trabajo se estudió la inmovilización de sGFP en soportes de agarosa, metacrilato, nanopartículas de oro y nanopartículas de sílica. Las químicas de unión de la proteína al soporte que se estudiaron son enlaces de coordinación con metales, enlaces covalentes irreversibles, enlaces disulfuro, intercambio iónico y química click. Además, el proceso de CFPS-i fue monitorizado en tiempo real mediante microscopía de fluorescencia para comprobar la eficiencia de este sistema.

Esta estrategia versátil para el diseño de nuevos biomateriales y biocatalizadores se aplicó a sistemas con varias proteínas. Para ello se expresaron e inmovilizaron al mismo tiempo y sobre el mismo soporte la proteína sGFP etiquetada con poly-(6x)Cys y la enzima alcohol deshidrogenasa (Bs-ADH) etiquetada con poly-(6x)His, usando dos químicas de unión diferente. Este experimento demuestra el alto potencial de la técnica CFPS-i para el diseño de células metabólicas artificiales basadas en cascadas enzimáticas. Finalmente, CFPS-i se aplicó también para el desarrollo de biosensores basados en anticuerpos. La proteína A, que es una proteína de unión universal a anticuerpos, se expresó e inmovilizó en un solo paso para posteriormente captar anticuerpos.

El segundo capítulo experimental de la presente tesis (capítulo 4) se centró en la puesta a punto de la inmovilización de cofactores redox en soportes sólidos. Anteriormente, se habían descrito varios métodos para inmovilizar cofactores en la fase sólida del biocatalizador heterogéneo. Pero desafortunadamente se hallaron problemas de reuso del cofactor, baja actividad de la enzima hacia el cofactor inmovilizado y dificultades para aumentar la escala del proceso. Durante este trabajo,

nuestro grupo ha desarrollado una estrategia para inmovilizar los cofactores en soportes de forma reversible mediante interacciones electrostáticas. Este tipo de inmovilización permite que los cofactores fosforilados (con carga negativa) se encuentren en un equilibrio asociación-disociación entre la superficie del soporte (con carga positiva) y el centro activo de la enzima, pero sin abandonar el microambiente del soporte poroso. A continuación, se diseñó una arquitectura para poder co-inmovilizar un sistema bi-enzimático y el cofactor NADH en la misma micropartícula. Para ello, una alcohol deshidrogenasa (Tt-ADH) fue inmovilizada covalentemente en micropartículas de agarosa funcionalizadas con grupos aldehídos. Posteriormente, se recubrió este biocatalizador con un polímero catiónico (PEI) para permitir la inmovilización del cofactor NADH y de una segunda deshidrogenasa (Cb-FDH) capaz de regenerar el cofactor. Los resultantes biocatalizadores heterogéneos se pusieron a prueba para la síntesis de un alcohol modelo, demostrando ser capaces de llevar a cabo la reacción durante al menos 4 ciclos manteniendo una conversión del 100% y de forma autosuficiente, es decir, sin adición exógena de cofactor. Mediante técnicas de microscopía de fluorescencia se analizó el progreso de la reacción en cada micropartícula. Aprovechando la autofluorescencia del cofactor se pudo monitorizar *in situ* el consumo de éste dentro de la micropartícula, pues la forma reducida del cofactor NADH presenta mayor fluorescencia que la forma oxidada (NAD^+).

Además de la inmovilización del cofactor, también se analizó el efecto de la distribución espacial de la enzima inmovilizada. En las células, las enzimas están distribuidas espacialmente para optimizar al máximo su función. Por tanto, estudiamos si la distribución de las enzimas inmovilizadas en las micropartículas afecta al progreso de las reacciones que catalizan. Para este estudio se inmovilizó una oxidasa (Tt-NOX), que al ser dependiente de oxígeno podría presentar problemas difusionales en el interior del biocatalizador heterogéneo. Nuestra hipótesis fue corroborada al determinar una mayor velocidad cinética en los biocatalizadores que presentaban la enzima inmovilizada de forma heterogénea en la parte externa de las micropartículas. Por el contrario, cuando la enzima estaba distribuida homogéneamente a través de la micropartícula, la velocidad cinética disminuía. Este sistema también fue analizado a nivel microscópico. En este caso, se consiguió monitorizar tanto la inmovilización de dos cofactores redox (NADH y FAD^+) como el consumo de NADH dentro de la célula metabólica artificial.

Una vez que tuvimos un diseño eficiente para la co-inmovilización de los cofactores expandimos nuestra estrategia a otro tipo de reacciones, concretamente a

reducciones asimétricas de cetonas. En el capítulo 5, co-inmovilizamos mediante intercambio iónico una cetoreductasa (KRED P1-A04) junto al cofactor NADPH. Este tipo de inmovilización de la enzima fue elegido de entre varios métodos utilizando diferentes soportes activados con diferentes grupos funcionales. La estrategia de unión reversible es aún más sostenible, ya que además de reusar el biocatalizador permite el reciclaje del soporte (de alto coste económico) cuando la enzima se inactiva. La actividad de este biocatalizador autosuficiente también fue constatada utilizando técnicas de microscopía de fluorescencia en tiempo real. Utilizando diferentes sustratos, se demostró que la misma enzima puede realizar la reducción del sustrato y la regeneración del cofactor de forma autosuficiente. Durante estos estudios, se halló un fenómeno interesante que relaciona el tamaño de las células metabólicas artificiales con su actividad catalítica. En las micropartículas más grandes se observó una tasa de actividad más baja que en las micropartículas de menor tamaño. Estos datos correlacionan con la cantidad de enzima inmovilizada que se detectó tras hacer estudios de microscopía confocal sobre la distribución espacial de la enzima inmovilizada. Las micropartículas más pequeñas presentaron una mayor congregación de enzimas y, por tanto, una mayor actividad. Por último, las células metabólicas artificiales basadas en cetoreductasa y NADPH fueron empacadas en un microreactor de flujo. Durante su funcionamiento, el microreactor mantuvo más del 80% de conversión durante 120 horas con tasas de reciclaje del cofactor cercanas a los requerimientos industriales. Estos resultados demostraron que nuestro diseño de co-inmovilización de enzimas y cofactores es eficiente y robusto incluso operando en flujo, condiciones más similares a las de uso en industria.

Por último, la misma estrategia de co-inmovilización se aplicó a otra enzima cetoreductasa (KRED P2-D11) que demostró ser más estable en presencia de solventes orgánicos. Sin embargo, en este caso la célula artificial metabólica no era eficiente porque la enzima no podía regenerar el cofactor.

En el capítulo 6 de esta tesis doctoral y, a diferencia de los trabajos anteriores, se amplió la técnica de co-inmovilización a cofactores que no participan en redacciones de oxido-reducción como por ejemplo pyridoxal-5'-fosfato (PLP). Las enzimas transaminasas (dependientes de PLP) han cobrado un papel importante en la biocatálisis en los últimos años debido a su intervención en la síntesis de productos farmacológicos. Por este motivo, se co-inmovilizó una transaminasa altamente activa y estable (He-ωTA) junto con el PLP en soportes de metacrilato. En primer lugar, se

exploraron diferentes tipos de co-inmovilización para la enzima y el cofactor. Una vez más, el mejor resultado se obtuvo con una estrategia basada en el diseño de co-inmovilización desarrollado en el capítulo 4. Primero, la transaminasa se unió de forma covalente al soporte. Posteriormente, se cubrió con el polímero PEI para la co-inmovilización del PLP. Las reacciones de transaminación se llevaron a cabo en reactores de flujo continuo durante más de 50 ciclos manteniendo al menos un 90% de conversión. Cabe destacar que estas células metábolicas artificiales llevaron a cabo síntesis de aminas a 1.4 mL x min^{-1}, el flujo más alto conseguido y reportado hasta el momento para reacciones biocatalíticas con enzimas y cofactores co-inmovilizados.

En vista de estos prometedores resultados, la misma técnica de co-inmovilización se aplicó a otras dos enzimas transaminasas (Cv-ωTA y (Pf-ωTA) con diferentes afinidades por el PLP. La enzima que presenta menor afinidad por el PLP, mostró ser la más ineficiente en reacciones en flujo. En último lugar, se eligió la transaminasa con mejores resultados para realizar en flujo continuo la síntesis de aminas de alto valor comercial empleando células metabólicas artificiales.

En definitiva, durante los trabajos presentados en esta tesis doctoral se ha demostrado que el diseño racional de biocatalizadores heterogéneos y su análisis a nivel de una sola partícula son esenciales para mejorar el funcionamiento de las reacciones biocatalíticas y poder aplicarlas a nivel industrial.

Chapter 1

General introduction

1. BIOCATALYSIS

Chemical reactions can happen spontaneously, but this process often takes a long time to be accomplished because of the high energy requirements. In order to overcome such issue, catalysts are molecules which are able to diminish the energy barriers of the reaction to speed up the transformation of a chemical substance into another one. Noteworthy, the catalysts remain unaltered after each reaction cycle. In nature, enzymes are the essential biological catalysts to perform both catabolic and anabolic reactions that form the cell metabolism to sustain life.[1] These protein-based catalysts present unique properties compared to chemical catalysts: a) since enzymes are naturally present in cells, they catalyze reactions under physiological conditions (pH and temperature) and are biocompatible; b) enzymes are greener catalysts because they are biodegradable and they do not produce waste products in excess; c) enzymes are capable to catalyze a broad spectrum of reactions, many of which are extremely complex to perform by chemical synthesis; d) the regio-, stereo- and chemoselectivity of reactions catalyzed by enzymes are also greater than the chemically-catalyzed reactions.[1]

Biotechnology has been using enzymes as biocatalysts since millennia ago already to produce certain foods (e. g. wine, bread, cheese and beer) by using whole-cell fermentations. Generally, microbial cells are preferred over plant and animal cells as biocatalysts due to their simplicity and easy handling. However, whole-cells biotransformations show some inconveniences in terms of product purification, resistance to harsh conditions, production of toxic by-products and diffusion limitations.[2] In the 1960s and 1970s, enzymes started to be isolated from cells to accomplish cell-free bioconversions. Fundamentally, free enzymes arrived to the general public of our society as additives in commercial detergents.[3] But the breakthrough of industrial enzymes started at the end of the past century with the emergence of directed-evolution of enzymes.[4, 5] These advances have driven the use of isolated enzymes for the synthesis of non-natural chemical compounds, the biomanufacturing of pharmaceuticals intermediates and their application in medical therapy.

The success of catalysis at industrial level depends ultimately on its sustainability at the three levels; economy, society and ecology.[6, 7] Although biotechnology is not necessarily more sustainable than organic chemistry, biocatalysis has demonstrated to be cleaner, safer and sometimes more efficient by continuously replacing traditional

chemical processes at industry in the last decades. In this sense, modern biocatalysis faces the transition from the petro-based economy to the renewable bio-based economies; addressing our society evolution but diminishing the human footprint in the world.[3, 7]

In an industrial context, enzymes still show undesirable features inherent to their natural origin.[8, 9] On the one hand, the high solubility of enzymes in aqueous solutions limits their reuse and recycling for in-line reactions, more dramatically for continuous-flow operations. On the other hand, the low stability at industrial conditions (extreme pH, high temperature, non-polar solvents, high substrates and products concentrations) challenges their implementation as free biocatalysts. Moreover, the multi-step protocols to produce and purify isolated enzymes are very time-consuming. Finally, natural enzymes show a restricted reactivity towards non-natural substrates.[10] Fortunately, new strategies for the rational development of biocatalysts, high-troughput screening and computational analysis are cooperating to sort out these drawbacks. Firstly, the novel protein engineering techniques are the *in vitro* directed evolution based on random mutagenesis of amino acids followed by cycles of selection from the resulting protein libraries.[4] Likewise, the growing number of available enzymes expands the catalytic reaction repertoire and eases the assembly of one-pot multi-enzyme cascade reactions to access more sophisticated synthetic schemes.[11, 12] Moreover, recent developments on metadata analysis as omics sciences (e. g. metagenomics[13]), computational protein engineering and the more recent high resolution analysis methods among others, let the rapid and extensive enhance of biocatalysts properties.[14, 15] Secondly, the progress of enzyme immobilization on solid surfaces during the last fifty years has been a huge advance to overcome the solubilization problems of free enzymes, allowing their reuse during several batch reactions and their incorporation in the growing field of flow reactions.[16-18]

2. ENZYME IMMOBILIZATION

Enzyme immobilization refers to the state of enzyme molecules confined into or attached to solid materials where enzymes are in a different phase from the reactants, but substrates and products can diffuse between the solid and liquid phase. These enzymatic systems are dubbed as heterogeneous biocatalysts. Hence, during the immobilization process, the enzyme becomes water-insoluble (solid) and presents

different properties compared to homogeneous biocatalysts (soluble enzyme) dissolved in an aqueous-liquid phase.[19]

Enzyme immobilization provides many advantages to overcome the limitations of free enzymes:[20]

- The solid-liquid composition of the heterogeneous biocatalysts facilitates the handling and separation of the product from the biocatalyst when the reaction is completed, minimizing the contamination of the product and simplifying the downstream processes.
- Enzyme inactivation triggered by inactivating agents (temperature, pH and organic solvents) can be minimized when the protein is immobilized, which allows using heterogeneous biocatalysts for longer operational times. Additionally, immobilized enzymes can be storaged for a long-term due its high stability.
- The facile separation of the immobilized enzymes (solid) from the reaction bulk (liquid) make possible the reuse and recycle of the biocatalyst and ease their integration into continuous flow systems. This is an essential concern for a cost-efficient application and intensification of enzymatic processes.

For those reasons, enzyme immobilization has been the most endorsed solution to defeat the solubility and robustness issues of free enzymes.[21] However, there are still some inconveniences derived from enzyme immobilization. Since enzymes are enclosed in a solid structure, mass transfer issues have to be solved in some cases. Moreover, the vast majority of enzymes lose activity when immobilized because of conformational distortions. Economically, the high price of the carrier is a limiting factor to implement enzyme biocatalysis in industry. In order to alleviate those drawbacks, many different studies about immobilization procedures, carrier materials and immobilization chemistries have come to light in the last five decades.[16-18, 21, 22]

2.1. Methodologies for enzyme immobilization

Hitherto, no immobilization protocol has proved to be universal for the enhancement of both activity and stability of the immobilized enzymes. In consequence, enzyme immobilization is still an empirical exercise based on trial-and-error experiments rather than a rational design. Underlying disciplines as materials science, protein structure,

enzymology and reactor engineering must converged during the fabrication of heterogeneous biocatalysts.[23]

The main immobilization chemistries between the enzyme and the carrier can be divided into reversible and irreversible immobilization (Figure 1). On the one hand, enzymes can be reversibly immobilized by hydrophobic, electrostatic or the called weak interactions (van der Waals and hydrogen bonds) with the surface of the carriers. Reversible immobilization can be easily reverted by changing the media conditions. This is an attractive point to reuse costly carriers because when enzymes become inactive, the carrier can be regenerated and reloaded with fresh enzyme. However, operational use may suffer from lixiviation issues that may decrease the long-term operational performance of the heterogeneous biocatalysts. On the other hand, irreversible immobilization involves covalent interactions to bind irreversibly the enzyme on the carrier surface. Therefore, the lixiviation issue is overcomed because the enzyme cannot be physically detached from the carrier. Despite the carrier cannot be regenerated once the enzyme is inactive, irreversible immobilization is frequently adopted to prolong the stability of the biocatalyst. Multivalent attachments foment the rigidification of the enzyme and consequently stabilize the enzyme structure.[24] As consequence, the operational life-time of the biocatalyst may significantly increase since the enzyme remains active for longer times. Nonetheless, the rigidification of enzymes must be balanced because a severe rigidification may cause a dramatic decrease of the protein activity.

Basically, the most used immobilization chemistries are the following:

- Physical adsorption: This is the most straightforward and oldest technique used to immobilize proteins. The physical adsorption is achieved by non-specific forces as hydrophobic or ionic reversible interactions.[25] Hydrophobic adsorption has been used since more than a century ago,[26] but the interaction can be disrupted under certain conditions (e. g. organic solvents, detergents). Ionic adsorption is usually preferred because enzymes surfaces are rich in charged residues (acid or basic) that establish strong interactions with the carrier surface activated with complementary charged groups. Nevertheless, the immobilized enzyme can be still removed by modifying the ionic strength or the pH.[27, 28]

- Affinity immobilization: This type of reversible immobilization relies on the selectivity and complementarity of biomolecules;[29] e. g. antibodies and antigens, avidin and biotin, polyhistidine tag and metal ions (Co^{2+}, Cu^{2+}, Zn^{2+} or

Ni^{2+}) hormones and receptors, lectins and glycosilated molecules, DNA and DNA-binding protein domains among others. The protein is usually genetically modified and the carrier is activated with the corresponding group before the immobilization process. The minimal conformational changes and the control of protein orientation during affinity immobilization turn out in a high enzymatic activity of the biocatalyst.[30] Unfortunately, the biocatalyst operational stability is low upon the immobilization protocol due to potential lixiviation of the enzyme.

- Covalent binding: Reversible (usually imine or disulfide bonds)[31] and irreversible covalent binding are applied to attach proteins to carriers. Although reversible covalent bounds (Schiff´s bases) are frequently reduced to become irreversible. The side chains of lysine, cysteine, tyrosine, histidine, arginine and glutamic / aspartic acid can perform a nucleophilic attack to the reactive groups (epoxy, aldehyde, vinyl and cyanogen bromide groups) of the carrier for the covalent binding.[24, 32-34] Afterwards, the enzyme remains bound to the carrier by multipoint covalent attachment which is a strong linking but does not specifically orient the enzyme.[24] Covalent binding offers benefits in terms of operational stability[32] and reuse which are crucial for industrial biocatalytic processes. However, the irreversible nature of the immobilization does not allow the recycle of the expensive carriers when enzyme activity tends to zero.

- Entrapment/encapsulation: Unlike the previous immobilization strategies, the entrapment and encapsulation are not carried out on a prefabricated matrix (carrier). In other words, this is a bottom-up approach. Typically, entrapment strategies need the presence of enzymes during the synthesis of the carrier. The most common carriers are polymeric matrices,[35, 36] hollow fibers[37] and microcapsules.[38] Entrapment physically confines the enzymes into micro/nanometric structures where the latter can freely move inside the materials without direct contact with the carrier. For this reason, this type of immobilization can be considered as a reversible approach although the carrier can be hardly reused. In some cases, the physical interactions between the enzymes and the matrices are so strong that the immobilization is considered quasi-irreversible. This is the case of enzyme entrapment into metal-organic frameworks where the enzyme is intimately interplaying with the interaction network that sustains the carrier architecture.[39] A particular case of entrapment is the encapsulation of proteins into capsules or vesicles. In this architecture, during the encapsulation the enzymes are retained into the lumen spaces of the

vesicles formed by a membrane. Depending on the composition we distinguish between liposomes, colloidosomes and proteinosemes built with lipids, nanoparticles and proteins, respectively.

- Crosslinked aggregates: This carrier-free immobilization methodology relies on the irreversible intermolecular cross-linkages between a cross-linking agent (commonly, glutaraldehyde) and the lysine residues of enzymes.[40] Cross-linked enzyme aggregates (CLEAs) are primarily prepared by precipitation of enzymes with organic solvents (acetone, ethanol or butanol), ammonium sulfate or other precipitating agents, followed by the cross-linking step. The great advantage of CLEAs is the lack of expensive carriers to immobilize enzymes[41] in an irreversible manner that avoids the enzyme lixiviation.[42] Nevertheless, loss of activity and mass transfer limitations are the main disadvantages of the high enzyme crowding on CLEAs. In the last years other cross-linked aggregates have been reported such as metal-phosphate biominerals that can also aggregate enzymes giving rise to highly active and stable heterogeneous biocatalysts. Unfortunately, their mechanical stability is too low for industrial application and their uses have been restricted for sensing or biomedical applications.[43]

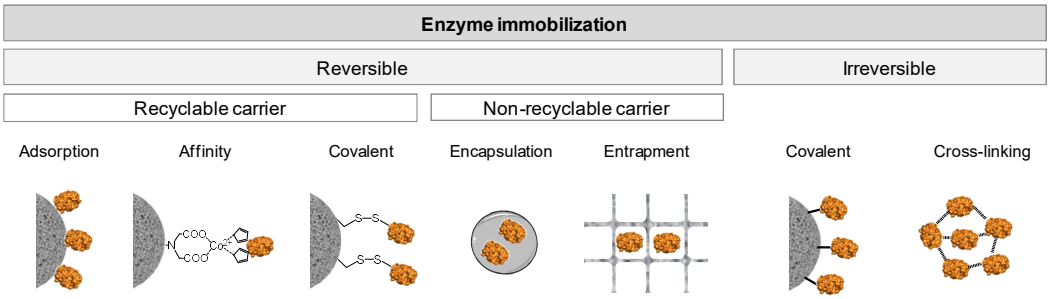

Figure 1. Scheme of main enzyme immobilization chemistries.

2.2. Materials for the fabrication of carriers

The selection of a suitable material for enzyme immobilization is the key to ultimately optimize the performance of the heterogeneous biocatalysts. However, an universal material has not been described for all different applications of immobilized enzymes. Ideally, the material should be hydrophilic, inert, biocompatible, endurable to microbial attack, inexpensive and resistant to physico-chemical degradation.[16, 18, 22] Porous

carriers are mostly chosen because their high surface area enables high enzyme loading and the enzymes are protected from the reaction bulk. Nowadays, nanostructures are also getting momentum in virtue of their quick synthesis, large surface area and fluent movement. Materials are chiefly classified into organic and inorganic according to their chemical composition:

- Organic materials: These carriers are commonly subclassified into natural and synthetic polymers according to their origin.
  - Natural polymers present interesting properties as high protein affinity, non-toxicity, hydrophilic nature and biodegradability for food industry, pharmaco-medical applications and agricultural procedures. The most common natural polymers are cellulose, agarose, pectins, chitin, chitosan, proteins (gelatin, albumin and collagen) and alginate.[44, 45]
  - Synthetic polymers are sometimes chosen as a result of their low cost, high stability and resistant to biodegradation. Polymethacrylate,[46] polyacrylamide and silicone are some examples of synthetic polymers for enzyme immobilization.

- Inorganic materials: Despite of these materials can be also subdivided as natural (silica, bentonite and activated carbon) and synthetic (glass, zeolite[47] and ceramics). The most widely used inorganic material for enzyme immobilization is silica.[48, 49] This material can be easily synthesized and activated with a plethora of reactive groups via silanization. Since silica is pretty stable to high temperatures, inert and low-cost, this material has been broadly used for industrial manufacturing and also for biomedical purposes.[50]

During the works developed in this PhD thesis, a broad spectrum of carrier materials, activation of the carriers and immobilization chemistries were applied for enzyme immobilization (Table1).

Table 1. Carriers applied for protein immobilization during this work.

Name	Material	Number of reactive groups	Reactive groups	Particle diameter (μm)	Pore diameter (nm)	Preparation protocol
AG-DVS	Agarose	Mono-functionalization	Vinyl groups	50-150	200	Page 121
AG-Co			Cobalt chelates	50-150	200	Commercial source
AG-PEI600			Aminated groups	50-150	300	Page 121
AG-TEA			Aminated groups	50-150	200	Page 89
AG-Oct			Octyne groups	50-150	200	This work (Page 56)
AuNRs	Gold		Thiol groups	0.05	Non-pororous	Page 55
Pu-E	Methacryllate		Epoxy groups	150-300	120-180	Commercial source
Pu-G			Aldehyde groups	150-300	120-180	Page 121
SiO_2NPs	Silica dioxide		Hydroxyl groups	0.1	Non-pororous	Page 55
Glass surface			Hydroxyl groups	-	Non-pororous	Commercial source
AG-Co/S	Agarose	Bi-functionalization	Cobalt chelates and thiol groups	50-150	200	This work (Page 56)
AG-G/PEI25			Aldehyde and aminated groups	50-150	200	Page 89
AG-DVS/PEI25			Vinyl and aminated groups	50-150	200	Page 89
AG-DEAE/G			Aldehyde and aminated groups	50-150	200	Page 121
EC-Co^{2+}/eA	Methacryllate		Cobalt chelates and aminated groups	100-300	10-20	This work (Page 156)
EC-Co^{2+}/PEI60			Cobalt chelates and aminated groups	100-300	10-20	This work (Page 156)
Pu-Co^{2+}/eA			Cobalt chelates and aminated groups	150-300	120-180	This work (Page 155)
Pu-Co^{2+}/hA			Cobalt chelates and aminated groups	150-300	120-180	This work (Page 155)
Pu-G/PEI25			Aldehyde groups and aminated groups	150-300	120-180	Page 90
Pu-DEAE/E			Epoxides and aminated groups	150-300	30-60	Page 121

3. SYNTHETIC BIOLOGY

Science has benefited from natural systems by mimicking their structures, properties and functions (e. g. biocatalytic routes). Almost two centuries ago, organic chemistry started to synthesize natural products rather than just analyzing and isolating them from natural samples.[51, 52] Following that roadmap, the emerging field of synthetic

biology develops nature-like systems for applications in biomedicine, biochemical synthesis and biotechnology.[53] This discipline has focused on two main approaches; a top-down strategy and a bottom-up strategy. The first approach is based on diminishing the multiple functions of an organism to maintain the essential properties of a living entity. The bottom-up approach starts from scratch and tries to build complex artificial entities by assembling biological and non-biological molecules.[52, 54] In this PhD thesis, the bottom-up approach was applied to design and engineering protein-based micro-systems with metabolic functionalities. This bottom-up approach can be dubbed as *in vitro* synthetic biology because non-living elements are normally created.

3.1. Cell-free protein synthesis

Proteins are the ultimately expression of biological function as enzymes. Thus, proteins represent many roles in chemical reactions as transporters, scaffolds, receptors, and protein signaling.[55] For these reasons, the production of pure proteins has become in an interesting objective from different disciplines. Traditionally, proteins have been produced using host organisms as bacteria, yeast and less commonly animal and plant cells. However, these heterologous expression systems require multiple time-consuming steps that include: cloning, transformation of the plasmid to compatible cells, selection of colonies hosting a foreign plasmid, culture growth for plasmid production, plasmid isolation, sequencing, transformation of the plasmid to compatible cells, culture growth for protein overexpression, harvesting, lysis and protein purification.[56]

In 1961, Nirenberg and Matthaei conducted the protein expression in a test tube rather in living cells.[57] They separated the cytoplasm from the cell membrane and they used the resulting cell extracts to perform the *in vitro* transcription and translation of proteins which is called cell-free protein synthesis (CFPS). Almost any class of cell can be used to prepared cell extracts for CFPS. The most conventional sources are *E. coli*, wheat germ and rabbit reticulocite, but also *Thermus sp., Leishmania tarentolae*, insect cells and even human cells have been used.[58, 59] Prokaryotic cells are more convenient to improve the productivity and scalability of CFPS. However, protein folding and post-translational modifications are more feasible in eukaryotic cells which are still emerging for preparation of cell extracts.[60]

Cell extracts basically contain the enzymatic machinery like ribosomes, the ATP regeneration system, aminoacyl-tRNA synthases and translation factors (initation,

elongation and termination factors). All these elements are used in their soluble form together with the substrates (amino acids and nucleotides), tRNAs for the 20 natural amino acids, energy cofactors (ATP, GTP, CoA, NAD^+ among others), and the DNA template to transcript and translate the target polypeptide (Figure 2). DNA templates can be added in three different forms: circular plasmid, linearized plasmid or linear PCR product. On the one hand, plasmids are of general choice because of the higher susceptibility of linear DNA fragments to be cleavaged by endonucleases.[61] On the other hand, linear DNA fragments are simpler since cloning steps (digestion, ligation, transformation to cells, culture growth, plasmid isolation and sequencing) are avoided.[62]

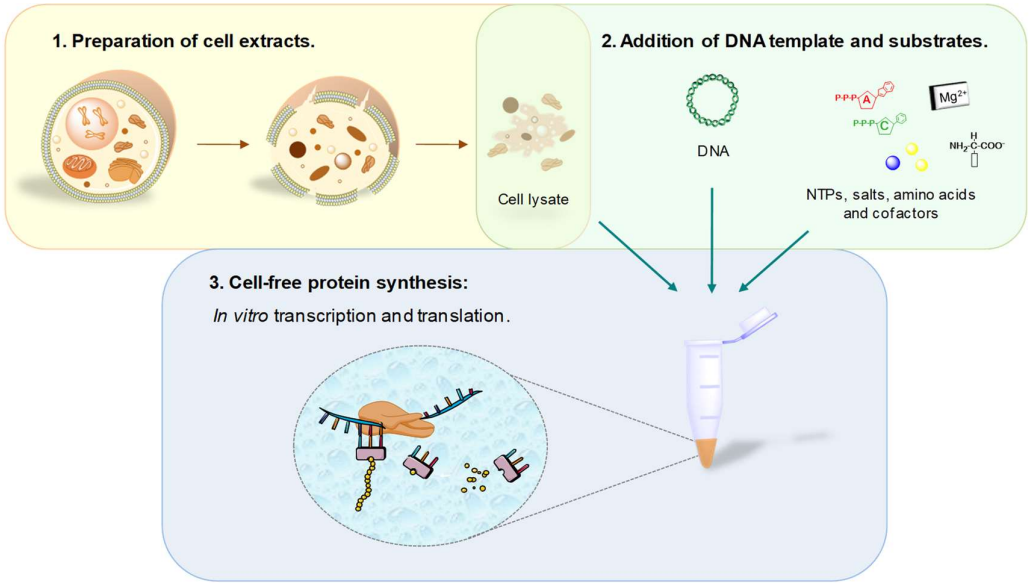

Figure 2. Cell-free protein synthesis. 1) Starting from a living cell, cell extracts are produced and stored for further on-demand CFPS. 2) Cell extracts must be supplemented with the fresh mix of substrates and the DNA template which is added to trigger the CFPS reaction. 3) The transcription of mRNA and the translation into proteins are accomplished in the same test tube to finally obtain the desired protein.

Hitherto, two main methods have been optimized to accomplish the CFPS. The cell lysate-based CFPS described above has been utilized since fifty years ago due its more facile preparation at lower cost. The second method was more recently described by Shimizu *et al.* and was named as PURE system.[63, 64] This cell-free system is reconstituted with purified components and contains His-tagged versions of all proteins which make easier the purification of the synthesized protein.[64] Due to the His-tag, the protein synthesis machinery can be immobilized onto microbeads to facilitate the

purification of the synthesized protein since it remains soluble in the supernatant.[65] Both systems are commercially available nowadays, but also many protocols for cell extracts preparation have colonized the field of CFPS in the last years.[66]

3.1.1. Applications of CFPS

CFPS is the synthetic-biological tool that has received the greatest interest from the scientific community because of the wide spectrum of applications.[49, 66-69] Due to the easy manipulation of cell extracts, fast sampling and direct monitoring, new applications are growing everyday. The most relevant strategies which can be involved on biocatalyst design are following summarized:

- Protein evolution: *In vivo* directed evolution has already shown a high potential for enzyme improvement, but applying CFPS for directed evolution of enzymes can definitively boost this strategy shortening time processes and financial costs.[70-72] In the same way, *in vitro* biocatalyst prototyping by using CFPS has been a helpful tool to discover new enzymes and biosynthetic pathways optimizing the cycle design-build-test.[67, 73]

- Incorporation of non-natural amino acids: The incorporation of non-natural amino acids into a specific site of the protein sequence has been addressed *in vivo*. But *in vitro* protein synthesis is more versatile to incorporate fluorescence-labels, photoactivable probes, redox active groups and natural post-translational modifications into proteins, creating a new toolbox for protein engineering.[74, 75] Since the expression of unnatural proteins may result toxic for living cells, CFPS has proven to overcome this issue even obtaining high yields of non-natural proteins.[76, 77]

- Therapeutics and vaccines: The synthesis of bioactive recombinant proteins has been improved by incorporation of CFPS. Exciting results on high-throughput production and fast protein screenings support CFPS also for development of new drugs and biocatalyst-based therapies.[78] Recent developments on microfluidic systems allow the production of protein-based therapeutics at the point-care.[79-81] Therefore, CFPS is opening new frontiers for personalized protein therapeutics which are very important for orphan drugs.

- Diagnostics and biosensing: Biosensors are very sensitive devices principally used for clinical diagnosis, environmental monitoring and food safety. Frequently, specialized instruments and high economical budgets are needed.[82] Several biosensing platforms have been created in the very last years, by using user-friendly and inexpensive CFPS strategies.[83] Thus, a new multivalent and robust biosensing platform has been developed for both biomedical and environmental purposes.[84, 85]

3.2. Cell-free metabolic engineering

Cells are highly advanced microreactors in nature that constitute the 'minimal building block of life'.[86] Their complex spatial organization and compartmentalization has attracted the attention of synthetic biologists since cells are capable to perform thousands of different functions simultaneously with an exquisite selectivity.[87] From a bottom-up approach, the intracellular components can be *in vitro* assembled to build a synthetic cell-mimic microstructure which is called 'artificial cell'. However, if biosynthetic pathways are the only elements confined into microstructures, we may instead name these systems as artificial metabolic cells. This approach was born as 'systems biocatalysis' based on the co-immobilization of isolated enzymes onto artificial carriers to perform cell-free metabolic pathways.[88, 89] The strategy merges the most complex synthetic focus of chemistry with the simplest modular design of biological systems. Systems biocatalysis has been already tested for mimicking several natural enzymatic pathways as cell-free ethanol fermentation, glycolysis or carbohydrate synthesis.[88] In this thesis, we went one step further integrating whole-enzyme cascades in the solid carrier and analyzing the resulting biocatalysts as single cells.

Inspired by the organization and confinement of both catabolic and anabolic pathways within living cells, enzymes and also their cofactors were co-immobilized into artificial solid chassis to develop robust and self-sufficient heterogeneous biocatalysts called artificial metabolic cells (Figure 3).[90-92]

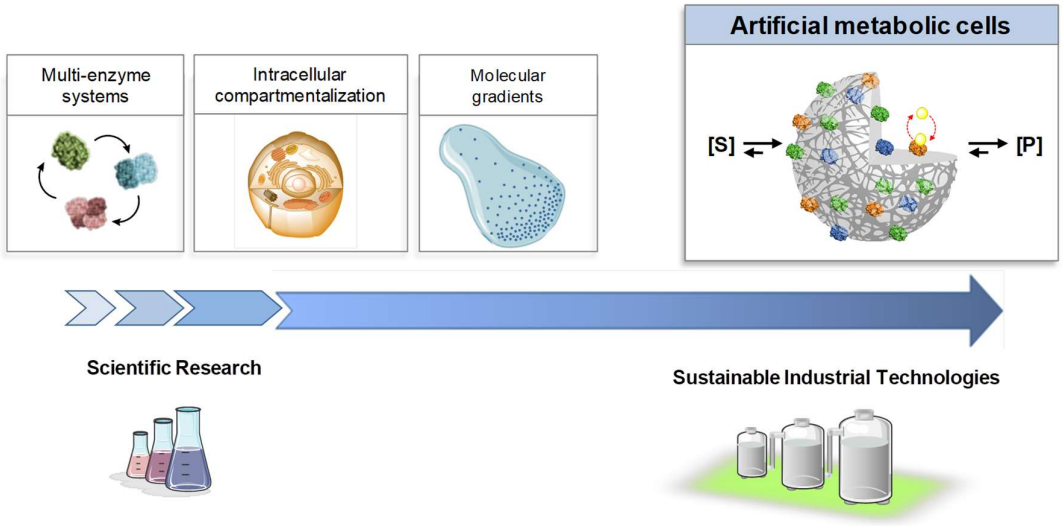

Figure 3. Development of artificial metabolic cells for advanced applications. The spatial organization and dynamics inside living cells are the basis for the design and engineering of artificial metabolic cells. These micro-structures not only help to better understand how cellular biology works, but also can perform industrially-interesting reactions in a more efficient fashion.

In an industrial context, growing demands to access a wider spectrum of new products maintaining the smaller ecological footprint have pushed the transition framework from natural cells as biocatalysts to new cell-free approaches.[93] Systems biocatalysis approaches for the co-immobilization of enzymes and cofactors (both natural and artificial) on different surfaces have been developed in the last years. For dehydrogenase-catalyzed reactions, several methodologies have been described to retain NAD(P)H in the solid phase.[94] Artificial cofactors like nanoparticles and metal complexes may be also integrated in biocatalytic reactions.[91] For instance, a lipase was covalently co-immobilized with metal nanoparticles into silanaceous mesoporous foam for tandem catalysis. Sadly, the enzyme was drastically inactivated due to the hard reaction conditions.[95] In a more precise strategy, metal complexes were covalently tethered to the surface of immobilized enzymes, giving rise to heterogeneous biocatalysts capable of hydrolyzing and reducing nitroarene esters in a one-pot tandem reaction.[96]

The last advances on protein engineering and immobilization techniques working synergistically with the focus of heterogeneous biocatalysts as self-sufficient artificial metabolic cells are poised to boost adapted and efficient biocatalystsfor sustainable chemistry purposes.[97]

4. SINGLE-PARTICLE STUDIES

Notwithstanding the advance of characterization studies of heterogeneous biocatalysts at macroscopic level, the performance of enzymes and cofactors inside solid carriers is still a black-box. Unfortunately, the intraparticle characterization and analysis of immobilized enzymes have received much less attention. For this reason, heterogeneous biocatalysts show unpredictable mass transfer issues, unknown internal gradients and inactivation facts which are harsh to overcome.[98, 99] Analogously to inside living cells, co-immobilized enzymes and cofactors on porous materials show a dynamic behavior. Therefore, the information elicited from the inside of microparticles is paramount to optimize the design and engineering of these self-sufficient heterogeneous biocatalysts (Figure 3).

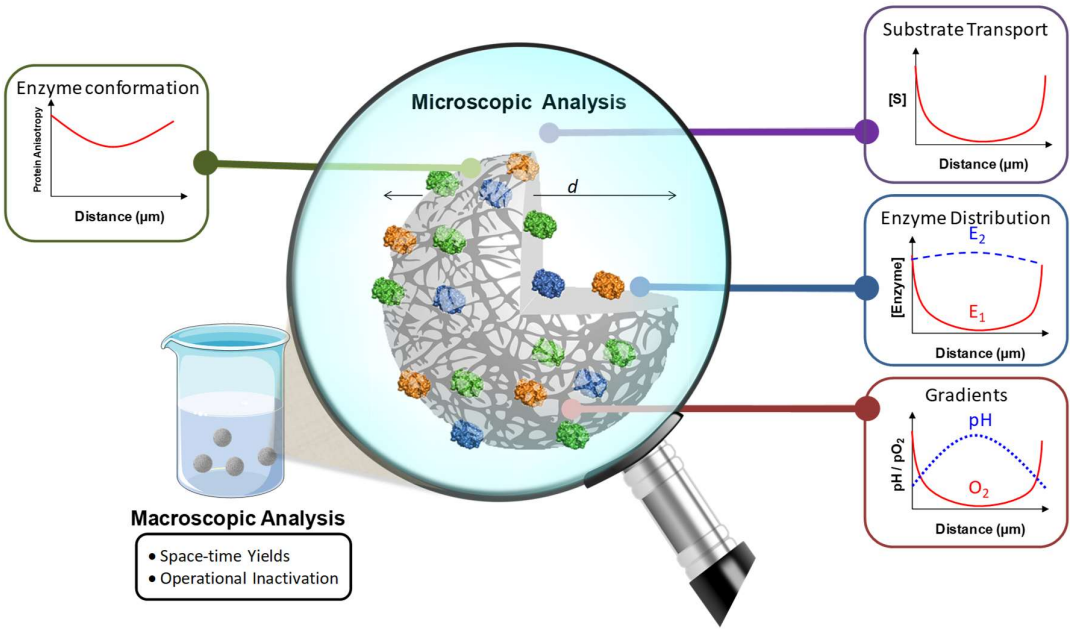

Figure 3. Scheme of information elicited from single-particle studies with spatio-temporal resolution.

In the last twenty years, single-molecule[100] and single-cell[101] studies have been key to understand biological processes and subsequently to boost the biotechnological applications of synthetic biology. In parallel, single-particle studies of artificial metabolic cells pretend to decipher mass transfer effects and enzyme kinetics at micro-scale to enhance the biocatalytic processes at macroscopic level.[102] On one hand, single-particle studies reveal morphological features of the solid materials as size dispersion and shape defects which will influence the final properties of the heterogeneous

biocatalysts. On the other hand, more functional aspects as spatio-temporal performance of immobilized enzymes and cofactors can be monitored and analyzed at real time. Although the intraparticle analytical techniques are not well-established yet, single-particle studies are getting momentum in biocatalyst community.[102, 103] These studies shine light on the extensive technical possibilities existing for microscopic characterization of artificial metabolic cells, which are much simpler and easier to control than living cells.

Hitherto, the information elicited from single-particle studies of artificial metabolic cells can be sorted in four main areas:

- Spatial distribution of immobilized enzymes across solid carriers: Immobilized enzymes have been traditionally assumed to be homogeneously distributed across the solid porous carriers. Consequently, the majority of immobilization protocols lack the control of the spatial distribution and also the orientation of the enzyme. Nonetheless, the 3D distribution and spatial localization of immobilized enzymes show a direct influence on the efficiency of the reaction kinetics.

  Over the last few decades, atomic force microscopy (AFM), low-temperature field-emission scanning electron microscopy (cryo-FESEM),[104] spherical aberration (Cs)-corrected (STEM),[105] micro infrared and RAMAN spectroscopy[106] among others have been applied to obtain spatial information from immobilized proteins. Apart from these high-specialized techniques, fluorescence imaging by confocal laser scanning microscopy (CLSM) is often preferred due to the high versatility and resolution with easy handling. The fluorophores can be either genetically encoded (e. g. fluorescent proteins) or organic labels (e. g. rhodamine). The use of fluorescent proteins allowed the analysis of the effects of immobilization rates on spatial distribution of immobilized enzymes.[107] Moreover, the kinetics of an immobilized multi-enzyme system was studied by the spatial distribution of fluorophore-labeled enzymes.[108]

- Stability of immobilized enzymes using spectroscopic methods: Enzyme immobilization is a well-known methodology to achieve a higher stabilization of the biocatalysts because of the enzyme rigidification. Conventionally, stability of the enzyme is determined through bulk studies where the samples are incubated in presence of the inactivating agent and the averaged enzymatic

activity is monitored along the time. These macroscopic studies lose the spatial resolution needed to analyze the enzyme stability at single-particle level. AFM has been used to perform spectroscopic studies that predict the thermal stability of immobilized proteins.[109] Likewise, the combination of fluorescence lifetime imaging and spatial resolved fluorescence polarization was also applied to determine the fluorescence anisotropy of immobilized proteins as innovative strategy to analyze the stability of immobilized enzymes.[110]

- Reaction kinetics of immobilized enzymes: The activity of biocatalysts is conventionally monitored by measuring either the depletion of substrates or the formation of products from the bulk solution. Due to the heterogeneity of the sample, all the microparticles immobilizing enzymes show different spatio-temporal kinetics. Monitoring and imaging the enzyme activity during the operational process (*in operando* studies) provide substantial information that is otherwise inaccessible. To this aim, many fluorogenic substrates are commercially available as useful reporter systems.[111] These fluorogenic substrates are enzymatically transformed into fluorescent products which are read out to monitor the system kinetics.[112, 113] CLSM benefits from fluorescence to record the local synthesis of products. The bi-enzymatic system formed by glucose oxidase and horseradish peroxidase has been the most studied immobilized cascade by using fluorogenic substrates.[114, 115]

  Harnessing the autofluorescence of cofactors, enzymatic reactions performed by cofactor-dependent enzymes can be monitored by a label-free strategy. FAD(H) and NAD(H) are excellent cofactors for these studies, because cofactor-enzyme electron transfer causes fluorescence fluctuations that may be attributed to different conformations states. The fluorescence intensity is higher for the reduced form than for the oxidized one. This phenomenon was profited using soluble NAD^+ to created pH micro-gradients with microelectrodes and monitored the local activity of an immobilized alcohol dehydrogenase.[116] The transition from soluble NAD^+ to NADH was recorded and imaged to monitor the immobilized enzyme kinetics. However, monitoring the cofactor utilization with spatial resolution is underexploited.

- Oxygen and pH resolution within immobilized enzymes: Mass transfer effects are sometimes limiting the scope of heterogeneous biocatalysts. O_2 and pH are two variables specially affected by the concentration gradients between the bulk

liquid and the solid carrier surface.[103, 117] In order to assess the significance of the diffusional limitations, the concentration gradients should be measured in the bulk solution and in the internal microenvironment of the particle at real-time.[23, 103] The intraparticle consumption of O_2 by immobilized oxidases was measured by labeling the carrier with an O_2-sensitive luminophore.[117] This stategy was further used to optimize the geometrical properties of carriers (avoiding O_2 transfer limitations) during the design of heterogenous biocatalysts.[118]

Fluorophore-labeling was also applied to immobilized enzymes in order to quantify acidification effects inside the microparticles during biocatalytic reactions.[119] In addition, CLSM was once more applied in a pioneer study to characterize different biocatalysts by measuring and imaging the intraparticle pH.[120]

5. FLOW BIOPROCESSES

In this age, biocatalysis is a robust tool to accomplish sustainable chemical processes. Until the early 20th century, biocatalytic reactions were carried out in batch reactors which are flexible and simple. Nevertheless, the modern industry demands the intensification of the process to achieve high space-time yields. Flow-reactors can be more productive, better controlled and more sustainable than reactions in batch.[121-123]

In the last two decades, the concept of flow chemistry has been quickly developed in academia and also transferred to industry. The methodology involves a fluid containing the starting materials that is pumped at known flow rates through plug-flow reactors, where the chemical reaction takes place to finally yield a stream of product. The pump can be semi-continuous (e. g. syringe that needs refilling with the starting material) or continuous which do not require refilling and hypothetically can work indefinitely.[122] The foremost advantages of flow biocatalysis are time and costs. Flow biotransformations are accelerated, from hours to minutes, as a result of the higher liquid-solid contact surface which allows larger synthesis of products in smaller equipments with higher space-time yields, up to 650-fold in comparison with batch reactions.[123, 124] The continuous flow nature facilitate a faster homogenization of the temperature (heating or cooling) and the diffusion of gases (O_2, N_2, H_2, CO_2).[125] Moreover, flow reactors are normally modular allowing a flexible increment of production volume by adding more

reactors either in series or in parallel. In consequence, energy requirements and waste are drastically reduced due to higher efficiencies derived from a better process control.[123]

Flow reactors migth be tube-in-tube reactors, cartridges, micro- or mesofluidic devices, reactor coils and packed-bed reactors. Microreactors are getting popular for organic synthesis even at industrial scale. The most highlighted benefits are the high surface/volume ratio, the energy efficiency, the easy mobility of process plants, the plug-and-play process configuration and the rapid process development.[126, 127] In the very last two years, a new type of 3D-printed flow reactors (known as 'reactionwares') were developed for efficient continuous transaminations in microreactors.[128] However, more conventional packed-bed reactors (PBR) are the most used type of flow reactor by reason of easy-handling and high stability. PBRs are usually constituted by a tube filled with particles of immobilized enzymes remaining in fixed positions. The particles are suspended and moving constantly through the reaction medium which must be pumped at high flow rates to achieve mass transfers. Since the particles keep a continuous movement, the clogging of the bed and the poor distribution of the flow are avoided.[123] Consequently, PBRs are usually the most nearby approximation to a plug flow reactor (PFR). The PFR is a model used in chemical engineering to describe a flowing system of cylindrical geometry. The main assumption is that the whole content is completely mixed in the radial direction, but no mixing happens in the axial direction (not with the elements downstream or upstream). Then, the residence time is the same for all the elements inside the reactor.[123]

Flow biocatalysis may be performed using whole-cells, immobilized enzymes or free enzymes. Immobilized enzymes are mostly chosen for flow biotransformations because the downstream processes are simpler, the reaction is performed faster than using whole-cells and immobilized enzymes are retained and reused unlike free enzymes.[122]

Flow-chemistry contributes to the progress of many synthetic applications. Pharmaceutical industry was the first one to exploit the power of flow biocatalysis to sustainable manufacturing fine chemicals.[129-131] Currently, flow biocatalysis is an increasingly trending topic to enhance biocatalytic transformations obtaining high conversion yields. Lipase-catalyzed amidations and esterifications have been accomplished in flow-reactors.[132, 133] Dehydrogenases,[134] lyases,[135] phosphatases and aldolases,[136] among others have been incorporated to flow-biocatalysis as well.

Noteworthy, transaminations have greatly impacted on flow biocatalysis in the last years.[128, 137-140]

REFERENCES

1. Illanes, A. Enzyme biocatalysis: principles and applications. Springer. **2008**.

2. Schmid-Dannert, C., López-Gallego, F. Advances and opportunities for the design of self-sufficient and spatially organized cell-free biocatalytic systems. *Current Opinion in Chemical Biology*. **2019**, *49*: 97-104.

3. Blamey, J. M., Fischer, F., Meyer, H. P., Sarmiento, F., Zinn, M. Enzymatic biocatalysis in chemical transformations: a promising and emerging field in green chemistry practice. In Biotechnology of microbial enzymes. Academic Press. **2017**, *14*: 347-403.

4. Moore, J. C., Jin, H. M., Kuchner, O., Arnold, F. H. Strategies for the in vitro evolution of protein function: enzyme evolution by random recombination of improved sequences. *Journal of Molecular Biology*. **1997**, *272*: 336-347.

5. Minshull, J., Willem Stemmer, P. C. Protein evolution by molecular breeding. *Current Opinion in Chemical Biology*. **1999**, *3*: 284-290.

6. Fessner, W. D. Biocatalysis: from discovery to application. Springer. **2000**.

7. Sheldon, R. A., Woodley, J. M. Role of biocatalysis in sustainable chemistry. *Chemical Reviews*. **2018**, *118*: 801-838.

8. Chapman, J., Ismail, E. A., Dinu, Z. C. Industrial applications of enzymes: recent advances, techniques, and outlooks. *Catalysts*. **2018**, *8*: 1443-1454.

9. Schmid, A., Dordick, J. S., Hauer, B., Kiener, A., Wubbolts, M., Witholt, B. Industrial biocatalysis today and tomorrow. *Nature*. **2001**, *409*: 258-268.

10. Homaei, A. A., Sariri, R., Vianello, F., Stevanato, R. Enzyme immobilization: an update. *Journal of Chemical Biology*. **2013**, *6*: 185-205.

11. García-Junceda, E., Lavandera, I., Rother, D., Schrittwieser, J. H. (Chemo)enzymatic cascades - nature's synthetic strategy transferred to the laboratory. *Journal of Molecular Catalysis B: Enzymatic*. **2015**, *114*: 1-6.

12. Sanchez-Moreno, I., Oroz-Guinea, I., Iturrate, L., Garcia-Junceda, E. ChemInform abstract: multienzyme reactions. *ChemInform*. **2013**, *44*.

13. Lorenz, P., Eck, J. Metagenomics and industrial applications. *Nature Reviews Microbiology*. **2005**, *3*: 510-516.

14. Bommarius, A. S. Biocatalysis: a status report. *Annual Review of Chemical and Biomolecular Engineering*. **2015**, *6*: 319-345.

15. Bornscheuer, U. T., Huisman, G. W., Kazlauskas, R. J., Lutz, S., Moore, J. C., Robins, K. Engineering the third wave of biocatalysis. *Nature*. **2012**, *485*: 185-194.

16. Datta, S., Christena, L. R., Rajaram, Y. R. S. Enzyme immobilization: an overview on techniques and support materials. *3 Biotech*. **2013**, *3*: 1-9.

17. Guisán, J. M. In Immobilization of enzymes and cells. Humana Press. **2006**.

18. Sheldon, R. A., Van Pelt, S. Enzyme immobilisation in biocatalysis: why, what and how. *Chemical Society Reviews*. **2013**, *42*: 6223-6235.

19. Hanefeld, U., Gardossi, L., Magner, E. Understanding enzyme immobilisation. *Chemical Society Reviews*. **2009**, *38*: 453-468.

20. Katchalski-Katzir, E. Immobilized enzymes, learning from past successes and failures. *Trends in Biotechnology*. **1993**, *11*: 471-478.

21. Bickerstaff, G. In Immobilization of enzymes and cells. Humana Press. **1996**.

22. Mohamad, N. R., Marzuki, N. H. C., Buang, N. A., Huyop, F., Wahab, R. A. An overview of technologies for immobilization of enzymes and surface analysis techniques for immobilized enzymes. *Biotechnology, biotechnological equipment*. **2015**, *29*: 205-220.

23. Bolivar, J. M., Eisl, I., Nidetzky, B. Advanced characterization of immobilized enzymes as heterogeneous biocatalysts. *Catalysis Today*. **2016**, *259*: 66-80.

24. Grazú, V., Abian, O., Mateo, C., Batista-Viera, F., Fernández-Lafuente, R., Guisán, J. M. Stabilization of enzymes by multipoint immobilization of thiolated proteins on new epoxy-thiol supports. *Biotechnology and Bioengineering*. **2005**, *90*: 597-605.

25. Jesionowski, T., Zdarta, J., Krajewska, B. Enzyme immobilization by adsorption: a review. *Adsorption*. **2014**, *20*: 801-821.

26. Nelson, J. M., Griffin, E. G. Adsorption of invertase. *Journal of the American Chemical Society*. **1916**, *38*: 1109-1115.

27. Mateo, C., Abian, O., Fernandez-Lafuente, R., Guisan, J. M. Reversible enzyme immobilization via a very strong and nondistorting ionic adsorption on support–polyethylenimine composites. *Biotechnology and Bioengineering*. **2000**, *68*: 98-105.

28. Mateo, C. *et al.* Very strong but reversible immobilization of enzymes on supports coated with ionic polymers. In Immobilization of enzymes and cells. Springer. **2006**, *22*: 205-216.

29. Roy, I., Gupta, M. N. Bioaffinity immobilization. In Immobilization of enzymes and cells. Springer. **2006**, 107-116.

30. Andreescu, S., Bucur, B., Marty, J. L. Affinity immobilization of tagged enzymes. In Immobilization of enzymes and cells. Springer. **2006**, 97-106.

31. Ovsejevi, K., Manta, C., Batista-Viera, F. Reversible covalent immobilization of enzymes via disulfide bonds. In Immobilization of enzymes and cells. Springer. **2013**, 89-116.

32. López-Gallego, F., Fernandez-Lorente, G., Rocha-Martin, J., Bolivar, J. M., Mateo, C., Guisan, J. M. Stabilization of enzymes by multipoint covalent immobilization on supports activated with glyoxyl groups. In Immobilization of enzymes and cells. Springer. **2013**, 59-71.

33. López-Gallego, F., Guisán, J. M., Betancor, L. Glutaraldehyde-mediated protein immobilization. In Immobilization of enzymes and cells. Springer. **2013**, 33-41.

34. Mateo, C., Grazu, V., Palomo, J. M., López-Gallego, F., Fernandez-Lafuente, R., Guisan, J. M. Immobilization of enzymes on heterofunctional epoxy supports. *Nature Protocols*. **2007**, *2*: 1022.

35. Reetz, M. T. Practical protocols for lipase immobilization via sol–gel techniques. In Immobilization of enzymes and cells. Springer. **2013**, 241-254.

36. Sassolas, A., Hayat, A., Marty, J.-L. Enzyme immobilization by entrapment within a gel network. In Immobilization of enzymes and cells. Springer. **2013**, 229-239.

37. Ji, X., Wang, P., Su, Z., Ma, G., Zhang, S. Enabling multi-enzyme biocatalysis using coaxial-electrospun hollow nanofibers: redesign of artificial cells. *Journal of Materials Chemistry B*. **2014**, *2*: 181-190.

38. Rother, C., Nidetzky, B. Enzyme immobilization by microencapsulation: methods, materials, and technological applications. *Encyclopedia of Industrial Biotechnology*. **2014**.

39. Chen, W. H., Vázquez-González, M., Zoabi, A., Abu-Reziq, R., Willner, I. Biocatalytic cascades driven by enzymes encapsulated in metal–organic framework nanoparticles. *Nature Catalysis*. **2018**, *1*: 689-695.

40. Cao, L., Langen, L. V., Sheldon, R. A. Immobilised enzymes: carrier-bound or carrier-free? *Current Opinion in Biotechnology*. **2003**, *14*: 387-394.

41. Sheldon, R. A. Characteristic features and biotechnological applications of cross-linked enzyme aggregates (CLEAs). *Applied microbiology and biotechnology*. **2011**, *92*: 467-477.

42. Velasco-Lozano, S., López-Gallego, F., Mateos-Díaz Juan, C., Favela-Torres, E. Cross-linked enzyme aggregates (CLEA) in enzyme improvement – a review. *Biocatalysis*. **2016**, *1*: 166-177.

43. Lee, S. W., Cheon, S. A., Kim, M. I., Park, T. J. Organic-inorganic hybrid nanoflowers: types, characteristics, and future prospects. *Journal of nanobiotechnology*. **2015**, *13*: 54-63.

44. Klein, M. P., Scheeren, C. W., Lorenzoni, A. S. G., Dupont, J., Frazzon, J., Hertz, P. F. Ionic liquid-cellulose film for enzyme immobilization. *Process Biochemistry*. **2011**, *46*: 1375-1379.

45. Zucca, P., Fernandez-Lafuente, R., Sanjust, E. Agarose and its derivatives as supports for enzyme immobilization. *Molecules*. **2016**, *21*: 1577-1601.

46. Palomo, J. M., Muñoz, G., Fernández-Lorente, G., Mateo, C., Fernández-Lafuente, R., Guisán, J. M. Interfacial adsorption of lipases on very hydrophobic support (octadecyl–Sepabeads): immobilization, hyperactivation and stabilization of the open form of lipases. *Journal of Molecular Catalysis B: Enzymatic*. **2002**, *19-20*: 279-286.

47. Díaz, J. F., Balkus, K. J. Enzyme immobilization in MCM-41 molecular sieve. *Journal of Molecular Catalysis B: Enzymatic*. **1996**, *2*: 115-126.

48. Blanco, R. M., Terreros, P., Fernández-Pérez, M., Otero, C., Díaz-González, G. Functionalization of mesoporous silica for lipase immobilization: Characterization of the support and the catalysts. *Journal of Molecular Catalysis B: Enzymatic*. **2004**, *30*: 83-93.

49. Carlson, E. D., Gan, R., Hodgman, C. E., Jewett, M. C. Cell-free protein synthesis: applications come of age. *Biotechnology Advances*. **2012**, *30*: 1185-1194.

50. Bharti, C., Nagaich, U., Pal, A. K., Gulati, N. Mesoporous silica nanoparticles in target drug delivery system: A review. *International journal of pharmaceutical investigation*. **2015**, *5*: 124-133.

51. Yeh, B. J., Lim, W. A. Synthetic biology: lessons from the history of synthetic organic chemistry. *Nature Chemical Biology*. **2007**, *3*: 521-525.

52. Boldt, J. Synthetic biology: origin, scope and ethics. *Minding nature*. **2010**, *3*.

53. Hodgman, C. E., Jewett, M. C. Cell-free synthetic biology: thinking outside the cell. *Metabolic Engineering*. **2012**, *14*: 261-269.

54. Xu, C., Hu, S., Chen, X. Artificial cells: from basic science to applications. *Materials Today*. **2016**, *19*: 516-532.

55. Whittaker, J. W. Cell-free protein synthesis: the state of the art. *Biotechnology Letters*. **2013**, *35*: 143-152.

56. Gräslund, S. *et al.* Protein production and purification. *Nature Methods*. **2008**, *5*: 135-146.

57. Nirenberg, M. W., Matthaei, J. H. The dependence of cell-free protein synthesis in E. coli upon naturally occurring or synthetic polyribonucleotides. *Proceedings of the National Academy of Sciences*. **1961**, *47*: 1588-1602.

58. Mikami, S., Kobayashi, T., Masutani, M., Yokoyama, S., Imataka, H. A human cell-derived in vitro coupled transcription/translation system optimized for

production of recombinant proteins. *Protein Expression and Purification*. **2008**, *62*: 190-198.

59. Mureev, S., Kovtun, O., Nguyen, U. T. T., Alexandrov, K. Species-independent translational leaders facilitate cell-free expression. *Nature Biotechnology*. **2009**, *27*: 747-752.

60. Zemella, A., Thoring, L., Hoffmeister, C., Kubick, S. Cell-free protein synthesis: pros and cons of prokaryotic and eukaryotic systems. *ChemBioChem*. **2015**, *16*: 2420-2431.

61. Yang, H. L., Ivashkiv, L., Chen, H. Z., Zubay, G., Cashel, M. Cell-free coupled transcription-translation system for investigation of linear DNA segments. *Proceedings of the National Academy of Sciences*. **1980**, *77*: 7029-7033.

62. Schinn, S. M., Broadbent, A., Bradley, W. T., Bundy, B. C. Protein synthesis directly from PCR: progress and applications of cell-free protein synthesis with linear DNA. *New Biotechnology*. **2016**, *33*: 480-487.

63. Shimizu, Y. *et al.* Cell-free translation reconstituted with purified components. *Nature Biotechnology*. **2001**, *19*: 751-755.

64. Shimizu, Y., Kanamori, T., Ueda, T. Protein synthesis by pure translation systems. *Methods*. **2005**, *36*: 299-304.

65. Kojima, T. *et al.* Immobilization of proteins onto microbeads using a DNA binding tag for enzymatic assays. *Journal of Bioscience and Bioengineering*. **2016**, *121*: 147-153.

66. Chong, S. Overview of cell-free protein synthesis: historic landmarks, commercial systems, and expanding applications. *Current protocols in molecular biology*. **2014**, *108*: 16.30.1-16.30.11.

67. Karim, A. S., Jewett, M. C. A cell-free framework for rapid biosynthetic pathway prototyping and enzyme discovery. *Metabolic Engineering*. **2016**, *36*: 116-126.

68. Villarreal, F., Tan, C. Cell-free systems in the new age of synthetic biology. *Frontiers of Chemical Science and Engineering*. **2017**, *11*: 58-65.

69. Liu, W.-Q., Zhang, L., Chen, M., Li, J. Cell-free protein synthesis: recent advances in bacterial extract sources and expanded applications. *Biochemical Engineering Journal*. **2019**, *141*: 182-189.

70. Fischlechner, M., Schaerli, Y., Mohamed, M. F., Patil, S., Abell, C., Hollfelder, F. Evolution of enzyme catalysts caged in biomimetic gel-shell beads. *Nature Chemistry*. **2014**, *6*: 791-796.

71. Nishikawa, T., Sunami, T., Matsuura, T., Yomo, T. Directed evolution of proteins through in vitro protein synthesis in liposomes. *Journal of nucleic acids*. **2012**, *2012*: 1-11.

72. Stapleton, J. A., Swartz, J. R. Development of an in vitro compartmentalization screen for high-throughput directed evolution of [FeFe] hydrogenases. *PLOS ONE*. **2010**, *5*: 1-8.

73. Swartz, J. Developing cell-free biology for industrial applications. *Journal of Industrial Microbiology and Biotechnology*. **2006**, *33*: 476-485.

74. Dumas, A., Lercher, L., Spicer, C. D., Davis, B. G. Designing logical codon reassignment – expanding the chemistry in biology. *Chemical Science*. **2015**, *6*: 50-69.

75. Chin, J. W. Expanding and reprogramming the genetic code. *Nature*. **2017**, *550*: 53-60.

76. Goerke, A. R., Swartz, J. R. High-level cell-free synthesis yields of proteins containing site-specific non-natural amino acids. *Biotechnology and Bioengineering*. **2009**, *102*: 400-416.

77. Martin, R. W. *et al.* Cell-free protein synthesis from genomically recoded bacteria enables multisite incorporation of noncanonical amino acids. *Nature Communications*. **2018**, *9*: 1-9.

78. Salehi, A. S. M., Smith, M. T., Bennett, A. M., Williams, J. B., Pitt, W. G., Bundy, B. C. Cell-free protein synthesis of a cytotoxic cancer therapeutic: onconase production and a just-add-water cell-free system. *Biotechnology Journal*. **2016**, *11*: 274-281.

79. Georgi, V. *et al.* On-chip automation of cell-free protein synthesis: new opportunities due to a novel reaction mode. *Lab on a Chip*. **2016**, *16*: 269-281.

80. Husser, M. C., Vo, P. Q. N., Sinha, H., Ahmadi, F., Shih, S. C. C. An automated induction microfluidics system for synthetic biology. *ACS Synthetic Biology*. **2018**, *7* (3): 933-944.

81. Sullivan, C. J. *et al.* A cell-free expression and purification process for rapid production of protein biologics. *Biotechnology Journal*. **2016**, *11*: 238-248.

82. Perumal, V., Hashim, U. Advances in biosensors: principle, architecture and applications. *Journal of Applied Biomedicine*. **2014**, *12*: 1-15.

83. Wen, K. Y. *et al.* A cell-free biosensor for detecting quorum sensing molecules in P. aeruginosa - infected respiratory samples. *ACS Synthetic Biology*. **2017**, *6*: 2293-2301.

84. Salehi, A. S. M. *et al.* Cell-free protein synthesis approach to biosensing hTRβ-specific endocrine disruptors. *Analytical Chemistry*. **2017**, *89*: 3395-3401.

85. Salehi, A. S. M. *et al.* Biosensing estrogenic endocrine disruptors in human blood and urine: a rapid cell-free protein synthesis approach. *Toxicology and Applied Pharmacology*. **2018**, *345*: 19-25.

86. Buddingh', B. C., Van Hest, J. C. M. Artificial cells: synthetic compartments with life-like functionality and adaptivity. *Accounts of Chemical Research*. **2017**, *50*: 769-777.

87. Mehta, S., Zhang, J. Illuminating the cell's biochemical activity architecture. *Biochemistry*. **2017**, *56*: 5210-5213.

88. Fessner, W.-D. Systems Biocatalysis: Development and engineering of cell-free "artificial metabolisms" for preparative multi-enzymatic synthesis. *New Biotechnology*. **2015**, *32*: 658-664.

89. Tessaro, D., Pollegioni, L., Piubelli, L., D'arrigo, P., Servi, S. Systems biocatalysis: an artificial metabolism for interconversion of functional groups. *ACS Catalysis*. **2015**, *5*: 1604-1608.

90. López-Gallego, F., Jackson, E., Betancor, L. Heterogeneous systems biocatalysis: the path to the fabrication of self-sufficient artificial metabolic cells. *Chemistry – A European Journal*. **2017**, *23*: 17841-17849.

91. Schmidt, S., Castiglione, K., Kourist, R. Overcoming the incompatibility challenge in chemoenzymatic and multi-catalytic cascade reactions. *Chemistry – A European Journal*. **2018**, *24*: 1755-1768.

92. Velasco-Lozano, S., Benítez-Mateos, A. I., López-Gallego, F. Co-immobilized phosphorylated cofactors and enzymes as self-sufficient heterogeneous biocatalysts for chemical processes. *Angewandte Chemie International Edition*. **2017**, *56*: 771-775.

93. Lee, J. W., Na, D., Park, J. M., Lee, J., Choi, S., Lee, S. Y. Systems metabolic engineering of microorganisms for natural and non-natural chemicals. *Nature Chemical Biology*. **2012**, *8*: 536-546.

94. Liu, W., Wang, P. Cofactor regeneration for sustainable enzymatic biosynthesis. *Biotechnology Advances*. **2007**, *25*: 369-384.

95. Engström, K. *et al.* Co-immobilization of an enzyme and a metal into the compartments of mesoporous silica for cooperative tandem catalysis: an artificial metalloenzyme. *Angewandte Chemie International Edition*. **2013**, *52*: 14006-14010.

96. Filice, M., Romero, O., Gutiérrez-Fernández, J., De Las Rivas, B., Hermoso, J. A., Palomo, J. M. Synthesis of a heterogeneous artificial metallolipase with chimeric catalytic activity. *Chemical Communications*. **2015**, *51*: 9324-9327.

97. Schmidt-Dannert, C., Lopez-Gallego, F. A roadmap for biocatalysis – functional and spatial orchestration of enzyme cascades. *Microbial Biotechnology*. **2016**, *9*: 601-609.

98. Bommarius, A. S., Paye, M. F. Stabilizing biocatalysts. *Chemical Society Reviews*. **2013**, *42*: 6534-6565.

99. Dicosimo, R., Mcauliffe, J., Poulose, A. J., Bohlmann, G. Industrial use of immobilized enzymes. *Chemical Society Reviews*. **2013**, *42*: 6437-6474.

100. Peterman, E. J. G., Wuite, G. J. L. Single molecule analysis. Humana Press. **2018**.

101. Yuan, G.C. *et al.* Challenges and emerging directions in single-cell analysis. *Genome Biology*. **2017**, *18*: 1-8.

102. Benítez-Mateos, A. I., Nidetzky, B., Bolivar, J. M., López-Gallego, F. Single-particle studies to advance the characterization of heterogeneous biocatalysts. *ChemCatChem*. **2018**, *10*: 654-665.

103. Bolivar, J. M., Consolati, T., Mayr, T., Nidetzky, B. Shine a light on immobilized enzymes: real-time sensing in solid supported biocatalysts. *Trends in Biotechnology*. **2013**, *31*: 194-203.

104. Hoenger, A. High-resolution cryo-electron microscopy on macromolecular complexes and cell organelles. *Protoplasma*. **2014**, *251*: 417-427.

105. Mayoral, A., Arenal, R., Gascón, V., Márquez-Álvarez, C., Blanco, R. M., Díaz, I. Designing functionalized mesoporous materials for enzyme immobilization: locating enzymes by using advanced TEM techniques. *ChemCatChem*. **2013**, *5*: 903-909.

106. López-Gallego, F., Yate, L. Selective biomineralization of $Co_3(PO_4)_2$-sponges triggered by His-tagged proteins: efficient heterogeneous biocatalysts for redox processes. *Chemical Communications*. **2015**, *51*: 8753-8756.

107. Bolivar, J. M., Hidalgo, A., Sánchez-Ruiloba, L., Berenguer, J., Guisán, J. M., López-Gallego, F. Modulation of the distribution of small proteins within porous matrixes by smart-control of the immobilization rate. *Journal of Biotechnology*. **2011**, *155*: 412-420.

108. Rocha-Martín, J., Rivas, B. D. L., Muñoz, R., Guisán, J. M., López-Gallego, F. Rational co-immobilization of bi-enzyme cascades on porous supports and their applications in bio-redox reactions with in situ recycling of soluble cofactors. *ChemCatChem*. **2012**, *4*: 1279-1288.

109. Gregurec, D., Velasco-Lozano, S., Moya, S. E., Vázquez, L., López-Gallego, F. Force spectroscopy predicts thermal stability of immobilized proteins by measuring microbead mechanics. *Soft Matter*. **2016**, *12*: 8718-8725.

110. Orrego, A. H., García, C., Mancheño, J. M., Guisán, J. M., Lillo, M. P., López-Gallego, F. Two-photon fluorescence anisotropy imaging to elucidate the dynamics and the stability of immobilized proteins. *The Journal of Physical Chemistry B*. **2016**, *120*: 485-491.

111. Turunen, P., Rowan, A. E., Blank, K. Single-enzyme kinetics with fluorogenic substrates: lessons learnt and future directions. *FEBS Letters*. **2014**, *588*: 3553-3563.

112. Aguanno, E., Altamura, E., Mavelli, F., Fahr, A., Stano, P., Luisi, L. P. Physical routes to primitive cells: an experimental model based on the spontaneous

entrapment of enzymes inside micrometer-sized liposomes. *Life*. **2015**, *5*: 969-996.

113. Wang, L. *et al.* Single-step fabrication of multi-compartmentalized biphasic proteinosomes. *Chemical Communications*. **2017**, *53*: 8537-8540.

114. Piwonski, H. M., Goomanovsky, M., Bensimon, D., Horovitz, A., Haran, G. Allosteric inhibition of individual enzyme molecules trapped in lipid vesicles. *Proceedings of the National Academy of Sciences*. **2012**, *109*: 1437-1443.

115. Tang, T. Y. D. *et al.* Gene-mediated chemical communication in synthetic protocell communities. *ACS Synthetic Biology*. **2018**, *7*: 339-346.

116. O'brien, J. C., Shumaker-Parry, J., Engstrom, R. C. Microelectrode control of surface-bound enzymatic activity. *Analytical Chemistry*. **1998**, *70*: 1307-1311.

117. Bolivar, J. M., Consolati, T., Mayr, T., Nidetzky, B. Quantitating intraparticle O_2 gradients in solid supported enzyme immobilizates: Experimental determination of their role in limiting the catalytic effectiveness of immobilized glucose oxidase. *Biotechnology and Bioengineering*. **2013**, *110*: 2086-2095.

118. Bolivar, J. M., Schelch, S., Pfeiffer, M., Nidetzky, B. Intensifying the O_2-dependent heterogeneous biocatalysis: Superoxygenation of solid support from H_2O_2 by a catalase tailor-made for effective immobilization. *Journal of Molecular Catalysis B: Enzymatic*. **2016**, *134*: 302-309.

119. Spieß, A., Schlothauer, R. C., Hinrichs, J., Scheidat, B., Kasche, V. pH gradients in immobilized amidases and their influence on rates and yields of β-lactam hydrolysis. *Biotechnology and Bioengineering*. **1999**, *62*: 267-277.

120. Spiess, A. C., Kasche, V. Direct measurement of pH profiles in immobilized enzyme carriers during kinetically controlled synthesis using CLSM. *Biotechnology Progress*. **2001**, *17*: 294-303.

121. Wiles, C., Watts, P. Continuous flow reactors: a perspective. *Green Chemistry*. **2012**, *14*: 38-54.

122. Britton, J., Majumdar, S., Weiss, G. A. Continuous flow biocatalysis. *Chemical Society Reviews*. **2018**, *47*: 5891-5918.

123. Tamborini, L., Fernandes, P., Paradisi, F., Molinari, F. Flow bioreactors as complementary tools for biocatalytic process intensification. *Trends in Biotechnology*. **2018**, *36*: 73-88.

124. Jones, E., Mcclean, K., Housden, S., Gasparini, G., Archer, I. Biocatalytic oxidase: batch to continuous. *Chemical Engineering Research and Design*. **2012**, *90*: 726-731.

125. Ley, S. V., Fitzpatrick, D. E., Myers, R. M., Battilocchio, C., Ingham, R. J. Machine-assisted organic synthesis. *Angewandte Chemie International Edition*. **2015**, *54*: 10122-10136.

126. Jensen, K. F. Flow chemistry - microreaction technology comes of age. *AIChE Journal*. **2017**, *63*: 858-869.

127. Wohlgemuth, R., Plazl, I., Žnidaršič-Plazl, P., Gernaey, K. V., Woodley, J. M. Microscale technology and biocatalytic processes: opportunities and challenges for synthesis. *Trends in Biotechnology*. **2015**, *33*: 302-314.

128. Peris, E. *et al.* Tuneable 3D printed bioreactors for transaminations under continuous-flow. *Green Chemistry*. **2017**, *19*: 5345-5349.

129. Adamo, A. *et al.* On-demand continuous-flow production of pharmaceuticals in a compact, reconfigurable system. *Science*. **2016**, *352*: 61-67.

130. Devine, P. N., Howard, R. M., Kumar, R., Thompson, M. P., Truppo, M. D., Turner, N. J. Extending the application of biocatalysis to meet the challenges of drug development. *Nature Reviews Chemistry*. **2018**, *2*: 409-421.

131. Jiménez-González, C. *et al.* Key green engineering research areas for sustainable manufacturing: a perspective from pharmaceutical and fine chemicals manufacturers. *Organic Process Research & Development*. **2011**, *15*: 900-911.

132. Le Joubioux, F., Bridiau, N., Sanekli, M., Graber, M., Maugard, T. Continuous lipase-catalyzed production of pseudo-ceramides in a packed-bed bioreactor. *Journal of Molecular Catalysis B: Enzymatic*. **2014**, *109*: 143-153.

133. Tamborini, L., Romano, D., Pinto, A., Bertolani, A., Molinari, F., Conti, P. An efficient method for the lipase-catalysed resolution and in-line purification of racemic flurbiprofen in a continuous-flow reactor. *Journal of Molecular Catalysis B: Enzymatic*. **2012**, *84*: 78-82.

134. Šalić, A., Zelić, B. ADH-catalysed hexanol oxidation with fully integrated NADH regeneration performed in microreactors connected in series. *RSC Advances*. **2014**, *4*: 41714-41721.

135. Ender, F. *et al.* Microfluidic multiple cell chip reactor filled with enzyme-coated magnetic nanoparticles — an efficient and flexible novel tool for enzyme catalyzed biotransformations. *Journal of Flow Chemistry*. **2016**, *6*: 43-52.

136. Babich, L., Hartog, A. F., Van Hemert, L. J. C., Rutjes, F. P. J. T., Wever, R. Synthesis of carbohydrates in a continuous flow reactor by immobilized phosphatase and aldolase. *ChemSusChem*. **2012**, *5*: 2348-2353.

137. Contente, M. L., Dall'oglio, F., Tamborini, L., Molinari, F., Paradisi, F. Highly Efficient Oxidation of Amines to Aldehydes with Flow-based Biocatalysis. *ChemCatChem*. **2017**, *9*: 3843-3848.

138. Contente, M. L., Paradisi, F. Self-sustaining closed-loop multienzyme-mediated conversion of amines into alcohols in continuous reactions. *Nature Catalysis*. **2018**, *1*: 452-459.

139. Gruber, P. *et al.* Enzymatic synthesis of chiral amino-alcohols by coupling transketolase and transaminase-catalyzed reactions in a cascading continuous-

flow microreactor system. *Biotechnology and Bioengineering*. **2018**, *115*: 586-596.

140. Planchestainer, M., Contente, M. L., Cassidy, J., Molinari, F., Tamborini, L., Paradisi, F. Continuous flow biocatalysis: production and in-line purification of amines by immobilised transaminase from Halomonas elongata. *Green Chemistry*. **2017**, *19*: 372-375.

Chapter 2

Background and objectives

1. BACKGROUND

The research in industrial biotechnology has been highly boosted around the world in the last decades. Many findings have been made in the use of enzymes as catalytic tools to sustainably manufacture demanded chemicals and materials from our developed society, aiming at replacing the conventional manufacturing that exploits fossil raw material. Protein engineering and enzyme cascades have allowed improving the operational yields of more complex synthetic schemes under non physiological conditions. Parallely, enzyme immobilization on solid supports has driven heterogeneous biocatalysis towards more economic pathways throguh easing the recycling and enhancing the robutness of the biocatalyts. More recently, a revolution in chemical manufacturing is happening thanks to the innovations in continuous flow biocatalysis. However, the efficiency of these top-down approaches is often rather low due to the lack of orcherstration and tunning between the individual enzymes that form the biosynthetic system. Likewise, the continuous supply of expensive additives (i.e cofactors) during the biocatalytic reactions hampers the scaling-up of theses process due to economic reasons. In this context tailor-made design studies and fast assembly strategies are unmet to fabricate more efficient and robust multi-functional heterogeneous biocatalysts. New efforts to contribute to the fundamental knowledge and technological develoment on this subject will contribute to establish and speed-up a safe path for the technological transfer from lab scale to industrial scale assuming the productivity and economy criteria posed by chemical industry .

These days, synthetic biology is getting momentum in the scientific community not only as a novel field itself but also as a new advanced tool to go beyond the limits of classic engineering strategies in biocatalysis and biotechnology. Applying those principles, the supervisor of this thesis Dr. López-Gallego visualized heterogeneous biocatalysts as artificial metabolic cells which are constituted by sub-micrometric particles rationally assembled and whose ultimate goal is to efficiently develope anabolic and catabolic reactions in flow.

Since I was motivated and keen on biocatalysis and synthetic biology, I was selected to join the Heterogeneous Biocatalysis team as PhD student on March 2016. The research group leaded by Dr. López-Gallego was founded in CIC biomaGUNE (San Sebastián, Spain), an international institute for research on biomaterials and where the work presented on this PhD thesis was mainly conducted. I started to work as part of the project BIOPROTOGEL (BIO2014-61838-EXP) on the development of applications

of cell-free protein synthesis and immobilization for biosensing, biomedicine and biocatalysts prototyping. Then, I focused on the co-immobilization of multienzyme cascades and cofactors, as well as evolving single-particle strategies to optimize the performance of self-sufficient heterogeneous biocatalysts at microenvironments. This second part of my PhD thesis was funded by the project HETMUBI (BIO2015-69887-R) related to the development of multifunctional heterogeneous biocatalysts as new horizons for synthetic biology in solid state.

2. OBJECTIVES

My PhD thesis, here presented, was born with the aim to advance on the fabrication of self-sufficient heterogeneous biocatalysts characterized at single-particle level. **The main goal of this thesis is therefore the fabrication and the characterization of artificial metabolic cells** based on multi-enzymes systems co-immobilized with the required cofactors on porous microparticles **to perform the continous synthesis of amine and alcohols** without the exogeneous addition of cofactors. To achieve the main objective, this PhD thesis has addressed the following goals:

1. The development of a prototyping-screening platform to make easier, quicker and massive the site-directed immobilization of proteins to optimize the fabrication of protein-based biomaterials and biocatalysts.

2. The co-immobilization of phosphorylated cofactors with enzyme systems on the same solid carrier to make self-sufficient heterogeneous biocatalysts.

3. To expand the strategy described in the goal 2 to develop more complex multi-enzyme systems as artificial metabolic cells for the synthesis of chiral alcohols and amines.

4. To understand how co-immobilized multi-enzyme systems and their cofactors work at micro-scale inside the solid particles with spatio-temporal characterization.

5. The integration of self-sufficient heterogeneous biocatalysts into flow reactors to test the potential applicability and feasibility under current industrial requirements.

The first task of this PhD thesis was to search into the state of the art of the main subjects in this work: biocatalysis, protein immobilization, flow biochemistry and

synthetic biology. A summarized description and the nexus among all of them are compiled in **Chapter 1**.

Considering the lack of easy-and-quick screening strategies to study protein immobilization and orientation, cell-free protein synthesis was combined with protein immobilization and published in Paper I. A genetic toolkit of plasmids for tagging proteins with different polipeptide-tags was also developed and incorporated into this novel platform. This strategy was applied for the immobilization of fluorescent proteins, enzymes and antibody-binding proteins onto different materials. The co-expression and co-immobilization of different proteins on the same carrier was also achieved. Encouraged to explore deeply the effects of the co-expression of different enzymes by cell-free protein synthesis, we collaborate with the Synthetic and Reconstructive Biology group of Prof. Mansy. The work carried out in CIBIO (Trento, Italy) was funded by a travelling fellowship (JCSTF-180501) that I received from The Company of Biologists (Journal of Cell Science). The objectives reached in this experimental part are presented in **Chapter 3**.

To the aim of engineering artificial metabolic cells, our group developed a cutting-edge strategy to co-immobilize phosphorylated cofactors on PEI-coated carriers. This platform was tested for a bi-enzyme system with two dehydrogenases that were co-immobilized with the cofactor. This pioneering work was published in Paper II. Considering the potential of cofactor co-immobilization observed, we also fabricated a microstructure co-immobilizing two different redox cofactors and an oxidoreductase onto the same solid carrier, demostrating the wide-ranging applicability of this methodology. For this system, we controlled the enzyme immobilization rate to tune the distribution of the enzymes across the porous carrier. The work developed in collaboration with Dr. Bolivar and Prof. Nidetzky is still ongoing and the results will be collected in Paper III. Finally, we investigated the state of the art of single-particle studies in order to characterize these heterogeneous biocatalysts and the reviewed information was collected in Paper IV. Due to the scarce sub-particle studies to design heterogeneous biocatalysts, we developed and applied microscopy and analytical tecniques to aid and guide the biocatalyst characterization step. All these results are summarized in **Chapter 4**.

Once enzymes and cofactors were efficiently co-immobilized onto solid carriers, we expanded this strategy to perform assymetric reduction of prochiral ketones. To this end, a ketoreductase-based biocatalyst was engineered by co-immobilizing the

enzyme and the cofactor on a positively-charged carrier. Single-particle studies were applied during the design and engineering process of the biocatalyst. Finally, the biocatalyst was tested in flow-reactions. The project was carried out in collaboration with the company EntreChem S.L., and the results are compiled in Paper V. Due to the satisfactory results obtained, the strategy was also applied for pharmaceutical synthesis using another more stable ketoreductase. Paper VI shows the work in partnership with the group of Prof. Berglund, the company EntreChem S.L. and the groupg of Prof. Kroutil. This work is deeply described in **Chapter 5**.

Since amines are industrially relevant, transaminases are becoming popular in organic synthesis. That demand aroused our motivation to fabricate self-sufficient heterogeneous biocatalyts based on transaminases from different organisms. In this case, the required coenzyme is not a redox cofactor but a phosphorylated cofactor. In addition, as indicated in the previous chapter, flow-biochemistry intensifies biocatalytic industrial processes. Therefore, we optimized the cofactor and enzyme immobilization conditions for flow-biocatalysis. Finally, the synthesis of high-valuable amines at the highest flow-rate ever reported for co-immobilized enzymes and cofactors was reported in Paper VII. This final work described in **Chapter 6** was carried out in collaboration with the group of Prof. Paradisi from the University of Nottingham (United Kingdom). This fruitful collaboration was supported by a travelling fellowship (N. 38377) from COST action CM1303.

3. SCIENTIFIC OUTCOME

These research findings has been published in the following scientific articles:

- **Paper I:** Benítez-Mateos, A. I., Llarena, I., Sánchez-Iglesias, A., López-Gallego, F. Expanding one-pot cell-free protein synthesis and immobilization for on-demand manufacturing of biomaterials. *ACS Synthetic Biology*. **2018**, *7*: 875-884.
- **Paper II:** Velasco-Lozano, S., Benítez-Mateos, A. I., López-Gallego, F. Co-immobilized phosphorylated cofactors and enzymes as self-sufficient heterogeneous biocatalysts for chemical processes. *Angewandte Chemie International Edition*. **2017**, *56*: 771-775.
- **Paper III:** Benítez-Mateos, A. I., Huber, C., Bolivar, J. M., Nidetzky, B., López-Gallego, F. Spatial distribution effects on the kinetic properties of co-immobilized enzymes and cofactors. *Manuscript in preparation.*

- **Paper IV:** Benítez-Mateos, A. I., Nidetzky, B., Bolivar, J. M., López-Gallego, F. Single-particle studies to advance the characterization of heterogeneous biocatalysts. *ChemCatChem*. **2018**, *10*: 654-665.
- **Paper V:** Benítez-Mateos, A. I., San Sebastian, E., Ríos-Lombardía, N., Morís, F., González-Sabín, J., López-Gallego, F. Asymmetric reduction of prochiral ketones by using self-sufficient heterogeneous biocatalysts based on NADPH-dependent ketoreductases. *Chemistry – A European Journal*. **2017**, *23*: 16843-16852.
- **Paper VI:** Marx, L., Ríos-Lombardía, N., Farnberger, J. F., Kroutil, W., Benítez-Mateos, A. I., López-Gallego, F., Morís, F., González-Sabín, J., Berglund, P. Chemoenzymatic approaches to the synthesis of the calcimimetic agent cinacalcet employing transaminases and ketoreductases. *Advanced Synthesis & Catalysis*. **2018**, *360*: 2157-2165.
- **Paper VII:** Benítez-Mateos, A. I., Contente, M. L., Velasco-Lozano, S., Paradisi, F., López-Gallego, F. Self-sufficient flow-biocatalysis by coimmobilization of pyridoxal 5′-phosphate and ω-transaminases onto porous carriers. *ACS Sustainable Chemistry & Engineering*. **2018**, *6*: 13151-13159.

Chapter 3

One-pot cell-free protein synthesis and immobilization for protein-carrier screening

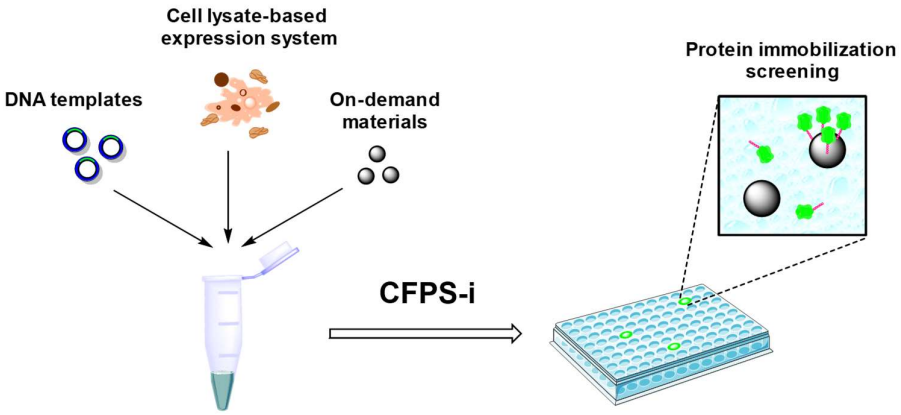

Expression, purification and immobilization of proteins are arduous work-up processeswhich may take a long time for the screening and further development of bio-molecule based materials. In this chapter, a molecular toolbox based on cell-free protein synthesis and oriented immobilization in one pot is proved to speed up the process from weeks to hours. A modular set of plasmids was constructed to fuse the N-terminal of superfolded green fluorescent protein (sGFP) with different peptide tags (poly(6X)Cys, poly(6X)His, and poly(6X)Lys), which drive the selective immobilization of the protein on the tailored material (agarose microbeads with different functionalities, gold nanorods and silica nanoparticles). This system also enables the incorporation of azide-based amino acids into the nascent protein for its site-directed immobilization through copper-free click reactions. Moreover, sGFP and an enzyme were co-expressed and co-immobilized by different binding chemistries on the same material. Finally, this technology has been expanded to the synthesis and oriented immobilization of proteins through antibody-binding proteins as a prototyping platform for the fabrication of more complex artificial metabolic cells.

The work presented in this chapter was published in *ACS Synthetic Biology*.[1]

1. INTRODUCTION

Cell-free protein synthesis (CFPS) in solution[2] is an emerging alternative to the conventional time-consuming methodologies for protein expression by using heterologous hosts as *E. coli* or *S. cerevisiae*. CFPS is an *in vitro* transcription-translation system which can synthesize proteins at mg x mL^{-1} concentration in several hours.[3] It is becoming a powerful and versatile technique to readily synthesize well-folded proteins and active enzymes, even toxic proteins which cannot be expressed using living hosts.[4-6] Despite of these unique features, this synthetic biological strategy still suffers a bottleneck when scaling-up the process to an industrial environment. Operational complexities like either inhibitory by-products or depletion of substrates and energy make it extremely impractical for high-scale protein production. Many efforts on improving the energy recycling systems[7, 8] and several compartmentalization strategies[9, 10] are currently alleviating those drawbacks. Contrastingly, *in vitro* protein expression system is an efficient approach in terms of both time and resources for R&D analysis and screenings of protein expression at lab scale. Recently, many advances have been reported for prototyping and microarrays of *in vitro* protein expression in solution.[11-16]

Once proteins have been synthesized, their immobilization is one of the major challenges of biomaterial manufacturing. In order to facilitate the fabrication of protein-based materials, CFPS and protein immobilization have been coupled in one pot (CFPS-i). The achievement of this goal requires the development of methodologies that selectively immobilize the nascent protein. To this aim, the immobilization chemistry must be orthogonal to the protein synthesis, avoid unspecific interactions between the protein synthesis machinery and the solid material, and correctly orient the protein to guarantee the functionality of the resulting biomaterial. A previous work showed CFPS-i of membrane proteins fused to GFP at their C-terminal and immobilized on PVDF membranes through hydrophobic interactions.[17] Unfortunately, this kind of hydrophobic interaction is not very selective to expand this technique for new applications. Protein tagging with polypeptides or protein domains is the most widespread strategy to purify proteins for biochemical and structural studies. Furthermore, the tag serves to control the orientation of proteins when immobilized on solid materials.[18, 19] Nowadays we have access to a large variety of peptide tags and domains that selectively bind silver,[20] gold,[21-23] nickel oxide[24] and iron oxide[25] through coordination and covalent bonds; silica particles[26] through ionic interactions; biopolymeric particles such as agarose

microbeads[27] through multivalent interactions based on hydrogen and Van der Waals bonds; and even oil-droplets[28] through hydrophobic interactions.

In several pioneering works, CFPS-i was utilized for the fabrication of self-assembling protein microarrays as NAPPA technology,[29] PISA method[30] and other protein array-based approaches.[17, 31, 32] One of the most well-known immunoassay technologies is the antibody microarray which is essentially based on functional immobilized antibodies onto solid surfaces.[33] To this end, the proper orientation of the immobilized inmunoglobulins is key for the correct recognition of the antigen.[34] Protein A and protein G contain an IgG-binding domain which is harnessed as an affinity IgG purification method. Furthermore, proteins A/G are specifically bound to the Fc region of the IgG allowing the orientation of the antibody during its immobilization.[22] This concept was further extended to the protein synthesis and selective immobilization by using (6x)-Histag.[35-37] These systems have been successfully applied for drug discovery[38] and protein engineering.[39]

Due to its extreme selectivity and biocompatibility, click reactions have also been exploited for bioconjugation of molecules and protein engineering.[40-42] Click chemistry has been already applied in cell-free protein synthesis for direct protein−protein click conjugation using Cu(I)-catalyzed cycloadditions and unnatural amino acids.[43] Similarly, virus-like particles (VLP) were assembled by using this technology after CFPS.[44] For that reasons, click chemistry could be another interesting approach to drive the immobilization of the newly synthesized protein onto materials. As far as we know, CFPS and copper-free click chemistry-mediated immobilization onto porous carriers has not been previously combined in one-pot.

The design, prototyping and development of biomaterials (mainly based on immobilized proteins on solid carriers) is paramount to fabricate heterogeneous biocatalysts, biosensors[45] and new therapeutics.[46] In the present chapter, cell-free protein synthesis has been coupled to the protein immobilization in one-pot, using different binding chemistries that assure the selective immobilization of the nascent protein. Harnessing the different chemical functionalities on the material surface, a novel toolkit was developed to synthesize and immobilize on-demand proteins on a plethora of materials. Firstly, a set of plasmids coding the desired protein with different polypeptide tags was designed for the selective immobilization onto solid materials. This system was further tested for the co-expression and selective co-immobilization of multi-protein systems on the same material. Secondly, unnatural amino acids were added to the

CFPS reaction to immobilize the nascent protein by click-chemistry. Finally, this strategy was also expanded to the fabrication of antibody-based materials mediated by protein A.[22, 33, 34] Bringing together all these strategies, an efficient screening and prototyping platform was developed for protein engineering and synthetic biology.

2. EXPERIMENTAL SECTION

2.1. Materials

AuNR and SiO_2NP were supplied by the colloidal nanofabrication platform from CIC-biomaGUNE. Agarose-based materials monofunctionalized with cyclooctyne groups and heterofunctionalized with both disulfide and cobalt-chelates groups were fabricated using plain agarose microbeads purchased from ABT technologies (Madrid, Spain). TALON Metal Affinity Resin was acquired from Clontech Laboratoires, Inc. S30 / T7 High-yield protein expression system was supplied by Promega Corporation (Fitchburg, WI). Rhodamine B isothiocyanate, dibenzocyclooctyne-amine, anti-rabbit IgG (whole molecule)–alkaline phosphatase antibody produced in goat, 4-nitrophenyl phosphate disodium salt hexahydrate (pNPP), 5,5′-dithiobis(2-nitrobenzoic acid), 1,4-dithiothreitol (DTT), 2-2'-2''-2'''-(ethane-1,2-diyldinitrilo)tetraacetic acid (EDTA), cyanogen bromide-activated sepharose 4B, L-Lysine, L-Cysteine, L-Histidine, p-nitrophenyl phosphate (pNPP), amicon ultra 0.5 mL centrifugal filters 10 kDa, kanamycin, horseradish peroxidise (HRP), Ampliflu Red, maltose, magnesium glutamate, polyethylene glycol (PEG8000), flavin-adenine-dinucleotide sodium salt (FAD^+), adenosine-5'-triphosphate (ATP), guanosine-5'-triphosphate (GTP), citydine-5'-triphosphate (CTP), uridine-5'-triphosphate (UTP), transfer RNA (tRNAs), coenzyme A (CoA), cyclic adenosine monophosphate (cAMP), folinic acid, spermidine, 3-phosphoglyceric acid (3-PGA), silver nitrate ($AgNO_3$, ≥ 99.0%), hexadecyltrimethylammonium bromide (CTAB, ≥ 99.0 %), hydrogen tetrachloroaurate trihydrate ($HAuCl_4$, ≥ 99.9%), L-ascorbic acid (AA, ≥ 99.0 %), sodium borohydride ($NaBH_4$, ≥ 96.0%), hydrochloric acid (HCl, 37%), tetraethyl orthosilicate (TEOS, 99%), ammonium hydroxide (NH_4OH, 29%), ethanol (EtOH, ≥ 99.8 %) and primers were acquired from Sigma-Aldrich (St. Louis, IL). Nicotinamide-adenine-dinucleotide sodium salt (NAD^+) was purchased from GERBU Biotechnik GmbH (Wieblingen, Germany). Click-it L-azidohomoalanine (AHA) was supplied by Thermo Fisher Scientific. Micro Bio-spinTM chromatographic columns were from BIORAD. 6-channel µ-Slide VI $^{0.4}$ was purchased from ibidi (Planegg, Germany) and epoxy methacrylate microbeads Lifetech ECR8204 were kindly donated by Purolite

Ltd (Llantrisant, UK). The plasmid *his-proa*_pET28b was donated by Dr. C. Araya-Callís and Dr. R. P. Richter. All other reagents were of analytical grade unless otherwise specified.

2.2. Methods

2.2.1. Gene cloning

The plasmid pET28b(+) (Novagen) was used for cloning and protein expression. The genetic construction *his-sgfp*_pET28b[47] and *his-adh*_pET28b[48] were developed in previous works. The plasmid encoding *his-proa* gene was already reported in a recent publication.[49] We designed eight primers (Table 1) for cloning *cys-sgfp*, *lys-sgfp* and *untagged-sgfp* genes using the plasmid *his-sgfp*_pET28b as template.

Table 1. List of primers for the genetic constructions.

Number	Primer name	Sequence	Length (bp)	Tm (ºC)
1	up_T7p_F	GCGTAGAGGATCGAG	15	51,5
2	down_T7t_R	CCGGATATAGTTCC	14	35,0
3	NcoI_sGFP_F	AAACCATGGAACATATGAGCAAAGGAGAAG	30	71,3
4	lacI_pET_F	AACTTAATGGGCCCGCTAACAG	22	66,8
5	AccII_down_T7t_R	CGTCCCATTCGCCATCC	17	67,8
6	LysTAG_F	AAAAAAAAAAAAAAAAAAAAGCAGCGGCCTGGTG	33	76,0
7	LysTAG_R	TTTTTTTTTTTTTTTTTTGCTGCTGCCCATG	31	74,1
8	CysTAG_F	TGTTGTTGTTGTTGTTGTAGCAGCGGCCTGGTG	31	79,1
9	CysTAG_R	ACAACAACAACAACAACAGCTGCTGCCCATG	33	81,5

Firstly, the sequence upstream of the *sgfp* gene was amplified by PCR using primers 3 and 8 for the construction of *cys-sgfp*_pET28b. Secondly, the downstream sequence was amplified with primers 7 and 4. Finally, an overlapping PCR was performed by using primers 3 and 4, and the previous PCR products as megaprimers. The vector pET28b was digested with the restriction enzymes NcoI and XhoI. Afterwards, the overlapping PCR product and the digested vector were purified and ligated by homologous recombination in *E. coli* strain DH10β (laboratory stock). The same procedure was carried out for the genetic construction of *lys-sgfp*_pET28b with primers 3 and 6; 5 and 4; 3 and 4, respectively. Cloning of *untagged-sgfp*_pET28b was accomplished with primers 1 and 2 for the amplification of *untagged-sgfp* sequence. The resulting PCR product and the vector were further digested with NcoI and XhoI. After the dephosphorylation and purification, DNA fragments were ligated and

transformed in BL21-Gold (DE3). All molecular biology protocols were performed using standard methods. [50]

2.2.2. Synthesis of nanomaterials

The colloidal nanofabrication platform from CICbiomaGUNE prepared the nanoparticles as follows. Milli-Q water (resistivity 18.2 MΩ x cm^{-1} at 25 °C) was used in all experiments.

- Synthesis of gold nanorods (AuNRs): AuNRs were prepared using Ag-assisted seeded growth.[51, 52] Seeds were prepared by fast reduction of 0.25 mM $HAuCl_4$ (5 mL) with freshly prepared 10 mM $NaBH_4$ (0.3 mL) in aqueous 100 mM CTAB solution. After 30 minutes, 24 µL of seed solution were added to 10 mL of growth solution containing 100mM CTAB, 0.5 mM $HAuCl_4$, 0.8 mM ascorbic acid, 0.12 mM $AgNO_3$, and 19 mM HCl. The mixture was left undisturbed at 30°C for 2 hours. The solution was centrifuged twice (8000 rpm, 30 min) to remove excess $AgNO_3$, AA and HCl, and redispersed in 15mM CTAB.

- Synthesis of silica nanoparticles (SiO_2NP): SiO_2NP were synthesized by Stöber method.[53, 54] 4.5 mL of TEOS were added to 100 mL of a mixture of ethanol, 10 M water and ammonium hydroxide (1 M in NH_3) under vigorous stirring. The mixture was stirred for 12 hours at room temperature. The SiO_2NP were washed three times with ethanol by centrifugation at 5000 rpm.

The fabricated nanoparticles were then characterized by transmission electron microscopy (TEM) with a JEOL JEM-1400PLUS transmission electron microscope operating at an acceleration voltage of 120 kV (Figure 1).

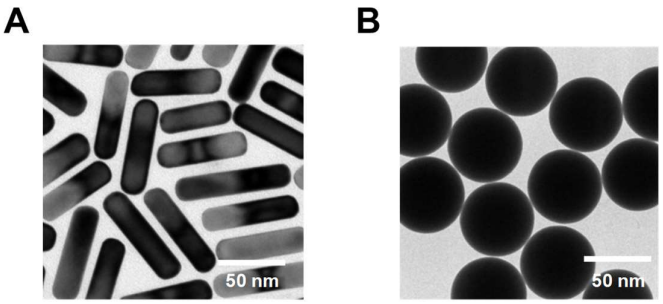

Figure 1. TEM imaging of AuNR (A) and SiO_2NP (B).

2.2.3. Preparation of heterofunctional cobalt and thiol activated agarose

100 mg of epoxy agarose microbeads (6BCL) were partially modified with 500 mM IDA (pH 11.0) for 3 hours and then filtered and washed with excess of water. Epoxy-carboxyl was mixed with 10 mM Na_2S dissolved in 100 mM $NaHCO_3$ solution (pH 10) for 1 hour. Later on, the thiolated support was filtered and washed. Such support (carboxyl-thiol) was incubated with a solution of 10 mM DTNB dissolved in 50 mM KH_2PO_4 (pH 8) for 2 hours. The resulting support was finally activated with cobalt by mixing with 30 mg x mL^{-1} of $CoCl_2$ in H_20 during at least 1 hour (Figure 2). All the steps during the functionalization of the support were carried out under mild stirring. The washing steps were performed at least 10 times with 20 volumes of water to make sure that soluble chemicals were fully removed.

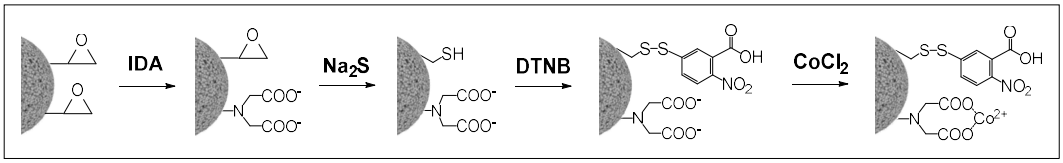

Figure 2. Protocol for the activation of heterofunctional cobalt and thiol activated agarose.

2.2.4. Preparation of AG-Oct (agarose activated with cyclooctyne groups)

0.3 grams of dry cyanogen bromide-activated sepharose (4BCL) were mixed with 10 mL of 1 mM HCl and incubated for 30 minutes at 25 ºC. The activated resin was filtered and incubated with 3 mL of 1 mM dibenzocyclooctyne-amine in water. As negative control, the activated resin was incubated with 50 mM of β-mercaptoethanol to decorate the agarose surface with inert hydroxyl groups (Figure 3).

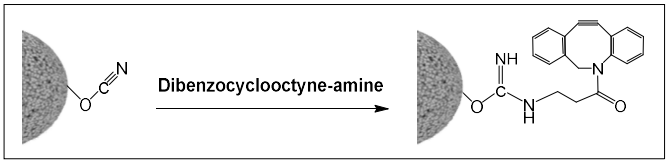

Figure 3. Protocol for the activation of agarose microbeads with cyclooctyne groups.

2.2.5. *In vitro* cell-free protein synthesis and immobilization (CFPS-i)

CFPS system was composed of 40% of S30 Premix Plus and 30% of T7/S30 cell extracts. In case of click reactions, we mixed 40% of S30 Premix without amino acids, 10% of amino acid mixture minus methionine, 10% of amino acid (methionine or L-

AHA) and 30% of T7/S30 cell extracts. 1 µg of DNA template and 1 mg of carriers were added to the cell lysate-based expression system at final volume of 50 µL, unless otherwise specified. The reactions were performed at 37 ºC and 1200 rpm for 12 hours in an Eppendorf Thermomixer R, unless otherwise specified. 1 mM CTAB was added to CFPS-i reactions with methacrylate microbeads activated with epoxy groups (Pu-E) and AuNR to avoid unspecific hydrophobic interactions and particle aggregation, respectively. Once the CFPS-i was finished, protein-based biomaterials can be easily purified from the reaction mixture by rapid and low-cost vaccum filtration using mini Bio-spin chromatography columns. In case of CFPS-i of Lys-sGFP by drop-casting, the reactions were incubated at 37 ºC without shaking inside a humidity chamber to avoid the evaporation of the reaction mix.

2.2.6. *In vitro* cell-free protein synthesis using 'lab-made' cell extracts

In collaboration with the group of Prof. Mansy, 'lab-made' cell extracts were prepared following the previously reported protocol by Sun *et al.*[55] The reaction mix contained 45% of cell extracts, 12 mM maltose, 5 mM magnesium glutamate, 2% PEG8000, 0.15 mM FAD^+, 1.5 mM amino acids mixture, 9.6% energy solution (700 mM HEPES pH 8, 21 mM ATP, 21 mM GTP, 12.6 mM CTP, 12.6 mM UTP, 2.8 mg x ml^{-1} tRNAs, 3.64 mM CoA, 4.62 mM NAD^+, 10.5 mM cAMP, 0.95 mM folinic acid, 14 mM spermidine, 420 mM 3-PGA), 5 nM *adh*_pET28b and 5 nM *nox*_pET22a at final reaction volume of 10.5 µL. The CFPS reactions were performed at 30 ºC for 17 hours in a PCR thermocycler.

2.2.7. On line monitoring the enzyme cascade after the CFPS using 'lab-made' cell extracts

Once the CFPS reaction was accomplished, 5 µg x mL^{-1} HRP, 1 mM NAD^+, 1 mM ethanol and 0.4 mM Ampliflu Red were added to the previous CFPS reaction mixture until reaching a final volume of 12 µL. The samples were incubated at 30 ºC in a Rotor-Gene Q (Qiagen) for 2 hours. The fluorescence (λ_{exc}: 571 nm and λ_{em}: 585 nm) was monitored every 30 seconds for 2 hours.

2.2.8. Fluorescence microscopy imaging

After CFPS-i was performed, 10 µL of the reaction mixture were placed inside a channel of a 6-channel µ-slide. The sGFP fluorescence was detected by using a Colibri LED illumination system incorporated into the fluorescence microscope (Axio Observer ZEISS). The sGFP fluorescence was observed using λ_{exc}: 470 nm and λ_{em}: 500-557 nm. In order to better visualize the nanoparticles, the confocal microscope LSM510

was used for AuNRs and SiO_2NPs with an excitation laser at 488 nm and the emission filter LP505. Images were analysed and processed with the software ZEN2012.

2.2.9. *In vivo* expression of sGFP

Briefly, 1 mL of an overnight culture of *E. coli* BL21-Gold cells transformed with the plasmid was inoculated in 50 mL of LB medium containing kanamycin (30 μg x mL^{-1}). Such culture was incubated at 37 °C and 200 rpm until the OD_{600nm} reached 0.6. At that point, the culture was induced with 1 mM IPTG. Cells were grown at 37 °C for 3 hours and then harvested by centrifugation at 10000 g during 30 minutes at 4 ºC. After sonication and centrifugation to discard cell debris, the His-sGFP concentration in the resulting protein solution was determined by measuring fluorescence in a Varioskan™ Flash Multimode Reader (Thermo Scientific) using 384-well plates.

2.2.10. Rhodamine-labeling of proteins

Inmunoglobulin G chemically conjugated with alkaline phosphatase (AP-IgG) was labeled with rhodamine B isothiocyanate following a modified protocol previously described elsewhere.[56] The protein solution in 100 mM sodium bicarbonate buffer at pH 8 was mixed (1:1 molar ratio) with a rhodamine B isothiocyanate solution in DMSO (1 mg x mL^{-1}) and incubated 1 hour with gentle agitation at 25 ºC in darkness. This step allows the acylation reaction between the primary amines from proteins and the isothiocyanates groups from rhodamine B to form a thiourea. Later, the unreacted rhodamine B was eliminated by filtering the mix solution trough a tangential ultrafiltration unit (10 kDa) using 25 mM sodium phosphate buffer at pH 7 until the flow-through solution was colourless.

2.2.11. Alkaline phosphatase activity assay

The substrate pNPP was dissolved 10 mg x mL^{-1} in 50 mM Tris-HCl buffer (pH 8.5). The reaction mixture containing 0.5 mM $MgCl_2$ and 1 mg x mL^{-1} of pNPP was added to 10 μL of a solution (90.6 μM) or suspension (0.2 mg of immobilizate) of IgG in a final volume of 100 μL. The reaction was incubated in darkness for 30 minutes at 37 ºC. Then, the absorbance of the product *p*-nitrophenol was monitored at 405 nm in a Varioskan™ Flash Multimode Reader using 96-well plates. For both soluble and immobilized enzyme the activity was measured under orbital shaking integrated into the reader.

2.2.12. ADH activity assay

200 µL of a reaction mixture containing 100 mM acetone and 0.25 mM NADH in 25 mM sodium phosphate buffer at pH 7.0 were incubated with 20 µL of suspension (0.2 mg of immobilizate) at 25 ºC. The activity of ADH was spectrophotometrically measured in a Varioskan™ Flash Multimode Reader using 96-well plates. The absorbance at 340 nm which decreased because of the enzymatic oxidation of NADH, was monitored along the time and under orbital shaking integrated into the reader.

3. RESULTS AND DISCUSSION

3.1. Development of a plasmid toolkit containing different polypeptide tags

A set of plasmids enconding sGFP fused to the N-terminal with different polypeptide tags was developed due to its great broad of applications.[57] In these genetic constructions, both the sGFP and the tag sequences can be easily exchanged by others just by enzymatic digestion (Figure 4A). Hence, the modular design of this genetic toolbox enables to easily fuse any target protein with any polypeptide tag. Specifically three plasmids expressing sGFP harboring at its N-terminal poly-(6x)His (His-sGFP), poly-(6x)Lys (Lys-sGFP) or poly-(6x)Cys (Cys-sGFP) peptides were designed to prove the modularity of this architecture. Additionally, we also genetically engineered a plasmid encoding untagged sGFP as control (Figure 4B).

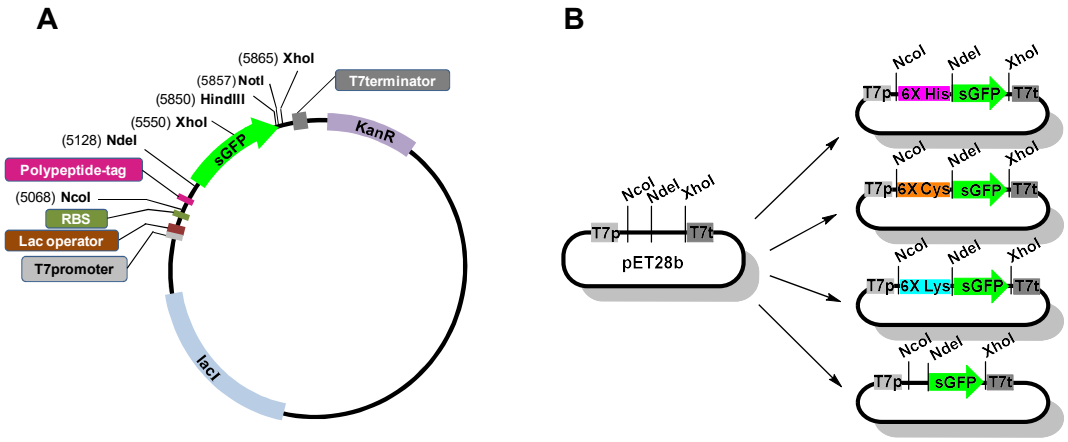

Figure 4. Genetic constructions. A) The pET28b plasmid map encoding *sgfp* gene. B) The plasmid tool-kit showing the restriction enzymes needed to modularly exchange the target protein and the tag.

After transformation in *E. Coli* strain BL21, all plasmids similarly expressed *in vivo* the sGFP tagged with the different tags (Figure 5). According to previous results, sGFP expression remained unaltered regardless the position (N- or C-terminal) of the tag.[58] Nevertheless, the *in vitro* expression of the untagged-sGFP using the commercially available T7/S30 cell extracts was significatly more efficient than the expression of the tagged variants which presented different expression levels among them (Figure 5). The *in vitro* expression of Lys-sGFP was lower than His-sGFP, and significantly much lower than Cys-sGFP. These data correlate with the amino acids content in the sGFP primary sequence; 20 lysines, 11 Histidines and 2 cysteines, which suggests that either the amino acid or tRNAs pools may be the limiting factor to achieve high protein yields of the tagged sGFP variants.

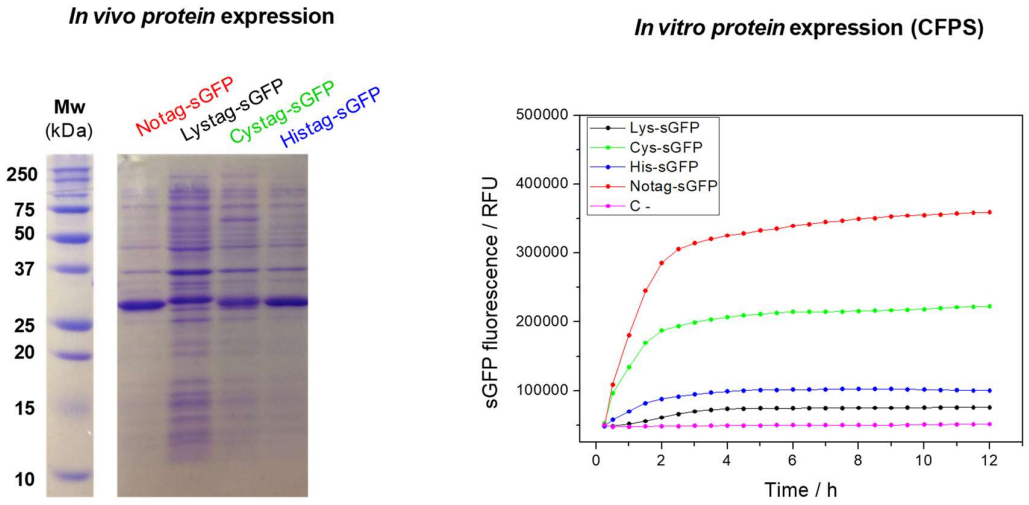

Figure 5. Expression levels of tagged sGFP variants. On the left, SDS-PAGE of soluble fractions after cell disruption by sonication. First line correspond to molecular weight markers (BioRad Precision Plus Protein All Blue Standard). On the rigth, the sGFP fluorescence was monitored on-line for 12 hours by StepOne™ Real-Time PCR System (Thermo Scientific) using λ_{ex}: 494 nm and λ_{em}: 518 nm. The empty plasmid pET28b was used as negative control.

In order to improve the portability and robustness of this system, the commercial preparation of cell extracts was freeze-dried according to recent studies.[59, 60] We pleasantly achieved the same protein synthesis yield after 12-hour reactions using either freeze-dried or no freeze-dried cell extracts. Although the synthesis rate was 2.63 times slower using the freeze-dried cell extracts rather than the no freeze-dried solution (Figure 6). Therefore, this strategy would be a portable device due to the endurance at high dehydration-rehydration conditions, although the freeze-drying should be optimized.

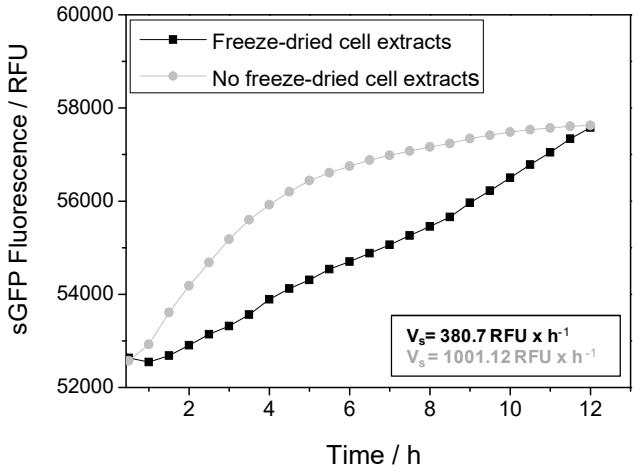

Figure 6. Comparing CFPS kinetics by using freeze-dried and no freeze-dried cell extracts. The freeze-dried T7/S30 cell extracts and S30 premix plus were rehydrated with the plasmid solution in a final reaction volume of 25 µL. These cell extracts were stored at -20ºC but no longer than a week before their reconstitution. sGFP fluorescence was on-line monitored by RT-PCR for 12 hours. Data below (V_s) show the initial rates of His-sGFP synthesis in the range of 0.5 to 4 hours.

3.2. Optimization of one-pot CFPS-i by using His-sGFP and AG-Co

To demostrate that protein synthesis and immobilization can occur orthogonally and simultaneously, we synthesized His-sGFP using T7/S30 cell extracts in presence of porous agarose particles activated with cobalt-chelates (AG-Co). Expectedly, protein synthesis was not observed when empty pET28b was used as negative control (Figure 7). Conversely, when the CFPS system was incubated with the plasmid encoding the *untagged-sgfp* gene and the microbeads, the fluorescence appeared but remained in the reaction bulk without selectively colonizing the microbeads (Figure 6).

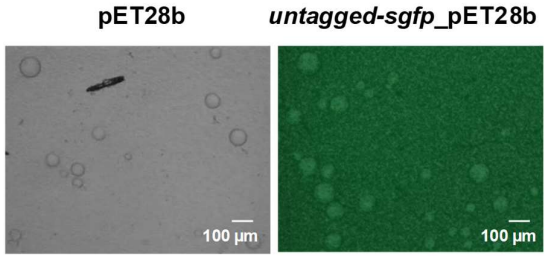

Figure 7. Control reactions of CFPS-i. Fluorescence microscopy images show the overlay of brightfield and sGFP signals after 12 hours of CFPS.

Finally, only when the plasmid *his-sgfp*_pET28b and AG-Co were incubated with the cell-free extracts, we observed the selective confinement of the fluorescence in the microbead surface (Figure 8A). These experimental results evidence the *in vitro* synthesis and concurrent selective immobilization of the protein but only when the protein tag/microbead pair is properly selected. To better understand the dynamics of this two-step/one-pot process, we performed the synthesis and immobilization of His-sGFP immobilized on AG-Co by measuring sGFP fluorescence along the time (Figure 8B). The on-line monitoring of the process reveals that *sgfp* gene under the control of T7 promoter is transcribed and translated producing a His-tagged nascent protein that is subsequently immobilized on the AG-Co. As we can see from the time-course images, fluorescence is barely accumulated in the bulk during the entire process (Figure 8B). This fact suggests that the immobilization rate is higher than the synthesis rate, converting the latter into the rate-limiting step. Despite CFPS reactions in solution normally reach the maximum protein yields in 2-4 hours,[61, 62] the accumulation of the nascent proteins inside the porous microbeads continued for more than 12 hours and never reached a plateau. Furthermore, the larger microbeads were more efficient in recruiting the nascent proteins due to their higher surface (Figure 8B).

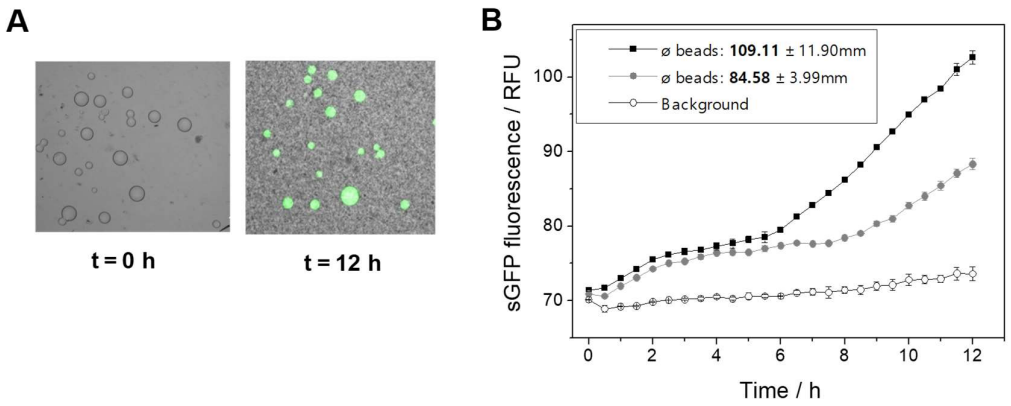

Figure 8. On-line monitoring CFPS-i kinetics by fluorescence microscopy. A) Fluorescence microscopy images overlaying brightfield and sGFP signals before (left) and after (right) the CFPS-i reaction was completed. B) sGFP fluorescence inside the microbeads and in the background (the reaction medium outside the microbeads) as a function of time. Microbeads were grouped according to their size. The fluorescence value at each time point corresponds to the average fluorescence of 3 microbeads. Reactions were carried out in the fluorescence microscope without shaking.

Once the CFPS-i system was demonstrated to be functional, we reused the cell extracts by separating the loaded microbeads and incubating the cell extracts with fresh and empty microbeads, substrates and reagents. Unfortunately, the protein

synthesis yield diminished 96.0% after the second reuse (Figure 9). We hypothesized that some fundamental elements for protein synthesis remained bound to the microbeads.

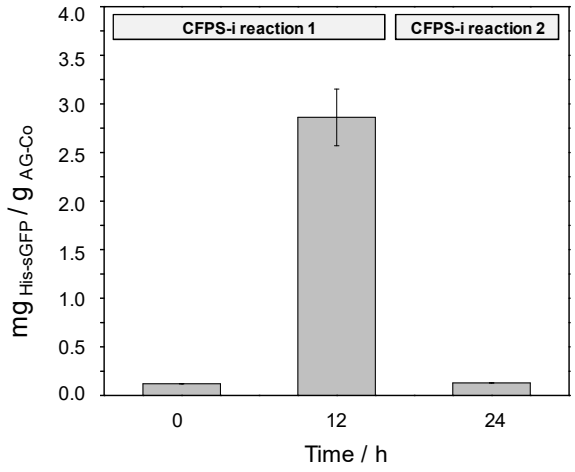

Figure 9. Reuse of CFPS machinery. CFPS-i of His-sGFP on AG-Co was quantified with a calibration curve (y = 1252.5x + 74.8; R^2 = 0.99) obtained from AG-Co with different loads of *in vivo* expressed His-sGFP. The data show the average of 5 microbeads. The final reaction volume was 25 µL.

3.3. Polypeptide tags as linkers to drive protein immobilization on a plethora of materials

First of all, the high selectivity of one-pot CFPS-i strategy was tested in simultaneous presence of two different materials (agarose and methacrylate) with different surface functionalizations. For this purpose, *cys-sgfp*_pET28b was incubated with CFPS system and two materials, AG-Co and methacrylate microbeads activated with epoxy groups (Pu-E). The nascent Cys-sGFP was exclusively immobilized on Pu-E (Figure 10), as result of the specific interaction between the thiol groups of the Cys-tag and the epoxy groups of the carrier.

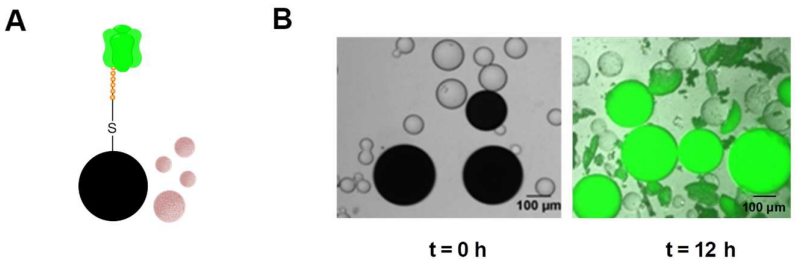

Figure 10. CFPS-i of Cys-sGFP in presence of AG-Co and Pu-E. A) Scheme of the selective binding between the Cys-GFP and Pu-E (black) in presence of AG-Co (pink). B) Fluorescence microscopy images overlaying brightfield and sGFP signals before and after the CFPS-i reaction was accomplished.

Expanding the scope of the CFPS-i methodology, the synthesis of Cys-sGFP and Lys-sGFP was coupled to their selective immobilization on gold nanorods (AuNRs) and silica nanoparticles (SiO_2NPs), respectively (Figure 11). Cys-sGFP was efficiently immobilized on AuNRs due to the formation of thiol-gold covalent bonds (Figure 11A). This binding chemistry has been extensively exploited in the biofunctionalization of gold-based nanomaterials.[21] Likewise, Lys-sGFP was selectively and stably absorbed on SiO_2NPs through the ionic interaction between the positive charges of the ε-NH_2 group of the poly-(6x)Lys and the negatively charged surface of these nanoparticles (Figure 11B), accordingly to the results obtained with other basic domains and tags fused to the protein of interest.[63]

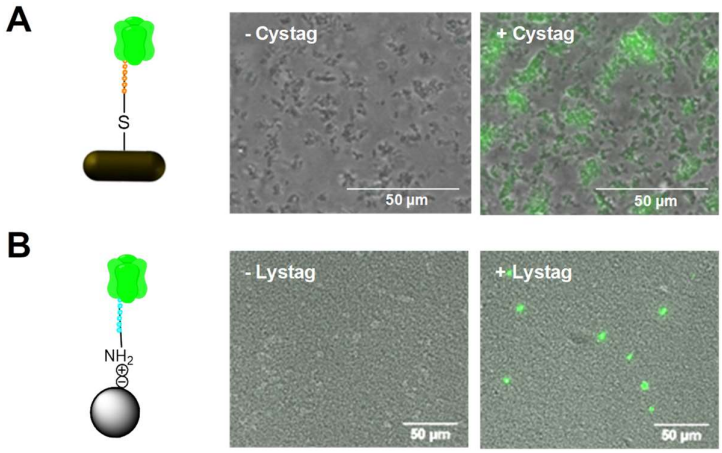

Figure 11. CFPS-i of sGFP onto on-demand materials by selective polypeptide-tags. A) Cys-sGFP. B) Lys-sGFP. From left to right, scheme of the selective binding between the polypeptide-tagged sGFP and the nanoparticle; fluorescence microscopy images overlaying brightfield and sGFP signals for the control reaction with untagged sGFP (- Cystag / - Lystag) and for the reaction with polypeptide-tagged sGFP (+ Cystag / + Lystag). All microscopy images were taken after a washing step with 10 mM sodium phosphate buffer at pH7.0.

In both cases, the untagged sGFP was synthesized but not immobilized on nanoparticles (Figure 11). The interaction between the Lys-tag and the silica surface was proven to be very selective, since the untagged-sGFP was not bound to the SiO_2NPs. However, minor unspecific interactions were observed between proteins from the CFPS machinery and the SiO_2NPs (Figure 12).

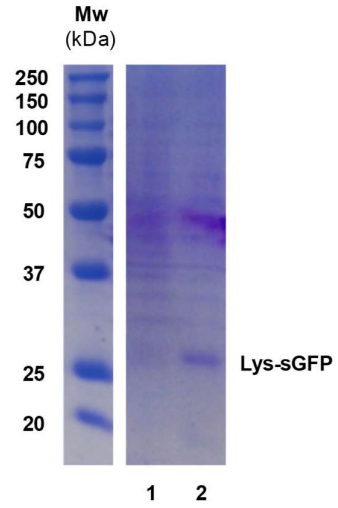

Figure 12. SDS-PAGE of CFPS-i of Lys-sGFP on SiO_2NP. The molecular weight markers are BioRad Precision Plus Protein All Blue Standard. Line 1: immobilized proteins on SiO_2NP after CFPS-i reaction with the plasmid *untagged-sgfp*_pET28b. Line 2: immobilized proteins on SiO_2NP after CFPS-i reaction with the plasmid *lys-sgfp*_pET28b.

In addition, the pool of free amino acids contained in the S30 premix plus was not competing with the polypeptide-tagged sGFP for the reactive groups of the carrier. This fact was demonstrated by incubation of *in vivo* expressed sGFP (cell debris without purification step) with the corresponding materials and a solution of the free amino acid. After 12 hours of incubation, similar protein immobilization yields were achieved in presence/absence of free amino acids in the reaction bulk. Likewise, the protein immobilization kinetics followed a similar trend in both cases (Figure 13).

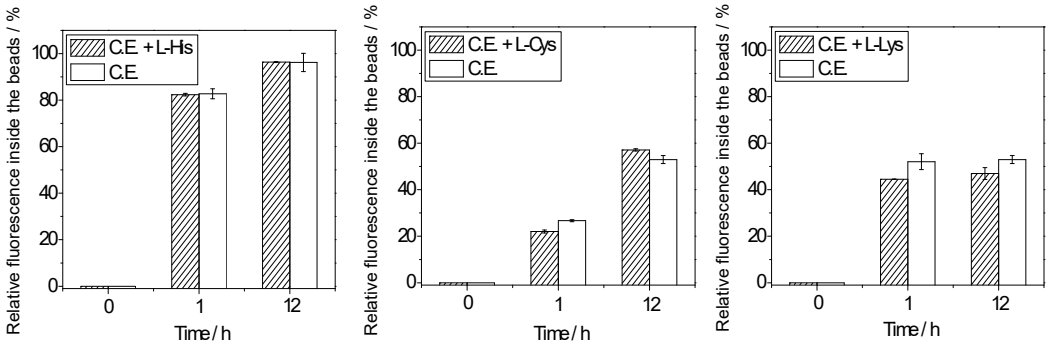

Figure 13. Comparing immobilization yields of *in vivo* expressed tagged sGFP adding or not external free amino acids. 1 mL (0.02 mg x mL^{-1}) of cell extracts from *in vivo* expression of tagged sGFP was incubated with the appropriate carrier and the same concentration of the free amino acid (0.3 mM) that CFPS-i reactions included. sGFP fluorescence of 200 µL from the bulk was measured in a 96-well plate using a Varioskan™ Flash Multimode Reader. From left to right, striped bars correspond to cell extracts (C.E.) with His-sGFP incubated with AG-Co and free L-Histidine, Cys-sGFP incubated with Pu-E and free L-Cysteine and Lys-sGFP incubated with SiO_2NPs and free L-Lysine. White bars represent the relative fluorescence of control reactions without adding free amino acids.

CFPS-i reaction was also carried out by drop-casting the corresponding plasmid to express Lys-sGFP and the cell-free protein synthesis machinery on the top of glass slides. The reaction mixture was incubated for 12 hours. Herein, the protein synthesis was successfully accomplished since fluorescence was detected in drops containing either tagged or untagged proteins after the reaction time (Figure 14). After the washing step, the drops containing the plasmid encoding Lys-sGFP displayed fluorescence spots on the glass, while no fluorescence was detected in those drops that *in vitro* expressed the untagged protein, since it was removed from the surface during the washing step (Figure 14). These experimental data corroborate that the Lys-tag drives the protein immobilization on silica-based materials and expand its utilization to other solid architectures. In spite of the low robustness which can be expected from an ionic interaction, the immobilization of oriented proteins using CFPS-i by drop-casting has been demonstrated even after washing the biomaterial. Furthermore, this technology skips the chemical functionalization steps of glass slides required for the conventional proceedings to prepare protein-based microarrays.[64]

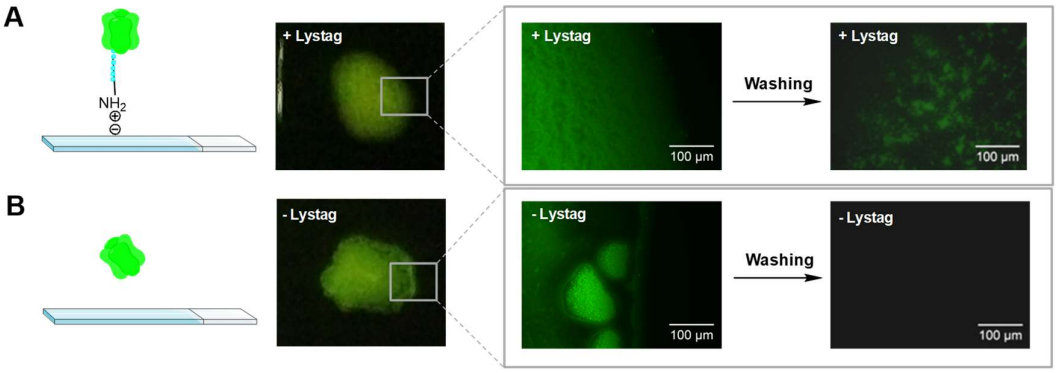

Figure 14. CFPS-i of Lys-sGFP onto glass slides. CFPS of A) Lys-sGFP and B) untagged sGFP. From left to right, scheme of the selective binding; macroscopic view of the drop-casting after a 12-hour CFPS-i reaction by using an UV transilluminator (λ_{ex}: 470 nm); fluorescence microscopy images overlaying brightfield and sGFP signals after CFPS-i reaction but before a washing step; and after both CFPS-i reaction and a washing step with milli-Q water.

3.4. Polypeptide tags to selectively co-immobilize proteins on the same carrier by using CFPS-i

The co-immobilization of different enzymes on the same carrier is a common strategy to assemble complex biological machineries like multi-enzyme systems.[65-68] In order to gain selectivity during the co-immobilization protocol, the toolbox of polypeptide-tags herein developed was applied to simultaneously synthesize two different proteins and selectively co-immobilize them on the same carrier through two different immobilization chemistries. As a proof of concept, Cys-sGFP and an alcohol dehydrogenase from *Bacillus stearothermophilus* tagged with 6 histidines at its N-terminal (Bs-ADH) were synthesized *in vitro*. In order to evaluate the orthogonality of the toolbox for CFPS-i, a new agarose-based heterofunctional carrier activated with both cobalt-chelates and disulfide groups (AG-Co/S) was prepared (Figure 2). This new surface theoretically allows the co-immobilization of Cys- and His-tagged proteins simultaneously through two different immobilization chemistries based on reversible covalent disulfide and reversible metal coordination bonds, respectively (Figure 15A). This concept was proved by incubating the heterofunctional carrier with the corresponding DNA plasmids and the cell-free extracts for the one-pot co-expression and co-immobilization of His-Bs-ADH and Cys-sGFP. As a control reaction, we also expressed only Cys-sGFP in presence of the heterofunctional carrier. To demonstrate the co-expression and co-immobilization of these two proteins, the fluorescence of Cys-sGFP was visualized (Figure 15B) and quantified (Figure 15B) by fluorescence microscopy.

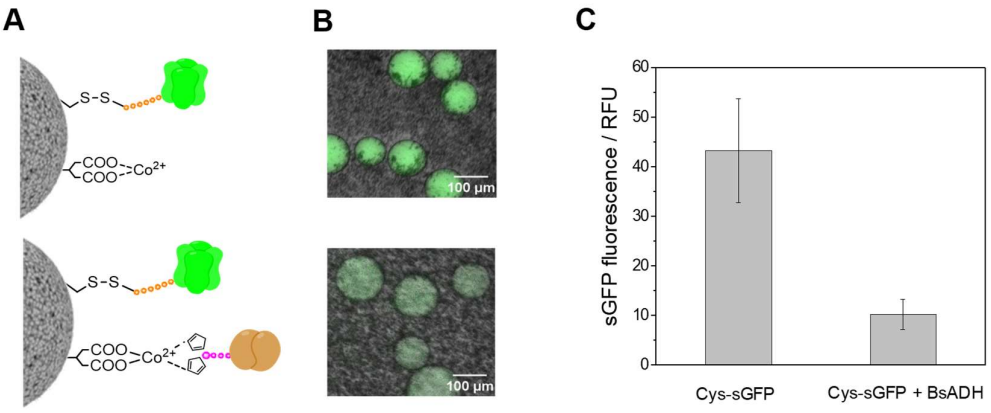

Figure 15. Co-expression and co-immobilization of two different proteins by two different chemistries. A) Scheme of the immobilization of Cys-sGFP (up) and the co-immobilization of Cys-sGFP and Bs-ADH (down) on AG-Co/S. B) Microsocopy images overlaying brightfield and sGFP signals after the CFPS-i reaction. C) sGFP fluorescence mean values correspond to the average of 5 microbeads after the CFPS-i reactions were completed (12 hours).

These experiments showed that Cys-sGFP and Bs-ADH are co-expressed and co-immobilized on the same microbeads. However when we performed the CFPS-i using only the plasmid for the expression of Cys-sGFP, the fluorescence intensity per microbead was 4.22 times higher than when using the two different plasmids (Figure 15C). This dissimilarity points out a possible competition between the two transcribed mRNA for the ribosomal machinery that may diminish the specific final yields for both Cys-sGFP and Bs-ADH. Karim and Jewett observed a similar decreasing effect on the protein expression levels when they tried the cell-free co-expression of several enzymes.[39] According to Park *et al.*, mRNA species must compete for a finite pool of ribosomes and aminoacyl-tRNAs when CFPS reaction mixtures are primed with several DNA templates, leading to an unequal expression level of different proteins. Indeed, sGFP fluorescence was reported to be inversely proportional to translation rates of the co-expressed genes.[69] Besides the fluorescence of the immobilized Cys-sGFP reveals its proper folding and structurally innocuous immobilization, *in vitro* synthesized and immobilized Bs-ADH was catalytically active after CFPS-i (Figure 16).

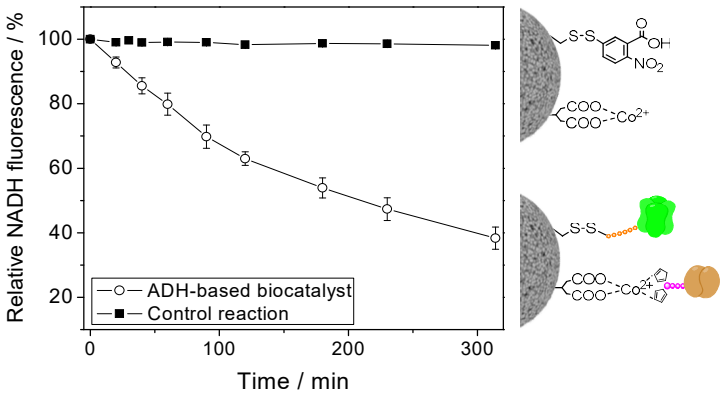

Figure 16. ADH activity assay. ADH activity of the biocatalyst containing co-immobilized His-Bs-ADH and Cys-sGFP (white circles) and the control reaction without proteins (black squares) was tested.

The multimeric nature of Bs-ADH was not a hurdle for its successful expression and *in situ* immobilization by using the CFPS-i system, validating the feasibility of this technology for quick and easy preliminary tests of enzyme co-immobilization. These results also guide the design of more complex biological micro-architectures for engineering artificial metabolic cells.

Additionally, the orthogonality and selectivity of these two immobilization chemistries was demonstrated by selective elution of Bs-ADH in presence of EDTA, while the Cys-sGFP remained attached to the surface. Alike, Cys-sGFP was eluted to the solution by using thiolated compounds (Figure 17). Hence, such orthogonality allow the modular assembly of multi-enzyme systems where one enzyme can be easily replaced by other (or by the same enzyme) when the first enzyme becomes inactive.

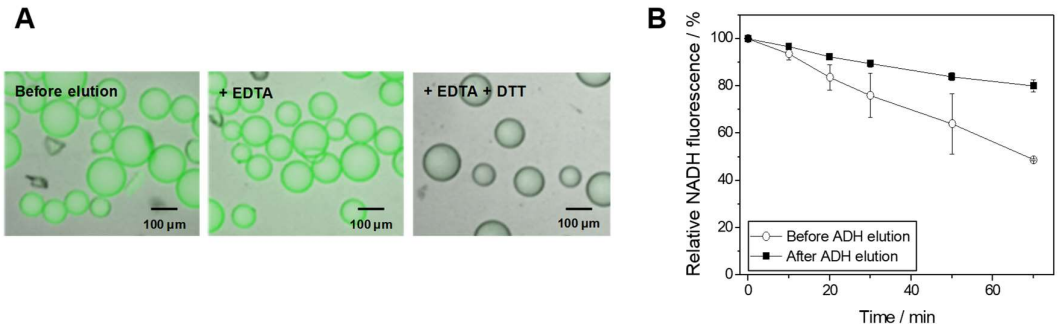

Figure 17. Selective elution of Cys-sGFP and Bs-ADH from the heterofunctional agarose. A) Overlay of brightfield and sGFP signals imaging. From left to right, images before the elution, after the elution with EDTA and after the elution with EDTA and DTT. B) ADH activity of the biocatalyst before (white circles) and after (black squares) EDTA and DTT elution.

3.5. CFPS for prototyping of enzyme cascades

Encouraged by the previous protein co-expression results, the co-expression of two enzymes was tested by CFPS in the same tube. For this purpose, the cell-free extracts were prepared in the laboratory[55] in collaboration with the group of Prof. Mansy instead of using cell extracts from a commercial source. The preparation of 'lab-made' cell extracts decreases the costs of using CFPS, becoming more feasible the implementation of CFPS as a regular tool for high-throughput screenings of enzymes at prototyping scale.

Two plasmids encoding genes to produce NADH oxidase from *Thermus thermophilus* (Tt-NOX)[67] and Bs-ADH were incubated with the CFPS system to simultaneously express the two enzymes (Figure 18A). The tetrameric (Bs-ADH) and the dimeric (Tt-NOX) enzymes perform a redox cascade reaction that may be monitored by exogenously adding a third enzyme, horseradish peroxidase (HRP) from a commercial source. HRP transforms the fluorogenic substrate Ampliflu Red into the product Resorufin which is easily monitored by its fluorescence (Figure 18B).

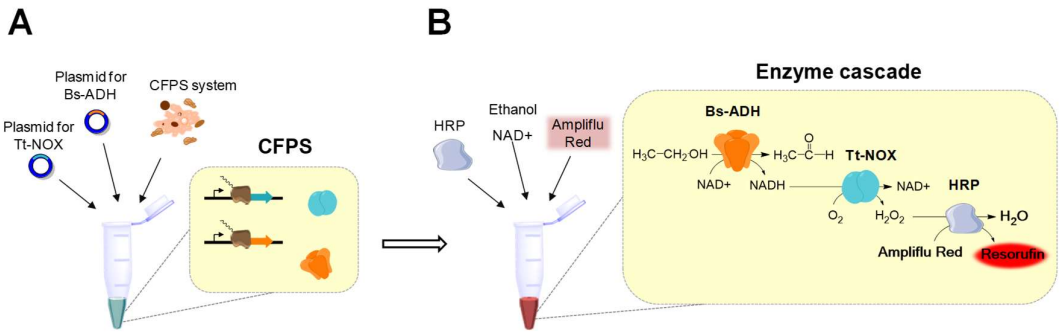

Figure 18. Co-expression of an enzyme cascade by CFPS. A) Two plasmids were incubated overnight with the CFPS system at 30ºC. B) After CFPS, the enzyme cascade was completed by adding substrates and HRP to monitor the final fluorescent product, resorufin.

The production of resorufin was monitored during two hours by using a Rotor-Gene Q (Figure 19). The results show an increase on fluorescence only when all components of the enzyme cascade were present in the reaction tube.

In spite of further analysis are needed to develop a robust prototyping platform using CFPS, this preliminary study reveals the promising potential of this synthetic biological tool for quick-and-easy assays to test a whole enzyme cascade in one pot. Therefore, this study contributes to the recently emerging applications of CFPS for biocatalysts development.[70]

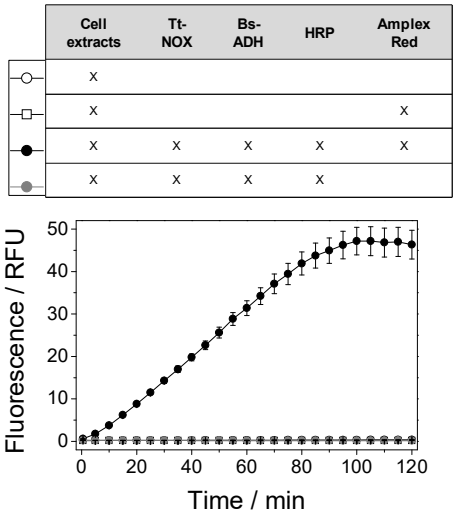

Figure 19. Monitoring the Resorufin production by the *in vitro* synthesized enzyme cascade. The table shows the conditions of each reaction mixture.

3.6. Incorporation of non-natural amino acids through CFPS to enable oriented protein immobilization mediated by copper-free click chemistry

In order to go beyond the chemistry offered by the nature, CFPS reactions have been already used for incorporating non-natural amino acids into target proteins.[43, 44] In many cases this non-natural amino acids are used as hubs to conjugate the target protein with other molecules or with solid materials. In this context, amino acids containing azides are extensively used to lead the immobilization of *in vivo* expressed proteins on surfaces activated with alkyne groups through click chemistry.[71] However, most of click chemistry schemes rely on copper(I)-catalyzed reactions, and the copper might negatively affect the *in vitro* protein synthesis. In this work, we have overcome the potential toxicity of the copper by expanding CFPS-i to copper-free click chemistry reactions. Here, we have incorporated non-natural amino acids harboring azide groups into the nascent proteins to drive their immobilization on materials functionalized with cyclooctyne groups. To this aim, we firstly activated agarose microbeads with cyclooctyne groups (AG-Oct) through a new surface chemistry protocol starting from commercially available agarose microbeads activated with cyanogen bromide (Figure 2). Figure 18 shows that protein synthesis fails when neither methionine nor L-AHA (L-azidohomoalanine) is included in the amino acid mixture. As expected, fluorescence can be detected neither in the bulk nor inside the microbeads. Furthermore, when the protein is synthesized with methionine, the protein is produced but the immobilization

on AG-Oct does not occur, remaining the nascent protein in the reaction bulk. Similarly, when the protein is synthesized with L-AHA but incubated with agarose microbeads activated with hydroxyl groups instead of AG-Oct, sGFP fluorescence is only detected in the reaction bulk.

These experimental data demonstrate that the synthesis and bio-orthogonal copper-free click immobilization of sGFP is only possible when azide side chains are displayed in the protein surface and the agarose surface is activated with cyclooctyne groups (Figure 20). The incorporation of non-natural amino acids for protein-based biomaterials manufacturing has been already described.[6, 72, 73] However, the protein synthesis have been here coupled with a cyclooctyne/azide click immobilization in one-pot concurrent process, unlike two-pot conventional methods where firstly azide- or alkyne-amino acids are incorporated either *in vivo* or *in vitro* into the protein. Then, the modified protein is purified and incubated with solid particles functionalized either with alkyne or azide groups.[43, 74]

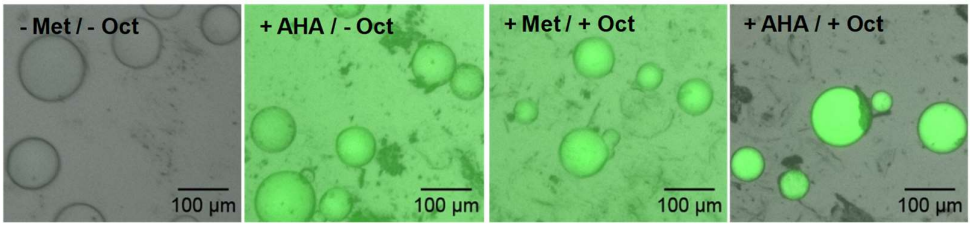

Figure 20. CFPS-i of sGFP incorporating AHA by copper-free click chemistry. Fluorescence microscopy imaging overlaying brightfield and sGFP signals after the CFPS-i was completed. The images show the reaction in presence of each amino acid: Met (methionine) or AHA (L-azidohomoalanine) and the agarose microbeads activated or not with cyclooctyne (Oct) groups.

According to the sGFP X-ray structure (PDB: 2B3P), L-AHA might be introduced at position 1, 76, 86 and 216 of the protein primary sequence. Positions 1, 76 and 86 cluster at the bottom part of the β-barrel where N- and C-terminal are located, while position 216 is located at the hollow of the barrel facing the chromophore (Figure 21). Due to that distribution of residues, the resulting protein can adopt different molecular orientations during the immobilization process. Likely, the protein is mainly oriented through the bottom part since the amino acid in position 1 is more exposed to the solvent. Subsequently, this strategy can be a potential tool for further protein orientation screenings.

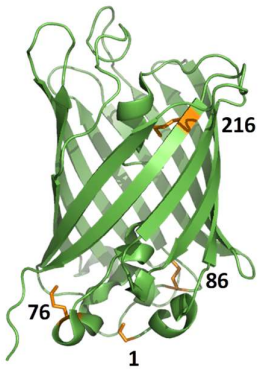

Figure 21. X-ray structure of sGFP. Met are represented in orange.

For a more precise site-selective immobilization, the CFPS-i developed here could be coupled to cell-free AMBER system by using specific tRNAs to insert non-natural amino acids in unique positions.[75] To sum up, cooper-free click immobilization based on cyclooctyne/azide pairs is compatible with the protein synthesis according to the broad bio-orthogonality of this chemistry.[76]

3.7. Antibody orientation and immobilization by two-pot CFPS-i

The demonstrated plasticity of the methodology presented in this chapter encorauged us to develop a novel strategy for oriented antibody immobilization. In order to conceive a wide-ranging device for oriented-immobilization of inmunoconjugates, Protein A was synthesized and immobilized by using CFPS-i. Materials functionalized with ProA mean a universal platform for binding to the Fc region of any immunoglobulin G (IgG).[77] A previously reported plasmid that encodes Protein A tagged with poly-(6x)His (His-ProA) at its N-terminal under the control of the T7 promoter was utilized.[49] In a first attempt, the plasmid, the cell-free extracts, AG-Co and an IgG chemically conjugated with both rhodamine and alkaline phosphatase (AP-IgG-Rh) were incubated in one test tube to perform the CFPS-i of His-ProA and the subsequent AP-IgG-Rh capture in one-pot. The fluorescence and the enzyme activity conjugated to the IgG enabled to trace the antibody capture reaction. Unfortunately, the antibody was not able to be bound to the microbeads functionalized with the nascent His-ProA under the protein synthesis and immobilization conditions (data not shown).

In the light of the previous unsatisfactory result, His-ProA was firstly expressed and immobilized on AG-Co in one pot (Figure 22A) and afterwards AP-IgG-Rh was incubated with that biomaterial in a second pot (Figure 22B). As a result, the

fluorescence of the AP-IgG-Rh was uniformly distributed on the AG-Co immobilizing His-ProA, pointing an optimal antibody density for antigen recognition as previously reported for the direct immobilization of IgG on porous agarose particles.[18, 78] Hence, we demonstrated that His-ProA can be synthesized and immobilized in one-pot retaining its capacity to selectively capture conjugated IgG, giving rise a two-step process for the site-directed immobilization of inmunoconjugates on solid carriers. These results suggest that the protein synthesis conditions inhibit the affinity interaction between the Fc region of the antibody and the His-ProA.

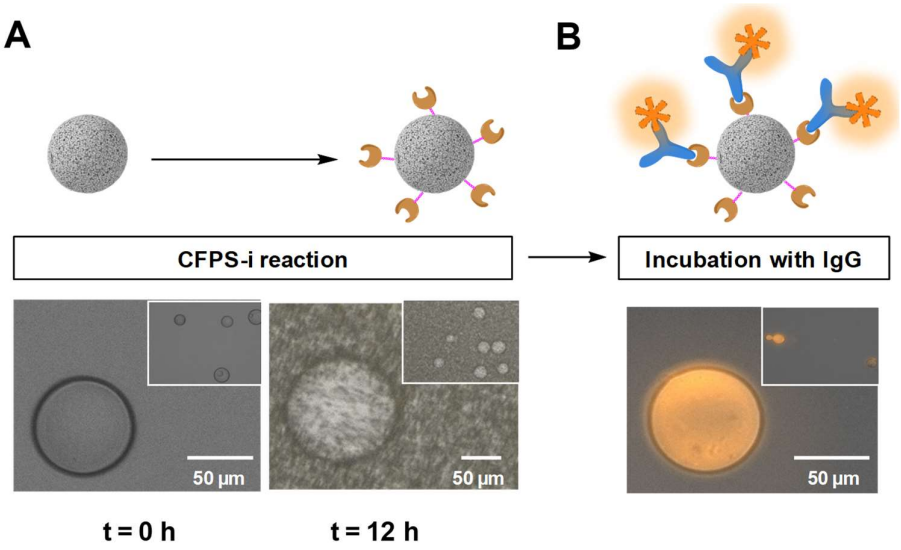

Figure 22. Two-pot fabrication of antibody-based biomaterials. A) CFPS-i of His-ProA (brown) on AG-Co (pink). B) Capturation of IgGs (blue) which are labeled with rhodamine (orange star) and by ProA immobilized on AG-Co. On the upper side, the schemes of protein immobilization. On the bottom side, the fluorescence microscopy images overlaying brigthfield and fluorescence (λ_{exc}: 530 nm, λ_{em}: 615-700 nm).

As control, when AP-IgG-Rh was incubated with AG-Co lacking the His-ProA, fluorescence was neither visualized inside the microbeads and enzyme activity was not detected neither after sample washing (Figure 23). However, the labeled antibody was not quantitatively captured by the microbeads immobilizing His-ProA; 43% of the offered antibody was captured (Figure 23).

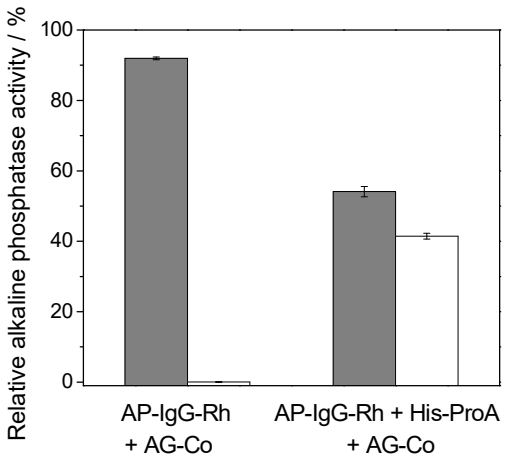

Figure 23. Alkaline phosphatase activity of control reactions for AP-IgG-Rh immobilization. AP-IgG-Rh was incubated with AG-Co and AG-Co containing His-ProA. Alkaline phosphatase activity was measured in the flow-through (grey bars) of the immobilization and in a suspension of microbeads (white bars) after the His-ProA immobilization.

Nevertheless, combining the last advances on CFPS of either antibody fragments[79, 80] or whole functional antibodies[81, 82] with the technique described here, the fabrication of antibody-based biomaterials could be successfully accomplished in one-pot. Ultimately, the optimization of CFPS-i of antibodies can contribute to develop innovative immunological screening platforms for manufacturing tailor-made biosensors, pull-down systems[83] and immunotherapy.[84]

4. CONCLUSION

Cell-free protein synthesis and immobilization has been successfully coordinated in one pot controlling the orientation and the immobilization chemistry of the nascent proteins. *In vitro* synthesis of different proteins has been performed orthogonally to a variety of solid materials as carriers and allowed screening a diversity of immobilization chemistries to selectively attach the nascent protein to the carrier (Table 2). Some of those protein-material pairs were designed and fabricated for first time.

Table 2. Description of protein-material pairs tested by using one-pot CFPS-i.

Tagged protein	Binding material	Binding interaction	Elution reagent
His-sGFP	AG-Co	Metal coordination bond	Imidazol
Bs-ADH	AG-Co/S	Metal coordination bond	Imidazol
His-ProA	AG-Co	Metal coordination bond	Imidazol
Cys-sGFP	Pu-E	Covalent	-
	Au-NRs	Covalent	-
	AG-Co/S	Thiol exchange	DTT
Lys-sGFP	SiO_2NPs	Ion exchange	Sodium chloride
	Glass slide	Ion exchange	Sodium chloride
sGFP containing AHA	AG-Oct	Copper-free click chemistry	-

Three main strategies were exploited for CFPS and orientation of selective protein immobilization: a toolkit of interchangeable polypeptide-tags; coupling the introduction of non-natural amino acids and click chemistry; and the synthesis of the IgG-binding His-ProA for site-directed immobilization of antibodies. The flexibility showed by those results supports this platform as a suitable prototyping technology for manufacturing protein-based materials. Taking advantage of its short processing time and versatility, this platform offers the opportunity to develop quick and easy assays for enzyme expression and immobilization screening onto a wide-ranging spectrum of materials. This system has already showed to be suitable for the production of multimeric enzymes and immobilized biological conjugates (IgG-ProA). Moreover, the co-expression and selective co-immobilization of a protein and an enzyme was for first time achieved by CFPS-i strategy, as far as we know. What is more, this technology is fully portable since it requires neither specialized equipment nor sophisticated infrastructures. However, the optimal synthesis of larger multimeric proteins and the *in situ* formation of biological complexes through specific protein-protein interactions will be some of the most important challenges this technology will must face in the near future.

REFERENCES

1. Benítez-Mateos, A. I., Llarena, I., Sánchez-Iglesias, A., López-Gallego, F. Expanding one-pot cell-free protein synthesis and immobilization for on-demand manufacturing of biomaterials. *ACS Synthetic Biology*. **2018**, *7*: 875-884.

2. Alexandrov, K., Johnston, W. A. Cell-free protein synthesis. Springer. **2013**.

3. Caschera, F., Noireaux, V. Synthesis of 2.3 mg/ml of protein with an all Escherichia coli cell-free transcription–translation system. *Biochimie*. **2014**, *99*: 162-168.

4. Katzen, F., Chang, G., Kudlicki, W. The past, present and future of cell-free protein synthesis. *Trends in Biotechnology*. **2005**, *23*: 150-156.

5. Rosenblum, G., Cooperman, B. S. Engine out of the chassis: cell-free protein synthesis and its uses. *FEBS Letters*. **2014**, *588*: 261-268.

6. Whittaker, J. W. Cell-free protein synthesis: the state of the art. *Biotechnology Letters*. **2013**, *35*: 143-152.

7. Anderson, M. J., Stark, J. C., Hodgman, C. E., Jewett, M. C. Energizing eukaryotic cell-free protein synthesis with glucose metabolism. *FEBS Letters*. **2015**, *589*: 1723-1727.

8. Caschera, F., Noireaux, V. A cost-effective polyphosphate-based metabolism fuels an all E. coli cell-free expression system. *Metabolic Engineering*. **2015**, *27*: 29-37.

9. Georgi, V. *et al.* On-chip automation of cell-free protein synthesis: new opportunities due to a novel reaction mode. *Lab on a Chip*. **2016**, *16*: 269-281.

10. Voloshin, A. M., Swartz, J. R. Efficient and scalable method for scaling up cell free protein synthesis in batch mode. *Biotechnology and Bioengineering*. **2005**, *91*: 516-521.

11. Chandrasekaran, A., Bharadwaj, R., Park, J. I., Sapra, R., Adams, P. D., Singh, A. K. A microscale platform for integrated cell-free expression and activity screening of cellulases. *Journal of Proteome Research*. **2010**, *9*: 5677-5683.

12. Chandrasekaran, A., Singh, A. K. One-pot, microscale cell-free enzyme expression and screening. In Cell-free protein synthesis: methods and protocols. Humana Press. **2014**, 55-69.

13. Jiang, L., Zhao, J., Lian, J., Xu, Z. Cell-free protein synthesis enabled rapid prototyping for metabolic engineering and synthetic biology. *Synthetic and Systems Biotechnology*. **2018**, *3*: 90-96.

14. Karim, A. S., Jewett, M. C. Cell-free synthetic biology for pathway prototyping. *Methods in enzymology*. **2018**, *608*: 31-57.

15. Kwon, Y. C., Song, J. K., Kim, D. M. Cloning-independent expression and screening of enzymes using cell-free protein synthesis systems. In Cell-free protein synthesis: methods and protocols. Humana Press. **2014**, 97-108.

16. Zárate, X., Galbraith, D. W. A cell-free expression platform for production of protein microarrays. In Cell-free protein synthesis: methods and protocols. Humana Press. **2014**, 297-307.

17. Bhide, M., Natarajan, S., Hresko, S., Aguilar, C., Bencurova, E. Rapid in vitro protein synthesis pipeline: a promising tool for cost-effective protein array design. *Molecular BioSystems*. **2014**, *10*: 1236-1245.

18. Batalla, P., Bolívar, J. M., Lopez-Gallego, F., Guisan, J. M. Oriented covalent immobilization of antibodies onto heterofunctional agarose supports: A highly efficient immuno-affinity chromatography platform. *Journal of Chromatography A*. **2012**, *1262*: 56-63.

19. Catherine, C. *et al.* Cell-Free expression and in situ immobilization of parasite proteins from clonorchis sinensis for rapid identification of antigenic candidates. *PLOS ONE*. **2015**, *10*: 1-9.

20. Hall Sedlak, R. *et al.* Engineered Escherichia coli silver-binding periplasmic protein that promotes silver tolerance. *Applied and Environmental Microbiology*. **2012**, *78*: 2289-2296.

21. Frasconi, M., Mazzei, F., Ferri, T. Protein immobilization at gold–thiol surfaces and potential for biosensing. *Analytical and Bioanalytical Chemistry*. **2010**, *398*: 1545-1564.

22. Lee, J. M., Park, H. K., Jung, Y., Kim, J. K., Jung, S. O., Chung, B. H. Direct immobilization of protein G variants with various numbers of cysteine residues on a gold surface. *Analytical Chemistry*. **2007**, *79*: 2680-2687.

23. Yang, M., Choi, B. G., Park, T. J., Heo, N. S., Hong, W. H., Lee, S. Y. Site-specific immobilization of gold binding polypeptide on gold nanoparticle-coated graphene sheet for biosensor application. *Nanoscale*. **2011**, *3*: 2950-2956.

24. Bodelón, G. *et al.* Imaging bacterial interspecies chemical interactions by surface-enhanced raman scattering. *ACS Nano*. **2017**, *11*: 4631-4640.

25. Schwaminger, S. P., Blank-Shim, S. A., Scheifele, I., Fraga-García, P., Berensmeier, S. Peptide binding to metal oxide nanoparticles. *Faraday Discussions*. **2017**, *204*: 233-250.

26. Cassimjee, K. E. *et al*. One-step enzyme extraction and immobilization for biocatalysis applications. *Biotechnology Journal*. **2011**, *6*: 463-469.

27. López-Gallego, F., Acebrón, I., Mancheño, J. M., Raja, S., Lillo, M. P., Guisán Seijas, J. M. Directed, strong, and reversible immobilization of proteins tagged with a β-trefoil lectin domain: a simple method to immobilize biomolecules on plain agarose matrixes. *Bioconjugate Chemistry*. **2012**, *23*: 565-573.

28. Yunker, P. J. *et al.* One-pot system for synthesis, assembly, and display of functional single-span membrane proteins on oil–water interfaces. *Proceedings of the National Academy of Sciences*. **2016**, *113*: 608-613.

29. Ramachandran, N. *et al.* Next-generation high-density self-assembling functional protein arrays. *Nature Methods*. **2008**, *5*: 535-538.

30. He, M., Taussig, M. J. Single step generation of protein arrays from DNA by cell-free expression and in situ immobilisation (PISA method). *Nucleic acids research*. **2001**, *29*: 1-6.

31. He, M., Stoevesandt, O., Taussig, M. J. In situ synthesis of protein arrays. *Current Opinion in Biotechnology*. **2008**, *19*: 4-9.

32. He, M., Liu, H., Turner, M., Taussig, M. J. Detection of protein–protein interactions by ribosome display and protein in situ immobilisation. *New Biotechnology*. **2009**, *26*: 277-281.

33. Chen, Z., Dodig-Crnković, T., Schwenk, J. M., Tao, S. C. Current applications of antibody microarrays. *Clinical Proteomics*. **2018**, *15*: 1-15.

34. Trilling, A. K., Beekwilder, J., Zuilhof, H. Antibody orientation on biosensor surfaces: a minireview. *Analyst*. **2013**, *138*: 1619-1627.

35. Lee, K. H., Kwon, Y. C., Yoo, S. J., Kim, D. M. Ribosomal synthesis and in situ isolation of peptide molecules in a cell-free translation system. *Protein Expression and Purification*. **2010**, *71*: 16-20.

36. Lee, K. H., Lee, K. Y., Byun, J. Y., Kim, B. G., Kim, D. M. On-bead expression of recombinant proteins in an agarose gel matrix coated on a glass slide. *Lab on a Chip*. **2012**, *12*: 1605-1610.

37. Byun, J.-Y., Lee, K.-H., Lee, K.-Y., Kim, M.-G., Kim, D.-M. In-gel expression and in situ immobilization of proteins for generation of three dimensional protein arrays in a hydrogel matrix. *Lab on a Chip*. **2013**, *13*: 886-891.

38. Karig, D. K., Bessling, S., Thielen, P., Zhang, S., Wolfe, J. Preservation of protein expression systems at elevated temperatures for portable therapeutic production. *Journal of the Royal Society, Interface*. **2017**, *14*: 1-8.

39. Karim, A. S., Jewett, M. C. A cell-free framework for rapid biosynthetic pathway prototyping and enzyme discovery. *Metabolic Engineering*. **2016**, *36*: 116-126.

40. Jewett, J. C., Bertozzi, C. R. Cu-free click cycloaddition reactions in chemical biology. *Chemical Society Reviews*. **2010**, *39*: 1272-1279.

41. Lallana, E., Riguera, R., Fernandez-Megia, E. Reliable and efficient procedures for the conjugation of biomolecules through huisgen azide–alkyne cycloadditions. *Angewandte Chemie International Edition*. **2011**, *50*: 8794-8804.

42. Palomo, J. M. Click reactions in protein chemistry: from the preparation of semisynthetic enzymes to new click enzymes. *Organic & Biomolecular Chemistry*. **2012**, *10*: 9309-9318.

43. Bundy, B. C., Swartz, J. R. Site-specific incorporation of p-propargyloxyphenylalanine in a cell-free environment for direct protein−protein click conjugation. *Bioconjugate Chemistry*. **2010**, *21*: 255-263.

44. Patel, K. G., Swartz, J. R. Surface functionalization of virus-like particles by direct conjugation using azide-alkyne click chemistry. *Bioconjugate Chemistry*. **2011**, *22*: 376-387.

45. Vigneshvar, S., Sudhakumari, C. C., Senthilkumaran, B., Prakash, H. Recent advances in biosensor technology for potential applications – an overview. *Frontiers in Bioengineering and Biotechnology*. **2016**, *4*: 1-9.

46. Smaglo, B. G., Aldeghaither, D., Weiner, L. M. The development of immunoconjugates for targeted cancer therapy. *Nature reviews Clinical oncology*. **2014**, *11*: 637-648.

47. Bolivar, J. M., Hidalgo, A., Sánchez-Ruiloba, L., Berenguer, J., Guisán, J. M., López-Gallego, F. Modulation of the distribution of small proteins within porous matrixes by smart-control of the immobilization rate. *Journal of Biotechnology*. **2011**, *155*: 412-420.

48. López-Gallego, F., Yate, L. Selective biomineralization of $Co_3(PO_4)_2$-sponges triggered by His-tagged proteins: efficient heterogeneous biocatalysts for redox processes. *Chemical Communications*. **2015**, *51*: 8753-8756.

49. Dubacheva, G. V. *et al.* Controlling multivalent binding through surface chemistry: model study on streptavidin. *Journal of the American Chemical Society*. **2017**, *139*: 4157-4167.

50. Denman, A. M. Molecular cloning: a laboratory manual. *Immunology*. **1983**, *49*: 411-411.

51. Liu, M., Guyot-Sionnest, P. Mechanism of silver(I)-assisted growth of gold nanorods and bipyramids. *The Journal of Physical Chemistry B*. **2005**, *109*: 22192-22200.

52. Scarabelli, L., Sánchez-Iglesias, A., Pérez-Juste, J., Liz-Marzán, L. M. A “tips and tricks” practical guide to the synthesis of gold nanorods. *The Journal of Physical Chemistry Letters*. **2015**, *6*: 4270-4279.

53. Stöber, W., Fink, A., Bohn, E. Controlled growth of monodisperse silica spheres in the micron size range. *Journal of Colloid and Interface Science*. **1968**, *26*: 62-69.

54. Bogush, G. H., Tracy, M. A., Zukoski, C. F. Preparation of monodisperse silica particles: Control of size and mass fraction. *Journal of Non-Crystalline Solids*. **1988**, *104*: 95-106.

55. Sun, Z. Z., Hayes, C. A., Shin, J., Caschera, F., Murray, R. M., Noireaux, V. Protocols for implementing an Escherichia coli based TX-TL cell-free expression system for synthetic biology. *Journal of visualized experiments*. **2013**, *79*: 1-14.

56. Rocha-Martín, J., Rivas, B. D. L., Muñoz, R., Guisán, J. M., López-Gallego, F. Rational co-immobilization of bi-enzyme cascades on porous supports and their applications in bio-redox reactions with in situ recycling of soluble cofactors. *ChemCatChem*. **2012**, *4*: 1279-1288

57. Tsien, R. Y. The green fluorescent protein. *Annual Review of Biochemistry*. **1998**, *67*: 509-544.

58. Singh, M. I., Jain, V. Tagging the expressed protein with 6 histidines: rapid cloning of an amplicon with three options. *PLOS ONE*. **2013**, *8*: 1-8.

59. Smith, M. T., Berkheimer, S. D., Werner, C. J., Bundy, B. C. Lyophilized Escherichia coli-based cell-free systems for robust, high-density, long-term storage. *BioTechniques*. **2014**, *56*: 186-193.

60. Pardee, K. *et al.* Portable, on-demand biomolecular manufacturing. *Cell*. **2016**, *167*: 248-259.

61. Tuckey, C., Asahara, H., Zhou, Y., Chong, S. Protein synthesis using a reconstituted cell-free system. *Current protocols in molecular biology*. **2014**, *108*: 16.31.11-16.31.22.

62. Kwon, Y. C., Jewett, M. C. High-throughput preparation methods of crude extract for robust cell-free protein synthesis. *Scientific Reports*. **2015**, *5*: 1-8.

63. Wiesbauer, J., Bolivar, J. M., Mueller, M., Schiller, M., Nidetzky, B. Oriented immobilization of enzymes made fit for applied biocatalysis: non-covalent attachment to anionic supports using Zbasic2 module. *ChemCatChem*. **2011**, *3*: 1299-1303.

64. Hall, D. A., Ptacek, J., Snyder, M. Protein microarray technology. *Mechanisms of ageing and development*. **2007**, *128*: 161-167.

65. Burdick, B. A., Schaeffer, J. R. Co-immobilized coupled enzyme systems on nylon mesh capable of gluconic and pyruvic acid production. *Biotechnology Letters*. **1987**, *9*: 253-258.

66. Mateo, C., Grazu, V., Palomo, J. M., Lopez-Gallego, F., Fernandez-Lafuente, R., Guisan, J. M. Immobilization of enzymes on heterofunctional epoxy supports. *Nature Protocols*. **2007**, *2*: 1022-1033.

67. Rocha-Martín, J. *et al.* New biotechnological perspectives of a NADH oxidase variant from Thermus thermophilus HB27 as NAD^+-recycling enzyme. *BMC Biotechnology*. **2011**, *11*: 1-11..

68. Velasco-Lozano, S., Da Silva, E. S., Llop, J., López-Gallego, F. Sustainable and continuous synthesis of enantiopure L-amino acids by using a versatile immobilised multienzyme system. *ChemBioChem*. **2018**, *19*: 395-403.

69. Park, Y. J., Lee, K. H., Kim, D. M. Assessing translational efficiency by a reporter protein co-expressed in a cell-free synthesis system. *Analytical Biochemistry*. **2017**, *518*: 139-142.

70. Rolf, J., Rosenthal, K., Lütz, S. Application of cell-free protein synthesis for faster biocatalyst development. *Catalysts*. **2019**, *9*: 1913-1921.

71. Kim, C. H., Axup, J. Y., Schultz, P. G. Protein conjugation with genetically encoded unnatural amino acids. *Current Opinion in Chemical Biology*. **2013**, *17*: 412-419.

72. Hatzenpichler, R., Scheller, S., Tavormina, P. L., Babin, B. M., Tirrell, D. A., Orphan, V. J. In situ visualization of newly synthesized proteins in environmental microbes using amino acid tagging and click chemistry. *Environmental microbiology*. **2014**, *16*: 2568-2590.

73. Wu, J. C. Y., Hutchings, C. H., Lindsay, M. J., Werner, C. J., Bundy, B. C. Enhanced enzyme stability through site-directed covalent immobilization. *Journal of Biotechnology*. **2015**, *193*: 83-90.

74. Smith, M. T., Wu, J. C., Varner, C. T., Bundy, B. C. Enhanced protein stability through minimally invasive, direct, covalent, and site-specific immobilization. *Biotechnology Progress*. **2013**, *29*: 247-254.

75. Drabkin, H. J., Rajbhandary, U. L. Initiation of protein synthesis in mammalian cells with codons other than AUG and amino acids other than methionine. *Molecular and Cellular Biology*. **1998**, *18*: 5140-5147.

76. Raliski, B. K., Howard, C. A., Young, D. D. Site-specific protein immobilization using unnatural amino acids. *Bioconjugate Chemistry*. **2014**, *25*: 1916-1920.

77. Tarrant, R. D. R., Velez-Suberbie, M. L., Tait, A. S., Smales, C. M., Bracewell, D. G. Host cell protein adsorption characteristics during protein a chromatography. *Biotechnology Progress*. **2012**, *28*: 1037-1044.

78. Ferrari, M., Barreto, R., Jackson, E., Guisan, J. M., Lopez-Gallego, F., Betancor, L. Optimizing the biological activity of Fab fragments by controlling their molecular orientation and spatial distribution across porous hydrogels. *Process Biochemistry*. **2015**, *50*: 1565-1571.

79. Merk, H., Gless, C., Maertens, B., Gerrits, M., Stiege, W. Cell-free synthesis of functional and endotoxin-free antibody Fab fragments by translocation into microsomes. *BioTechniques*. **2012**, *53*: 153-160.

80. Matsuda, T. *et al.* Cell-free synthesis of functional antibody fragments to provide a structural basis for antibody–antigen interaction. *PLOS ONE*. **2018**, *13*: 1-19.

81. Stech, M. *et al.* Cell-free synthesis of functional antibodies using a coupled in vitro transcription-translation system based on CHO cell lysates. *Scientific Reports*. **2017**, *7*: 1-15.

82. Murakami, S., Matsumoto, R., Kanamori, T. Constructive approach for synthesis of a functional IgG using a reconstituted cell-free protein synthesis system. *Scientific Reports*. **2019**, *9*: 1-13.

83. Brymora, A., Valova, V. A., Robinson, P. J. Protein-protein interactions identified by pull-down experiments and mass spectrometry. *Current Protocols in Cell Biology*. **2004**, *22*: 17.15.11-17.15.51.

84. Wang, C., Ye, Y., Hu, Q., Bellotti, A., Gu, Z. Tailoring biomaterials for cancer immunotherapy: emerging trends and future outlook. *Advanced Materials*. **2017**, *29*: 1-24.

Chapter 4

Optimizing the co-immobilization of enzymes and redox cofactors to develop artificial metabolic cells

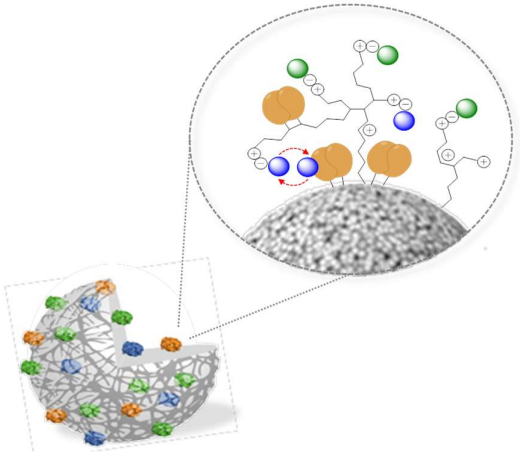

A new concept of artificial metabolic cells was developed in this chapter. The reversible immobilization of phosphorylated cofactors (FAD^+ and NAD^+) onto PEI-coated agarose microbeads was firstly optimized. In order to develop self-sufficient heterogeneous biocatalysts, covalent immobilization of enzymes was followed by electrostatic adsorption of cofactors onto the positively charged polymer attached to the carrier surface. To proof this principle, two dehydrogenases were co-immobilized with NAD^+ to asymmetrically reduce a model prochiral ketone, giving rise to 100% of conversion yield during 4 reaction cycles and without adding exogenous cofactor. This principle was expanded to the co-immobilization of an O_2-dependent oxidase and two cofactors (NADH and FAD^+). The spatial localization of the enzyme across the carrier was tuned by controlling the immobilization kinetics to get a heterogeneous distribution. For the better understanding of these systems, *in operando* analysis by using fluorescence microscopy at single-particle level were coupled to the rational design.

The co-immobilization of two dehydrogenases and NAD^+ was published in *Angewandte Chemie.*[1] The co-immobilization of an oxidase with NADH and FAD^+ is in preparation.

1. INTRODUCTION

Biocatalysis is a smart path towards more cost-effective and environmentally friendly chemical processes.[2] Furthermore, the most interesting reactions in industrial biocatalysis are mainly catalyzed by cofactor-dependent enzymes such as NAD(P)H-dependent reductases and oxidases, PLP-dependent transaminases and FAD^+-dependent oxygenases.[3-6] Consequently, the regeneration and reutilization of the expensive cofactors is a key requirement for the implementation of enzymatic processes at large scale.[7, 8] Hitherto, whole cells are still preferred as biocatalysts for those cofactor-dependent reactions because of their high efficiency and re-usability without exogenous addition of cofactors. However, whole cells often produce undesired metabolic by-products which may be toxic and difficult to separate.[9] Many endeavours have been invested in cell-free systems based on enzymatic and chemical reactions to regenerate the cofactors[10, 11] allowing their use in catalytic amounts, but they still must be exogenously added. Bio-inspired pioneering works have immobilized biological or artificial cofactors (mostly NADH) and enzymes on solid materials as cell-free systems aiming at their solid phase recycling and reusability for several operational cycles.[7, 12-14] Genereally, the success of these works have been limited because the immobilized cofactors show limited turnover numbers,[15] the enzymatic activity towards the immobilized cofactors is low,[16] the enzymes and cofactors can be hardly reused[16, 17] and the fabrication of these systems is hardly scalable.[18]

Due to its easy handling and recycling, a more promising approach for industry is the electrostatic adsorption of the cofactors and enzyme systems to solid and porous materials in organic media.[19] These solid materials modified with polyelectrolytes that display positive charges allow the electrostatic interactions with phosphorylated cofactors that are negatively charged under the binding conditions. As result, the cofactor was physically adsorbed through reversible ionic interactions which allow the cofactor molecules simultaneously existing attached to the solid surface and free in the porous space.[20] Based on such association-dissociation equilibrium, the cofactor becomes accessible for the immobilized enzymes but concurrently may also be released to the reaction bulk, leaving the solid surface. This strategy has been proven profitably in organic media[19] but fails in aqueous media owing to the lixiviation of both NAD(P)H and enzymes.[21] In a recent work, a multi-enzyme system and NADH have been co-immobilized into a membrane-based hollow nanofibers doped with polyallylamine to transform CO_2 into methanol in aqueous media.[22] Unfortunately, the cofactor regeneration in each cycle was very low (total turnover number (TTN) = 1),

although the enzymes and cofactor could be reused up to 10 cycles without activity loss.

The micro-architecture design for the cofactor immobilization is as important as the rational design for the enzyme immobilization.[23, 24] Traditionally, enzymes have been immobilized by trial-and-error approaches and characterized at macroscopic level based on observable parameters. These averaged measurements are collected from information gathered at the liquid bulk solution without considering the spatial heterogeneity of the sample. Frequently, the distribution of immobilized enzymes may affect positively/negatively to the efficiency of the heterogeneous biocatalyst. Immobilized enzymes might be inhibited by phisico-chemical changes inside microparticles (e.g. pH gradients,[25] substrates/product gradients[24]) or suffer substrate transfer limitations.[26, 27] Specifically, immobilized oxygen-dependent enzymes suffer loss of activity because of diffusional restrictions in the inner regions of the microparticles which have been studied at intra-particle level.[28-30] In the scenario of multi-enzymes cascades, the proper localization of each enzyme on different microparticles and the spatial distribution inside a single-particle was also demonstrated to make the difference during redox reactions.[31-33] More recently, rational design and single-particle/single-molecule studies have demonstrated to have an impact on the catalytic yield of the heterogeneous biocatalysts.[23, 29] These microscopic studies have received less attention, but reveal vital information about the spatio-temporal performance at the intra-particle environment of the heterogeneous biocatalysts.

In this chapter, a new design is proposed by assembling enzymes and cofactors into artificial solid supports to build artificial metabolic cells. To this end, the co-immobilization of both enzyme and cofactors have been rationally designed and optimized to perform more efficient chemical reactions. Thus, fluorescence techniques were implemented for the spatio-temporal monitoring of enzyme kinetics at single-particle level for a better understanding of enzyme behavior inside artificial metabolic cells.

2. EXPERIMENTAL SECTION

2.1. Materials

Substrates and reagents as 2,2,2-trifluoroacetophenone (TFAF), N-succinimidyl-3-(2-pyridyldithio)-propionate, FAD^+, sodium formate, fluorescein isothiocyanate (FITC),

rhodamine B isothiocyanate, polyethyleneimine 25 kDa (PEI25), $NaBH_4$, triethylamine (TEA), kanamycin, ampicillin, amicon ultra 0.5 mL centrifugal filters 10 kDa were acquired from Sigma-Aldrich (St. Louis, IL). NAD^+ and Nicotinamide-adenine-dinucleotide-reduced sodium salt (NADH) were purchased from GERBU Biotechnik GmbH (Wieblingen, Germany). 1,4-butanediol diglycidyl ether (BDE) was purchased from Thermo Scientific-Alfa Aesar (Karlsruhe, Germany). Plain agarose microbeads were purchased from ABT technologies (Madrid, Spain) to fabricate the derivatives. TALON Metal Affinity Resin was acquired from Clontech Laboratoires. PD-10 columns were from GE healthcare. Inc. 8-well μslides were purchased from ibidi (Planegg, Germany). All other reagents and solvents were of analytical grade or superior.

2.2. Methods

2.2.1. Activation of carriers:

- AG-DVS/PEI25 (6BCL agarose activated with vinyl groups and coated with polyethileneimine). AG-DVS was prepared by strictly following the protocol described by dos Santos *et al.*[34] Then, AG-DVS/PEI25 was prepared by mixing 100 mg of AG-DVS and 1 mL of a PEI solution (25 kDa, at final concentration of 10 mg x mL^{-1}) in 100 mM bicarbonate buffer at pH 10 under orbital agitation for 1 hour at 25 ºC. Finally, the AG-DVS/PEI25 was washed 5 times with 10 volumes of water and stored at 4 ºC. The supports modified with PEI were characterized by using N-succinimidyl-3-(2-pyridyldithio)-propionate that specifically reacts with the primary amines and the product can be quantified by measuring absorbance at 343 nm.[35]

- AG-G/PEI25 (6BCL agarose microbeads activated with glyoxyl groups and coated with polyethileneimine). AG-G was prepared as described elsewhere.[36] Then, AG-G/PEI25 was prepared by mixing 100 mg of AG-G and 1 mL of a PEI solution (25 kDa, at final concentration of 10 mg x mL^{-1}) in 100 mM bicarbonate buffer solution at pH 10 under orbital agitation for 1 hour at 25 ºC. Later on, solid $NaBH_4$ was added (1 mg x mL^{-1}) and incubated for 30 min at 4 ºC. Finally, the AG-GPEI was washed 5 times with 10 volumes of water and stored at 4 ºC.

- AG-TEA (6BCL agarose activated with triethylamine). Agarose activated with epoxy groups was modified with 1 M triethylamine in 50 % water/acetone at pH 12 for 24 hours at 25 ºC, following a previously reported protocol.[36]

- Pu-G/PEI25 (purolite activated with glyoxyl and coated with polyethileneimine). The same protocol carried out to prepare AG/PEI25 was followed but using Pu-G as starting carrier.

2.2.2. Expression and purification of enzymes

Alcohol dehydrogenase from *Thermus thermophilus* (Tt-ADH)[37], formate dehydrogenase from *Candida boidinii* (Cb-FDH)[38] and Tt-NOX[39] were overexpressed in *E. coli* as follows. Shortly, 1 mL of an overnight culture of *E. coli* BL21 transformed with the respective plasmid (*adh*_pET22a, *fdh*_pET28b and *nox*_pET22a) was inoculated in a 50 mL of LB medium containing kanamycin (30 μg x mL^{-1}) for Cb-FDH, and ampicillin (100 μg x mL^{-1}) for Tt-ADH and Tt-NOX. For the overexpression of Tt-ADH and Tt-NOX, the resulting culture was incubated at 37 °C and 200 rpm until the OD_{600nm} reached 0.6. At that point, the culture was induced with 1 mM IPTG. Cells were grown at 37 °C for 3 hours and then harvested by centrifugation at 10000 g during 30 minutes at 4 ºC. For Cb-FDH, the resulting culture was incubated at 21 °C with energetic shaking until the OD_{600nm} reached 0.6, and then the culture was induced with 1 mM IPTG. Cells were grown at 21 °C for 18 hours and then harvested by centrifugation at 10000 g during 30 minutes at 4 ºC.

2.2.3. Protein purification

The resulting pellets (0.5 g) were resuspended in 5 mL of binding buffer (25 mM sodium phosphate at pH 7). Cells were broken by sonication (LABSONIC P, Sartorius Stedim biotech) at 30% of amplitude (1 second ON, 1 second OFF) during 30 minutes. The suspension was centrifuged at 10000 g during 30 minutes at 4 ºC. For Cb-FDH the supernatant containing the enzyme was collected and passed through a TALON resin equilibrated with binding buffer. Following the protein binding to the column, the column was washed three times with binding buffer before the protein elution with elution buffer (binding buffer supplemented with 300 mM imidazole). The eluted protein was gel-filtered by using PD-10 columns to remove the imidazole and exchange. In case of Tt-ADH, the sonicated crude extract that contains the enzyme was incubated at 70 ºC during 1 hour to remove all mesophilic proteins, the thermophilic one remain at the supernatant and was separated by centrifugation at 10000 g during 30 min at 4 ºC. For Tt-NOX, the sonicated crude extract was incubated at 80 ºC during 45 minutes. The protein solution was then centrifugated at 10000 g during 30 minutes at 4 ºC to separate Tt-NOX in the supernatant.

The purification process of Cb-FDH, Tt-ADH and Tt-NOX was followed by SDS-PAGE (Figure 1).

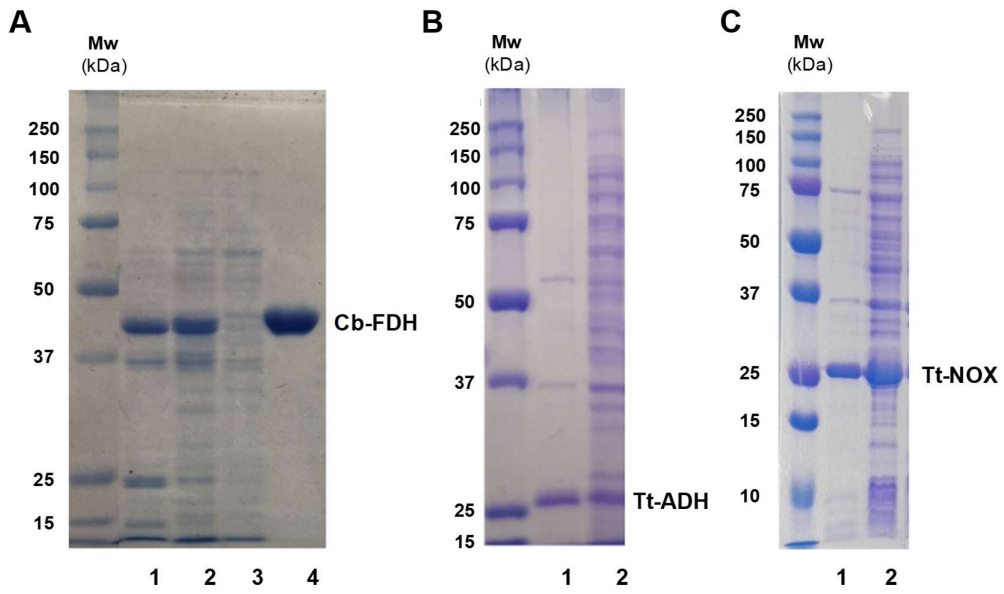

Figure 1. SDS-PAGE of protein purifications. All molecular weight markers are BioRad Precision Plus Protein All Blue Standard. A) Cb-FDH. Line A1: crude extract, line A2: soluble fraction after cell disruption by sonication, line A3: elution fraction, line A4: pure Cb-FDH (band 40 kDa). B) Tt-ADH. Line B1: pure Tt-ADH (band 27 kDa), line B2: Soluble fraction after cell disruption by sonication. C) Tt-NOX. Line C1: pure Tt-NOX (band 27 kDa), line C2: soluble fraction after cell disruption by sonication.

2.2.4. Protein quantification

Protein concentration was quantified by Bradford protein assay[40] adapted to 96-well plates. Briefly, 5 µL of enzyme solution were mixed with 200 µL of Bradford reagent and incubated at room temperature for 5 min. Then the absorbance was measured at 595 nm and the protein content was estimated employing a calibration curve using BSA as a standard.

2.2.5. Enzymatic activity assays

The enzymatic activities were spectrophotometrically measured in 96-well plates by monitoring the absorbance at the corresponding wavelenght in a Varioska^{nTM} Flash Multimode Reader. One unit of activity was defined as the amount of enzyme that was needed to either reduce or oxidize 1 µmol of the corresponding nicotinamide cofactor at 25 ºC at pH 7.

- Tt-ADH activity. 200 µL of a reaction mixture containing 10 mM of TFAF, 0.25 mM of NADH in 25 mM sodium phosphate buffer at pH 7 were incubated with 5 µL of enzymatic solution or suspension at 25 ºC. The decrease in the absorbance was monitored at 340 nm.

- Cb-FDH activity. 200 µL of 1 mM NAD^+ and 100 mM formic acid in 25 mM sodium phosphate buffer at pH 7 were incubated with 5 µL of enzymatic solution at 25 ºC. The increase in the absorbance was monitored at 340 nm.

- Tt-NOX activity. 200 µL of 0.15 mM FAD^+ and 0.2 mM NAD^+ in 25 mM sodium phosphate buffer at pH 7 were incubated with 20 µL of enzymatic solution at 25 ºC. The increase in the absorbance was monitored at 340 nm.

2.2.6. Enzyme immobilization:

- Co-immobilization of Tt-ADH and Cb-FDH on AG-G/PEI25. 10 mL of Tt-ADH (0.078 mg x mL^{-1}) in 100 mM sodium bicarbonate buffer at pH 10 were mixed with 1 gram of AG-G and incubated at room temperature with orbital shaking for 2 hours. Immobilization course was followed spectrophotometrically by measuring the activity of both suspension and supernatant. Later, the suspension was filtered and 10 mL of a PEI solution (10 mg x mL^{-1}) in the same buffer were added. After 1 hour of incubation at room temperature, 1 mg x mL^{-1} solid $NaBH_4$ was added and incubated 30 minutes at 4 ºC. Then, the suspension was filtered and washed 5 times with 10 mL of 10 mM sodium phosphate buffer at pH 7. Afterwards, the immobilization of the second enzyme was conducted by adding 10 mL of Cb-FDH solution (4.5 mg x mL^{-1}) in 10 mM sodium phosphate buffere at pH 7 and incubating 1 hour at room temperature with orbital shaking. Then, the suspension was filtered and the solid was incubated with 10 mL of 30 mM BDE at pH 7 for 1 hour at room temperature. Finally, the suspension was filtered and washed twice with 5 volumes of 10 mM sodium phosphate buffer at pH 7 and stored at 4 ºC.

- Immobilization of Tt-NOX on AG-G/PEI25. 10 mL of Tt-NOX (0.1 mg x mL^{-1}) in 100 mM sodium bicarbonate buffer at pH 10 were mixed with 1 gram of AG-G and incubated at room temperature under orbital shaking for 3 hours. Immobilization course was followed spectrophotometrically by measuring the activity of both suspension and supernatant. In case of homogeneous immobilization (slow immobilization process), 10 or 100 mM hydroxylamine was

added to the suspension. Later on, PEI-coating was performed as described above.

2.2.7. Parameters of immobilized enzymes:

- Protein load. The amount of protein that has been immobilized per gram of carrier. This parameter is defined as mg x g^{-1}.

- Immobilization Yield. The percentage of enzyme that has been immobilized from the initial enzyme solution which was offered to the carrier. This parameter was calculated by using values of either the enzymatic activity (U x mL^{-1}) or the protein concentration (mg x mL^{-1}).

$$\Psi\ (\%) = \left(\frac{\text{enzyme}_{\text{offered}} - \text{enzyme}_{\text{supernatant}}}{\text{enzyme}_{\text{offered}}} \right) \text{x } 100$$

- Final expressed activity. The measured activity of the immobilized enzyme on the carrier after washing. This parameter is defined as U x $g_{carrier}^{-1}$.

- Specific activity. The activity of the soluble/immobilized enzyme per miligram of enzyme.

  - Soluble enzyme: A_e (U x mg^{-1}) = $\left(\frac{\text{Enzyme activity (U x mL}^{-1})}{\text{Protein concentration (mg x mL}^{-1})} \right)$

  - Immobilized enzyme: A_e (U x mg^{-1}) = $\left(\frac{\text{Expressed activity (U x g}^{1})}{\text{Protein loading (mg x g}^{-1})} \right)$

- Relative recovered specific activity. The percentage of specific activity which has been immobilized in comparision with the specific activity of the soluble enzyme which was offered to the carrier.

$$A_r\ (\%) = \left(\frac{A_e \text{ immobilized enzyme}}{A_e \text{ soluble enzyme}} \right) \text{ x } 100$$

2.2.8. Cofactor immobilization

Ionic immobilization of phosphorylated cofactors was achieved by incubating 10 mL of soluble cofactor at the indicated concentration in 10 mM sodium phosphate at pH 7 with 1 gram of agarose microbeads (with or without previously immobilized enzymes). The suspension was kept under orbital agitation for 1 hour at room temperature. Afterwards, the resin was filtered and washed three times with 1 mL of 10 mM sodium phosphate at pH 7. The concentration of the immobilized cofactors were calculated by

measuring the absorbance of the supernatant after the adsorption process and after each washing step at the proper wavelength (260 nm for NAD^+, 340 nm for NADH and 450 nm for FAD^+) in the microplate-reader.

- Cofactor load. The amount of cofactor that has been immobilized per gram of carrier. This parameter is defined as μmol x g^{-1}.

- Immobilization Yield. The percentage of cofactors that has been immobilized from the initial cofcator solution which was offered to the carrier. This parameter was calculated by using the values of cofactor concentration (μmol x g^{-1}) as follows:

$$\Psi\ (\%) = \left(\frac{cofactor_{offered} - cofactor_{supernatant}}{cofactor_{offered}} \right) \text{ x } 100$$

2.2.9. FITC/Rhodamine-labeling of enzymes

Enzymes were labeled with either fluorophore FITC or rhodamine B following the protocol described in Chapter 3 (page 58).

2.2.10. Spatial localization studies by fluorescence microscopy

The immobilization of enzymes onto the microparticles was confirmed by using a Colibri LED illumination system incorporated into the fluorescence microscope to image rhodamine (λ_{ex}: 530 nm, λ_{em}: 615-700 nm) and FITC (λ_{ex}: 470 nm, λ_{em}: 500-557 nm).

2.2.11. Single-microbead kinetics (*In operando* experiments)

Reactions were performed under the fluorescence microscope using 8-well μslides. Images were processed with the software ZEN2012.

- Tt-ADH and Cb-FDH. 180 μL of 1:200 (w/v) suspension of the self-sufficient heterogeneous biocatalyst (0.63 $mg_{Tt\text{-}ADH}$, 43.7 $mg_{Cb\text{-}FDH}$ and 17.5 μmol_{NADH} x $g_{carrier}^{-1}$) in 10 mM sodium phosphate buffer at pH 7 were placed into the well. Reactions were triggered with 20 μL of substrate at a final concentration of 5 mM TFAF, 10 mM formic acid and 5% acetonitrile in 10 mM sodium phosphate buffer pH 7. The fluorescence monitoring of NADH (λ_{ex}: 365 nm, λ_{em}: 402-448 nm) was carried out every 20 seconds during 15 minutes at room temperature.

- Tt-NOX. 184 µL of 1:200 (w/v) suspension of the immobilized enzyme (0.1 $mg_{Tt\text{-}NOX}$ x $g_{carrier}^{-1}$) in 10 mM of sodium phosphate buffered solution pH 7 were placed into the well. Substrate mixtures with both substrates (111 µM NADH and 5.5 µM FAD^+), with 10 mM sodium phosphate buffer at pH 7, with only 5.5 µM FAD^+ and with only 111 µM NADH were used to trigger different reactions. The fluorescence monitoring of NADH (λ_{ex}: 365 nm, λ_{em}: 402-448 nm) and FAD^+ (λ_{ex}: 470 nm, λ_{em}: 500-557 nm) was carried out every minute during 30 minutes at room temperature.

3. RESULTS AND DISCUSSION

3.1. Optimization of phosphorylated redox cofactor immobilization

Firstly, the electrostatic adsorption of phosphorylated cofactors to solid porous microbeads was tested on two different anionic exchangers that have been broadly used in purification and immobilization of proteins.[36, 41-44] AG-TEA and AG-G/PEI25 were fabricated with agarose microbeads activated with triethylamine (TEA) and polyethyleneimine (PEI), respectively. The cationic groups were introduced by nucleophilic attack of the amine-containing molecule (TEA/PEI) to the epoxy or aldehyde groups, respectively, on the agarose surface followed by mild reduction that establishes covalent irreversible bonds. As a model phosphorylated cofactor, NAD^+ was adsorbed on both cationic microbeads at different pH (Table 1).

Table 1. Effect of the pH and chemistry bound in the immobilization of NAD^+.

	NAD^+ (µmol x $g_{carrier}^{-1}$)			
	AG-TEA		AG-G/PEI25	
Washing number	pH 7	pH 9	pH 7	pH 9
0	11.2	18.4	17.5	18.2
1	0	1.9	6.7	3.0
2	0	0	4.9	1.0
3	0	0	4.4	0.4
4	0	0	4.0	0.2
5	0	0	3.8	0.1

Washing steps were performed by adding 10 volumes of 10 mM sodium phosphate or carbonate at pH 7 or 9, respectively.

AG-G/PEI25 loaded 1.6-fold more NAD^+ than AG-TEA and retained 4 $\mu mol_{NAD} x\ g^{-1}$ after 5 washing steps (10 volumes each), while 100% of NAD^+ bound to AG-TEA was

lixiviated under the same conditions. Although the pKa values of TEA and PEI are similar (around 10),[45-47] PEI build a 3D-polymeric bed inside the pores displaying a larger and denser cationic surface that may explain its higher cofactor loading capacity compared to those surfaces modified with TEA. Noteworthy, although the cofactor adsorption was similar at both pHs, the cofactor lixiviation increased at pH 9 because alkaline conditions neutralize the positive charge of the amine groups, dramatically weakening NAD^+-PEI interactions.

Remarkably, the loading yield and cofactor lixiviation were not affected when PEI was irreversibly attached to polyacrylic porous microbeads (Pu-G/PEI25) or to agarose microbeads activated with vinyl groups (AG-DVS/PEI25). Figure 2 shows that 4-5 $\mu mol_{NAD+} \times g_{carrier}^{-1}$ remained bound to the positively charged surfaces after 8 washing steps.

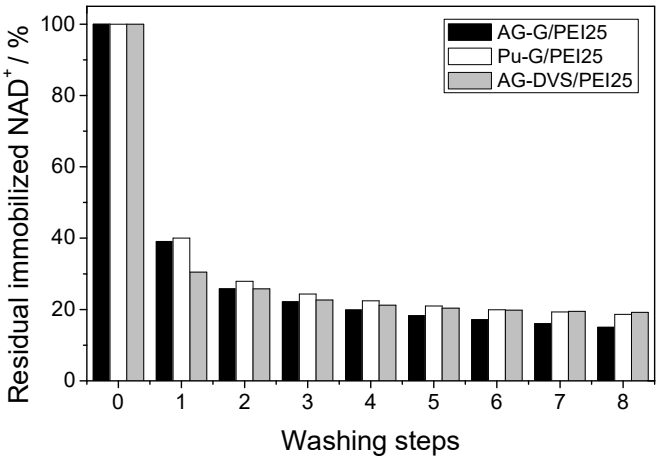

Figure 2. Immobilization of NAD^+ on different PEI-coated supports. In all cases washing steps were carried out by adding 10 volumes of 10 mM sodium phosphate buffer at pH 7. The initial immobilized NAD^+ in each case corresponds to 24, 23 and 22 $\mu mol_{NAD+} \times g_{carrier}^{-1}$, respectively.

In addition, AG-G/PEI25 was also able to efficiently bind another phosphorylated redox cofactors such as flavin adenine dinucleotide (FAD^+) which is required for other industrially relevant enzymes (flavin-dependent oxidases[3] and enoate reductases[48]). Figure 3A shows that the absorption yield of FAD^+ was 3 times higher than NAD^+. Nevertheless, more than 90% of the adsorbed FAD^+ was lixiviated after 8 washing steps (Figure 3B).

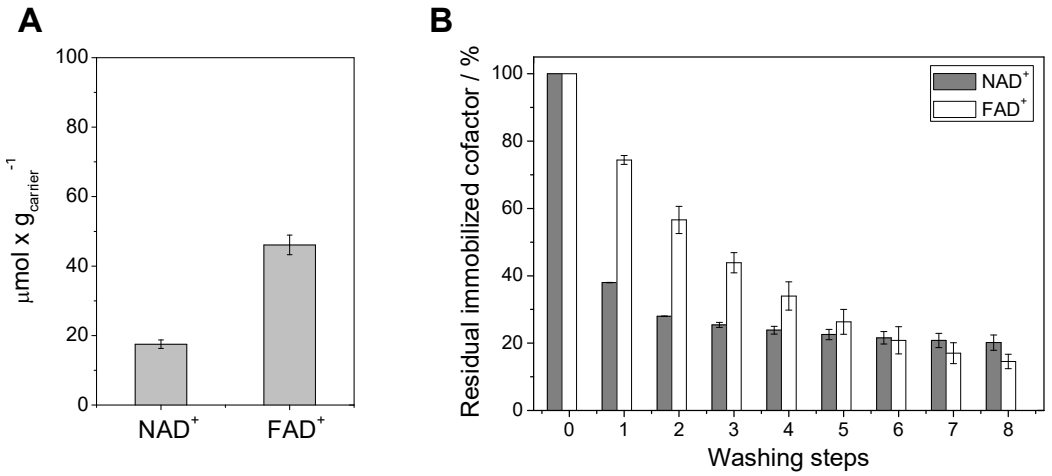

Figure 3. Immobilization of phosphorylated cofactors on AG-G/PEI25. A) Cofactor loading (the offered cofactor was 100 $\mu mol_{cofactor}$ x $g_{support}^{-1}$). B) Residual cofactors which remain bound to AG-G/PEI25 after washing treatments. In all cases, the washing steps were carried out by adding 10 volumes of 10 mM sodium phosphate buffer at pH 7 per volume of AG-G/PEI25 microbeads.

We suggest that the cofactor lixiviation relies on the association-dissociation equilibrium of the cofactor-PEI interactions, and such interactions are specific for each cofactor. To prove this hypothesis, we determined the apparent dissociation constants (K_d^{app}) for the electrostatic binding of the cofactors to the AG-G/PEI25 (Table 2).

Table 2. Apparent dissociation constants of redox cofactors ionically absorbed to AG-G/PEI25.

Cofactor	$[Cof^{(-)}]_{bound}$ ($\mu mol \times g^{-1}$)	$[Cof^{(-)}]_{free}$ ($\mu mol \times g^{-1}$)	K_d^{app} ($\mu mol \times g^{-1}$)
NAD^+	17.5	82.5	3283
FAD^+	46.1	53.9	781

The K_d^{app} was calculated as described elsewhere.[1] The free and bound cofactors were calculated by incubating 1 mL of 10 mM cofactor in 10 mM sodium phosphate buffer at pH 7 with 0.1 gram of AG-G/PEI25 for 60 minutes when the concentration of the free cofactor was constant (equilibrium in batch).

Actually, the K_d^{app} of FAD^+ was 4.2 times lower than the K_d^{app} of NAD^+. These results show a higher affinity of AG-G/PEI25 towards FAD^+ according to the higher immobilization yield of FAD^+ (Figure 3A). The adsorption of the cofactor to the microbeads is mainly driven by reversible ion-exchange interactions between the negatively charged phosphate groups of the cofactors and the positively charged

amine groups coating the agarose fibers. Therefore, the strength of such electrostatic interactions relies on the association-dissociation equilibrium that is affected by the ionization state (pH/cofactor-dependent) and the density of the amine groups coating the solid surface.

3.2. Co-immobilization of two enzymes and one redox cofactor

Having now in hand a versatile and simple strategy to incorporate phosphorylated cofactors to porous carriers, we tested the catalytic availability of these cofactors to carry out redox reactions by enzymes. Usually, enzymes display lower activity towards reversible or irreversible tethered cofactors on solid materials.[13, 15, 17] To test the performance of these reversibly immobilized cofactors, steady-state kinetics of NAD^+-dependent formiate dehydrogenase (Cb-FDH) towards both soluble and immobilized cofactors were studied. Using soluble NAD^+, the K_M of soluble Cb-FDH was 12 times lower than its immobilized form (Figure 4). Unfortunately, the apparent Michaelis-Menten constant could not be calculated using the immobilized NAD^+ because neither the soluble nor the immobilized enzymes were saturated at any concentration of immobilized cofactor.

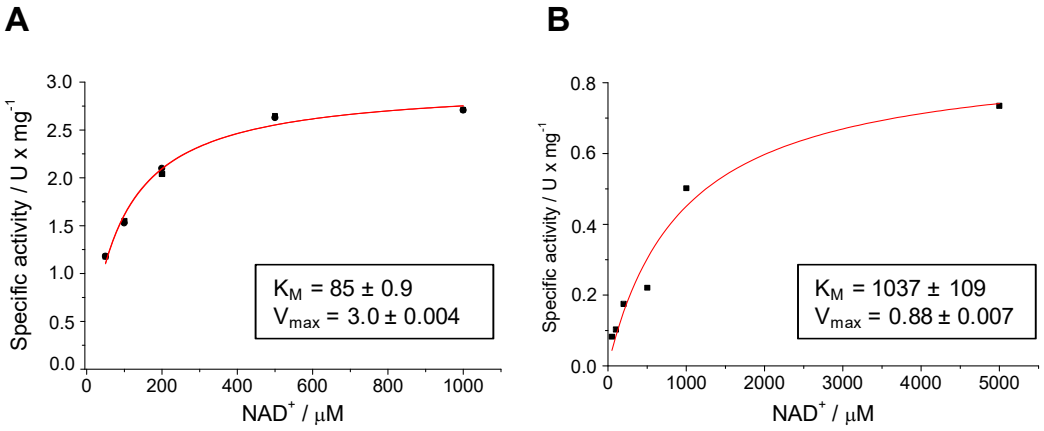

Figure 4. Kinetic parameters of soluble (A) and immobilized (B) Cb-FDH with soluble NAD^+.

The immobilized Cb-FDH showed the same specific activity by using either soluble or co-immobilized NAD^+ (166 µM) (Table 3). This fact suggests that the available cofactor is nearly the same regardless NAD^+ is in its free or immobilized form.

Table 3. Cofactor catalytic availability.

Cb-FDH form	Cofactor form	Specific activity (U x mg^{-1})	NAD^+ available (μM)	NAD^+ available (%)
Soluble	Soluble	1.97 ± 0.005 [a]	166	100
	Immobilized	0.19 ± 0.06 [b]	5.8 ± 1.9 [c]	3.5 ± 1.1
Immobilized	Soluble	0.12 ± 0.01 [a]	166	100
	Immobilized	0.13 ± 0.01 [b]	177 ± 21.2 [c]	107.2 ± 12.8

Soluble and immobilized Cb-FDH with free (166 μM in bulk) and immobilized NAD^+ (6.6 μmol x $g_{carrier}^{-1}$ = 166 μmol in bulk). Ae = specific activity in U x mg^{-1}, Vmax = maximum specific activity in U x mg^{-1} and K_M = Michaelis-Menten constant in μM. [a] The specific activities were calculated by inserting 166 μM of soluble NAD^+ as substrate concentration in the Michaelis-Menten equation using the corresponding kinetics parameters (Vmax and K_M) experimentally determined. Ae = (Vmax x 166) / K_M +166). [b] The specific activities were experimentally determined using 166 μM of immobilized NAD^+. [c] The catalytically available NAD^+ concentration was calculated by inserting the specific activity experimentally determined [b] in the Michaelis-Menten equation using the corresponding kinetics parameters (Vmax and K_M) for the soluble and the immobilized Cb-FDH experimentally determined. $[NAD^+]$ = (Ae x K_M) / (Vmax - Ae), where $[NAD^+]$ is the catalytically available immobilized NAD^+ concentration in μM.

However, when the activity values of the Cb-FDH were introduced in the Michaelis-Menten fitting corresponding to either the soluble or the immobilized enzyme, the estimated available concentration of immobilized NAD^+ was 30-fold higher for the immobilized enzyme than for the soluble one. We suggest that the physical proximity between the enzymes and the cofactor molecules within the pores where both species are co-immobilized explains the higher available cofactor concentration, compared to the soluble enzyme that needs to diffuse into the pores to reach the cofactors.[49] Therefore, NAD^+ bound to AG-G/PEI25 can be catalytically utilized and retained in the solid phase, demonstrating that the association-dissociation equilibrium directly impacts on the cofactor availability for the enzymes that determines the reaction kinetics.

Due to these promising results, two different enzymes; alcohol dehydrogenase (Tt-ADH) and Cb-FDH, were co-immobilized with the corresponding cofactor; NAD^+ (Scheme 1), to develop a self-sufficient heterogeneous biocatalyst to carry out the asymmetric reduction of TFAF to yield *S*-(trifluoromethyl)bencylalcohol.

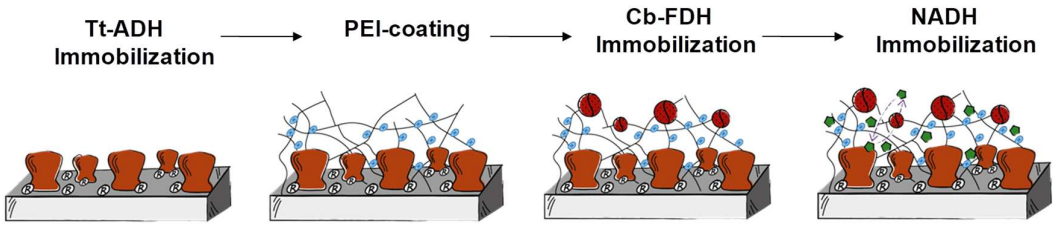

Scheme 1. Co-immobilization process of two enzymes and one cofactor onto the same microbeads.

Tt-ADH was firstly immobilized on AG-G[50] and then the agarose fibers immobilizing the enzymes were coated with PEI through the same amine-aldehyde chemistry[51], followed by a mild reduction step that turns the reversible imines resulted from the amine-aldehyde interaction into irreversible secondary amines. Unfortunately, when Cb-FDH was immobilized by the aldehyde immobilization chemistry, the enzyme was inactivated. Thereby, this enzyme was co-immobilized by ionic adsorption on the PEI-bed and subsequently cross-linked with BDE to assure its irreversible attachment. In this architecture, both enzymes and PEI are irreversibly bound to the agarose microbeads leaving the enzymes surrounded by the cationic polymer with the ionically adsorbed cofactor. The different enzymes were immobilized with yields ranging 79-100% and recovering 52–100% of their specific activities upon the immobilization process (Table 4).

Table 4. Immobilization yields and expressed activities of co-immobilized Tt-ADH and Cb-FDH on AG-G/PEI25.

Enzymes	Protein load (mg x $g_{carrier}^{-1}$)	Immobilization yield (%)	Final expressed activity (U x $g_{carrier}^{-1}$)	Relative recovered specific activity (%)
Tt-ADH	0.63	79	6.15	113
Cb-FDH	43.7	100	59.60	52

[a] After 5 washes with a mixture of 10 mM formic acid, 5 mM TFAF and 10 mM sodium phosphate buffer at pH 7, the heterogeneous biocatalyst maintained > 95% of residual Cb-FDH activity; and after a final wash with 0.5 M of NaCl, more than 85% of the Cb-FDH activity was retained in the heterogeneous biocatalyst.

The co-immobilization of two enzymes and NAD^+ onto the porous carrier was confirmed by fluorescence microscopy. Figure 5 shows the localization of both cofactor and enzymes across the surface of the same agarose microbeads, without presence of fluorescence in the bulk.

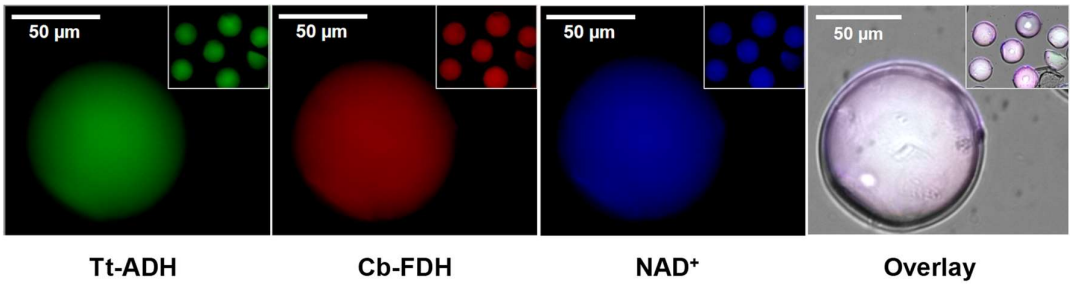

Figure 5. Spatial localization of enzymes and cofactor by fluorescence microscopy. Tt-ADH was labeled with FITC, Cb-FDH was labeled with rhodamine and NAD^+ showed autofluorescence.

Fluorescence microscopy techniques were also set up to monitor the enzyme kinetics at single-particle level. *In operando* monitoring of fluorescence at single-particle level was applied to demonstrate that the ionically adsorbed cofactors are available for the enzymes and remain inside the porous structure. To this end, single-particle experiments served to monitor the oxidation of formic acid in parallel with the asymmetric reduction of TFAF catalyzed by the co-immobilized bi-enzymatic system. The autofluorescence of NADH immobilized on single-agarose microbeads together the use of fluorescence microscopy (Figure 6B) allowed these single-particle studies. When the self-sufficient heterogeneous biocatalyst was operated under the microscope using formic acid as the only substrate, the fluorescence intensity within the microbeads increased due the concomitant production of NADH (which fluorescence is higher than the oxidized form NAD^+) resulted from the Cb-FDH oxidation activity. Under the same conditions but in the presence of both TFAF and formic acid, the fluorescence intensity of the microbeads remained practically constant along the time because the oxidized cofactor was recycled inside the particle by the orthogonal activities of the two enzymes (Figure 6B). The *in operando* experiments demonstrated that the immobilized cofactor is available for the immobilized enzymes but does not diffuse out the porous microbeads during the reaction. This innovative but straightforward application of fluorescence microscopy opens new pathways for a better characterization of heterogeneous biocatalysts.

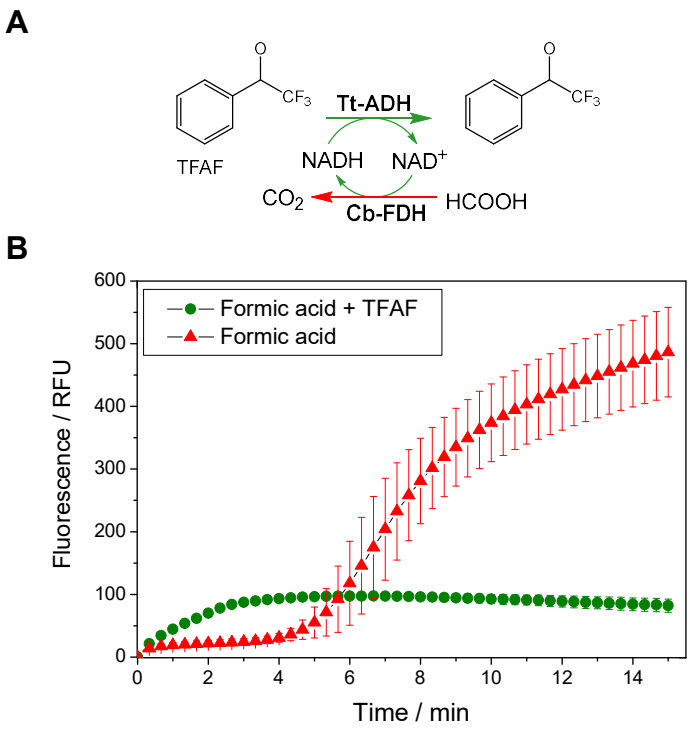

Figure 6. Single-particle monitoring redox biotransformations by self-sufficient heterogenous biocatalysts. A) Reaction scheme. B) *In operando* NADH production with (green circles) and without (red triangles) NAD^+ recycling within a single microbead. The fluorescence value at each time point corresponds to average fluorescence of 10 microbeads.

Afterwards, the efficiency of this self-sufficient multi-functional heterogeneous biocatalyst was tested for the asymmetric reduction of TFAF without addition of exogenous cofactor in batch mode (Figure 7). The conversion and reaction rates of the self-sufficient heterogeneous biocatalysts were similar than the co-immobilized Tt-ADH and Cb-FDH with exogenous NAD^+ (Figure 7A).

The next step was to test the reusability of the self-sufficient heterogeneous biocatalyst without adding exogenous NAD^+. The self-sufficient heterogeneous biocatalyst was reused for 4 batch cycles achieving the maximum conversion in each cycle and accumulating a total turnovernumber (TTN) of 40 (the theoretical maximum) (Figure 7). In this system, the immobilized NAD^+ performs as well as the soluble one with the advantage that the former can be reused for several reaction cycles increasing its TTN. When using porous microbeads, the cofactors must be co-immobilized with the enzymes on the same porous microbeads to guarantee the cofactor shuttling between the different enzyme active sites, enabling the intra-particle cofactor recycling and the operational reusing of the self-sufficient biocatalyst. In terms of cofactor recycling, the

architecture herein presented improves the reported TTN_{NADH} of 10 after 10 reaction cycles for a multi-enzyme system co-entrapped with NADH into hollow nanofibers doped with polyallyamine.[22] Alike, our system performs much better than the system where the enzymes and the cofactors are separately and irreversibly immobilized on non-porous polystyrene nanoparticles achieving an accumulated TTN <1 after 11 operational cycles of methanol production.[13] In this system, the cofactor is recycled by colloidal collisions between the nanoparticles unlike in our system where the cofactor shuttles between the active sites inside the porous surface, explaining the higher efficiency in the NAD^+ recycling.

A

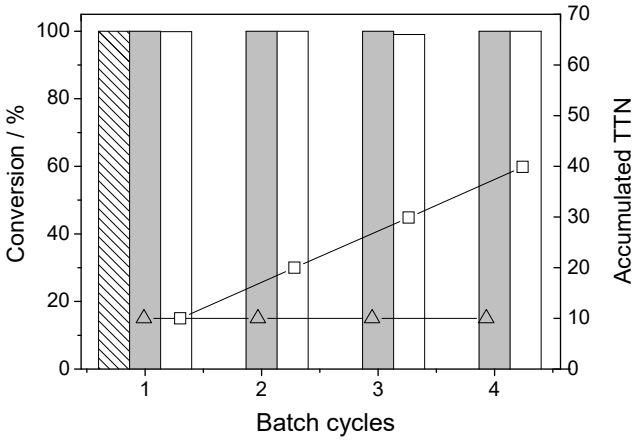

B

Enzymes form	Cofactor form	Specific activity ((µmol x mg^{-1}) min^{-1}) [1]	Conversion (%) [1]	TOF (min^{-1})	Accumulated TTN ($mol_{product}$ x mol_{NAD+}^{-1}) [2]
Immobilized	Soluble	0.77	100	0.079	10
Immobilized	Immobilized	0.69	100	0.064	40

Figure 7. Efficiency and reusability of the self-sufficient heterogeneous biocatalysts. A) Asymmetric reduction of TFAF catalyzed by co-immobilized NAD^+, Tt-ADH and Cb-FDH (white bars and squares), by co-immobilized Tt-ADH and Cb-FDH using soluble NAD^+ (grey bars and triangles) and by soluble enzymes and cofactor (dashed white bar). Reactions were carried out with 5 mM TFAF and 0.5 mM soluble or immobilized NAD^+, 10 mM formic acid, 5% of acetonitrile in 10 mM phosphate buffer at pH 7 and 25 ºC. Bars correspond to conversion degree, while symbols correspond to the accumulated TTN. Accumulated TTN was calculated as µmol of released product after each batch cycle per mol of immobilized cofactor. B) Catalytic efficiency and reuse of heterogeneous biocatalysts with soluble and immobilized cofactors. [1] Obtained specific activity or yield in the first cycle. [2] Accumulated TTN after 4 batch cycles. TOF was calculated as µmol of released product per µmol of cofactor in one hour.

3.3. Co-immobilization of one enzyme and two redox cofactors

In the context of design and engineering more efficient heterogeneous biocatalysts, the enzyme distribution across the porous particle is another important parameter to enhance the catalytic performance of the biocatalyst.[33, 52-54] In the second part of the present chapter, the spatial organization of co-immobilized enzymes and cofactors was more profoundly studied using as a proof of concept an O_2-dependent enzyme. Based on a previous work,[55] the immobilization rate of NADH-dependent oxidase (Tt-NOX) on AG-G was tuned to obtain different distributions of the enzyme across the porous carrier. Hydroxilamine (HA) was added during the enzyme immobilization process as a competitor for the aldehyde groups of the carrier surface (Figure 8).

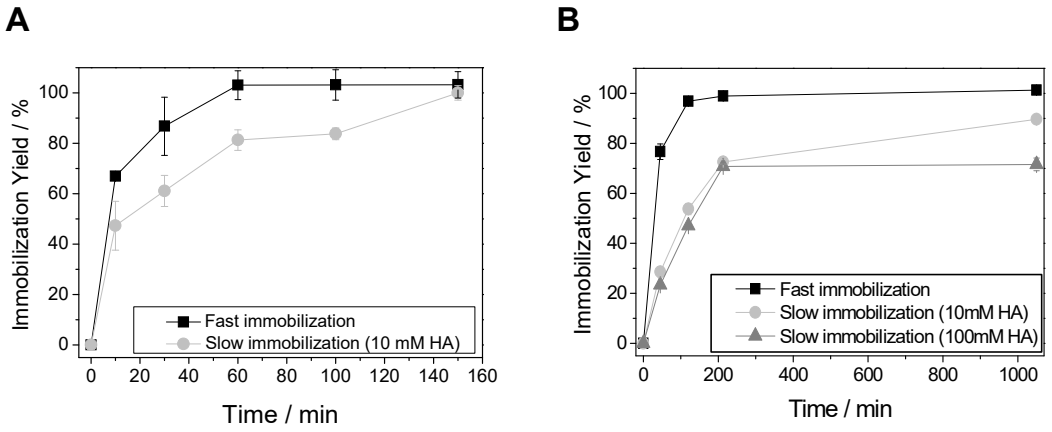

Figure 8. Modulation of the immobilization rate of Tt-NOX on AG-G. A) Low protein concentration (protein offered: 0.1 mg x $g_{carrier}^{-1}$). B) High protein concentration. (protein offered: 1 mg x $g_{carrier}^{-1}$).

A slowdown of the immobilization rate was observed in presence of HA when Tt-NOX was offered to AG-G at 0.1 mg x $g_{carrier}^{-1}$ (Figure 8A). Similar effects were obtained with a higher protein loading (Figure 8B). In this case, the influence of different concentrations of HA (10 and 100 mM) was negligible during the first phase of the immobilization, although the immobilization yield was lower at higher concentration of the competitor (100 mM HA).

To study the effect of the immobilization rate on the protein distribution, Tt-NOX was labeled with rhodamine and further immobilized. The immobilized preparations were analyzed by CLSM[56] (Figure 9). The fast immobilization rate (no adding HA) resulted in a heterogeneous distribution of the enzyme, while a homogenous distribution was achieved with a slower immobilization rate (adding HA). When the distribution was

heterogeneous, the enzyme was mainly immobilized on the outer phase of the microbeads. Same results were obtained when the intrinsic fluorescence of FAD^+ bound to unlabeled Tt-NOX was analyzed.

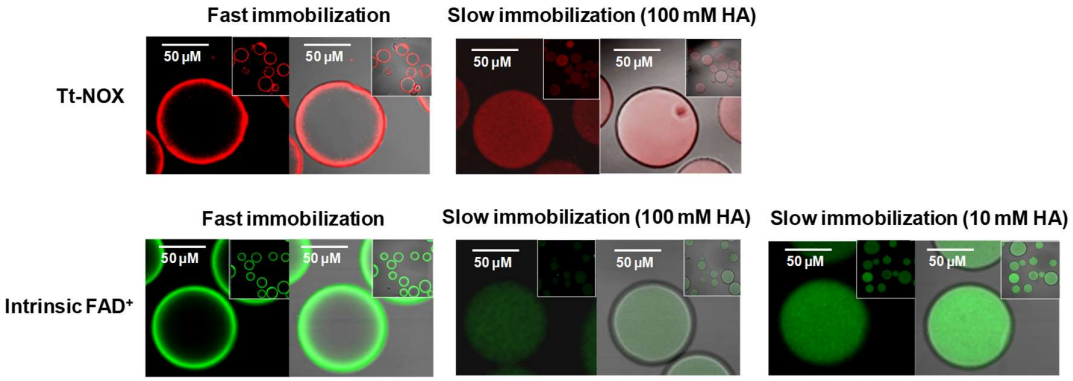

Figure 9. Spatial distribution of immobilized Tt-NOX on AG-G by CLSM. The fluorescence of rhodamine-labeled enzyme was measured at λ_{ex}: 561 nm, λ_{em}: filter LP565 nm. The intrinsic FAD^+ of Tt-NOX showed autofluorescence and was detected at λ_{ex}: 488 nm, λ_{em}: filter LP505 nm. The initial protein offered was 1 mg x $g_{carrier}^{-1}$ in all experiments.

Different enzyme distributions have been found to have beneficial/detrimental effects in the performance of the biocatalysts. For instance, enzymes located at the outer phase of the microparticle suffer less diffusion limitations of the substrates.[53, 57, 58] Conversely, when enzymes are distributed within the inner phase of the microparticle, they may be protected from inactivating agents that barely penetrate inside the porous particles.[52, 59] In this case, since Tt-NOX is an oxygen-dependent enzyme, a homogeneous distribution might be harmful for the catalytic efficiency of the biocatalyst due to diffusion limitations of the oxygen across the microstructure of the porous microbeads. In fact, biocatalysts with a uniform enzyme distribution showed a slower enzyme kinetics when the activity was tested, although the heterogeneous biocatalysts were tested at different protein loadings (Figure 10).

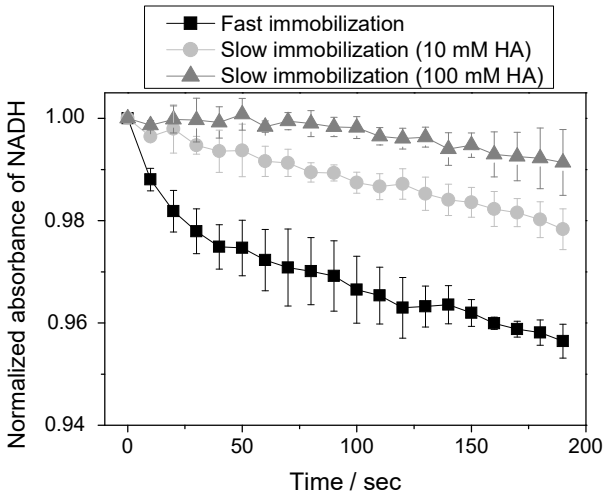

Figure 10. Monitoring enzyme kinetics. The protein loads were 1 mg x g^{-1} (black squares), 0.9 mg x g^{-1} (light grey squares) and 0.72 mg x g^{-1} (dark grey triangles).

According to the kinetic results, the final expressed activity of the biocatalyst with a heterogeneous distribution was 1.28 times higher than the expressed activity of the biocatalyst with a homogeneous distribution (Table 4).

Table 4. Immobilization yields and expressed activities of immobilized Tt-NOX on AG-G/PEI25.

	Protein load (mg x $g_{carrier}^{-1}$)	Immobilization Yield (%)	Final expressed activity (U x $g_{carrier}^{-1}$)	Relative recovered specific activity (%)
Heterogeneous distribution	1	100	5.03	5.59
Homogeneous distribution	0.9	89.61	3.92	4.87

Once the enzyme distribution was optimized, our new cofactor co-immobilization strategy was also applied to fabricate self-sufficient heterogeneous biocatalysts with Tt-NOX. Going a step further, two phosphorylated cofactors (NADH and FAD^+) were co-immobilized with Tt-NOX on agarose micromicrobeads (Scheme 2).

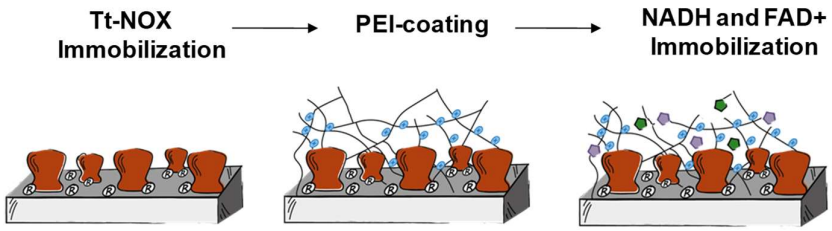

Scheme 2. Co-immobilization process of one enzyme and two cofactors onto the same microbeads.

Since PEI is largely and successfully used for protein immobilization in biocatalyst design,[60] the polymer was chosen again for the co-immobilization of two cofactors. Following the previously micro-architecture designed in this chapter, AG-G micromicrobeads were coated with PEI to enable the ion-exchange co-immobilization of NADH and FAD^+ onto the same microbeads (Figure 11). Actually, when no PEI was coating the microbeads, the cofactors were found homogenously in both the bulk solution and the microbeads (Figure 11). This experiment evinces the essential role of PEI as a support for the reversible immobilization of cofactors on AG-G.

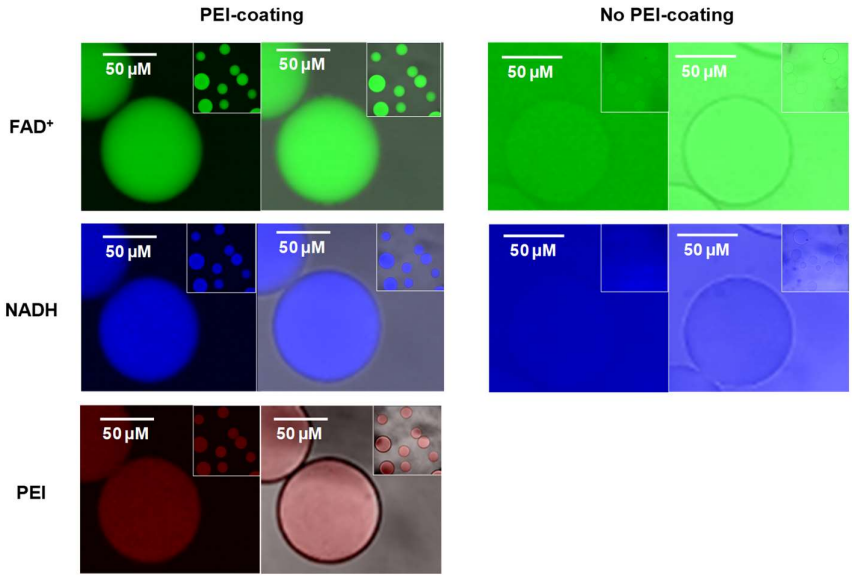

Figure 11. CLSM imaging the co-immobilization of NADH and FAD^+ by using PEI as coating agent. On the left side, colocalization of FAD^+ (green) and NADH (blue) on agarose micromicrobeads coated with rhodamine-labeled PEI (red). On the right side, the addition of FAD^+ (green) and NADH (blue) to AG-G without PEI-coating. The left columns are fluorescence images and the rigth columns are overlay of fluorescence and brigthfield signals.

Availing the autofluorescence of cofactors, the immobilization rate of NADH and FAD^+ on AG-G/PEI25 was monitored by CLSM (Figure 12). In less than 1 minute, both cofactors were homogeneously immobilized across the microbeads. Moreover, the cofactor remained bound to the microbeads after 1 hour in 10 mM buffered solution without being lixiviated to the reaction bulk.

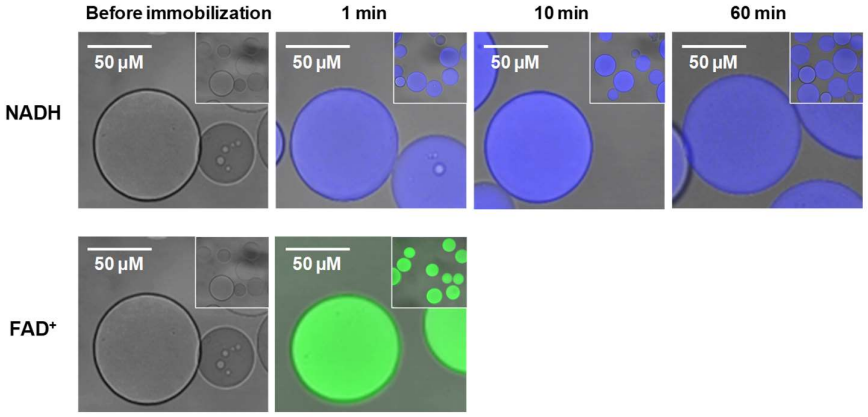

Figure 12. Monitoring the immobilization of NADH and FAD^+ on AG-G/PEI25 by CLSM. The offered cofactor was 20 µmol x $g_{carrier}^{-1}$ and 15 µmol x $g_{carrier}^{-1}$ of NADH and FAD^+, respectively. All images show the overlay of fluorescence and brigthfield signals.

After testing the co-immobilization of NADH and FAD^+ on AG-G/PEI25, the self-sufficient biocatalyst was fabricated. Firstly, Tt-NOX was immobilized on AG/G by imine bonds. After PEI-coating, a reduction step was carried out to become covalent the binding of both Tt-NOX and PEI to AG/G. Finally, both cofactors were simultaneously co-immobilized onto polymeric bed by ion-exchange with the amino groups from the PEI. The colocalization of both two cofactors and Tt-NOX onto the same microbeads was evinced by CLSM (Figure 13). As far as we know, this is the first heterogeneous biocatalyst where two different cofactors were co-immobilized with an oxidase enzyme.

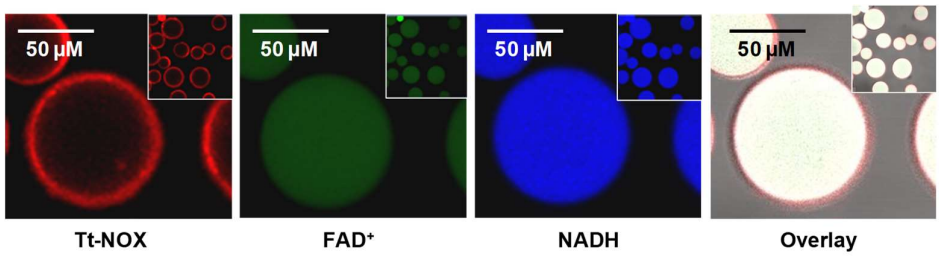

Figure 13. Colocalization of Tt-NOX, NADH and FAD^+ on AG-G/PEI25. The load of rhodamine-labeled Tt-NOX (red) was 1 mg x $g_{carrier}^{-1}$. The offered cofactor was 15 µmol x $g_{carrier}^{-1}$ and 20 µmol x $g_{carrier}^{-1}$ of FAD^+ (green) and NADH (blue), respectively.

Ultimately, *in operando* fuorescence microscopy analysis were employed not only to monitor the enzyme kinetics but also to follow the cofactor co-immobilization during the same experiment. To this end, a solution of free cofactors was added to a suspension of Tt-NOX immobilized on AG-G/PEI (Figure 14). As it was previously observed in Figure 12, most of the cofactor molecules (79.87 ± 0.64 % of NADH and 81.23 ± 5.96 % of FAD^+) were immobilized in less than 1 minute (Figure 14B, Figure 14C and Figure 14D). When the only cofactor added to the suspension was NADH, the cofactor was immobilized on the microbead and the fluorescence inside the microparticle remained stable along the time (Figure 14B). In the same way, FAD^+ persisted inside the microparticles without being lixiviated to the outside (Figure 14C). However, when both cofcators NADH and FAD^+ were added, the biocatalytic reaction was triggered (Figure 14D).

Since both redox forms $FADH_2$ and FAD^+ displayed a similar autofluorescence,[61] its autofluorescence inside the microparticles remained constant along the time after the cofactor immobilization. Contrarily, NADH fluorescence was diminished inside the microparticles due to the lower fluorescence of its oxidized form (NAD^+). These results confirm the intraparticle NADH oxidation catalyzed by the immobilized Tt-NOX. Noteworthy, as soon as NADH was immobilized, the redox reaction started (Figure 14D).

Figure 14D also suggests that the enzymatic activity was faster than the cofactor immobilization under the assayed conditions. These observations support that the cofactor is catalytically available for the enzyme as soon as it is co-immobilized.

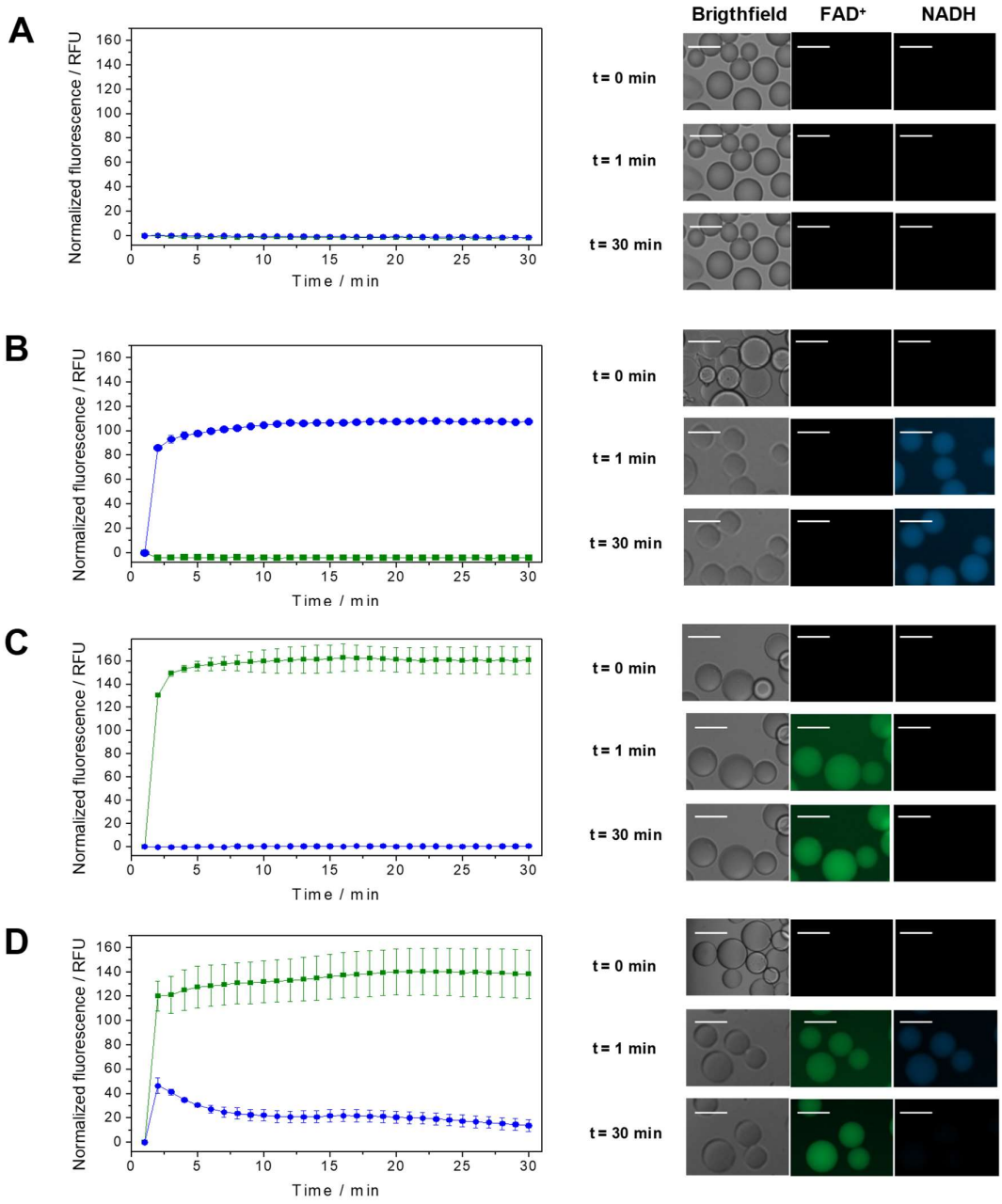

Figure 14. *In operando* monitoring of cofactors immobilization and NADH consumption by the self-sufficient heterogeneous biocatalysts. A) No cofactor was added to the suspension, only buffer. B) NADH was added. C) FAD^+ was added. D) Both cofactors were added. On the left side, the fluorescence values of FAD^+ (green squares) and NADH (blue circles) inside the microbeads (n=5) along the time. On the right side, fluorescence imaging during the reactions at different time points. The solution with the cofactors was added to the microbeads suspension just before the 1-minute image. White scale bars correspond to 100 µm.

In order to demonstrate that NADH did not disappeared because of NADH diffusion outside the microparticle, NADH fluorescence from the reaction bulk was measured after filtration of the reaction suspension (Figure 15).

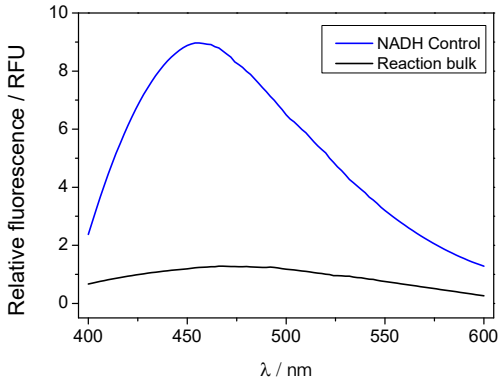

Figure 15. Demonstrating that NADH remained bound to the microparticle during the reaction. The NADH control is the supernatant after 1 hour of incubating AG-G and 20 μM NADH. The reaction bulk corresponds to the supernatant after 1 hour of the reaction with both cofactors co-immobilized and Tt-NOX co-immobilized on AG-G/PEI25.

4. CONCLUSION

We have introduced the successful fabrication of self-sufficient heterogeneous biocatalysts integrating enzymes and phosphorylated cofactors within the same porous microbeads through an innovative architecture where the enzymes and PEI are irreversibly bound to the solid surface, while the negatively charged cofactors are reversibly adsorbed to the cationic polymers through ion-exchange interactions. The micro-architecture was functional for several reaction cycles without adding exogenous cofactors, demonstrating its feasibility for sustainable processes. This strategy was expanded to co-immobilize two cofactors with an enzyme for first time. Thus, the optimal control to organize immobilized enzymes on the carrier has been of outstanding relevance to achieve the best catalytic properties of heterogeneous biocatalysts. Likewise, single-particle studies have provided useful information to develop more rational, reliable and reproducible proceedings when characterizing self-sufficient heterogeneous biocatalysts. Ultimately, the expansion of these co-immobilization strategies and single-particle approaches for more complex multi-enzymatic systems is a driving force to boost biocatalysis in different areas as chemical manufacturing, bioenergy and biosensing.

REFERENCES

1. Velasco-Lozano, S., Benítez-Mateos, A. I., López-Gallego, F. Co-immobilized phosphorylated cofactors and enzymes as self-sufficient heterogeneous biocatalysts for chemical processes. *Angewandte Chemie International Edition*. **2017**, *56*: 771-775.

2. Schmidt-Dannert, C., Lopez-Gallego, F. A roadmap for biocatalysis - functional and spatial orchestration of enzyme cascades. *Microb Biotechnol*. **2016**, *9*: 601-609.

3. Nestl, B. M., Hammer, S. C., Nebel, B. A., Hauer, B. New generation of biocatalysts for organic synthesis. *Angewandte Chemie International Edition*. **2014**, *53*: 3070-3095.

4. Sigrist, R., Costa, B. Z. D., Marsaioli, A. J., De Oliveira, L. G. Nature-inspired enzymatic cascades to build valuable compounds. *Biotechnology Advances*. **2015**, *33*: 394-411.

5. Malik, M. S., Park, E. S., Shin, J. S. Features and technical applications of ω-transaminases. *Applied Microbiology and Biotechnology*. **2012**, *94*: 1163-1171.

6. Simon, R. C., Richter, N., Busto, E., Kroutil, W. Recent developments of cascade reactions involving ω-transaminases. *ACS Catalysis*. **2014**, *4*: 129-143.

7. Liu, W., Wang, P. Cofactor regeneration for sustainable enzymatic biosynthesis. *Biotechnology Advances*. **2007**, *25*: 369-384.

8. Hollmann, F., Arends, I. W. C. E., Buehler, K. Biocatalytic redox reactions for organic synthesis: nonconventional regeneration methods. *ChemCatChem*. **2010**, *2*: 762-782.

9. Lin, B., Tao, Y. Whole-cell biocatalysts by design. *Microbial Cell Factories*. **2017**, *16*: 1-12.

10. Fessner, W. D. Systems Biocatalysis: Development and engineering of cell-free “artificial metabolisms” for preparative multi-enzymatic synthesis. *New Biotechnology*. **2015**, *32*: 658-664.

11. Truppo, M. D. Cofactor recycling for enzyme catalyzed processes. In Comprehensive chirality. Elsevier Science. **2012**.

12. Gestrelius, S., Månsson, M.-O., Mosbach, K. Preparation of an alcohol-dehydrogenase–NAD(H)–sepharose complex showing no requirement of soluble coenzyme for its activity. *European Journal of Biochemistry*. **1975**, *57*: 529-535.

13. El-Zahab, B., Donnelly, D., Wang, P. Particle-tethered NADH for production of methanol from CO2 catalyzed by coimmobilized enzymes. *Biotechnology and Bioengineering*. **2008**, *99*: 508-514.

14. Dicosimo, R., Mcauliffe, J., Poulose, A. J., Bohlmann, G. Industrial use of immobilized enzymes. *Chemical Society Reviews*. **2013**, *42*: 6437-6474.

15. Beauchamp, J., Vieille, C. Activity of select dehydrogenases with sepharose-immobilized N6-carboxymethyl-NAD. *Bioengineered*. **2015**, *6*: 106-110.

16. Vieille, C. Activity of select dehydrogenases with Sepharose-immobilized N6-carboxymethyl-NAD AU - Beauchamp, Justin. *Bioengineered*. **2015**, *6*: 106-110.

17. Ji, X., Wang, P., Su, Z., Ma, G., Zhang, S. Enabling multi-enzyme biocatalysis using coaxial-electrospun hollow nanofibers: Redesign of artificial cells. *Journal of Materials Chemistry B*. **2014**, *2*: 181-190.

18. Fu, J. *et al.* Multi-enzyme complexes on DNA scaffolds capable of substrate channelling with an artificial swinging arm. *Nature Nanotechnology*. **2014**, *9*: 531-536.

19. Heidlindemann, M., Rulli, G., Berkessel, A., Hummel, W., Gröger, H. Combination of asymmetric organo- and biocatalytic reactions in organic media using immobilized catalysts in different compartments. *ACS Catalysis*. **2014**, *4*: 1099-1103.

20. Da Silva, E. S., Gómez-Vallejo, V., Llop, J., López-Gallego, F. Efficient nitrogen-13 radiochemistry catalyzed by a highly stable immobilized biocatalyst. *Catalysis Science and Technology*. **2015**, *5*: 2705-2713.

21. Rulli, G., Heidlindemann, M., Berkessel, A., Hummel, W., Gröger, H. Towards catalyst compartimentation in combined chemo- and biocatalytic processes: Immobilization of alcohol dehydrogenases for the diastereoselective reduction of a β-hydroxy ketone obtained from an organocatalytic aldol reaction. *Journal of Biotechnology*. **2013**, *168*: 271-276.

22. Ji, X., Su, Z., Wang, P., Ma, G., Zhang, S. Tethering of nicotinamide adenine dinucleotide inside hollow nanofibers for high-yield synthesis of methanol from carbon dioxide catalyzed by coencapsulated multienzymes. *ACS Nano*. **2015**, *9*: 4600-4610.

23. Benítez-Mateos, A. I., Nidetzky, B., Bolivar, J. M., López-Gallego, F. Single-particle studies to advance the characterization of heterogeneous biocatalysts. *ChemCatChem*. **2018**, *10*: 654-665.

24. Rodrigues, R. C., Ortiz, C., Berenguer-Murcia, Á., Torres, R., Fernández-Lafuente, R. Modifying enzyme activity and selectivity by immobilization. *Chemical Society Reviews*. **2013**, *42*: 6290-6307.

25. Luo, H. *et al.* Microenvironmental pH changes in immobilized cephalosporin C acylase during a proton-producing reaction and regulation by a two-stage catalytic process. *Bioresource Technology*. **2017**, *223*: 157-165.

26. Xiu, G.-H., Jiang, L., Li, P. Mass-transfer limitations for immobilized enzyme-catalyzed kinetic resolution of racemate in a batch reactor. *Industrial & Engineering Chemistry Research*. **2000**, *39*: 4054-4062.

27. Kheirolomoom, A., Khorasheh, F., Fazelinia, H. Influence of external mass transfer limitation on apparent kinetic parameters of penicillin G acylase immobilized on nonporous ultrafine silica particles. *Journal of Bioscience and Bioengineering*. **2002**, *93*: 125-129.

28. Bolivar, J. M., Consolati, T., Mayr, T., Nidetzky, B. Quantitating intraparticle O_2 gradients in solid supported enzyme immobilizates: Experimental determination of their role in limiting the catalytic effectiveness of immobilized glucose oxidase. *Biotechnology and Bioengineering*. **2013**, *110*: 2086-2095.

29. Bolivar, J. M., Consolati, T., Mayr, T., Nidetzky, B. Shine a light on immobilized enzymes: real-time sensing in solid supported biocatalysts. *Trends in Biotechnology*. **2013**, *31*: 194-203.

30. Bolivar, J. M., Schelch, S., Pfeiffer, M., Nidetzky, B. Intensifying the O_2-dependent heterogeneous biocatalysis: Superoxygenation of solid support from H_2O_2 by a catalase tailor-made for effective immobilization. *Journal of Molecular Catalysis B: Enzymatic*. **2016**, *134*: 302-309.

31. García-García, P., Rocha-Martin, J., Fernandez-Lorente, G., Guisan, J. M. Co-localization of oxidase and catalase inside a porous support to improve the elimination of hydrogen peroxide: Oxidation of biogenic amines by amino oxidase from Pisum sativum. *Enzyme and Microbial Technology*. **2018**, *115*: 73-80.

32. Li, Z., Zhang, Y., Su, Y., Ouyang, P., Ge, J., Liu, Z. Spatial co-localization of multi-enzymes by inorganic nanocrystal–protein complexes. *Chemical Communications*. **2014**, *50*: 12465-12468.

33. Rocha-Martín, J., Rivas, B. D. L., Muñoz, R., Guisán, J. M., López-Gallego, F. Rational co-immobilization of bi-enzyme cascades on porous supports and their applications in bio-redox reactions with in situ recycling of soluble cofactors. *ChemCatChem*. **2012**, *4*: 1279-1288.

34. Dos Santos, J. C. S. *et al.* Characterization of supports activated with divinyl sulfone as a tool to immobilize and stabilize enzymes via multipoint covalent attachment. Application to chymotrypsin. *RSC Advances*. **2015**, *5*: 20639-20649.

35. Montes, T. *et al.* Improved stabilization of genetically modified penicillin G acylase in the presence of organic cosolvents by co-immobilization of the enzyme with polyethyleneimine. *Advanced Synthesis & Catalysis*. **2007**, *349*: 459-464.

36. Mateo, C. *et al.* Improvement of enzyme properties with a two-step immobilizaton process on novel heterofunctional supports. *Biomacromolecules*. **2010**, *11*: 3112-3117.

37. Rocha-Martin, J. *et al.* Purification, immobilization and stabilization of a highly enantioselective alcohol dehydrogenase from Thermus thermophilus HB27 cloned in E. coli. *Process Biochemistry*. **2009**, *44*: 1004-1012.

38. Schütte, H., Flossdorf, J., Sahm, H., Kula, M. R. Purification and properties of formaldehyde dehydrogenase and formate dehydrogenase from Candida boidinii. *European Journal of Biochemistry*. **1976**, *62*: 151-160.

39. Rocha-Martín, J. *et al.* New biotechnological perspectives of a NADH oxidase variant from Thermus thermophilus HB27 as NAD^+-recycling enzyme. *BMC Biotechnology*. **2011**, *11*: 1-11.

40. Bradford, M. M. A rapid and sensitive method for the quantitation of microgram quantities of protein utilizing the principle of protein-dye binding. *Analytical Biochemistry*. **1976**, *72*: 248-254.

41. Fernandez-Lafuente, R. *et al.* Preparation of activated supports containing low pK amino groups. A new tool for protein immobilization via the carboxyl coupling method. *Enzyme and Microbial Technology*. **1993**, *15*: 546-550.

42. Guisan, J. M. *et al.* Preparation of new lipases derivatives with high activity–stability in anhydrous media: adsorption on hydrophobic supports plus hydrophilization with polyethylenimine. *Journal of Molecular Catalysis B: Enzymatic*. **2001**, *11*: 817-824.

43. López-Gallego, F. *et al.* Preparation of a robust biocatalyst of d-amino acid oxidase on sepabeads supports using the glutaraldehyde crosslinking method. *Enzyme and Microbial Technology*. **2005**, *37*: 750-756.

44. Palomo, J. M., Segura, R. L., Fernandez-Lorente, G., Fernandez-Lafuente, R., Guisán, J. M. Glutaraldehyde modification of lipases adsorbed on aminated supports: A simple way to improve their behaviour as enantioselective biocatalyst. *Enzyme and Microbial Technology*. **2007**, *40*: 704-707.

45. Bickmore, B. R., Hochella Jr, M. F., Bosbach, D., Charlet, L. Methods for performing atomic force microscopy imaging of clay minerals in aqueous solutions. *Clays and Clay Minerals*. **1999**, *47*: 573-581.

46. Lin, D. Q., Brixius, P. J., Hubbuch, J. J., Thömmes, J., Kula, M. R. Biomass/adsorbent electrostatic interactions in expanded bed adsorption: A zeta potential study. *Biotechnology and Bioengineering*. **2003**, *83*: 149-157.

47. Wang, F., Liu, P., Nie, T., Wei, H., Cui, Z. Characterization of a polyamine microsphere and its adsorption for protein. *International Journal of Molecular Sciences*. **2013**, *14*: 17-29.

48. Moore, J. C., Savile, C. K., Pannuri, S., Kosjek, B., Janey, J. M. Industrially relevant enzymatic reductions. In Comprehensive Chirality. Elsevier Science. **2012**, 318-341.

49. Liu, W., Wang, P. Cofactor regeneration for sustainable enzymatic biosynthesis. *Biotechnology Advances*. **2007**, *25*: 369-384.

50. Mateo, C. *et al.* Glyoxyl agarose: A fully inert and hydrophilic support for immobilization and high stabilization of proteins. *Enzyme and Microbial Technology*. **2006**, *39*: 274-280.

51. Montes, T. *et al.* Improved stabilization of genetically modified penicillin G acylase in the presence of organic cosolvents by co-immobilization of the enzyme with polyethyleneimine. *Advanced Synthesis and Catalysis*. **2007**, *349*: 459-464.

52. Van Roon, J., Beeftink, R., Schroën, K., Tramper, H. Assessment of intraparticle biocatalytic distributions as a tool in rational formulation. *Current Opinion in Biotechnology*. **2002**, *13*: 398-405.

53. Van Roon, J. L., Joerink, M., Rijkers, M. P. W. M., Tramper, J., P. H. Schroën, C. G., Beeftink, H. H. Enzyme distribution derived from macroscopic particle behavior of an industrial immobilized penicillin-G acylase. *Biotechnology Progress*. **2003**, *19*: 1510-1518.

54. Nabavi Zadeh, P. S., Åkerman, B. Distribution of immobilized enzymes on the surface and into the mesoporous silica particle. *Biophysical Journal*. **2016**, *110*: 550.

55. Bolivar, J. M., Hidalgo, A., Sánchez-Ruiloba, L., Berenguer, J., Guisán, J. M., López-Gallego, F. Modulation of the distribution of small proteins within porous matrixes by smart-control of the immobilization rate. *Journal of Biotechnology*. **2011**, *155*: 412-420.

56. Pinto, M. C., Macías, P. Determination of intraparticle immobilized enzyme distribution in porous support by confocal scanning microscopy. *Biotechnology Techniques*. **1995**, *9*: 481-486.

57. Hossain, M. M., Do, D. D. Effects of nonuniform immobilized enzyme distribution in porous solid supports on the performance of a continuous reactor. *The Chemical Engineering Journal*. **1987**, *34*: 35-47.

58. Ladero, M., Santos, A., García-Ochoa, F. Diffusion and chemical reaction rates with nonuniform enzyme distribution: An experimental approach. *Biotechnology and Bioengineering*. **2001**, *72*: 458-467.

59. Dennis, K. E., Clark, D. S., Bailey, J. E., Cho, Y. K., Park, Y. H. Immobilization of enzymes in porous supports: Effects of support–enzyme solution contacting. *Biotechnology and Bioengineering*. **1984**, *26*: 892-900.

60. Virgen-Ortíz, J. J., Dos Santos, J. C. S., Berenguer-Murcia, Á., Barbosa, O., Rodrigues, R. C., Fernandez-Lafuente, R. Polyethylenimine: a very useful ionic polymer in the design of immobilized enzyme biocatalysts. *Journal of Materials Chemistry B*. **2017**, *5*: 7461-7490.

61. Galbán, J., Sanz-Vicente, I., Navarro, J., De Marcos, S. The intrinsic fluorescence of FAD and its application in analytical chemistry: a review. *Methods and Applications in Fluorescence*. **2016**, *4*: 1-19.

Chapter 5

Expanding the concept of artificial metabolic cells to ketoreductase-based biocatalysts

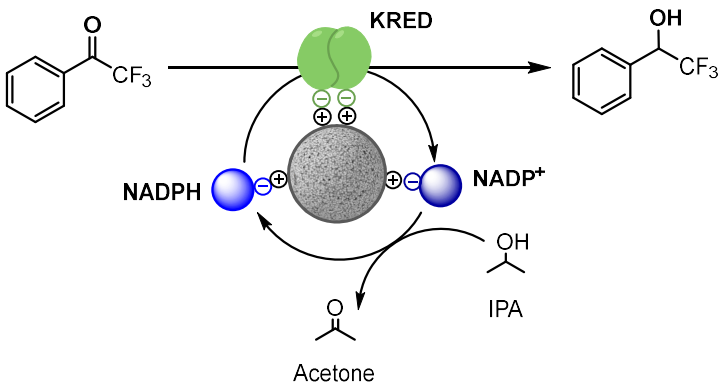

Cell-free and self-sufficient biocatalytic systems are here expanded to ketoreductases. Particularly, a commercially available NADPH-dependent ketoreductase was co-immobilized with NADPH to catalyze the asymmetric reduction of prochiral ketones without exogenous addition of the cofactor. As a result, the immobilized cofactor is accessible and thus efficiently recycled by the same enzyme inside the porous structure without diffusing out to the bulk as demonstrated by single-particle *in operando* studies. As a proof-of-concept, the self-sufficient heterogeneous biocatalyst was integrated into a flow-plug reactor for the continuous synthesis of one model secondary alcohol, giving rise to 97-112 g x L^{-1} x day^{-1} space-time yield. Furthermore, the immobilized cofactor accumulated a total turnover number of 1076 for 120 hours. Encouraged by these results, the same biocatalyst architecture was also applied to another commercial ketoreductase exploited in the preparation of key optically pure pharmaceutical precursors. These examples contribute to the handful of self-sufficient heterogeneous biocatalysts co-immobilizing both enzyme and cofactor.

This work was previously published in *Chemistry - A European Journal*[1] and *Advanced Synthesis and Catalysis*.[2]

1. INTRODUCTION

Asymmetric reduction of ketones is an elegant synthetic reaction because it enables to access highly-demanded secondary alcohols with quantitative yields without requiring deracemization steps.[3] The greatest challenges of this reaction are finding highly selective catalysts that yield exclusively one enantiomer (ee > 99%) and performing the synthetic reaction in an economically viable fashion. The selectivity is extremely important for pharmaceutical chemistry where traces of the other enantiomer can cause fatalities in public health as sadly confirmed by the thalidomide tragedy.[4] In this context, biocatalysis emerges as an enabling technology to address cost-effective asymmetric processes where enantiopurity of the products is compulsory.[5] Ketoreductases (KRED) (EC 1.1.1.X) have proven an excellent enantioselectivity for the asymmetric reduction of large variety of ketones with excellent yields and productivities.[6, 7] Whole-cell biocatalysts are widely involved in low-cost reactions to produce chiral alcohols from ketones by using endogenous KREDs.[8-11] However, whole-cell biotransformations are still time-consuming and often require purification steps that turn the process more expensive and hard to manage at industrial scale. Isolated KRED enzymes are an attractive alternative, but industrial implementation is often hampered by their cofactor dependency that requires the exogenous addition of very expensive redox cofactors endangering the economic viability of the process.[12, 13] This issue becomes even more dramatic considering that the most exploited KREDs[14-16] in large scale processes (i.e KRED from *Lactobacillus kefiri)*[17] use NADPH whose price is an order of magnitude higher than the price of NADH.[6] Moreover, the former cofactor is significantly less stable than the latter one. Therefore, both price and stability considerably limit the industrial application of NADPH-dependent enzymes.[17, 18]

Utilization of synthetic and cheaper analogues of nicotinamide cofactors have emerged as alternative to NAD(P)H.[19] Nevertheless, the enzymatic efficiencies towards these artificial cofactors are substantially lower than towards the natural ones. Alternatively, a more consolidated strategy is based on enzymatic or chemical cofactor regeneration that reduces the amount of needed cofactor at the expense of sacrificing reductants.[18, 20] In both strategies, we still need to exogenously add the cofactor increasing the process costs and complicating the work-up once the reaction is completed. In the 80´s, chemical engineers started to tether cofactors to large polymers achieving the successful integration of enzymatic systems dependent upon NAD(P)H into ultrafiltration membrane reactors for continuous reduction processes without adding exogenous cofactors.[13, 21-23] These systems reached cofactor total turnover numbers

(TTN) of up to 7000. Nevertheless, the high cost of the ultra- and nano-filtration membranes jeopardizes the economic viability of such processes. As shown in Chapter 4, NAD^+/NADH and enzymes can be efficiently co-immobilized on solid carriers giving raise to self-sufficient heterogeneous biocatalysts that do not require exogenous cofactor supply during the reaction.[15, 24-30] Furthermore, the immobilization of enzyme eases the reaction work-up and may improve the biocatalyst properties when the immobilization protocol is properly selected. In an industrial context, the most promising approach to fabricate self-sufficient heterogeneous biocatalyst relies on the electrostatic adsorption of phosphorylated cofactors and enzymes to solid and porous materials.[15, 26, 28, 29] This strategy has been proven successful for asymmetric reductions catalyzed by KREDs in organic media, but fails in aqueous media due to the lixiviation of both cofactors and enzymes.[15] Hence, such equilibrium makes the cofactor accessible for the immobilized enzyme but simultaneously may cause the cofactor lixiviation to the reaction bulk, overall when buffered media is used. As explained in Chapter 4, our group has originally designed a versatile and simple architecture for the fabrication of self-sufficient heterogeneous biocatalysts based on commercial carriers coated with PEI. In this architecture, enzymes and PEI are irreversibly bound to the agarose microbeads leaving the enzymes surrounded by NAD^+ ionically absorbed to cationic polymer.[27]

In the present chapter, we have collaborated with the company EntreChem S.L. to optimize the co-immobilization of commercially available KREDs (P1-A04 and P2-D11). KRED P1-A04 presents a wide substrate scope, an exquisite *R*-selectivity and self-regenerates the reduced cofactor by oxidizing IPA to acetone in a parallel reaction.[6, 31] By using porous agarose microbeads activated with tertiary amine groups, both KRED and NADPH were co-immobilized and co-localized on the same surface, enabling the enzymatic utilization of the cofactor and avoiding its lixiviation. Final operational studies demonstrated the re-usability and efficiency of these self-sufficient heterogeneous biocatalysts.

2. EXPERIMENTAL SECTION

2.1. Materials

SYPRO® Orange Protein Gel Stain, PEI, ethylendiamine, FITC, 2,2,2-trifluoroacetophenone (TFAF), 1-acetonaphtone (AN), isopropanol (IPA), DTT, polyethileneimine 600-1000 kDa (PEI600), sodium periodate and amicon ultra 0.5 mL

centrifugal filters 10 kDa were acquired from Sigma-Aldrich (St. Louis, IL). Ketoreductases P1-A04 and P2-D11 were purchased from Codexis. Nicotinamide-adenine-dinucleotide-phosphate reduced sodium salt (NADPH) was purchased from GERBU Biotechnik GmbH (Wieblingen, Germany). Agarose 6BCL and 4BCL were purchased from ABT (Madrid, Spain), DEAE-sepharose (AG-DEAE) was purchased from GE-healthcare (Little Chalfont, UK) and epoxy methacrylate microbeads Lifetech ECR8204 were kindly donated by Purolite Ltd (Llantrisant, UK). Micro Bio-spinTM chromatographic columns were from BIORAD. 8-well µslides were purchased from ibidi (Planegg, Germany). All other salts and reagents were of analytical grade.

2.2. Methods

2.2.1. Activation of carriers:

- AG-DVS (6BCL agarose activated with vinyl groups). This carrier was prepared by strictly following the protocol described by dos Santos *et al.*[32] using plain agarose.
- AG-DEAE/G (6BCL agarose activated with glyoxyl and tertiary amine groups). This heterofunctional carrier was prepared according to the protocol previously described by Mateo *et al.*[33] using agarose as plain carrier that finally was activated with 23 µmol of tertiary amines and 75 µmol of glyoxyl groups per gram of carrier.
- AG-PEI600 (4BCL agarose coated with high molecular weigth PEI 600-1000kDa).This carrier was prepared using plain agarose as described elsewhere.[34]
- Pu-G (Purolite lifetech ECR8204 microbead activated with glyoxyl groups). We followed an adapted protocol described elsewhere.[33] In brief, 10 grams of commercial carrier were incubated with 100 mL of 0.5 M sulphuric acid for 2 hours under gentle stirring at room temperature in order to hydrolyze the epoxy groups. Then, the carrie**r** was thoroughly washed with distilled water and further incubated with 100 mL of 10 mM sodium periodate to oxidize the vicinal diols resulted from the acidic hydrolysis of the starting epoxy groups. Finally, the carrier was washed with excess of water and stored at 4 ºC.
- Pu-DEAE/E (Purolite lifetech ECR8204 microbead activated with epoxy and diethyl-aminoethyl groups). This carrier was prepared and quantified by adapting the protocol described by Bolivar *et al.*[35] 10 grams of Purolite lifetech

ECR8204 microbeads were incubated with 100 mL of 1 M ethylendiamine at pH 10 for 2 hours under gentle stirring at room temperature. Then, the solid material was washed with an excess of water to remove the unreacted ethylendiamine. The resulting carrier contained 29 μmol of amino groups and 29 μmol of epoxy groups per gram of carrier.

2.2.2. Protein immobilization

Typically, 1 mL of 0.025-0.65 mg x mL^{-1} KRED P1-A04 were incubated with 100 mg of each carrier and incubated for 1 hour at room temperature and under the specific buffer conditions for each immobilization protocol. The immobilization on AG-DVS, AG-DEAE, AG-PEI600, AG-DEAE/G and Pu-DEAE/E was carried with an enzyme solution prepared in 10 mM sodium phosphate pH 7. For the immobilization on Pu-G, the enzyme was prepared in 100 mM sodium bicarbonate at pH 10 or in 100 mM sodium phosphate and 10 mM DTT at pH 8. Upon the enzyme immobilization on carrier containing glyoxyl groups, 100 mg of microbeads were incubated with 1 mL of $NaBH_4$ (1 mg x mL^{-1}) in 100 mM sodium bicarbonate at pH 10 and 4 ºC for 30 minutes in order to reduce the enzyme-carrier imine bonds into irreversible secondary amine bonds. In case of KRED P2-D11, 1 gram of AG-DEAE was incubated with 10 mL of 0.1–0.65 mg x mL^{-1} enzyme in 10 mM sodium phosphate pH 7.0 for 1 hour at room temperature. For each immobilization experiment, the enzyme solution was incubated under the same immobilization conditions but without the carrier as blank sample.

2.2.3. Parameters of immobilized enzymes

The immobilization yield, the specific activity and the final expressed activity were calculated as described in Chapter 4 (page 93) unless otherwise specified.

2.2.4. Protein quantification

The Bradford assay was carried out following the protocol described in Chapter 4 (page 91).

2.2.5. Enzymatic assays

The activity of KRED was spectrophotometrically measured by monitoring the absorbance at 340 nm along the time, which decreased because of the enzymatic reduction of NADPH. The enzymatic assays were carried out in a Varioskan™ Flash

Multimode Reader using 96-well plates. For both soluble and immobilized enzymes the activity was measured under orbital shaking integrated into the reader. One unit of activity was defined as the amount of enzyme that was required to either reduce or oxidize 1 µmol of NADPH at 25 ºC and the corresponding pH.

- KRED P1-A04 activity. 200 µL of a reaction mixture containing 10 mM TFAF and 0.25 mM NADPH in 10mM sodium phosphate buffer at pH 7 was incubated with 20 µL of enzymatic solution or suspension at 25 ºC.
- KRED P2-D11 activity. 200 µL of a reaction mixture containing 1 mM AN, 1 mM $MgCl_2$ and 0.25 mM NADPH in 10 mM sodium phosphate buffer at pH 7 was incubated with 20 µL of enzymatic solution or suspension at 25 ºC.

2.2.6. Thermal and isopropanol inactivation:

- Thermal Stability. Thermal stability was determined by incubating soluble and immobilized KRED P1-A04 in 10 mM sodium phosphate buffer at pH 7 at 40 °C. Samples were withdrawn at different incubation times and the residual enzymatic activity was measured as described above. The experimental data were fitted to different first-kinetic equation and first-kinetic equation with residual activity using Origin 8.0.
- Organic solvent stability. Enzyme stability against IPA was determined by incubating soluble and immobilized enzyme in 10 mM sodium phosphate buffer at pH 7 containing IPA. For KRED P1-A04, 1.55% of IPA was added to the incubation at 25 ºC. In case of KRED P2-D11, the incubation was carried out with 17% of IPA at 30 ºC. Samples were withdrawn at different times and the residual enzymatic activity was measured as described above.

2.2.7. Co-immobilization of NADPH on AG-DEAE

1 gram of AG-DEAE immobilizing KRED were incubated with 10 mL of 1 mM NADPH in 10 mM Tris-HCl at pH 7 and room temperature. Aliquots of supernatant were withdrawn after 1 hour and spectrophotometrically measured at 340 nm to quantify the adsorption of NADPH to the carrier. After the adsorption process, the solid samples were washed with 10 volumes of 10 mM Tris-HCl at pH 7 and utilized in further experiments. The cofactor load and the cofactor immobilization yield were calculated as described in Chapter 4 (page 94).

2.2.8. Fluorescence studies

- FITC-labeling of KRED P1-A04. The enzyme was labeled with FITC following the protocol described in Chapter 3 (page 58). The labeled KRED P1-A04 was used for further localization studies of the immobilized enzyme by CLSM. The images were analyzed with the softwares FIJI and ZEN2012.

- Intrinsic protein fluorescence. Intrinsic fluorescence of 10 µg of soluble or immobilized KRED P1-A04 ($1mg_{KRED}$ x $g_{carrier}^{-1}$) prepared in 25 mM sodium phosphate buffer at pH 7 was measured in 96-well plates. The study was performed by exciting at 280 nm and recording the emission spectrum at 300-500 nm in a Varioskan™ Flash Multimode reader at 25º C.

- Thermal shift assay. 0.5 µg x mL^{-1} of soluble or 0.23 µg x mL^{-1} of immobilized KRED P1-A04 in 25 mM sodium phosphate buffer and 0.3% of SYPRO® Orange at pH 7 were incubated in a StepOnePlus™ Real-Time PCR System by using a temperature ramp program from 25-95°C with a ramp rate of 0.5 °C x min^{-1}.

2.2.9. Single-microbead kinetics (*in operando* experiments)

Different redox reactions were performed under the fluorescence microscope using 8-well µslides. 184 µL of 1:200 (w/v) suspension of the self-sufficient heterogeneous biocatalyst ($6.5mg_{KRED\ P1-A04}$ and 10 μmol_{NADPH} x $g_{carrier}^{-1}$) in 10 mM Tris-HCl, 1 mM $MgCl_2$ at pH 7.3 were placed in the wells. Reactions were triggered with 36 µL of substrate mix to achieve a well concentration of 1 mM TFAF (in acetonitrile) and 17% IPA. Substrate mixtures with both substrates, with only buffer, with only TFAF and with only IPA were used to trigger different *in operando* experiments. The fluorescence measurements of NADPH were carried out every 20 seconds until 20 minutes in a cell axio observer microscope (λ_{ex}: 365 nm, λ_{em}: 402-448 nm) at room temperature. Images were processed with the software ZEN2012.

- Image analytics. The molecular imaging platform from CIC biomaGUNE carried out the following analysis. The 60 frames were analyzed by using MATLAB Release R2012b (The MathWorks, Inc., Natick, Massachusetts, United States). The reference area occupied by each microbead was calculated by segmenting the brightfield image, which was also considered as the functional area occupied by the autofluorescence of the immobilized NADPH. Pixel-wise time

courses extraction was performed and fitted to a first-order reaction equation ($F=F_o*e^{-k*t}$; F is the fluorescence per pixel at each time, F_o is the fluorescence per pixel at t = 0 and t is the time of each frame). Statistically, only those pixels that present fittings with $R^2 > 0.95$ were considered. Then, the pixel-wise initial rate (V_o) was determined from the linear regression fitting considering only the time frames where the microbead fluorescence was higher than 80% of the microbead fluorescence at time 0. The relative V_o per pixel were mapped by normalizing the V_o of each pixel regarding to the maximum V_o within the same microbead (see Figure 8).

2.2.10. General procedure for the continuous asymmetric reduction of TFAF by KRED P1-A04

0.28 g of self-sufficient heterogeneous biocatalyst (6.5mg_{KRED} and 10 μmol_{NADPH} x $g_{carrier}^{-1}$) were packed into a column (2 x 0.4 cm) and connected to a flow system driven by a syringe pump. A reaction mixture containing 10 mM TFAF, 1 mM $MgCl_2$ and 17% IPA in 10 mM Tris-HCl at pH 7 passed through the column at different flow rates (50-200 µL x min^{-1}) and 25 ºC. Different samples were collected from the outlet of the system and analyzed by UPLC.

2.2.11. In-batch asymmetric reduction of AN by KRED P2-D11

In a micro-chromatographic column, a reaction mixture containing 27 mM AN, 17% IPA and 1 mM $MgCl_2$ in 10 mM Tris-HCl at pH 7.0 was incubated with 30 mg of self-sufficient heterogeneous biocatalysts (6.5 mg_{KRED} and 10 $mmol_{NADPH}$ x $g_{carrier}^{-1}$) and maintained under gentle rotational agitation (50 rpm) at 25 ºC. As control reaction, same amount of KRED immobilized on AG-DEAE and soluble and exogenous NADPH were mixed in the same conditions. The reaction was stopped by vacuum filtration. Next, the immobilized biocatalyst was washed with 10 volumes of 10 mM Tris-HCl at pH 7.0 to be reused in the next batch cycle.

2.2.12. General procedure for the continuous asymmetric reduction of AN by KRED P2-D11

1 gram of self-sufficient heterogeneous biocatalyst (5.85 mg_{KRED} and 10 $mmol_{NADPH}$ x $g_{carrier}^{-1}$) were packed into a column (230.4 cm) and connected to a flow system driven by a syringe pump. A reaction mixture containing 27 mM AN, 1 mM MgCl, 4.9% DMSO

and 17% IPA in a 10 mM Tris-HCl buffer solution at pH 7.0 passed through the column at different flow rates (50-200 µL x min^{-1}) and 25 ºC. Different samples were collected from the outlet of the system and analyzed by UPLC.

2.2.13. HPLC analysis:

- Asymmetric reduction of TFAF: The reaction products were monitored by HPLC coupled to a spectrophotometer unit (UPLC Waters or 1120 compact LC Agilent). Isocratic flow of 0.3 mL x min^{-1} with a mobile phase of 0.1% formic acid in water/acetonitrile (65:35) through an ACQUITY UPLC BEH C18 column (50 x 2.1 mm) was used to determine the conversion at 254 nm. The retention time of the product from the asymmetric reduction of TFAF was 3.8 minutes.

- Asymmetric reduction of AN: The reaction products were monitored in an Agilent chromatographic system in collaboration with Prof. Berglund´s group. A reversed phase column (Zorbax Eclipse XDB-C18, RR, 1.8 µm, 4.6 x 50 mm, Agilent) was used with acetonitrile and 0.1% trifluoroacetic acid in water as solvents. Samples were eluted with three linear gradients from 10% to 60% acetonitrile during 5.70 min, followed by another from 60% to 100% Acetonitrile during 0.5 min and a third gradient from 100% to 10% acetonitrile during 1.90 min, at flow rate of 2 mL x min^{-1}. Detection and spectral characterization of peaks (UV absorption maximum at 210 nm) were performed with a diode array detector and ChemStation Rev.B.03.01 software (Agilent). The *ee* was determined by using an OJ-H column with 0.8 mL x min^{-1} flow rate and using 90:60 Hex: *i*-PrOH at 40 ºC. The retention times were 13.8 minutes (*S*-product) and 18.8 minutes (*R*-product) at 215 nm.

3. RESULTS AND DISCUSSION

3.1. Immobilization of KRED on different porous carriers

Even though the commercial supplier of KRED cannot disclose any sequence and structural information of these enzymes, KRED P1-A04 was immobilized on porous microbeads using 7 immobilization protocols that involved 6 different immobilization chemistries and two type of materials; crosslinked porous agarose and polyacrylic porous microbeads with different pore size and particle size (see Chapter 1, Table 1 for more information). Commercial agarose and methacrylate microbeads were activated

with one or two different reactive groups according to literature procedures.[32-35] An empirical approach was followed until finding the best surface and the best immobilization chemistry to maximize the enzyme loading (mg x $g_{carrier}^{-1}$) and the volumetric activity (U x $g_{carrier}^{-1}$) for the asymmetric reduction of TFAF as model substrate and using IPA as sacrificing substrate for the *in situ* NADPH recycling (Table 1).

Table 1. Immobilization parameters of KRED P1-A04 on different carriers.

Name	Reactive group	Immobilization chemistry	Protein load (mg x g^{-1})	Immobilization yield (%)	Conversion (%)
Pu-G	Aldehyde	Covalent irreversible bonds at pH 10 followed by a reduction step	0.24	95	0
	Aldehyde in presence of thiols	Covalent irreversible bonds at pH 8 followed by reduction step	0.23	92	0
AG-DVS	Divinyl-Sulphone	Covalent irreversible bonds at pH 8	0.13	53	0
AG-DEAE	Diethyl-aminoethyl	Reversible Ionic bonds	0.25	100	98
AG-PEI600	Poly-ethylenimine		0.15	62	9
Pu-A/E	Primary amines and epoxy	Ionic and irreversible covalent bonds at pH 8	0.23	93	1.5
AG-DEAE/G	Diethyl-aminoethyl and aldehydes	Ionic and irreversible covalent bonds at pH 10 followed by reduction step	0.25	100	46

In all cases 0.25 mg of KRED were offered per gram of carrier. Conversion was determined by incubating 100 mg of immobilized enzyme with 20 mM TFAF, 1 mM NADPH, 1 mM $MgCl_2$ in 10 mM KH_2PO_4 at pH 7 and 25 ºC during 14 hours (rotational shaking 50 rpm). Equal amount of soluble enzyme was incubated under the same reaction conditions achieving 87% of conversion.

The immobilization of KRED P1-A04 on Pu-G (methacrylate microbeads activated with aldehyde groups) under alkaline conditions yielded 100%, but the immobilized enzyme lost all its initial activity. The alkaline pH may cause the enzyme inactivation as occurs with other enzymes immobilized on agarose microbeads through the same chemistry and under similar conditions.[36] However, when KRED P1-A04 was immobilized on the same carrier at pH 8 in presence of thiols to favour the covalent immobilization through the aldehyde chemistry at neutral pH,[37] the immobilization yield was >90% but immobilized enzyme also became inactive. Therefore, the enzyme inactivation must be due to other reasons rather than the pH. The aldehyde chemistry requires a mild

reduction step upon immobilization to turn the reversible imine enzyme-carrier bonds into irreversible secondary amines. Such reduction step might cause the enzyme inactivation upon the immobilization as observed with other enzymes.[15, 38] Furthermore, the enzyme could be dramatically inactivated upon their immobilization on polyacrilyc microbeads because of the hydrophobic nature of the carrier. In order to overcome these two issues, a more hydrophilic and biocompatible material such agarose microbeads with vinyl groups (AG-DVS) was activated in order to enable the enzyme immobilization under pH 8 avoiding the reduction step.[32] Unfortunately, by using AG-DVS, the immobilization yield was lower than 40% and reaction product was not observed (Table 1). These data indicate that the enzyme does not tolerate the covalent immobilization because it may lose some structural flexibility required for the catalysis, which may explain the dramatic activity reduction upon the immobilization.

In the light of these unsatisfactory results, KRED P1-A04 was alternatively immobilized through a reversible chemistry based on ionic interactions between acid residues on the protein surface (Asp and Glu) and cationic groups on the carrier surface. To this end, two types of agarose-based cationic carriers were tested. Firstly, agarose microbeads activated with PEI600 containing a polymeric bed of primary, secondary and tertiary amine groups positively charged (AG-PEI600) were used, based in the previous architectures exposed in Chapter 4. Secondly, a commercial carrier based on a monolayer of tertiary amine groups (AG-DEAE) was tested. The positive surface allowed a rapid immobilization of KRED P1-A04 with high yields although the type of surface was decisive to recover high enzyme activity upon the immobilization process.

While the KRED P1-A04 immobilized on AG-PEI600 only transformed 9% of substrate after 14 hours, the same enzyme immobilized on AG-DEAE achieved 98% conversion under the same conditions (Table 1). Noteworthy, the same amount of soluble enzyme under the same conditions reached 82% conversion. It has been widely demonstrated that AG-PEI600 binds proteins stronger and more three-dimensionally than AG-DEAE though the immobilization on both carriers is driven by reversible ionic interactions.[34] Such stronger and 3D binding promoted by the PEI bed may either limit the protein conformational flexibility required for the enzymatic catalysis or cause negative structural distortions that reduce enzyme activity. However, the monolayer of tertiary amine groups displayed in the AG-DEAE surface seems to establish protein-carrier interactions strong enough to anchor the protein to the solid phase, but weak enough to provide KRED P1-A04 with some conformational flexibility for its optimal performance, without inducing negative structural rearrangements. Similar insights were found for

other oxidoreductases whose catalytic mechanism demands high structural flexibility such as the nitrate reductase that was significantly more active when immobilized on AG-DEAE than on AG-PEI600.[39] To support that KRED P1-A04 did not undergo any structural distortion upon its immobilization on AG-DEAE, we measured the intrinsic fluorescence spectrum of this protein in both soluble and immobilized forms (Figure 1A). The fluorescence studies clearly show that protein conformations of both soluble and immobilized enzymes are practically identical with similar maximum emission wavelengths (λ_{max}) and spectrum widths.

One of the main concerns about the immobilization of KRED P1-A04 on AG-DEAE was the enzyme lixiviation during the operational process due to reversible protein-carrier interactions, threatening the process purity and the operational stability of the heterogeneous biocatalysts. As solution, we incorporated other reactive groups such as aldehydes and epoxy groups besides the amine monolayer to establish irreversible protein-carrier attachments.

A

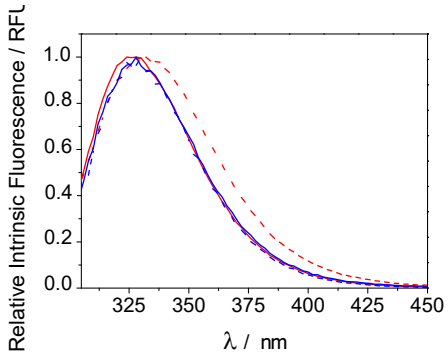

B

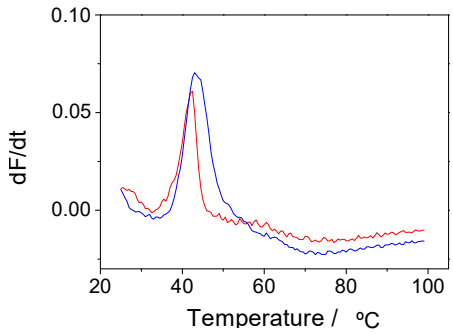

C

Enzyme form	Λ_{max} (nm) [a]	λ_{max} (nm) [b]	Peak Width (nm) [a]	Peak Width (nm) [b]	Tm[c]
Soluble	330	328	48	50	43
Immobilized	326 ± 2	330 ± 2	51	60	42.5 ± 0.3

Figure 1. Fluorescence assays of KRED. A) Relative intrinsic protein fluorescence of soluble (blue line) and immobilized KRED (red line) before (solid) and after (dashed line) being incubated at 40 ºC during 290 minutes. B) Thermal shift assay of soluble (blue line) and immobilized (red line) KRED. C) Analysis of Figure 1A and Figure 1B. [a] Intrinsic fluorescence of soluble and immobilized KRED. [b] Intrinsic fluorescence of soluble and immobilized KRED after being incubated for 290 min at 40ºC [c] Thermal-shift assay based on SYPRO fluorescence. The parameters were calculated from three independent measurements being the mean values represented in Figure 1B.

The fabrication of tailor-made heterofunctional carriers have been widely used to optimally and irreversibly orient the enzymes on the solid surface through a two-step mechanism.[35] Unfortunately, although this heterofunctional chemistry gave rise active immobilized preparations, conversions were lower than 50% for the asymmetric reduction of TFAF (Table 1). As described above, KRED P1-A04 seems to be very sensitive to the formation of a multivalent and irreversible attachment with the solid surface, which drives to the enzyme inactivation. Actually, inactivation of KRED P1-A04 by irreversibly immobilization has been also observed when a similar enzyme was attached to Sepabead EC resins activated with epoxy groups.[15] Hence, only those immobilization chemistries where the interactions protein-carrier is weak and reversible enough seem to retain an active conformation of the enzyme. SDS-PAGE analysis demonstrates that the 29 kDa major band of the commercial preparation is quantitatively absorbed to the carrier surface and partially eluted after incubation under denaturing conditions, demonstrating a reversible but stable protein immobilization on AG-DEAE (Figure 2). In the light of these results, homofunctional AG-DEAE was chosen as best functionalized carrier to continue working with since it results in a highly active heterogeneous biocatalyst.

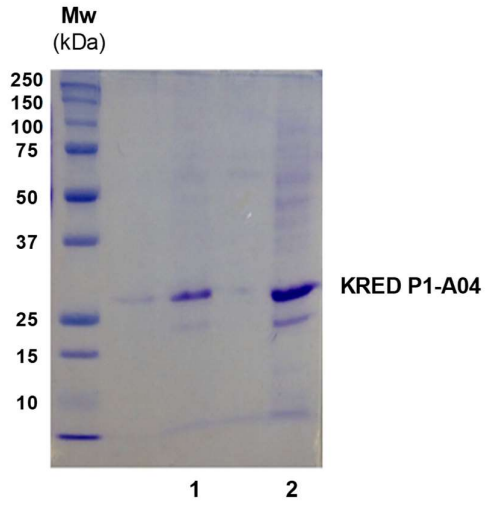

Figure 2. The SDS-PAGE analysis of KRED P1-A04 immobilization on AG-DEAE. Line 1 is the initial commercial extract of KRED P1-A04 before immobilization. Line 2 corresponds to the supernatant of KRED P1-A04 immobilized on AG-DEAE incubated with Laemmli buffer under denaturing conditions. The molecular weight marker is from BioRad (Precision Plus Protein All Blue Standard).

3.2. Apparent Kinetic parameters of soluble and immobilized KREDP1-A04

The apparent kinetic parameters of KRED P1-A04 immobilized on AG-DEAE were evaluated towards different NADPH concentrations and compared with the real parameters obtained for the soluble enzyme. Table 2 shows that K_M^{app} of the immobilized enzyme is approximately 4-fold higher towards NADPH than its soluble counterpart under saturating conditions of TFAF.

Table 2. Michaelis-Menten kinetic parameters of soluble and immobilized KRED towards NADPH.

Parameters	Soluble	Immobilized
V_{max} (U x mg^{-1})	0.46 ± 0.01	0.69 ± 0.18 [1]
K_M (mM)	0.47 ± 0.06	1.81 ± 0.69 [1]
k_{cat} (s^{-1})	0.40 ± 0.01	0.52 ± 0.06 [1]
k_{cat}/K_M (M^{-1} x s^{-1})	0.86 ± 0.10	0.37 ± 0.08 [1]

The kinetic parameters were measured with 10 mM TFAF at pH 7 and 25ºC varying the NADPH concentration. [1] Apparent kinetic parameters.

The Michaelis-Menten plots indicate that immobilized KRED P1-A04 requires a much higher concentration of NADPH than the soluble one to become saturated and consequently reach the maximum velocity (Figure 3).

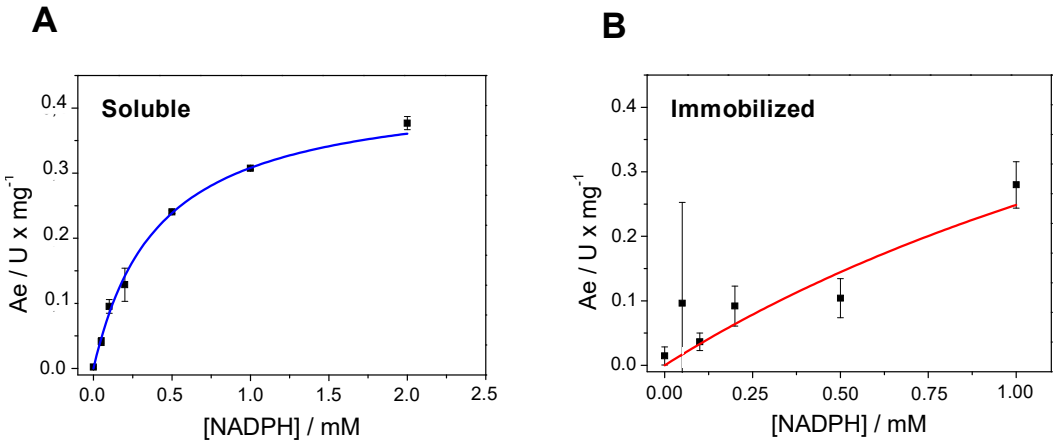

Figure 3. Michaelis-Menten plots. The reactions were carried out with 10 mM TFAF at pH 7 and 25 ºC varying the NADPH concentration. Ae means the specific activity of the enzyme. A) Soluble KRED P1-A04. B) Immobilized KRED P1-A04 on AG-DEAE.

On the contrary, the immobilized KRED P1-A04 on AG-DEAE presented an apparent V_{max} 1.8 times higher than the soluble one. Nevertheless, such higher catalytic activity

under cofactor saturating conditions cannot be explained by major structural distortions according to the fluorescence studies in absence of cofactor (Figure 1A). Therefore, the 2.3-fold lower apparent catalytic efficiency of the immobilized enzyme relies on the high K_M^{app} value; this fact suggests a lower effective NADPH concentration surrounding the immobilized enzymes than surrounding the enzymes in solution. The confinement of enzymes within the porous environment of AG-DEAE may impose mass transfer limitations to the enzymatic reaction that notably hamper the diffusion of the soluble cofactor across the pores of the carrier to access the enzyme active sites. These issues can explain the high K_M^{app} towards NADPH when the KRED P1-A04 is immobilized on porous microbeads even when the enzyme does not suffer dramatic structural distortions upon the immobilization. High K_M^{app} values towards redox cofactors are a common pattern when using immobilized oxidoreductases on porous carriers.[27, 39, 40]

3.3. Stability of KRED P1-A04 immobilized on AG-DEAE

Soluble and immobilized KRED P1-A04 were incubated at high temperature and in presence of IPA (Figure 4).The inactivation constant (k_i) of soluble KRED P1-A04 at 40 ºC was 10 ± 2 h^{-1}, while the immobilized enzyme presented a k_i = 0.8± 0.1 h^{-1} under the same conditions. Based on such inactivation kinetics, the half-life times of soluble and immobilized KRED P1-A04 are 0.06 and 0.88 hours, respectively, which means that the enzyme immobilized on AG-DEAE is thermally stabilized by a factor of 15 (Figure 4A).

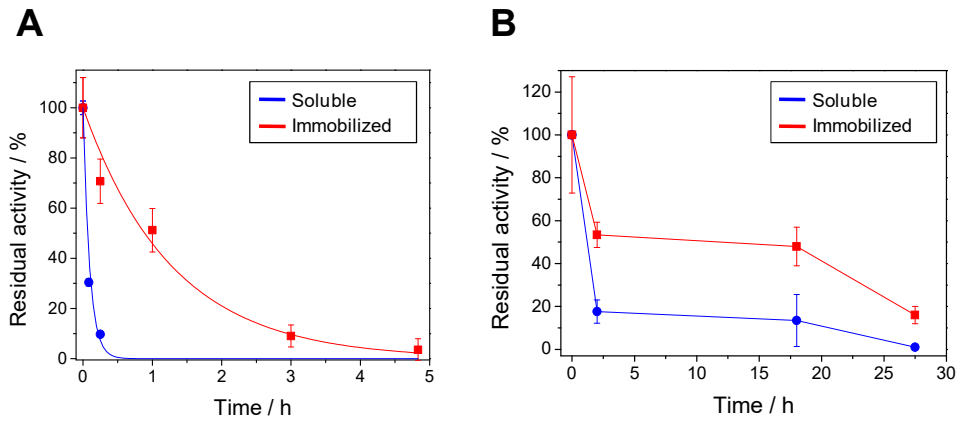

Figure 4. Stability studies of KRED P1-A04 against temperature and solvent. A) Thermal stability at 40 ºC. B) Stability against 1.55% of IPA.

The immobilized KRED P1-A04 was also more stable in presence of organic solvent such as IPA. In this case, the stability of the enzyme in presence of IPA is highly important because this enzyme uses IPA as sacrificing substrate to self-replenish the NADPH pool during the asymmetric reduction reactions.[14, 15, 41] Figure 4B shows that immobilized enzyme preserves 50% of its initial activity after 18 hours of incubation with 1.5% IPA, but the soluble enzyme loses 90% activity under the same conditions. Therefore, the ionic interactions of KRED P1-A04 with the cationic surface of AG-DEAE seem to increase the intrinsic stability of the protein against different denaturing agents. Surprisingly, the kinetic thermal inactivation does not match with the thermodynamic denaturalization since both soluble and immobilized enzymes presented similar melting temperatures (Tm) using a thermal-shift assay (Figure 1B). Unlike other proteins,[40, 42] the thermal inactivation of soluble KRED P1-A04 does not alter its intrinsic fluorescence spectrum. In contrast, the temperature shifted the fluorescence spectrum of the immobilized protein towards red wavelengths (Figure 1A). These temperature-induced conformational changes have been previously observed with other enzymes immobilized on AG-DEAE that were similarly stabilized by this immobilization chemistry.[39] Hence, the structural distortions observed when the immobilized KRED P1-A04 is exposed to moderate temperatures might induce more stable protein conformations.

3.4. Co-immobilization of NADPH and KRED P1-A04 on AG-DEAE: Single-particle studies of the resulting self-sufficient heterogeneous biocatalyst

The excellent stability and activity of KREDP1-A04 immobilized on AG-DEAE made this immobilization protocol suitable to fabricate self-sufficient heterogeneous biocatalysts. Considering the cationic nature of this carrier, a similar architecture as those ones recently reported in the previous Chapter 4[30] was here developed to co-immobilize the cofactor. In these architectures the enzyme must be strongly or irreversibly bound to the carrier, while the cofactor needs to be ionically adsorbed establishing an association-dissociation equilibrium that allows the cofactor shuttling from the solid surface to the enzyme active sites without leaving the porous microstructure of the microbead. To this aim, 6.5 mg of KRED P1-A04 and 10 μmol of NADPH per gram of carrier were quantitatively immobilized. Figure 5A shows that the cofactor remained bound to the solid surface after washing the resin with 10 volumes of buffer.

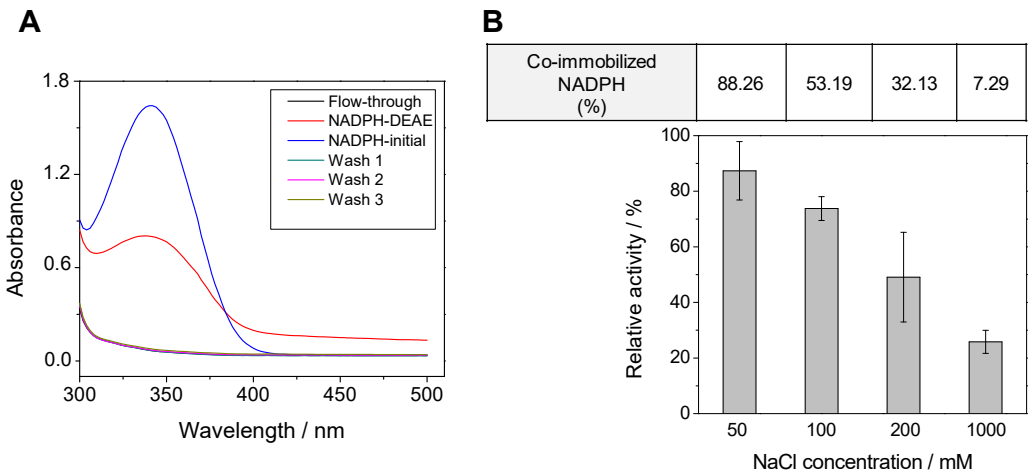

Figure 5. Reversible co-immobilization of KRED P1-A04 and NADPH onto AG-DEAE. A) Immobilization of NADPH on AG-DEAE. The immobilization was monitored by measuring the NADPH absorbance at 340 nm. After immobilization, the supernatant (flow-through) was collected and the resin immobilizing the cofactor was washed with 10 volumes of 10 mM Tris-HCl at pH 7. No cofactor was detected in the flow-through or in the washing supernatant. NADPH immobilized on AG-DEAE shows a maximum absorbance at 340 nm as well as the soluble one. B) Elution of co-immobilized KREDP1-A04 and NADPH from AG-DEAE. NADPH absorbance at 340 nm (top) and enzymatic activity of biocatalyst (bar graph) after 1 hour in presence of different ionic strengths.

Both the enzyme and the cofactor were ionically immobilized on AG-DEAE, as demonstrated by releasing them in presence of high ionic strength (Figure 5B). Hence, the reversible immobilization enables the reuse of the carrier once the enzyme become inactive.

To demonstrate that both enzyme and cofactor co-localize inside the same particle, the spatial distribution of the autofluorescence NADPH and the fluorophore-labeled KREDP1-A04 across the porous microbeads was analyzed by using CLSM. The microscopic images demonstrate that both enzyme and cofactor were uniformly distributed within microbeads. Nonetheless, the protein density was higher within the small microbeads than withinin the large ones (Figure 6).

A

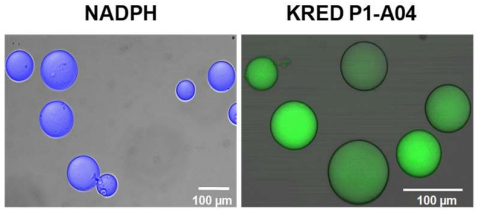

B

Fluorescence/area (RFU / µm²)	Diameter (µm)
0.008 ± 0.004	112 ± 16
0.027 ± 0.009	71 ± 10

Figure 6. Single-particle analysis of the spatial localization and distribution of co-immobilized KRED P1-A04 and NAPH. A) Confocal microscopy images of immobilized cofactor (blue) and FITC-labeled enzyme (green) on AG-DEA. B) Effect of the microbead size on the protein density of the immobilized KRED P1-A04. The average diameter was calculated from the microscopy images of large (n=8) and small (n=9) microbeads.

Then, the catalytic utilization of the cofactor within the porous microstructure of the agarose microbeads was proven by *in operando* fluorescence studies where different substrates were incubated with the self-sufficient heterogeneous biocatalyst under the microscope (Figure 7). Primarily, lixiviation of NADPH to the reaction medium resulted negligible since fluorescence within the particles was constant during the operation time in a control experiment without adding the substrates (Figure 7A). When TFAF was added to the reaction media, the autofluorescence of NADPH decayed along the time, indicating that immobilized KRED P1-A04 utilizes the immobilized NADPH to produce (*S*)-(+)-α-(Trifluoromethyl)benzyl alcohol (product detected in the bulk after the *in operando* experiment). By contrast, when both substrates TFAF and IPA were added to the reaction media, >90% of the cofactor fluorescence was detected within the particles during the reaction, indicating that the NADPH consumed by KRED P1-A04 during the asymmetric reduction of TFAF is replenished by the same enzyme using IPA as electron donor and yielding acetone as by-product. Using the two substrates, the cofactor fluorescence slightly decreased along the time. This effect suggests that KRED P1-A04 is more efficient reducing ketones than oxidizing alcohols under these assay conditions. Besides, the hypothesis that such fluorescence decreasing may be attributed to the cofactor lixiviation was discarded since no fluorescence was detected in the bulk.

These experiments demonstrate that the cofactor shuttles between the solid phase and the enzyme active sites, but it never diffuses out the porous microbeads. Remarkably, the aqueous media reaction was not a hindrance for the proper cofactor immobilization unlike former studies where high concentrations of solvents were needed to avoid the lixiviation of the ionically-immobilized cofactor.[15, 27, 29]

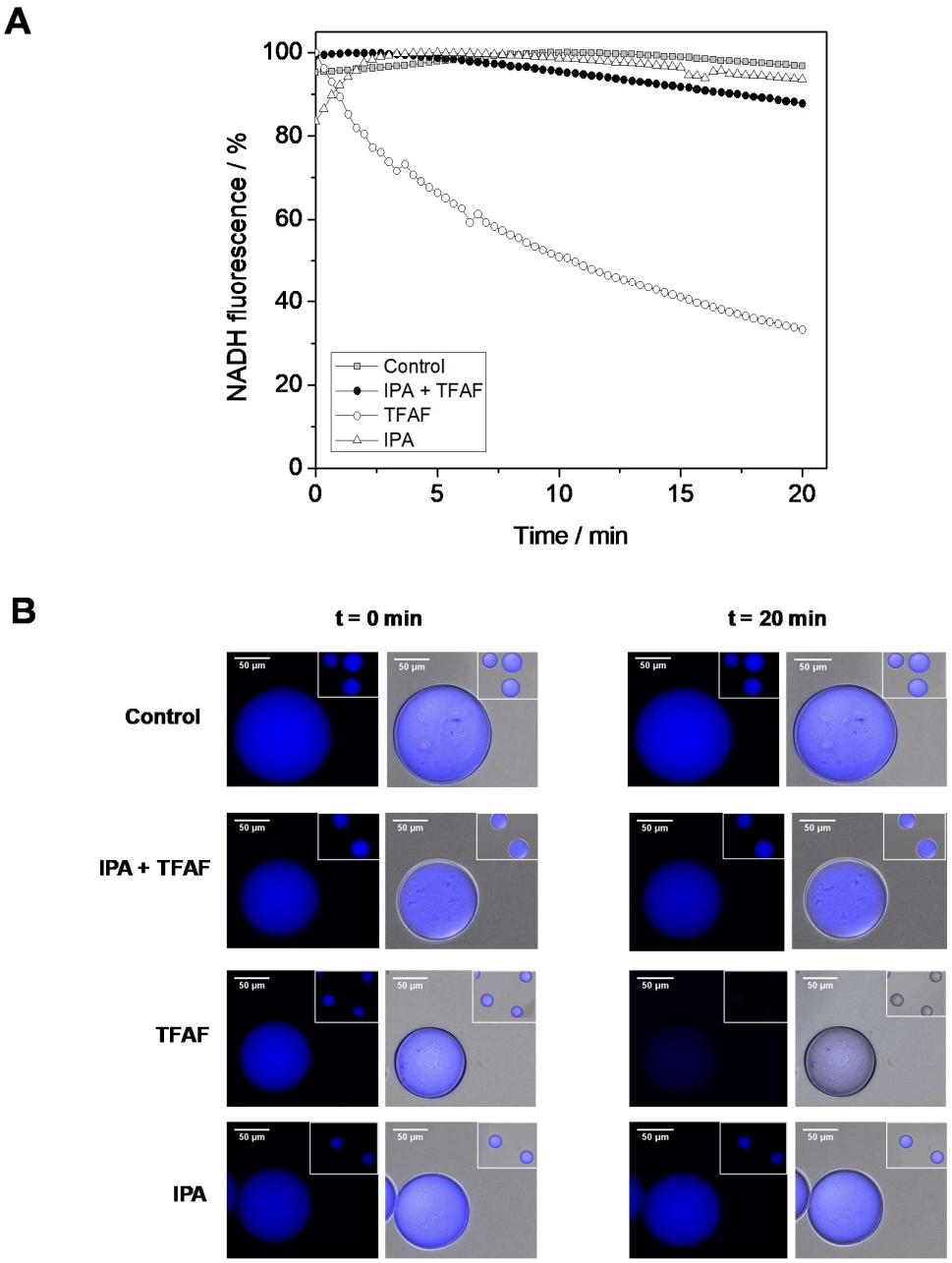

Figure 7. Single-particle kinetics of KRED P1-A04 and NADPH co-immobilized on AG-DEAE. A) Reactions were triggered with different substrates. Control reaction was triggered without substrate. Data are the mean value of 5 microbeads (diameter = 92 ± 13 µm). B) Fluorescence microscopy images at the beginning and the end of the reaction. Left side, autofluorescence signal of NADPH; right side, overlay of the signals of NADPH and brightfield.

Additionally, image analytics reveal two main microbead populations with different diameters that present different catalytic performance (Figure 8). The smallest microbeads (diameter = 71 ± 10 μm) present a uniform distribution of the initial reaction rate across the sub-micrometrical area of a single microbead. Conversely, in the largest microbeads (diameter = 112 ± 16 μm), the enzymes immobilized on the inner surface showed 20-30% lower initial reaction rate than the enzymes located at inner positions within the same particle. Moreover, Figure 8 shows a clear trend between the enzyme activity and the microbead size; the smaller the microbead diameter, the higher the initial reaction rate. This trend can be attributed to the lower protein density found in larger particles (Figure 8), but also suggests that the immobilized KRED P1-A04 on larger microbeads undergoes more severe external mass transport limitations of substrate TFAF. These diffusion restrictions are aligned with the engineering principles that rule the catalytic efficiency of any enzyme immobilized on porous carriers.[43] For example, D-amino acid oxidase immobilized on large porous silica particles suffered significant mass transfer restrictions due to the limitations in the diffusion of one of the substrates; the oxygen.[44] Actually, a similar mass restriction influence on enzyme kinetics has been pointed out when Tt-NOX was immobilized on agarose microbeads in the previous Chapter 4.

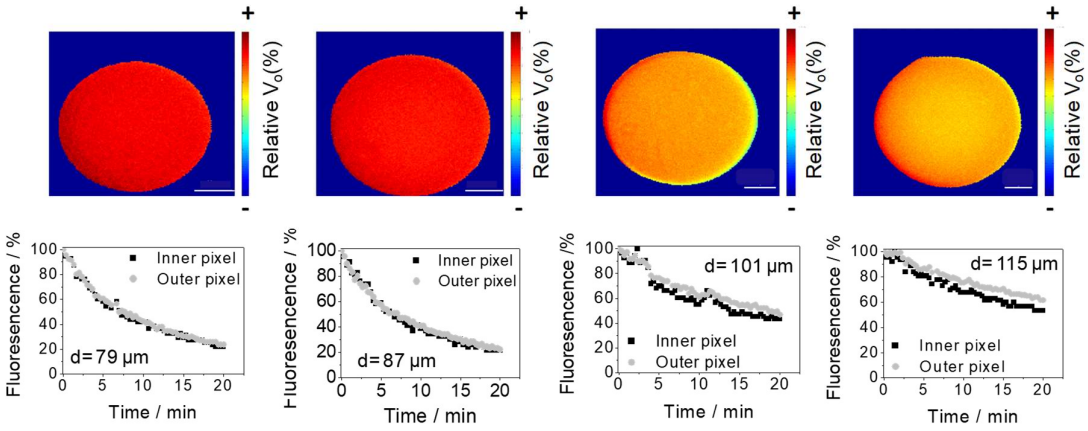

Figure 8. Image analytics of *in operando* asymmetric reduction of TFAF without IPA catalyzed by KRED P1-A04 co-immobilized with NADPH on AG-DEAE. Maps of initial reaction rates of microbeads with different diameters (up) and the reaction courses at inner and outer pixels (down). White lines corresponds to 20 μm.

3.5. Re-utilization of the self-sufficient heterogeneous biocatalyst in batch

Once we demonstrated that reduction and oxidation reactions occurred simultaneously inside the same porous microbeads where NADPH and KRED were co-immobilized, this self-sufficient heterogeneous biocatalyst was used to perform the asymmetric reduction of TFAF without exogenous addition of the redox cofactor. Firstly, the asymmetric reduction was performed with KRED immobilized on Ag-DEAE but using soluble cofactor. To achieve the maximum yields, we optimized the load of the heterogeneous catalyst at 2% of biocatalyst. Using the immobilized enzymes and the soluble cofactor, the reaction yield was 100%, obtaining *ee* >99%. Moreover, the immobilized enzyme was reused up to 5 operational cycles without losing effectiveness. When the reactions were catalyzed by the enzyme and the cofactor co-immobilized on the same microbead and without exogenous addition of NADPH, the conversion reached a quantitative yield of 100% (Table 3). Expectedly, the selectivity of the process was maintained (*ee* >99%) regardless of using soluble or immobilized NADPH. Finally, this self-sufficient heterogeneous biocatalyst was reused for up to 5 cycles without adding exogenous NADPH and obtaining the maximum yield in each cycle.

Table 3. Recycling of KRED P1-A04 and NADPH co-immobilized on AG-DEAE for the reduction of TFAF.

Cycle	Time (h)	Conversion (%)	*ee* *(S)*-1-(1-naphtyl)ethanol (%)
1	24	>99	>99
2	24	>99	>99
3	24	>99	>99
4	24	>99	>99
5	24	>99	>99

The reutilization of the self-sufficient heterogeneous biocatalyst significantly increased the total turnover number (TTN) of both enzyme and cofactor (Table 4). The TTN values reached are closed to industrial demands. Another important parameter that can be withdrawn from the batch experiments is the turnover frequency (TOF) of NADPH per cycle that gives an idea about how fast the utilization of the cofactor inside the porous environment occurs (Table 4).

Table 4. Total turnover of KRED and NADPH co-immobilized on Ag-DEAE during the asymmetric reduction of TFAF.

TTN_{NADPH}[a]	TTN_{KRED}[b]	TOF_{NADPH}/cycle (h^{-1}) [c]
333	19980	2.8

[a] TTN_{NADPH} = mol of product accumulated during 5 cycles/mol of immobilized NADPH.
[b] TTN_{KRED} = mol of product accumulated during 5 cycles/mol of immobilized KRED.
[c] TTN_{NADPH}/reaction time (hours) in every cycle.

The efficient re-utilization of immobilized NADPH and product yields may rely on the excellent activity of KRED P1-A04 to self-regenerate NADPH under extremely low cofactor concentrations using excess of IPA as hydride donor.[45] Using a similar approach, Merk *et al.* co-immobilized NADPH and a different KRED from the same commercial source on commercial methacrylate porous microbeads, obtaining good reusability using high IPA concentration (90%).[15] Unfortunately, the immobilization of the KRED P1-A04 in such resin inactivated the 95% of the immobilized protein unlike the immobilization on AG-DEAE where KRED P1-A04 showed 43% catalytic efficiency (Table 2) and 100% product yield (Table 1) compared to the soluble enzyme. Additionally, using methacrylate resin, the enzyme was covalently and irreversibly attached to the microbeads and the cofactor was ionically absorbed to the amine groups. Therefore, once the enzyme becomes inactive the carrier cannot be reused. Contrarily, in the system presented in this work, the enzyme can be removed from the matrix under drastic conditions after the enzyme inactivation. The vast majority of systems where the cofactors are ionically absorbed to the solid materials efficiently work under high solvent concentration[15, 27, 29] (conditions where cofactor-carrier interactions are favoured) but fail in buffered reaction media because of the cofactor lixiviation. Remarkably, the cofactor absorbed on Ag-DEAE remains adsorbed in a stable manner to the matrix, even with IPA concentrations as low as 17%.

3.6. Continuous synthesis of a model chiral alcohol using a mini-column packed with the self-sufficient heterogeneous biocatalyst.

The excellent operational stability in batch of the self-sufficient heterogeneous biocatalysts was the motivation to carry out the continuous asymmetric reduction of TFAF in packed-bed flow minireactors. To this aim, 280 mg of self-sufficient heterogeneous biocatalyst were packed into a plug-flow minicolumn and fed the reactor with the corresponding reaction mixture without exogenous NADPH. Figure 9A shows

the effect of the flow rate in the conversion, expectedly the faster the flow, the lower the product yield because the residence times are shorter and consequently the enzyme-substrate contact was briefer. 80% of conversion was achieved using 50 µL x min^{-1} flow giving rise to space-time yield (STY) of 104 g x L^{-1} x day^{-1}.

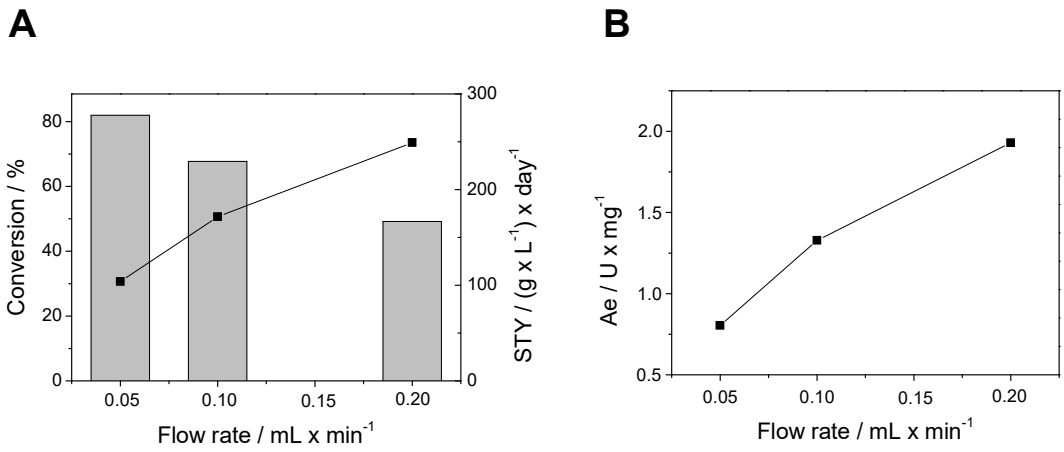

Figure 9. Operational characterization in flow. A) Effect of flow rate on the conversion (grey bars, left Y axis) and space time yield (black line with squares, right Y axis) of continuous asymmetric reduction of TFAF catalyzed by KRED P1-A04 and NADPH co-immobilized on AG-DEAE. B) Effect of flow rate on the specific activity of the KRED P1-A04 co-immobilized with NADPH on AG-DEAE during the continuous asymmetric reduction of TFAF.

Although the conversion dropped to 50%, both the STY and the apparent specific activity of the enzyme increased by a factor of 2.4 when the flow was four times faster (Figure 9).

By using a flow rate of 50 µL x min^{-1}, the reactor operated for 120 hours constantly yielding around 80% of product, observing neither enzyme inactivation nor cofactor lixiviation as supported by the constant specific activity of the enzyme during the whole operation time (Figure 10). Under these conditions, 1275 residence volumes were flushed through the self-sufficient heterogeneous biocatalyst giving rise to an accumulated TTN_{NADPH} of 1076. In this experiment, 2912 µmol of product were detected with 2.8 µmol of immobilized NADPH, while producing the same amount of product requires 54.6 µmol of exogenously added cofactor (0.15 mM NADPH in the reaction mixture). In addition, The STY range of 97-112 g x L^{-1} x day^{-1} remained unaltered for 120 hours of continuous operation (Figure 10B). This STY values falls in the range of the reported STY values for other continuous asymmetric reduction reactions catalyzed with either soluble or immobilized enzymes.[21-23, 46] The continuous

asymmetric reduction reaction demonstrates that neither the enzyme nor the cofactor are inactivated or lixiviated during the process, this behaviour aligns with the previous *in operando* single-particle studies (Figure 7).

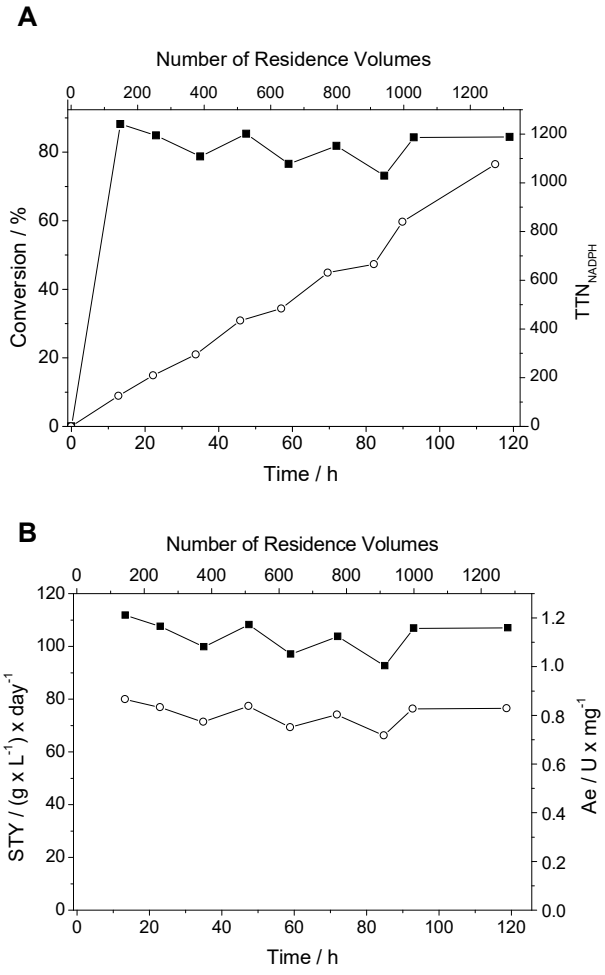

Figure 10. Continuous flow asymmetric reduction of TFAF catalyzed by KRED P1-A04 and NADPH co-immobilized on AG-DEAE. A) Conversion of TFAF into (*S*)-(+)-α-(Trifluoromethyl)benzyl alcohol (full squares) and accumulated TTN of NADPH (open circles) were determined at different times. B) Evolution of STY (full squares) of the reaction and specific activity (open circles) of KRED P1-A04**.** The STY was defined as grams of desired product released per liter of reaction during one day.

The accumulated TTN of NADPH under flow conditions was approximately 10-fold higher than the values found for NADH co-immobilized with two alcohol dehydrogenases onto AG-G/PEI25 (Chapter 4).[30] Unlike the KRED systems, the two alcohol dehydrogenases are irreversibly bound to the solid surface and must work in coordination to recycle the immobilized cofactor. Consequently, the regeneration of cofactors attached to solid surface by using recycling enzymes seems to be less

efficient than when the same enzyme catalyzes the main reaction and self-recycles the cofactor. In fact, this strategy has been elected for the process development and scale-up of many industrially relevant chiral alcohols.[14-16, 41, 47, 48] Hence, this heterogeneous self-sufficient biocatalyst meets the industrial requirements since the accumulated TTN_{NADPH} was higher than 1000. Remarkably, this system presents an even slightly better accumulated TTN for NADPH than those systems using ultrafiltration membrane reactors with soluble enzymes and polymeric cofactors.[21, 22, 46] For example, a membrane reactor containing NADPH tethered to polyethyelenglycol and two soluble alcohol deydrogenases was able to be re-cycled up to 540 times in 5 days, 2 times less than this system operated in the same time-span.[21]

3.7. Broadening the scope of KRED-based biocatalysts

Since stereoselective reduction of ketones is one of the most useful reactions in organic synthesis, it is not surprising that ketoreductases have become crucial in synthesis of chiral alcohols.[49] Therefore, a wide spectrum of biocatalysts with different operational stabilities and properties are desired. To this purpose, another promising ketoreductase variant (KRED P2-D11) was studied. Encouraged by the results obtained for KRED P1-A04, we followed the same protocol for immobilizing KRED P2-D11 on AG-DEAE through ion-exchange. The immobilized enzyme show a high expressed activity compared to those reported for other KREDs.[1, 15, 50] Remarkably, the immobilized enzyme was 9 times more thermostable than its soluble counterpart under the operational conditions tested (Table 5).

Table 5. Immobilization and stability parameters of KRED P2-D11 on AG-DEAE.

Parameters	Soluble	Immobilized
Protein loading (mg x g^{-1})	-	0.96
Immobilization yield (%)	-	96
Specific activity (U x mg^{-1})	2.26	2.25
Final expressed activity (%)	-	105 ± 10
Inactivation constant (h^{-1}) [a]	0.33	0.07
Half-life time (h) [a]	4.47	40.2
Stabilization factor [b]	-	9

[a] Stability parameters were calculated by non-linear fitting of inactivation.
[b] Stabilization factor = Half-life time immobilized enzyme / Half-life time soluble enzyme.

Moreover, the stability of the cofactor-dependent KRED P2-D11 against organic solvent was assessed. Since IPA is used as sacrificing molecule for cofactor recycling, the stability of KRED P2-D11 against IPA has a major significance for the development of an optimal biocatalyst. Fortunately, both soluble and immobilized KRED P2-D11 showed a high stability in presence of 17% IPA (Figure 11). In fact, soluble KRED P2-D11 only loses 38% of activity after 2 hours of incubation with 17% IPA while soluble KRED P1-A04 loses 85% during the same time (Figure 4B). These results demonstrate that KRED P2-D11 is significantly more robust than KRED P1-A04. Besides, the immobilized KRED P2-D11 retains more than 60% of initial activity after 18 hours (Figure 11) while KRED P1-A04 retains 50% of activity with 11 times lower concentration of IPA (Figure 4B).

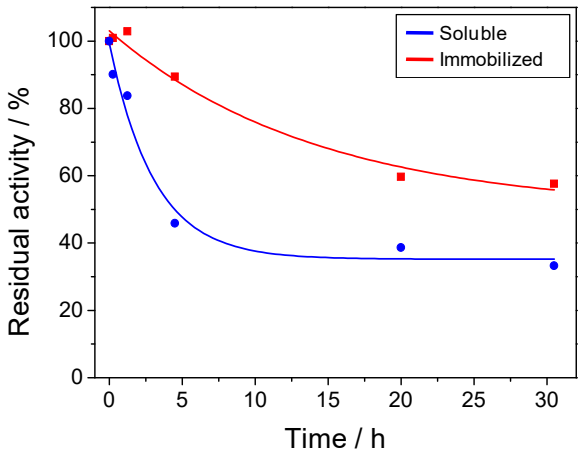

Figure 11. Stability of KRED P2-D11 against organic solvent (IPA).

The high activity and stability of the immobilized KRED P2-D11 was the incentive to develop self-sufficient heterogeneous biocatalysts that co-immobilize the enzyme (6.5 mg x $g_{carrier}^{-1}$) with NADPH (10 μmol_{NADPH} x $g_{carrier}^{-1}$). Then, the resulting self-sufficient heterogeneous biocatalyst was tested for the reduction of AN containing 3% of biocatalyst (0.195 $mg_{KRED\ P2\text{-}D11}$ x mL^{-1}) and IPA as reductant agent. We found a conversion of >99% after 24 h preserving the enantioselectivity of the KRED P2-D11 (>99% *ee* for *S*-1-(1-naphtyl)ethanol) without exogenous supply of NADPH. Moreover, this self-sufficient biocatalyst was reused up in 5 consecutive batch cycles without losing effectiveness (Table 6). The recyclability of the biocatalyst significantly increased the total turnover number (TTN) of both enzyme and cofactor. Hence, the co-immobilized NADPH accumulated a TTN of 675 whereas the KRED P2-D11 did 5400.

Table 6. Recycling of KRED P2-D11 and NADPH co-immobilized on AG-DEAE for the reduction of AN.

Cycle	Time (h)	Conversion (%)	*ee* *(S)*-1-(1-naphtyl)ethanol (%)
1	24	>99	>99
2	24	>99	>99
3	24	>99	>99
4	24	>99	>99
5	24	>99	>99

Going one step further, the continuous asymmetric reduction of AN was performed in a packed-bed flow minireactor using the self-sufficient heterogeneous biocatalysts based on KRED P2-D11. Unpleasantly, the system failed observing conversions < 5% at 50-200 µL x min^{-1} flow rates.

Unlike KRED P1-A04 immobilized on AG-DEAE, KRED P2-D11 immobilized on the same matrix was incapable to efficiently recycle the immobilized redox cofactor which burdened the continuous production of *S*-1-(1-naphtyl)ethanol. This hypothesis was supported by measuring the fluorescence of NADPH before and after the flow-reaction was accomplished. Immobilized NADPH was reduced to $NADP^+$ during the operation of the packed-bed reactor, but could not be regenerated in presence of IPA as sacrificing reductant. No NADPH fluorescence was detected on the microbeads after the flow-reaction (Figure 12A). Furthermore, the addition of soluble KRED P1-A04 that is inactive towards AN but highly active towards IPA, was able to regenerate the NADPH pool within the agarose microbead (Figure 12B). This fact was demonstrated by measuring the activity of the biocatalysts after the flow-reaction was accomplished. Therefore, these insights suggest that under flow conditions the quantitative conversion of AN is limited by the low oxidation rate of KRED P2-D11 towards IPA required to recycle the intraparticle pool of NADPH.

A

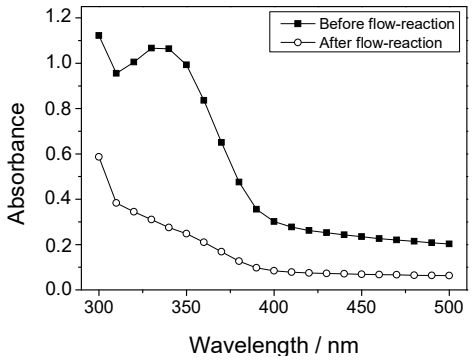

B

	Activity (slope)
AG-DEAE-KRED (P2-D11)	0.001
AG-DEAE-KRED(P2-D11) + KRED(P1-A04)	0.016

Figure 12. Inefficiency of KRED P2-D11 reducing $NADP^+$. A) Absorbance spectra before and after operating the packed-bed minireactor. NADPH immobilized on AG-DEAE shows a maximum absorbance at 340 nm before the flow-reaction. B) Activity measurement of the co-immobilized KRED P2-D11 and NADPH on AG-DEAE and the same biocatalyst adding soluble KRED P1-A04 after the operating packed-bed reaction.

4. CONCLUSIONS

In this chapter, the approach of self-sufficient heterogeneous biocatalysts was tried for the asymmetric reduction of carbonyl compounds without the addition of exogenous cofactors. Two biocatalysts with different operational stabilities were engineered by optimally co-immobilizing NADPH and KRED on commercially available agarose microbeads activated with tertiary amine groups. The first immobilized biocatalyst based on a versatile *R*-selective and NADPH-dependent KRED P1-A04, catalyzes the main reaction (carbonyl reduction) and self-recycles the cofactor (oxidation of isopropyl alcohol). As a result, this heterogeneous biocatalyst was successfully operated in a plug-flow minireactor during more than 200 hours without addition of exogenous NADPH. The integration of NADPH into the solid phase for the continuous synthesis of chiral alcohol has decreased almost 20 times the contribution of NADPH to the process costs since the TTN values are 333 and near 20000 for the cofactor and the enzyme, respectively. The second heterogeneous biocatalyst containing KRED P2-D11 presents a higher stability but fails recycling the cofactor during flow reaction. These results firmly confirm the cofactor as part of the biocatalyst avoiding the exogenous addition of costly cofactors to the reaction media and expanding the spectrum of enzymatic activities of self-sufficient heterogeneous biocatalysts.

REFERENCES

1. Benítez-Mateos, A. I., San Sebastian, E., Ríos-Lombardía, N., Morís, F., González-Sabín, J., López-Gallego, F. Asymmetric reduction of prochiral ketones by using self-sufficient heterogeneous biocatalysts based on NADPH-dependent ketoreductases. *Chemistry – A European Journal*. **2017**, *23*: 16843-16852.

2. Marx, L. *et al.* Chemoenzymatic approaches to the synthesis of the calcimimetic agent cinacalcet employing transaminases and ketoreductases. *Advanced Synthesis & Catalysis*. **2018**, *360*: 2157-2165.

3. Nakamura, K., Yamanaka, R., Matsuda, T., Harada, T. Recent developments in asymmetric reduction of ketones with biocatalysts. *Tetrahedron: Asymmetry*. **2003**, *14*: 2659-2681.

4. Kim, J. H., Scialli, A. R. Thalidomide: the tragedy of birth defects and the effective treatment of disease. *Toxicological Sciences*. **2011**, *122*: 1-6.

5. Nestl, B. M., Hammer, S. C., Nebel, B. A., Hauer, B. New generation of biocatalysts for organic synthesis. *Angewandte Chemie International Edition*. **2014**, *53*: 3070-3095.

6. Sorgedrager, M. J., Van Rantwijk, F., Huisman, G. W., Sheldon, R. A. Asymmetric carbonyl reductions with microbial ketoreductases. *Advanced Synthesis & Catalysis*. **2008**, *350*: 2322-2328.

7. Matsuda, T., Yamanaka, R., Nakamura, K. Recent progress in biocatalysis for asymmetric oxidation and reduction. *Tetrahedron: Asymmetry*. **2009**, *20*: 513-557.

8. Haq, S. F. *et al.* A strategy to identify a ketoreductase that preferentially synthesizes pharmaceutically relevant (S)-alcohols using whole-cell biotransformation. *Microbial Cell Factories*. **2018**, *17*: 1-14.

9. Li, B. *et al.* Whole-cell biotransformation systems for reduction of prochiral carbonyl compounds to chiral alcohol in Escherichia coli. *Scientific Reports*. **2014**, *4*: 1-5.

10. Liu, H., Chen, B.-S., De Souza, F. Z. R., Liu, L. A comparative study on asymmetric reduction of ketones using the growing and resting cells of marine-derived fungi. *Marine drugs*. **2018**, *16*: 1-15.

11. Milner, S. E., Maguire, A. R. Recent trends in whole cell and isolated enzymes in enantioselective synthesis. *Reviews and Accounts*. **2012**, *i*: 321-382.

12. Wichmann, R., Vasic-Racki, D. Cofactor regeneration at the lab scale. *Advances in biochemical engineering/biotechnology*. **2005**, 225-260.

13. Liu, W., Wang, P. Cofactor regeneration for sustainable enzymatic biosynthesis. *Biotechnology Advances*. **2007**, *25*: 369-384.

14. Liang, J. *et al.* Development of a biocatalytic process as an alternative to the (−)-DIP-Cl-mediated asymmetric reduction of a key intermediate of montelukast. *Organic Process Research & Development*. **2010**, *14*: 193-198.

15. Li, H., Moncecchi, J., Truppo, M. D. Development of an Immobilized Ketoreductase for Enzymatic (R)-1-(3,5-Bis(trifluoromethyl)phenyl)ethanol Production. *Organic Process Research & Development*. **2015**, *19*: 695-700.

16. Zuhse, R., Leggewie, C., Hollmann, F., Kara, S. Scaling-up of "smart cosubstrate" 1,4-butanediol promoted asymmetric reduction of ethyl-4,4,4-trifluoroacetoacetate in organic media. *Organic Process Research & Development*. **2015**, *19*: 369-372.

17. Noey, E. L. *et al.* Origins of stereoselectivity in evolved ketoreductases. *Proceedings of the National Academy of Sciences*. **2015**, *112*: 7065-7072.

18. Truppo, M. D. Cofactor recycling for enzyme catalyzed processes. In Comprehensive chirality. Elsevier Science. **2012**.

19. Knaus, T. *et al.* Better than nature: nicotinamide biomimetics that outperform natural coenzymes. *Journal of the American Chemical Society*. **2016**, *138*: 1033-1039.

20. Wang, X., Saba, T., Yiu, H. H. P., Howe, R. F., Anderson, J. A., Shi, J. Cofactor NAD(P)H regeneration inspired by heterogeneous pathways. *Chem*. **2017**, *2*: 621-654.

21. Wichmann, R., Wandrey, C., Bückmann, A. F., Kula, M. R. Continuous enzymatic transformation in an enzyme membrane reactor with simultaneous NAD(H) regeneration. *Biotechnology and Bioengineering*. **1981**, *23*: 2789-2802.

22. Obón, J., Almagro, M. J., Manjón, A., Iborra, J. Continuous retention of native NADP(H) in an enzyme membrane reactor for gluconate and glutamate production. *Journal of Biotechnology*. **1996**, *50*: 27-36.

23. Seelbach, K., Kragl, U. Nanofiltration membranes for cofactor retention in continuous enzymatic synthesis. *Enzyme and Microbial Technology*. **1997**, *20*: 389-392.

24. El-Zahab, B., Donnelly, D., Wang, P. Particle-tethered NADH for production of methanol from CO_2 catalyzed by coimmobilized enzymes. *Biotechnology and Bioengineering*. **2008**, *99*: 508-514.

25. Fu, J. *et al.* Multi-enzyme complexes on DNA scaffolds capable of substrate channelling with an artificial swinging arm. *Nature Nanotechnology*. **2014**, *9*: 531-536.

26. Garcia-Galan, C., Berenguer-Murcia, Á., Fernandez-Lafuente, R., Rodrigues, R. C. Potential of different enzyme immobilization strategies to improve enzyme performance. *Advanced Synthesis & Catalysis*. **2011**, *353*: 2885-2904.

27. Heidlindemann, M., Rulli, G., Berkessel, A., Hummel, W., Gröger, H. Combination of asymmetric organo- and biocatalytic reactions in organic media

using immobilized catalysts in different compartments. *ACS Catalysis*. **2014**, *4*: 1099-1103.

28. Ji, X., Su, Z., Wang, P., Ma, G., Zhang, S. Tethering of nicotinamide adenine dinucleotide inside hollow nanofibers for high-yield synthesis of methanol from carbon dioxide catalyzed by coencapsulated multienzymes. *ACS Nano*. **2015**, *9*: 4600-4610.

29. Rulli, G., Heidlindemann, M., Berkessel, A., Hummel, W., Gröger, H. Towards catalyst compartimentation in combined chemo- and biocatalytic processes: Immobilization of alcohol dehydrogenases for the diastereoselective reduction of a β-hydroxy ketone obtained from an organocatalytic aldol reaction. *Journal of Biotechnology*. **2013**, *168*: 271-276.

30. Velasco-Lozano, S., Benítez-Mateos, A. I., López-Gallego, F. Co-immobilized phosphorylated cofactors and enzymes as self-sufficient heterogeneous biocatalysts for chemical processes. *Angewandte Chemie International Edition*. **2017**, *56*: 771-775.

31. Dicosimo, R., Mcauliffe, J., Poulose, A. J., Bohlmann, G. Industrial use of immobilized enzymes. *Chemical Society Reviews*. **2013**, *42*: 6437-6474.

32. Dos Santos, J. C. S. *et al.* Characterization of supports activated with divinyl sulfone as a tool to immobilize and stabilize enzymes via multipoint covalent attachment. Application to chymotrypsin. *RSC Advances*. **2015**, *5*: 20639-20649.

33. Mateo, C. *et al.* Improvement of enzyme properties with a two-step immobilizaton process on novel heterofunctional supports. *Biomacromolecules*. **2010**, *11*: 3112-3117.

34. Mateo, C., Abian, O., Fernandez-Lafuente, R., Guisan, J. M. Reversible enzyme immobilization via a very strong and nondistorting ionic adsorption on support–polyethylenimine composites. *Biotechnology and Bioengineering*. **2000**, *68*: 98-105.

35. Bolivar, J. M., Mateo, C., Grazu, V., Carrascosa, A. V., Pessela, B. C., Guisan, J. M. Heterofunctional supports for the one-step purification, immobilization and stabilization of large multimeric enzymes: Amino-glyoxyl versus amino-epoxy supports. *Process Biochemistry*. **2010**, *45*: 1692-1698.

36. Rivero, C. W., Palomo, J. M. Covalent immobilization of candida rugosa lipase at alkaline pH and their application in the regioselective deprotection of per-O-acetylated thymidine. *Catalysts*. **2016**, *6*: 115.

37. Bolivar, J. M. *et al.* The presence of thiolated compounds allows the immobilization of enzymes on glyoxyl agarose at mild pH values: New strategies of stabilization by multipoint covalent attachment. *Enzyme and Microbial Technology*. **2009**, *45*: 477-483.

38. López-Gallego, F. *et al.* Preparation of a robust biocatalyst of d-amino acid oxidase on sepabeads supports using the glutaraldehyde crosslinking method. *Enzyme and Microbial Technology*. **2005**, *37*: 750-756.

39. Da Silva, E. S., Gómez-Vallejo, V., Llop, J., López-Gallego, F. Efficient nitrogen-13 radiochemistry catalyzed by a highly stable immobilized biocatalyst. *Catalysis Science & Technology*. **2015**, *5*: 2705-2713.

40. Da Silva, E. S., Gómez-Vallejo, V., Llop, J., López-Gallego, F. Structural, kinetic and operational characterization of an immobilized l-aminoacid dehydrogenase. *Process Biochemistry*. **2017**, *57*: 80-86.

41. Ju, X., Tang, Y., Liang, X., Hou, M., Wan, Z., Tao, J. Development of a biocatalytic process to prepare (S)-N-boc-3-hydroxypiperidine. *Organic Process Research & Development*. **2014**, *18*: 827-830.

42. Gouda, M. D., Singh, S. A., Rao, A. G. A., Thakur, M. S., Karanth, N. G. Thermal inactivation of glucose oxidase: mechanism and stabilization using additives. *Journal of Biological Chemistry*. **2003**, *278*: 24324-24333.

43. Liese, A., Hilterhaus, L. Evaluation of immobilized enzymes for industrial applications. *Chemical Society Reviews*. **2013**, *42*: 6236-6249.

44. Bolivar, J. M., Schelch, S., Mayr, T., Nidetzky, B. Mesoporous silica materials labeled for optical oxygen sensing and their application to development of a silica-supported oxidoreductase biocatalyst. *ACS Catalysis*. **2015**, *5*: 5984-5993.

45. Ríos-Lombardía, N., Vidal, C., Liardo, E., Morís, F., García-Álvarez, J., González-Sabín, J. From a sequential to a concurrent reaction in aqueous medium: ruthenium-catalyzed allylic alcohol isomerization and asymmetric bioreduction. *Angewandte Chemie International Edition*. **2016**, *55*: 8691-8695.

46. Hummel, W., Schütte, H., Kula, M.-R. d-(-)-Mandelic acid dehydrogenase from Lactobacillus curvatus. *Applied microbiology and biotechnology*. **1988**, *28*: 433-439.

47. Villela Filho, M., Stillger, T., Müller, M., Liese, A., Wandrey, C. Is log P a convenient criterion to guide the choice of solvents for biphasic enzymatic reactions? *Angewandte Chemie International Edition*. **2003**, *115*: 3101-3104.

48. Wolberg, M. *et al.* Chemoenzymatic synthesis of the chiral side-chain of statins: application of an alcohol dehydrogenase catalysed ketone reduction on a large scale. *Bioprocess and Biosystems Engineering*. **2008**, *31*: 183-191.

49. Kaluzna, I. A., David Rozzell, J., Kambourakis, S. Ketoreductases: stereoselective catalysts for the facile synthesis of chiral alcohols. *Tetrahedron: Asymmetry*. **2005**, *16*: 3682-3689.

50. Petkova, G. A., Záruba, K., Král, V. Synthesis of silica particles and their application as supports for alcohol dehydrogenases and cofactor immobilizations: conformational changes that lead to switch in enzyme stereoselectivity. *Biochimica et biophysica acta*. **2012**, *1824*: 792-801.

Chapter 6

Self-sufficient heterogeneous biocatalysts based on ω-transaminases and PLP for flow-biocatalysis

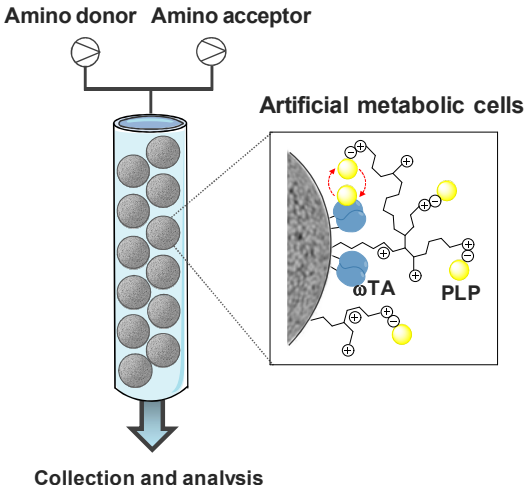

The design of artificial metabolic cells was here applied for flow transaminations. Since transaminases are an attractive alternative for chemical synthesis, a ω-transaminase from *Halomonas elongata* was co-immobilized with PLP onto porous methacrylate-based carriers coated with polyethyleneimine. The packed-bed reactor was operated continuously for up to 10 column volumes at 1.45 mL x min^{-1} in the enantioselective deamination of model amines yielding >90% conversion in all cycles without exogenous addition of cofactor. The architecture of self-sufficient heterogeneous biocatalysts was expanded to other ω-transaminases such as the ones from *Chromobacterium violaceum* and *Pseudomonas fluorescens*. We found that enzymes with lower affinities towards PLP present lower operational stabilities in flow, even when co-immobilizing PLP. Finally, these self-sufficient heterogeneous biocatalysts were successfully implemented for the synthesis of chiral amines exploiting the concept of artificial metabolic cells under industrial-like continuous transaminations.

This chapter was previously published in *ACS Sustainable Chemistry and Engineering*.[1]

1. INTRODUCTION

In the last few decades, the application of enzymes on traditional chemical processes has already proven as an essential solution for sustainable chemistry.[2-4] However, there are still several drawbacks in terms of process intensification when scaling-up the biocatalytic reactions. In this scenario, continuous-flow biocatalysis has emerged as a powerful instrument to shorten reaction times, increase conversion yields and remove undesired by-products, making the process economically more attractive too.[5, 6] Due to its easy-to-use and low-cost properties, the use of whole cell biocatalysis was foremost implemented in flow chemistry.[7, 8] Later, purified enzymes were found to offer more advantages avoiding the generation of toxic by-products and the mass transfer limitations posed by cell membranes.[9] But either expensive cofactors or exogenous partners must be exogenously added to the reaction. The artificial metabolic cells concept pursues meeting an intermediate state harnessing benefits provided by the co-immobilization of purified multi-enzyme systems and their cofactors on the same carrier.[10]

Aminations and de-aminations are important reactions in industrial processes. More specifically, the synthesis of optically pure amines is gaining momentum in the manufacturing of a plethora of commodities, agrochemicals and pharmaceuticals.[11] In the last decade, biocatalysis has offered efficient and environmentally sustainable solutions to incorporate amine groups into organic molecules under mild conditions with exquisite region and stereoselectivies.[12-14] Amidases,[15] transaminases,[16, 17] ammonia lyases,[18] amino acid dehydrogenases[19] and the recently engineered amine dehydrogenases[20] are among the most relevant enzymes exploited for the synthesis of chiral amines. PLP-dependent ω-transaminases (EC 2.6.1.X.) efficiently transfers amino groups from sacrificing amines or amino acids to the starting ketones or aldehydes with quantitative yields.[21, 22] There are dozens of examples where different ωTAs have been engineered to aminate industrially relevant molecules.[21, 23] Although the PLP is bound to ωTAs through a reversible imine bond, scaled-up biotransformations using high substrate concentrations require exogenous PLP to achieve high amine yields (50-100 mM).[24, 25] Like other cofactor-dependent enzymes, the exogenous addition of PLP complicates the work-up because it must be primarily added to the reaction and then separated from the final products increasing the process costs. Fortunately, catalytic amounts of PLP (0.1-2 mM) are enough to accomplish the amine transfer reaction because ωTAs recycle such cofactor during

their catalytic cycle. Nevertheless, the separation of both soluble cofactors and biocatalysts beside the low stability of ωTA pose important hurdles to scale-up processes.

Immobilization of ωTAs is proven an efficient approach to increase the operational stability of these biocatalysts as well as to intensify the amination process with the aim of achieving both higher productivities and yields.[26] Several ωTAs have been immobilized onto a great variety of carriers and using different immobilization strategies, but some of them dramatically failed to keep the enzyme active and stable. In some cases the performance of the immobilized ωTA was significantly worse than its soluble counterpart.[26-29] This fact means that the immobilization protocol must be carefully selected to keep catalytic efficiency and gain enzyme stability.[30] In the particular case of ωTAs, their immobilization is challenging because a random multi-point covalent attachment through short irreversible bonds often distort their 3D structures, dramatically inactivating them. In spite of these difficulties, some immobilization protocols provided highly robust heterogeneous biocatalysts enabling process intensification of amine synthesis using packed-bed reactors (PBR).[28, 29] Flow-biocatalysis can lead the development of more sustainable chemical synthesis since it gains control over several key reactor and reaction parameters. For example, the oriented immobilization and further covalent attachment of ωTA from *Halomonas elongata*[31] onto methacrylate porous beads has been integrated into a continuous process coupled with a scavenger for the in-line synthesis and purification of different optically pure amines.[29]

Continuous operation of enzymatic transaminations contributes to process intensification so far. However, those systems still require the exogenous addition of PLP that can limit their economic feasibility for the synthesis of low-added value products.[28, 29] Ideally, PLP and enzyme should be co-reused to increase their operational life-span and thus increasing the cost efficiency of the processes. Just one example has been reported where PLP has been incorporated into the solid phase of heterogeneous biocatalysts to continuously synthesize amines.[32] Andrade *et al.* used whole cells harboring a ωTA physically adsorbed together with PLP onto methacrylate polymeric beads. The newly generated biocatalyst was able to synthesize optically pure α-alkoxy- and α-aryloxy isopropyl amines in flow with negligible lixiviation of PLP. However, this system was limited to organic reaction environment to avoid the cofactor lixiviation.

In this chapter, several ωTAs from *Halomonas elongata* (He-ωTA)[31] *Chromobacterium violaceum (*Cv-ωTA)[33] and *Pseudomonas fluorescens* (Pf-ωTA),[34] have been co-immobilized with PLP and exploited for flow transaminations. ωTA and PLP were co-immobilized onto commercial methacrylate beads functionalized with different reactive groups; cobalt-chelates, epoxy groups and positively charged amines (Table 1). These self-sufficient heterogeneous biocatalysts have been successfully integrated into flow PBR to perform the synthesis of chiral amines in buffer environment and without exogenous supply of PLP.

2. EXPERIMENTAL SECTION

2.1. Materials

LifetechPurolite ECR 8215F and Sepabeads EC-EP/S were kindly donated by Purolite Ltd. (Llantrisant, U.K.) and Resindion S.R.L., respectively. Polyethyleneimine 60 kDa 50%wt aq. solution, branched (PEI60) was purchased from ACROS Organics™. Ethanolamine, hydroxylamine, (S)-phenylethylamine, rhodamine B isothiocyanate, IDA, cobalt (II) chloride, trans-cinnamaldehyde, *p*-nitrobenzaldehyde, sodium borate, sodium pyruvate, *S*-(α)-Methylbenzylamine (*S*-MBA), kanamycin, ampicillin, amicon ultra 0.5 mL centrifugal filters 10 kDa, Supelcosil LC-18-T column (250 mm x 4.6 mm, 5 µm particle size; Supelco) and PLP were acquired from Sigma-Aldrich (St. Louis, IL). UV transparent 96-well plates and 1 mL cuvettes were purchased from Thermo Fisher Scientific. µ-Slides with 8 wells were purchased from ibidi (Planegg, Germany). All other salts and reagents were of analytical grade.

2.2. Methods

2.2.1. Activation of Purolite-based carriers

Epoxy-purolite (Pu-E) was incubated with 0.5 M IDA at pH 11.0 for 3 hours at room temperature and orbital shaking. Afterwards, samples were intensively washed with distilled H_2O. A solution of 30 mg x mL^{-1} $CoCl_2$ was added (1:10 w/v) and incubated for 1 hour. After a washing step, Pu-Co^{2+}/eA and Pu-Co^{2+}/hA were prepared adding 0.5 M ethanolamine and 0.5 M hydroxylamine at pH 11.0 and incubated overnight under orbital shaking. Finally, the resin was intensively washed with distilled water, filtered and stored at 4 ºC until use

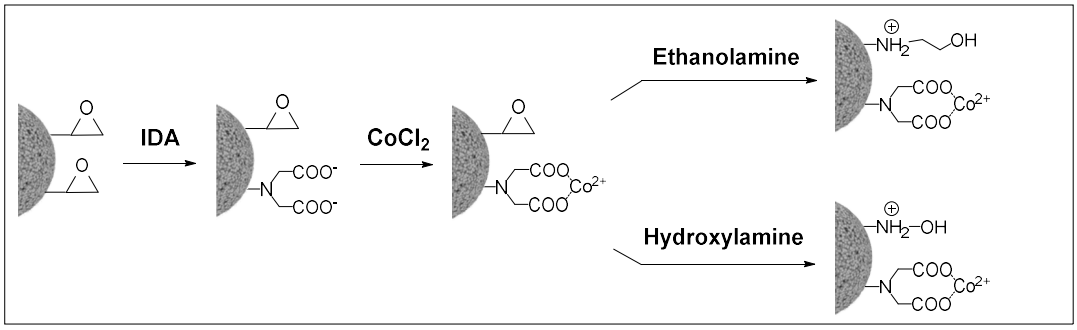

Figure 1. Protocol for the activation of Purolite-based carriers.

2.2.2. Activation of Sepabead-based carriers

Epoxy-sepabeads were firstly activated with cobalt as previously described.[29] Briefly, 5 g of epoxy-sepabeads were treated with 10 mL of modification buffer (100 mM sodium borate and 2 M IDA in 50 mM Tris-HCl buffer pH 8.5) under gentile shaking for two hours at room temperature. The sample was then filtered and washed with distilled water. 25 mL of metal buffer (1 M of sodium chloride and 5 mg x mL^{-1} $CoCl_2$ in 50 mM phosphate buffer at pH 6.0) applied for two hours. The sample was then filtered and washed with distilled water. EC-Co^{2+}/eA was prepared by adding 0.5 M ethanolamine at pH 11.0 and incubating overnight under orbital shaking. For preparation of EC-Co^{2+}/PEI60, a solution of 10 mg x mL^{-1} PEI60 (50% v/v in water) in 100 mM sodium bicarbonate buffer at pH 10.0 was added after protein immobilization and incubated for 1 hour under orbital shaking. In all cases, the resins were finally intensively washed with distilled water, filtered and stored at 4 ºC until use.

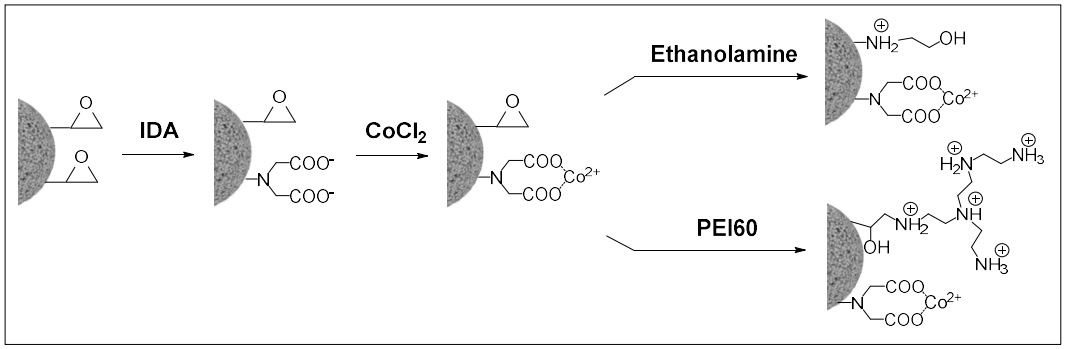

Figure 2. Protocol for the activation of Sepabead-based carriers.

2.2.3. Expression and purification of enzymes

He-ωTA and Cv-ωTA were expressed and purified following a modified version of a previously reported protocol.[31] Concisely, the cells were grown in 50 mL of ZYM-5052 medium for auto-induction at 37 ºC overnight. Then, the cells were harvested by centrifugation (4211 g, 4 ºC, 30 min). The pellet was resuspended in 7.5 mL of the lysis buffer (50 mM potassium phosphate buffer pH 8.0 and 0.1 mM PLP). The cells were disrupted by sonication at 4 °C using Sonics VCX 130 with 10 cycles of 30 sec ON and 30 sec OFF. After centrifugation (38.000 g, 4 °C, 45 min), the supernatant was clarified by filtration (0.45 µm filter). For the expression of Pf-ωTA, cells were grown in 50 mL of LB medium at 37 °C with energetic shaking until the OD_{600nm} reached 0.6. At that point, the culture was induced with 0.01 mM IPTG. Cells were grown at 21 °C for 16 hours and then harvested by centrifugation (4211 g, 4 ºC, 30 min). The resulting pellet was resuspended in 5 mL of 10 mM sodium phosphate buffer at pH 7.3 containing 0.1 mM PLP. Cells were sonicated (Sonics Vibracell VCX750) at amplitude= 20 %, during 15 min of 5 sec ON, 5 sec OFF. After centrifugation (10528 g, 30 min, 4 ºC), the supernatant was collected and stored at 4 ºC. The protein purification was followed by SDS-PAGE (Figure 3).

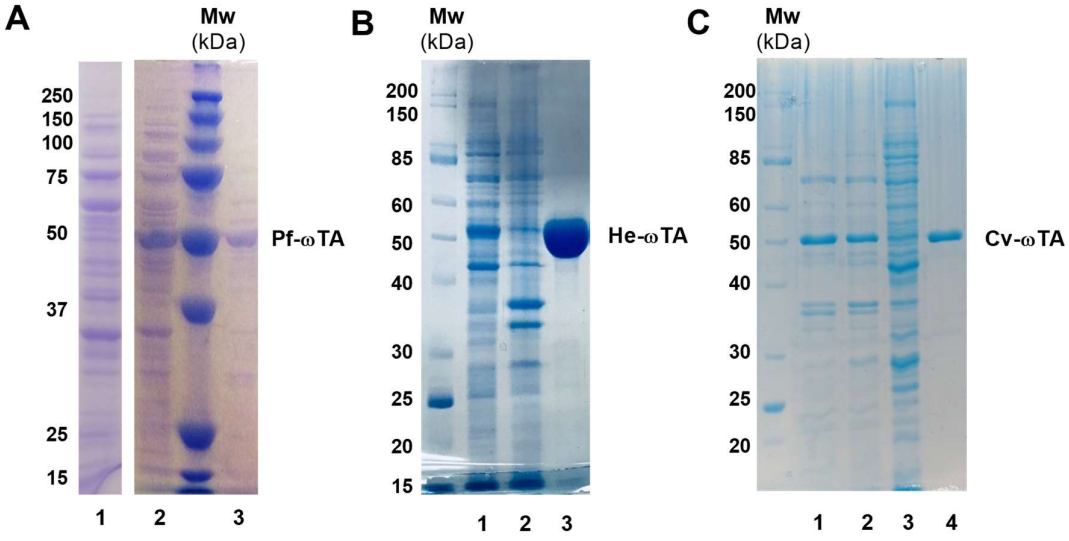

Figure 3. SDS-PAGE of protein purifications. The molecular weight markers are BioRad Precision Plus Protein All Blue Standard for (A) and NEB (Broad Range 10-200 kDa) for (B) and (C). A) Pf-ωTA. Line A1: affinity column flow-through, line A2: soluble fraction after cell disruption by sonication and line A3: purified Pf-ωTA. B) He-ωTA. Line B1: crude extract, line B2: pellet after sonication and line B3: purified He-ωTA. C) Cv-ωTA. Line C1: crude extract, line C2: soluble fraction after sonication, line C3: insoluble fraction after sonication and line C4: purified Cv-ωTA.

2.2.4. Protein quantification

The protein concentration was quantified by Bradford assay as described in Chapter 4 (page 91).

2.2.5. Enzyme immobilization

10 mL of enzyme solution (0.1 – 0.5 mg x mL^{-1}) containing 0.1 mM PLP in 50 mM sodium phosphate buffer at pH 8, were added to 1 g of carrier and incubated under orbital shaking for 4 hours (He-ωTA and Cv-ωTA), or for 1 hour (Pf-ωTA) at room temperature. Then, the suspension was filtered and washed 3 times with 10 volumes of phosphate buffer. When the enzyme was immobilized on EC-Co^{2+}/PEI60, the PEI coating was performed after protein immobilization, as described in Chapter 4.

2.2.6. Parameters of immobilized enzymes

The immobilization yield and the specific activity were calculated as described in Chapter 4 (page 93) unless otherwise specified.

2.2.7. Cofactor immobilization

Immobilization of PLP was achieved as described by Velasco-Lozano *et al.*[35] Briefly, 10 mL of 1 mM PLP in 10 mM sodium phosphate buffer at pH 7.3 were incubated with 1 gram of methacrylate beads with previously immobilized enzymes. The suspension was kept under orbital shaking for 1 hour at room temperature. The sample was then filtered and washed three times with 10 mM sodium phosphate buffer at pH 7.3. The immobilized PLP was determined by measuring the absorbance at 390 nm of 100 µL of the flow-through in a 96-well microplate using a Varian Cary 50 scan UV-visible spectrophotometer. The cofactor load and the cofactor immobilization yield were calculated as described in Chapter 4 (page 94).

2.2.8. Enzyme activity assays

The activity of immobilized ω-TAs was determined by mixing 50 mg of biocatalyst and 10 mL of reaction mixture (2.5 mM pyruvate, 2.5 mM *S*-MBA and 0.25 % DMSO in 10 mM phosphate buffer pH 7.3) in a 15 mL reaction tube cap. The final reaction mixture

was incubated at room temperature under orbital shaking. The absorbance at 245 nm was measured along the time as single readings using Brand UV-cuvettes in a Varian Cary 50 scan UV-visible spectrophotometer. One unit of ω-transaminase activity was defined as the amount of enzyme required for the production of 1 µmol of acetophenone per minute.

2.2.9. Rhodamine-labeling of He-ωTA

The enzyme was labeled as described in Chapter 3 (page 58).

2.2.10. CLSM imaging

Enzyme distribution was analyzed using a ZEISS confocal microscope LSM510 using λ_{ex}: 514 nm and the emission filter LP550. Since PLP exhibits autofluorescence, the spatial distribution of PLP across the EC-Co^{2+}/PEI60 beads was determined using an UV excitation laser (405 nm) and the emission filter LP420. Images were processed with the software ZEN2012.

- Spatial distribution study. The labeled enzyme was further immobilized at 1 mg x g^{-1} onto EC-Co^{2+} beads. After PEI coating, PLP was co-immobilized at 7.5 µmol x g^{-1}. The beads suspension was filtered and placed on a microscope slide. In order to improve the match in refractive index between the medium and the opaque beads, a drop of glycerol was added to the filtered beads onto the slide.
- PLP immobilization kinetics. 20 mg of EC-Co^{2+}/PEI60 were incubated with 200 µL of 1 mM PLP solution containing 50% glycerol in sodium phosphate buffer pH 7.3 in a 8-well µslide. PLP autofluorescence was monitored along the time.
- Desorption experiments. Three desorption experiments of PLP were carried out using different buffer compositions. 50 mg of EC-Co^{2+}/PEI60 with immobilized PLP were incubated with 500 µL of 4 M NaCl, 1 M ethanolamine or a mixed solution with 4 M NaCl and 1 M ethanolamine. The suspensions were incubated at room temperature for 1 hour. After filtration, three washing steps with phosphate buffer were performed. The beads were observed by adding a drop of glycerol. Finally, PLP was immobilized for second time by adding 400 µL of 1 mM PLP solution to 40 mg of EC-Co^{2+}/PEI60 (previously treated with ethanolamine).

2.2.11. Flow deamination reactions

The continuous flow biotransformations were performed in collaboration with Prof. Paradisi's group by using a R2+/R4 flow reactor commercially available from Vapourtec equipped with an Omnifit glass column (6.6 mm i.d x 100 mm lenght) filled with 1 gram of biocatalyst. An amino acceptor substrate solution (20 mM pyruvate in phosphate buffer) and an amino donor solution (50 mM *S*-MBA and 5% DMSO in phosphate buffer) were prepared. After mixing with a T-tube the resulting concentrations were 10 mM for the amino acceptor and 25 mM for the amino donor. 50 mM phosphate buffer at pH 8.0 was used for flow-reactions with exogenously added PLP (0.1 mM) and when no PLP was added. 10 mM phosphate buffer at pH 7.3 was used for flow-reactions when PLP was co-immobilized. The resulting flow stream was driven to the column packed-bed reactor with the biocatalyst (PBR volume: 1.3 - 1.45 mL). A first washing step with a flow rate of 0.4 mL x min^{-1} was performed for 30 minutes. Then, the flow rate was varied in order to obtain the desired residence time. The resulting flow product was analysed by HPLC following a previously reported protocol.[29] In short, 100 µL aliquots were quenched with 50% of acetonitrile, 50% of HCl (0.2% v/v) and then analysed by HPLC equipped with a Supelcosil LC-18-T column. The compounds were detected using an UV detector at 210 nm or 250 nm after an isocratic run with 25% acetonitrile / 75% water with TFA (0.1% v/v) at 45 °C with a flow rate of 1 mL x min^{-1}. The retention times were: (*S*)-(−)-1-phenylethylamine (1.9 min), acetophenone (2.1 min).

2.2.12. Flow synthesis of amines

The continuous flow synthesis of cinnamylamine and *p*-nitrobenzylamine were performed in collaboration with Prof. Paradisi´s group by using the equipment described above. The synthesis of cinnamylamine was performed preparing two solutions; solution 1: 20 mM *trans*-cinnamaldehyde, and 10% of DMSO in phosphate buffer and solution 2: 1 M L-alanine in 10 mM phosphate buffer. After the mixing, the concentrations of *trans*-cinnamaldehyde and L-alanine were 10 mM and 500 mM, respectively. In the synthesis of *p*-nitrobenzylamine, the amino acceptor solution (10 mM *p*-nitrobenzaldehyde and 20 % of DMSO in phosphate buffer) was mixed with the amino donor solution (1 M L-alanine in phosphate buffer). After the mixing, the concentrations of *p*-nitrobenzaldehyde and L-alanine were 5 mM and 500 mM,

respectively. The resulting flow product was analysed by HPLC as described in the previous section.

3. RESULTS AND DISCUSSION

3.1. Optimization of the micro-architecture for the co-immobilization of ω-TA and PLP

Expanding the concept of self-sufficient heterogeneous biocatalysts to amine synthesis using PLP-dependent ωTAs, commercial porous methacrylate beads activated with epoxy groups were firstly functionalized with cobalt-chelates and then blocked with either hydroxylamine or ethanolamine (Figure 1, Table 1), giving rise to carriers named as Pu-Co^{2+}/hA and Pu-Co^{2+}/eA, respectively. The immobilization conditions were optimized using these Purolite-based resins as carriers.

Table 1. Different architectures of self-sufficient heterogeneous biocatalysts based on co-immobilized ωTA and PLP.

Carriers				
Code	**Pu-Co^{2+}/hA**	**Pu-Co^{2+}/eA**	**EC-Co^{2+}/eA**	**EC-Co^{2+}/PEI60**
Commercial name	ECR8215F	ECR8215F	EC-EP/S	EC-EP/S
Particle size	150-300µm	150-300µm	100-300µm	100-300µm
Pore size	120-180 nm	120-180 nm	10-20 nm	10-20 nm
Aminated molecule	Hydroxylamine	Ethanolamine	Ethanolamine	PEI60
Scheme		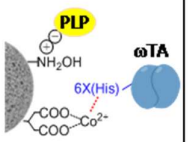	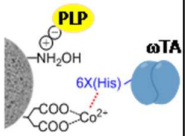	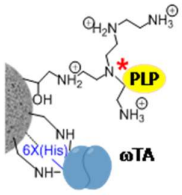

Pu-Co^{2+} and EC-Co^{2+} carriers were activated with different aminated molecules; hydroxylamine (/hA), ethanolamine (/eA) and polyethileneimine (PEI60). Red dashed bonds are the coordination bonds between His-tag and cobalt chelates. Red dashed lines represent the metal coordination bond between the enzyme and the cobalt groups. Red asterisk show the dual binding mode of PLP immobilization (see Figure 11 for more details).

In our group, we previously achieved the co-immobilization of an ωTA and PLP onto agarose beads by using low ionic strength (10 mM) phosphate buffer at pH 7 to favour

the ionic interactions between PLP and the positively charged surface of the carrier.[35] However, flow-reactions using immobilized He-ωTA were performed in 50 mM phosphate buffer at pH 8 at Prof. Paradisi´s laboratory.[29] These conditions match with another work which showed that an increased buffer concentration might prevent PLP release from the enzyme, and hence enhance the structural holoform stability of ωTA from *Vibrio fluvialis*.[36] But, paradoxically, an increased buffer concentration could also result in decreased enzyme residual activity.[37] Therefore, different conditions to co-immobilize the enzyme and the cofactor were tested to avoid its lixiviation into the reaction medium. To this aim, He-ωTA and PLP were co-immobilized onto Pu-Co^{2+}/eA under several buffered solutions. It must point out that both enzyme and cofactor were reversibly bound to this carrier through coordination and ionic bonds, respectively. As expectedly, 10 mM phosphate buffer and Tris-HCl buffer at pH 7.3 were the most effective conditions to minimize PLP and enzyme lixiviation after 3 consecutive washes (Figure 4). The use of phosphate buffer instead Tris-HCl buffer is indeed beneficial for the process since phosphate promotes the stability of the apoenzyme and prevents its irreversible unfolding.[38] For these reasons, phosphate buffer was selected to carry out the enzymatic reactions.

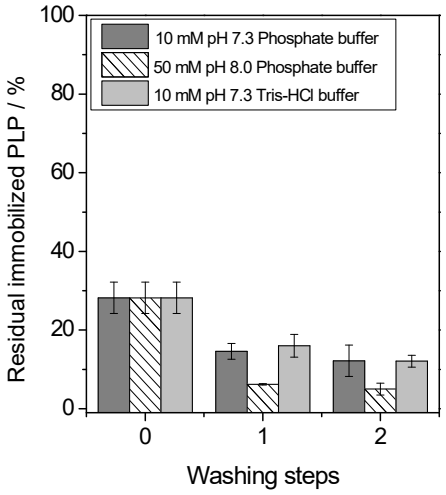

Figure 4. Optimization of ionic strength and pH of the buffer for the PLP immobilization. Pu-Co^{2+}/eA beads were incubated with 1 mM PLP prepared in different buffered solutions for 1 hour at room temperature.

Afterwards, different functionalizations of Purolite-based carriers (Pu-Co^{2+}/hA and Pu-Co^{2+}/eA) were analyzed for the co-immobilization of PLP. Once tested the deamination activity of the immobilized biocatalyst towards *S*-MBA, the activity of He-ωTA was

significantly lower when PLP was adsorbed onto Pu-Co^{2+}/hA than onto Pu-Co^{2+}/eA (Figure 5), indicating that the cofactor was catalytically more available when the solid surface was activated with ethanolamine. Due to the higher pKa of ethanolamine (pKa: 9.5) compared with hydroxylamine (pKa: 6.03), the ionic exchange between PLP and amines groups could be better maintained on Pu-Co^{2+}/eA.

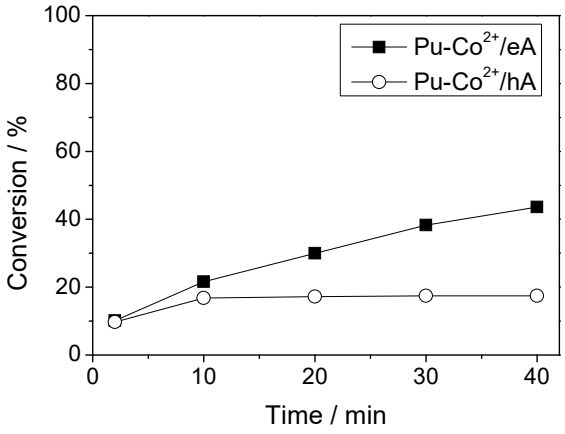

Figure 5. Effect of amine group on the enzyme kinetics. He-ωTA was immobilized onto Pu-Co^{2+}/eA and Pu-Co^{2+}/hA beads at 1 mg x g^{-1}. PLP was co-immobilized at 1.7 ± 0.09 µmol x g^{-1} onto Pu-Co^{2+}/eA and 6.5 ± 0.01 µmol x g^{-1}onto Pu-Co^{2+}/hA.

Finally, we tested the effect of the carrier architecture on PLP binding by using methacrylate carriers activated with ethanolamine at two different pore sizes (Table 1). Methacrylate beads (EC-Co^{2+}/eA) with smaller pores (size = 10-20 nm) loaded up to 8.6 μmol_{PLP} x $g_{carrier}^{-1}$ and 90% of the cofactor remained bound to the carrier after three washes. On the contrary, Pu-Co^{2+}/eA with larger pores (size = 120-180 nm) loaded 3 times less PLP (2.8μmol_{PLP} x $g_{carrier}^{-1}$) than EC-Co^{2+}/eA and the 43% of the bound cofactor was lixiviated after three washing steps (Figure 6A). Although the carriers were loaded with different amounts of PLP, co-immobilized He-ωTA expressed similar deamination rate and ketone yield without adding exogenous cofactor after the first batch cycle (Figure 6B).

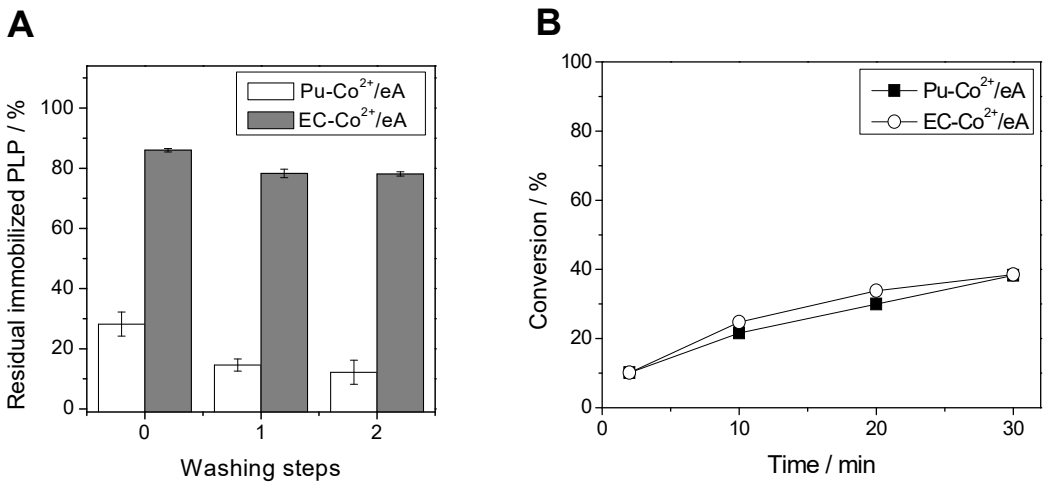

Figure 6. Effect of pore size on PLP immobilization yield and biocatalytic activity. A) Co-immobilization of PLP. EC-Co^{2+}/eA and Pu-Co^{2+}/eA were incubated with 1 mM PLP (1:10 v/w) in 10 mM phosphate buffer at pH 7.3. Washing steps were carried out with the same buffer. B) Enzyme kinetics of co-immobilized He-ωTA and PLP. The protein loading was 1 mg x g^{-1}. PLP was at 1.7 ± 0.09 µmol x g^{-1} onto Pu-Co^{2+}/eA and 7.8 ± 0.03 µmol x g^{-1} onto EC-Co^{2+}/eA.

3.2. Stability tests for deamination flow reactions

The final goal of the work developed in this chapter is the secondment of artificial metabolic cells to flow biocatalysis. For this purpose, the above described micro-architectures were tested in flow for the deamination reaction of *S*-MBA. After the first column volume in flow, He-ωTA co-immobilized with the cofactor on both EC-Co^{2+}/eA and Pu-Co^{2+}/eA showed a similar conversion yield (Figure 7). However, EC-Co^{2+}/eA biocatalyst presented a longer operational half-life time (133 minutes) in flow than the Pu-Co^{2+}/eA one (115 minutes). Nevertheless, the activation of methacrylate beads with ethanolamine and cobalt chelates (EC-Co^{2+}/eA) was not enough to operate the self-sufficient heterogeneous biocatalyst for longer times with high yields (Figure 7).

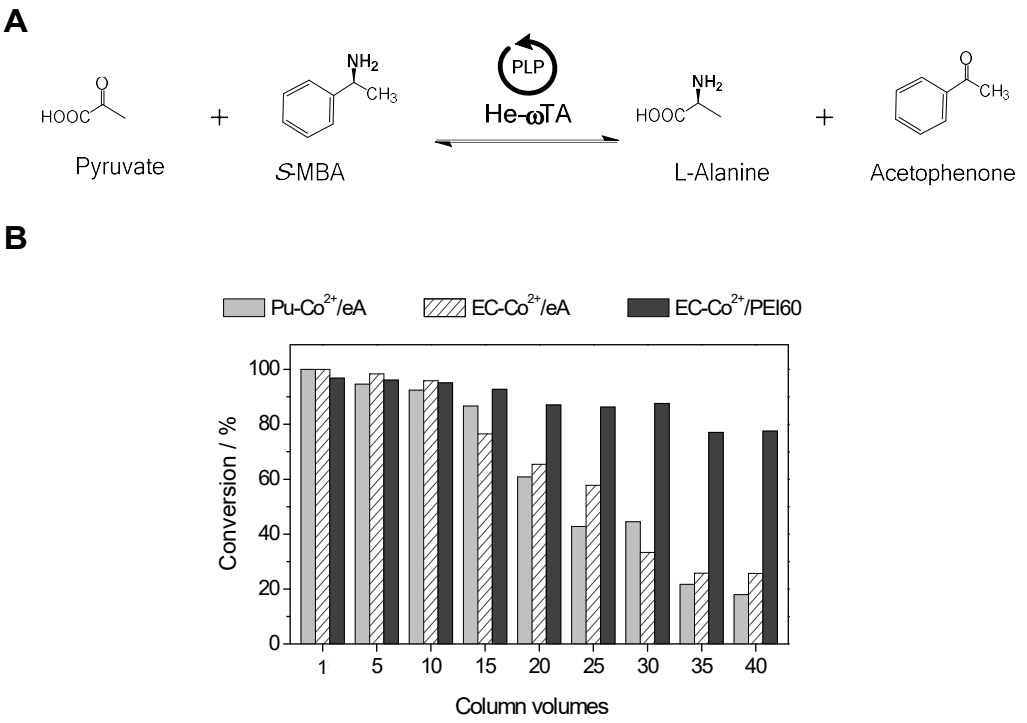

Figure 7. Stability test of different self-sufficient biocatalysts operating in flow at 0.3 mL x min^{-1}. He-ωTA was immobilized at 1 mg x g^{-1} onto three different carriers; Pu-Co^{2+}/eA, EC-Co^{2+}/eA and EC-Co^{2+}/PEI, that loaded 1.7, 7.8 and 7.5 μmol_{PLP} x $g_{carrier}^{-1}$, respectively. Each column volume corresponds to 5 minutes. A) Deamination reaction scheme. B) Conversion yields along the time.

PLP was observed in the flow-through after 20 minutes, suggesting that its lixiviation might explain the activity lost of the packed biocatalyst. In order to recover the activity of this self-sufficient biocatalyst, a new and fresh solution of PLP was offered to the EC-Co^{2+}/eA biocatalyst. Unfortunately, the biocatalytic activity was less than 11% for the flow deamination reaction, suggesting that the cofactor lixiviation inactivation was also explained by either the enzyme lixiviation or inactivation (Figure 8). The enzyme was immobilized through reversible metal coordination bonds between the poly-(6x)His at the N-terminal and the cobalt-chelates groups of the carrier surface (Figure 1). This well-known strategy for protein purification has been recently exploited for a ten-minute protein purification followed by an efficient continuous-flow production of *p*-nitrophenol by a bi-enzimatic (alkaline phosphatase and phosphodiesterase) immobilized system.[39] However, in our case the reversible immobilization of He-ωTA could be reverted during the operational process, provoking the enzyme release and causing the yield decay observed in Figure 8. The immobilization of proteins through one-point and long spacer

arms does not lead to high stabilization factors as Orrego *et al.* previously demonstrated by fluorescence anisotropy.[40]

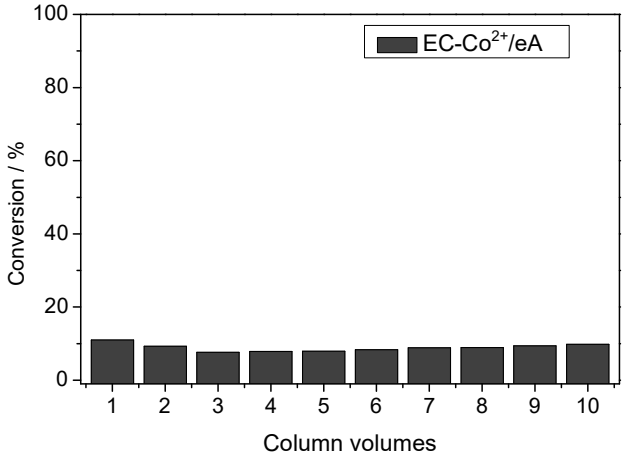

Figure 8. Stability test of EC-Co^{2+}/eA biocatalyst after second co-immobilization of PLP. The cofactor was again loaded at 7.8 μmol_{PLP} x $g_{carrier}^{-1}$, respectively. Flow reactor operated at 0.3 mL x min^{-1}. Each column volume corresponds to 5 minutes.

To avoid both enzyme and cofactor lixiviation, and consequently improve the performance of the biocatalyst, we modified the functionalization of the carrier to establish irreversible bonds between the enzyme and the solid surface and optimize the reversible interactions between PLP and the surface matrix. Firstly, the His-tagged enzyme was driven towards the carrier surface by cobalt-chelates. Secondly, amino groups from the enzyme stablished a covalent bond with the epoxy groups of the carrier. After site-directed immobilization of He-ωTA, the remaining epoxy groups were exploited to allow the PEI coating upon the immobilization (EC-Co^{2+}/PEI60, Table 1). In this thesis, similar approaches using PEI coating have been already described for efficient co-immobilization of cofactors on agarose beads (Chapter 4[35]). Herein, PLP was also co-immobilized onto PEI coated-methacrylate beads containing covalently immobilized He-ωTA. This architecture was utilized in continuous deamination reactions, significantly increasing the operational life of the self-sufficient heterogeneous biocatalyst since the reaction conversion decayed less than 20% after 200 minutes (40 column volumes) (Figure 9).

Flow rate is also another crucial parameter that governs productivity of continuous operations. Once both PLP and He-ωTA were optimally co-immobilized onto EC-

Co^{2+}/PEI60, this self-sufficient heterogeneous biocatalyst was tested at two different flow rates; 0.3 and 1.45 mL x min^{-1} (Figure 9).

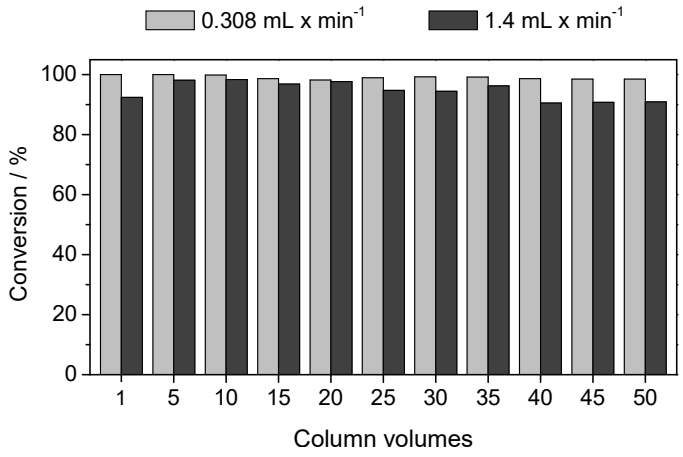

Figure 9. Stability test of He-ωTA and PLP co-immobilized on EC-Co^{2+}/PEI60 at different flow rates. Enzyme and cofactor loading were 5 mg x g^{-1} and 7.8 µmol x g^{-1}, respectively. For the flow rate at 0.308 mL x min^{-1}, each column volume corresponds to 5 minutes and for the flow rate at 1.45 mL x min^{-1}, each column volume took 1 minute.

Operating the PBR at higher flows, the specific productivity of He-ωTA increased from 6.79 to 33.95 $\mu mol_{product}$ x min^{-1} x mg_{enzyme}^{-1} and remained constant after processing 56 mL of reaction mixture (40 column volumes). This result clearly indicates that bound PLP is not lixiviated even under high flow rates, strongly favouring enzymatic productivity. Therefore, this PBR successfully operated at 1.45 mL x min^{-1}, the highest flow rate ever reported using co-immobilized enzyme and cofactor[32, 35, 41] and one of the highest (0.1-1.7 mL x min^{-1}) using immobilized enzymes supplied with exogenous cofactor.[27-29, 42]

3.3. Single-particle analysis of EC-Co^{2+}/PEI60 biocatalyst and PLP immobilization

In order to understand the performance of the EC-Co^{2+}/PEI60 self-sufficient heterogeneous biocatalysts under flow conditions, the sub-particle environment was deeply analyzed to better understand the properties of those biocatalysts. PLP binding monitored by time-lapse fluorescence microscopy demonstrates the reversible nature of PLP interaction since such cofactor is primarily adsorbed to the outer surface of the beads (when immobilizing in short times), to further migrate across their porous structures along the time (Figure 10).

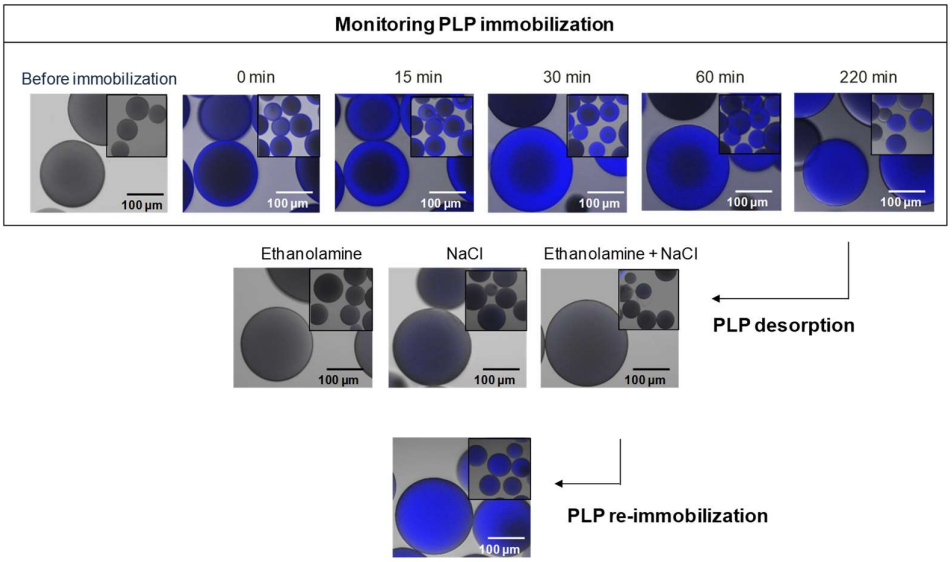

Figure 10. Reversible PLP immobilization. Single-particle studies of PLP immobilization kinetics by CLSM imaging. Images show the overlay of fluorescence and brightfield signals.

The cofactor migration proves that PLP molecules can reach enzyme active sites within the carrier microstructure but without diffusing out to the reaction bulk. Functional data together with microscopic analysis indicate that the nature and the density of positively charged groups as well as the pore size of the methacrylate beads are determinant parameters to allow the PLP shuttling between the enzyme active sites without leaving the pore microenvironment.

As mentioned above, the enzyme was oriented and irreversibly immobilized through a multivalent attachment, while PLP established an association-dissociation equilibrium with the PEI layer, through both ionic bridges and reversible imine bonds (Schiff´s bases) (Figure 11). Such dual interaction was supported by desorption experiments that demonstrate quantitative PLP elution from EC-Co^{2+}/PEI60 requires both high salt and ethanolamine concentrations to break ionic bonds and Schiff´s bases, respectively (Figure 10). Unlike other phosphorylated cofactor such as NAD(P)H, aldehyde groups and phosphate groups in PLP can establish that dual interaction with the primary amines and the positively charged amine groups of PEI, respectively (Figure 11). The reversible imines bonds between PLP and PEI mimic the chemistry that anchors such cofactor into the ωTA active site.[43] Moreover, once PLP is fully eluted, the carrier can be equilibrated and re-charged with fresh PLP (Figure 10).

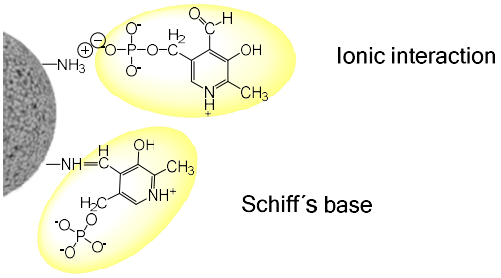

Figure 11. Scheme of the dual-binding mode of PLP on EC-Co^{2+}/PEI60.

The higher capacity of EC-Co^{2+}/PEI60 to reversibly bound PLP through a dual binding is supported by its K_d = 20.4 ± 0.9 µmol x g^{-1}, which is significantly lower than K_d values determined for EC-Co^{2+}/eA (K_d = 27.4 ± 1.2 µmolx g^{-1}) and Pu-Co^{2+}/hA (K_d = 121.4 ± 5.8 µmol x g^{-1}) carriers. These equilibrium constants were determined by fitting experimental data to Langmuir isotherm equation (Figure 12). The PLP adsorbed in EC-Co^{2+}/PEI60 falls in the same order or magnitude that the PLP equilibrium constants determined with similar positively charged surfaces.[35] Hence, the nature of the interaction between PLP and carrier surface dictates how strong PLP is bound to the matrix. Therefore, PEI containing primary, secondary and tertiary amines are capable to establish two type of interactions with PLP, salt bridges and imine bonds retaining more efficiently the cofactor that surfaces only activated with secondary amines (EC-Co^{2+}/hA and eA) that limit PLP adsorption to ionic interactions.

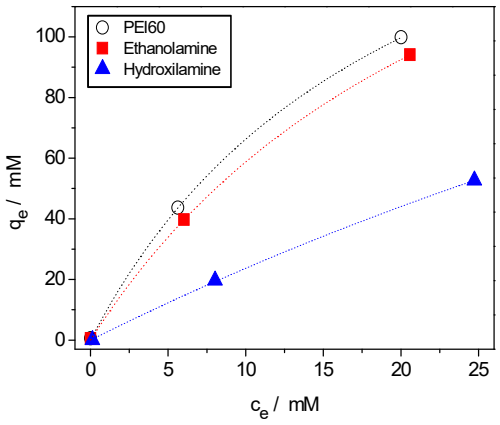

Figure 12. Adsorption isotherms of PLP. Three methacrylate-based carriers activated with different aminated groups (PEI60, ethanolamine, and hydroxylamine) were used to immobilize PLP. The X-axis shows the PLP load at the equilibrium (C_e) and the Y-axis the free PLP at the equilibrium (q_e) in the supernatant.

Additionally, confocal microscopy of EC-Co^{2+}/PEI60 co-immobilizing PLP and He-ωTA revealed that both molecules co-localized within the same particle but with different spatial distributions (Figure 13). The spatial organization of both PLP and enzyme remained stable even after one-week storages at 4 ºC, demonstrating that the enzyme cannot migrate inside the porous surface because it is irreversibly bound, while the cofactor is unable to diffuse out of the beads (Figure 13). While He-ωTA is located at the outer surface of the porous beads, PLP is homogenously distributed across the whole carrier surface. As it was revealed in Chapter 4, the heterogeneous distribution of the enzyme across the porous particles influences the enzyme kinetics of the biocatalyst. The enzyme localization in the outer phase of the particle may benefit the substrate-product exchange between the biocatalysts and the external reaction media.

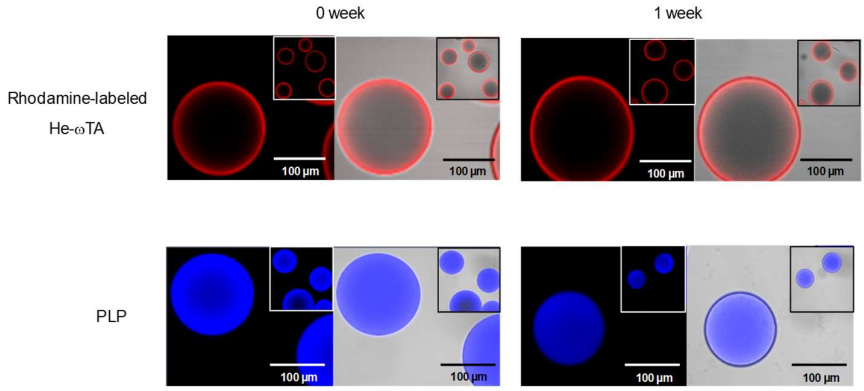

Figure 13. Single-particle studies of EC-Co^{2+}/PEI60 by CLSM imaging along the time. Spatial distribution of rhodamine-labeled He-ωTA (red) and PLP (blue) within the porous particles. The left side image of each panel shows the fluorescence signal and the right one merges the fluorescence and the brightfield signals.

3.4. Expanding the scope of ωTA-based artificial metabolic cells for flow reactions

In principle, this promising approach may be expanded to other ωTAs in order to fabricate a battery of self-sufficient heterogeneous biocatalysts with different catalytic properties (stability, selectivity, kinetics). Based on the same architecture, two additional N-terminal His-tagged ωTAs, Cv-ωTA and Pf-ωTA, were immobilized onto EC-Co^{2+} and further coated with PEI to finally absorb PLP as described above. In all cases, >90 % of offered activity (5 mg_{enzyme} x $g_{carrier}^{-1}$) was immobilized and each heterogeneous biocatalyst loaded 7-7.5 μmol_{PLP} x $g_{carrier}^{-1}$ (Table 2).

Table 2. Immobilization yields and specific activities of immobilized ω-transaminases onto EC-Co^{2+}/PEI60.

Enzyme	Protein load ($mg \times g^{-1}$)	Immobilization yield (%)	Cofactor load ($\mu mol_{PLP} \times g_{carrier}^{-1}$)	Immobilized specific activity ($U \times mg^{-1}$) and [Relative recovered activity (%)]	
				Free PLP	*Co-immobilized PLP*
He-ωTA	4.95	99 ± 1.81	7.5 ± 0.08	0.29 ± 0.02 [11]	0.27 ± 0.02 [10]
Cv-ωTA	4.62	92 ± 3.42	7.4 ± 0.15	0.13 ± 0.03 [7]	0.11 ± 0.00 [6]
Pf-ωTA	5	100 ± 0.90	7 ± 0.21	0.16 ± 0.00 [8]	0.14 ± 0.01 [7]

Protein load of He-ωTA and Cv-ωTA was determined by Bradford assay. SDS-PAGE analysis by using ImageJ was carried out to determine the Pf-ωTA load. The enzymatic activities were measured in 96-well plates by monitoring absorbance at 245 nm. Briefly, 200 µL of a reaction mixture (2.5 mM pyruvate, 2.5 mM *S*-MBA, 0.25% of DMSO and 37.5 µM PLP in 10 mM sodium phosphate buffer at pH 7.3) were incubated with 10 µL of enzymatic solution or suspension (1:10 w/v).

As shown in Table 1, the enzymes were oriented and irreversibly immobilized through a multi-valent attachment, while cofactor establishes an association-dissociation equilibrium with the PEI layer. Upon the immobilization process, the three ωTAs recovered 8-11% of their specific activity in solution (Table 2). The low recovered activities might be caused by mass transport restrictions underlying the measurement set up. Enzyme activities were determined by spectrophotometric analysis using plate readers whose orbital shaking is not optimized to measure highly dense carriers with large particle size such as the porous methacrylate beads utilized in this work. In this context, the substrate likely suffers important diffusion barriers for being transported from the reaction bulk to the porous surface of the carrier, where both enzyme and cofactor are located. In fact, when enzyme activity was further measured under more vigorous shaking, the expressed activity of ωTA upon immobilization was increased up to 90% (Table 3) compared with the previous results (Table 2).

Table 3. Immobilization and activity parameters of co-immobilized Pf-ωTA and PLP on EC-Co^{2+}/PEI60.

Enzyme	Cofactor load ($\mu mol_{PLP} \times g_{carrier}^{-1}$)	Immobilization yield (%)	Relative recovered activity (%)
Pf-ωTA	0	92 ± 0.26	78 ± 1.2
	1	91 ± 0.04	120 ± 10
	10	94 ± 0.22	111 ± 15

The activity was monitored at high shaking orbital speed (800 rpm).

Noteworthy, the three ωTAs herein studied showed similar specific activity towards soluble and immobilized PLP, which demonstrates that the cofactor is fully available and can access to the ωTA active sites (Table 2).

Encouraged by the excellent enzymatic activity towards the immobilized cofactor, we tested the three different self-sufficient heterogeneous biocatalysts in the continuous deamination of *S*-MBA at 1.45 mL x min^{-1} (Figure 14A).

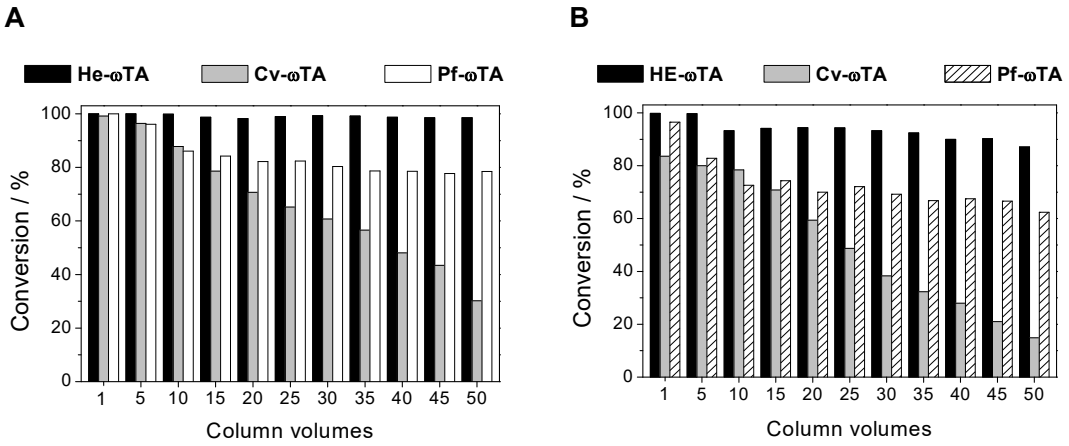

Figure 14. Stability test of the biocatalysts immobilizing ω-TA and with co-immobilized PLP (A) or without PLP at all (B). ω-transaminases were immobilized at 5 mg x g^{-1} onto EC-Co^{2+}/PEI60. The flow reactions were performed at 1.45 mL x min^{-1}. Each reaction cycle corresponds to 1 minute.

Interestingly, the operational performance of each biocatalyst relied on which ωTA was immobilized onto. He-ωTA maintained maximum conversion during the whole operational test producing 70 mL of 25 mM product after 10 column volumes. On the contrary, when the reactor was packed with Cv-ωTA co-immobilized with PLP, we observed a linear decay of conversion down to 30% after 10 column volumes (Figure 14A). Under the same conditions, Pf-ωTA performed notably better than Cv-ωTA but slightly worse than He-ωTA. Such differences on deamination efficiencies may rely on the affinity of each enzyme towards PLP. In fact, when flow reactions were performed using the different immobilized ωTAs with naturally bound PLP (not exogenously added), we observed a similar trend: He-ωTA preserved the highest conversion whereas Cv-ωTA showed the lowest one after 50 cycles (Figure 14B). These results suggest that high flows can detach more easily the natively bound PLP from Cv-ωTA than from He-ωTA. The unsatisfactory performance of Cv-ωTA can be explained by the

low affinity of this enzyme towards PLP (K_d = 78 μM)[37] compared to other ωTAs (K_d = 0.25-10 μM).[44] Hence, the operational stabilities shown in Figure 14, suggest that Pf-ωTA binds PLP better than Cv-ωTA but worse than He-ωTA. Actually, comparing conversion yields showed in Figure 14, Cv-ωTA biocatalyst increased 102% its stability after 50 cycles when the cofactor was co-immobilized while Pf-ωTA and He-ωTA only improved 45% and 6% respectively.

These results motivated us to understand whether the enzyme is stabilized by the immobilization itself, by the high effective PLP concentration in the enzyme vicinity or by a synergy of both effects. To answer that question, we immobilized Pf-ωTA with and without PLP on porous carriers functionalized with PEI, and the resulting preparations were thermally inactivated (Figure 15). Likewise, soluble enzyme was inactivated either in presence or absence of PLP. Soluble Pf-ωTA suffered a dramatic inactivation in absence of PLP, as well as the enzyme immobilized without the cofactor. Conversely, the co-immobilization of Pf-ωTA and PLP significantly stabilizes the enzyme against high temperatures (Figure 15).

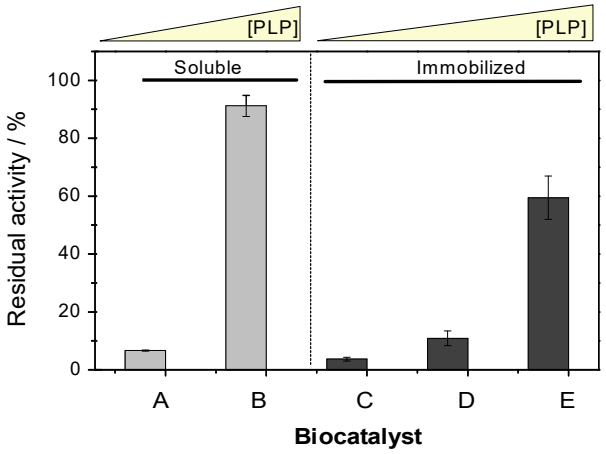

Figure 15. Stability of Pf-ωTA at different PLP concentrations. Bars represent the residual activity of the biocatalysts after 30 min of incubation at 65ºC: A) Soluble Pf-ωTA. B) Soluble Pf-ωTA at 0.1 mM PLP. C) Immobilized Pf-ωTA on EC-Co^{2+}/PEI60. D) Co-immobilized Pf-ωTA and PLP on EC-Co^{2+}/PEI60 at 1 $\mu mol_{PLP} \times g_{carrier}^{-1}$and E) Co-immobilized Pf-ωTA and PLP on EC-Co^{2+}/PEI60 at 10 $\mu mol_{PLP} \times g_{carrier}^{-1}$.

In fact, we observed a trend between the concentration of immobilized PLP and the enzyme thermal stability. When ωTA was surrounded by the highest PLP intraparticle concentration tested herein, the enzyme was 10 times more stable (Figure 15). This result indicates that the available concentration of PLP for ωTA relies on the

concentration of bound PLP. Hence, enzymes surrounded by more molecules of PLP are more stable (comparing C-E samples), because this cofactor stabilizes protein quaternary structure avoiding subunit dissociation.[29] When soluble PLP was incubated with soluble Pf-ωTA (comparing A and B samples), we observed a similar stabilization effect in agreement with the data published elsewhere for Cv-ωTA.[37] These experimental evidences point out that immobilization itself is not significantly stabilizing the enzyme (see soluble (sample A) and immobilized (sample B) preparation without being incubated with PLP), while the presence of PLP (both soluble (sample A) and co-immobilized forms (sample D and E)) enormously enhances the enzyme stability.

3.5. Flow-synthesis of chiral amines

Finally, to expand the application scope of this self-sufficient system, we performed the continuous synthesis of highly-valuable amines without exogenous supply of PLP (Figure 16).

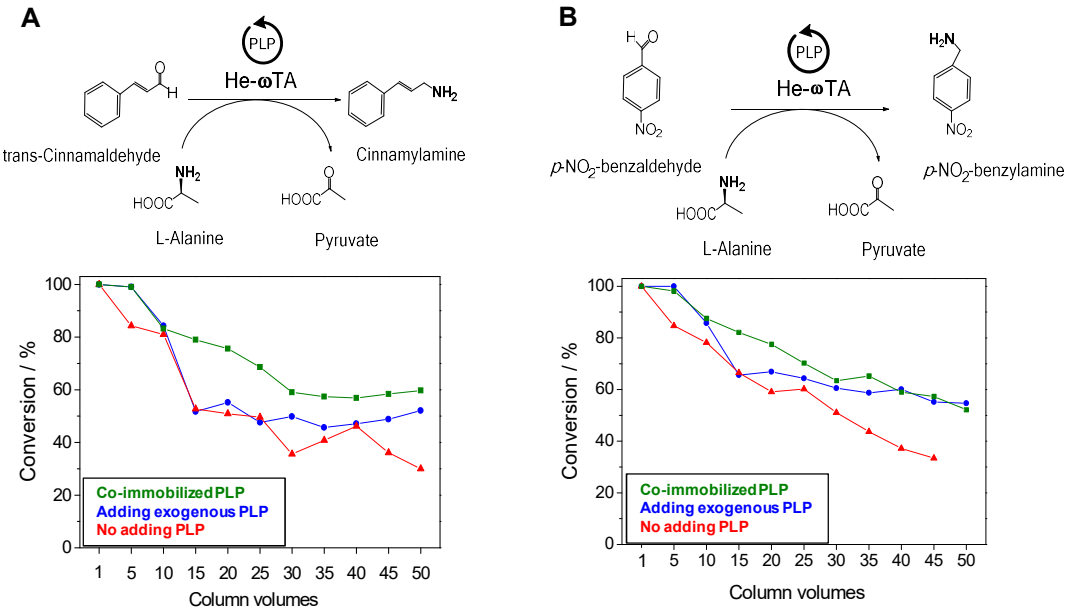

Figure 16. Synthesis of amines by EC-Co^{2+}/PEI60 biocatalysts. On the top side, the reaction schemes. On the bottom side, the conversion yields along the time. He-ωTA was immobilized onto EC-Co^{2+}/PEI60 at 5 mg x g^{-1}. The flow reactions were performed at flow-rate 0.725 mL x min^{-1}. Each column volume corresponds to 2 minutes. A) Synthesis of cinnamylamine. B) Synthesis of *p*-nitrobenzylamine.

A column packed with He-ωTA and co-immobilized PLP onto EC-Co^{2+}/PEI60 was fed with cinnamaldehyde to continuously synthesize cinnamylamine, a starting substrate for the synthesis of biologically active molecules.[45] Figure 14 shows as the self-sufficient heterogeneous biocatalyst is operationally slightly more stable than the system supplied with exogenous PLP. A similar trend was found for the synthesis of *p*-nitrobenzylamine (Figure 16B). The amine synthesis required double residence times than the deamination reaction to achieve a complete conversion, according to recently reported results with immobilized He-ωTA for the synthesis of chiral amines.[29] In addition, the operational stability under amination conditions was significantly lower than under deamination conditions. Likely, such decreased stability was due to the high concentration of L-Ala that may elute some of the bound PLP, since amine donor molecules contains amine and carboxylic groups that can compete with the dual interaction mode of PLP; imine and ionic bonds, respectively. Hence, the alanine would provoke the cofactor lixiviation which may explain the lower yields for the amination reaction compared to the deamination one.

4. CONCLUSIONS

In summary, the fabrication of self-sufficient biocatalytic systems has been prosperously implemented for transamination reactions in flow. To this aim, the co-immobilization of ωTAs from different origins with PLP was optimized onto the same porous methacrylate beads. Within these solid materials, His-tagged ωTA is irreversibly and multivalently attached to the carrier surface, whereas PLP is bound on a polymeric bed through reversible interactions (ionic bridges and imine bonds). As result, PBRs were operated using ωTAs from different sources with different operational stability results. We suggest that such stability relies on the affinity of each immobilized enzyme towards PLP. Finally, these self-sufficient heterogeneous biocatalysts were also applied for the continuous synthesis of valuable amines, obtaining high amine yields along the column volumes. This work proved that the architecture of artificial metabolic cells base on ωTAs and PLP is a functional and appealing alternative for chemical manufacturing of amines in flow. Moreover, these advances make up the path towards more environmentally-friendly industrial processes.

REFERENCES

1. Benítez-Mateos, A. I., Contente, M. L., Velasco-Lozano, S., Paradisi, F., López-Gallego, F. Self-sufficient flow-biocatalysis by coimmobilization of pyridoxal 5′-phosphate and ω-transaminases onto porous carriers. *ACS Sustainable Chemistry & Engineering*. **2018**, *6*: 13151-13159.

2. Wenda, S., Illner, S., Mell, A., Kragl, U. Industrial biotechnology—the future of green chemistry? *Green Chemistry*. **2011**, *13*: 3007-3047.

3. Nestl, B. M., Hammer, S. C., Nebel, B. A., Hauer, B. New generation of biocatalysts for organic synthesis. *Angewandte Chemie International Edition*. **2014**, *53*: 3070-3095.

4. Sheldon, R. A., Woodley, J. M. Role of biocatalysis in sustainable chemistry. *Chemical Reviews*. **2018**, *118*: 801-838.

5. Britton, J., Majumdar, S., Weiss, G. A. Continuous flow biocatalysis. *Chemical Society Reviews*. **2018**, *47*: 5891-5918.

6. Tamborini, L., Fernandes, P., Paradisi, F., Molinari, F. Flow bioreactors as complementary tools for biocatalytic process intensification. *Trends in Biotechnology*. **2018**, *36*: 73-88.

7. Lin, B., Tao, Y. Whole-cell biocatalysts by design. *Microbial Cell Factories*. **2017**, *16*: 1-12.

8. Wachtmeister, J., Rother, D. Recent advances in whole cell biocatalysis techniques bridging from investigative to industrial scale. *Current Opinion in Biotechnology*. **2016**, *42*: 169-177.

9. Chapman, J., Ismail, A., Dinu, C. Industrial applications of enzymes: recent advances, techniques, and outlooks. *Catalysts*. **2018**, *8*: 238: 1443-1454..

10. López-Gallego, F., Jackson, E., Betancor, L. Heterogeneous systems biocatalysis: the path to the fabrication of self-sufficient artificial metabolic cells. *Chemistry – A European Journal*. **2017**, *23*: 17841-17849.

11. Constable, D. J. C. *et al.* Key green chemistry research areas - a perspective from pharmaceutical manufacturers. *Green Chemistry*. **2007**, *9*: 411-420.

12. Abrahamson, M. J., Vázquez-Figueroa, E., Woodall, N. B., Moore, J. C., Bommarius, A. S. Development of an amine dehydrogenase for synthesis of chiral amines. *Angewandte Chemie International Edition*. **2012**, *51*: 3969-3972.

13. Park, E. S., Dong, J. Y., Shin, J.-S. ω-Transaminase-catalyzed asymmetric synthesis of unnatural amino acids using isopropylamine as an amino donor. *Organic & Biomolecular Chemistry*. **2013**, *11*: 6929-6933.

14. Yasukawa, K., Nakano, S., Asano, Y. Tailoring D-amino acid oxidase from the pig kidney to R-stereoselective amine oxidase and its use in the deracemization of α-methylbenzylamine. *Angewandte Chemie International Edition*. **2014**, *53*: 4428-4431.

15. Yamaguchi, S., Komeda, H., Asano, Y. New enzymatic method of chiral amino acid synthesis by dynamic kinetic resolution of amino acid amides: use of stereoselective amino acid amidases in the presence of α-amino-ε-caprolactam racemase. *Applied and Environmental Microbiology*. **2007**, *73*: 5370-5373.

16. Genz, M. *et al.* Engineering the amine transaminase from Vibrio fluvialis towards branched-chain substrates. *ChemCatChem*. **2016**, *8*: 3199-3202.

17. Savile, C. K. *et al.* Biocatalytic asymmetric synthesis of chiral amines from ketones applied to sitagliptin manufacture. *Science*. **2010**, *329*: 305-309.

18. Weise, N. J., Parmeggiani, F., Ahmed, S. T., Turner, N. J. The bacterial ammonia lyase EncP: a tunable biocatalyst for the synthesis of unnatural amino acids. *Journal of the American Chemical Society*. **2015**, *137*: 12977-12983.

19. Fernandes, P. *et al.* Alteration of substrate specificity of alanine dehydrogenase. *Protein engineering, design & selection : PEDS*. **2015**, *28*: 29-35.

20. Knaus, T., Böhmer, W., Mutti, F. G. Amine dehydrogenases: efficient biocatalysts for the reductive amination of carbonyl compounds. *Green Chemistry*. **2017**, *19*: 453-463.

21. Guo, F., Berglund, P. Transaminase biocatalysis: optimization and application. *Green Chemistry*. **2017**, *19*: 333-360.

22. Kelly, S. A. *et al.* Application of ω-transaminases in the pharmaceutical industry. *Chemical Reviews*. **2018**, *118*: 349-367.

23. Slabu, I., Galman, J. L., Lloyd, R. C., Turner, N. J. Discovery, engineering, and synthetic application of transaminase biocatalysts. *ACS Catalysis*. **2017**, *7* (12): 8263-8284.

24. Weber, N., Gorwa-Grauslund, M., Carlquist, M. Exploiting cell metabolism for biocatalytic whole-cell transamination by recombinant Saccharomyces cerevisiae. *Applied microbiology and biotechnology*. **2014**, *98* (10): 4615-4624.

25. Hyun Joong Kim, Y. H. K., Ji-Hyun Shin, Shashi Kant Bhatia, Ganesan Sathiyanarayanan, Hyung-Min Seo, Kwon Young Choi, Yung-Hun Yang, Kyungmoon Park. Optimization of direct lysine decarboxylase biotransformation for cadaverine production with whole-cell biocatalysts at high lysine concentration. *J Microbiol Biotechnol*. **2015**, *25* (7): 6.

26. Neto, W., Schürmann, M., Panella, L., Vogel, A., Woodley, J. M. Immobilisation of ω-transaminase for industrial application: Screening and characterisation of commercial ready to use enzyme carriers. *Journal of Molecular Catalysis B: Enzymatic*. **2015**, *117*: 54-61.

27. Abaházi, E. *et al.* Covalently immobilized Trp60Cys mutant of ω-transaminase from Chromobacterium violaceum for kinetic resolution of racemic amines in batch and continuous-flow modes. *Biochemical Engineering Journal*. **2018**, *132*: 270-278.

28. Bajić, M. Development of a miniaturized packed bed reactor with ω-transaminase immobilized in LentiKats®. *Process Biochemistry*. **2017**, *v. 52*: pp. 10-72-2017 v.2052.

29. Planchestainer, M., Contente, M. L., Cassidy, J., Molinari, F., Tamborini, L., Paradisi, F. Continuous flow biocatalysis: production and in-line purification of amines by immobilised transaminase from Halomonas elongata. *Green Chemistry*. **2017**, *19*: 372-375.

30. Sheldon, R. A., Van Pelt, S. Enzyme immobilisation in biocatalysis: why, what and how. *Chemical Society Reviews*. **2013**, *42*: 6223-6235.

31. Cerioli, L., Planchestainer, M., Cassidy, J., Tessaro, D., Paradisi, F. Characterization of a novel amine transaminase from Halomonas elongata. *Journal of Molecular Catalysis B: Enzymatic*. **2015**, *120*: 141-150.

32. Andrade, L. H., Kroutil, W., Jamison, T. F. Continuous flow synthesis of chiral amines in organic solvents: immobilization of *E. coli* cells containing both ω-transaminase and PLP. *Organic Letters*. **2014**, *16*: 6092-6095.

33. Kaulmann, U., Smithies, K., Smith, M. E. B., Hailes, H. C., Ward, J. M. Substrate spectrum of ω-transaminase from Chromobacterium violaceum DSM30191 and its potential for biocatalysis. *Enzyme and Microbial Technology*. **2007**, *41*: 628-637.

34. Ito, N., Kawano, S., Hasegawa, J., Yasohara, Y. purification and characterization of a novel (S)-enantioselective transaminase from Pseudomonas fluorescens KNK08-18 for the synthesis of optically active amines. *Bioscience, Biotechnology, and Biochemistry*. **2011**, *75*: 2093-2098.

35. Velasco-Lozano, S., Benítez-Mateos, A. I., López-Gallego, F. Co-immobilized phosphorylated cofactors and enzymes as self-sufficient heterogeneous biocatalysts for chemical processes. *Angewandte Chemie International Edition.* **2017**, *56*: 771-775.

36. Chen, S., Campillo-Brocal, J. C., Berglund, P., Humble, M. S. Characterization of the stability of Vibrio fluvialis JS17 amine transaminase. *Journal of Biotechnology*. **2018**, *282*: 10-17.

37. Humble, M. S. at al. Crystal structures of the Cromobacterium violaceum ω-transmainase reveal major structural rearrengements upon binding of coenzyme PLP. *The FEBS Journal*. **2012**, *279*: 779-792.

38. Chen, S., Berglund, P., Humble, M. S. The effect of phosphate group binding cup coordination on the stability of the amine transaminase from Chromobacterium violaceum. *Molecular Catalysis*. **2018**, *446*: 115-123.

39. Britton, J., Dyer, R. P., Majumdar, S., Raston, C. L., Weiss, G. A. Ten-minute protein purification and surface tethering for continuous-flow biocatalysis. *Angewandte Chemie International Edition*. **2017**, *56*: 2296-2301.

40. Orrego, A. H., García, C., Mancheño, J. M., Guisán, J. M., Lillo, M. P., López-Gallego, F. Two-photon fluorescence anisotropy imaging to elucidate the dynamics and the stability of immobilized proteins. *The Journal of Physical Chemistry B*. **2016**, *120*: 485-491.

41. Benítez-Mateos, A. I., San Sebastian, E., Ríos-Lombardía, N., Morís, F., González-Sabín, J., López-Gallego, F. Asymmetric reduction of prochiral ketones by using self-sufficient heterogeneous biocatalysts based on NADPH-dependent ketoreductases. *Chemistry – A European Journal*. **2017**, *23*: 16843-16852.

42. Van Den Biggelaar, L., Soumillion, P., Debecker, D. P. Enantioselective transamination in continuous flow mode with transaminase immobilized in a macrocellular silica monolith. *Catalysts*. **2017**, *7*: 1-13.

43. Dajnowicz, S. *et al.* Direct visualization of critical hydrogen atoms in a pyridoxal 5′-phosphate enzyme. *Nature Communications*. **2017**, *8*: 955.

44. Chen, S. Stability and inactivation mechanisms of two transaminases (Doctoral dissertation). Stockholm University. **2018**.

45. Kotipalli, T., Kavala, V., Janreddy, D., Bandi, V., Kuo, C. W., Yao, C. F. Synthesis of 2,3-disubstituted quinazolinone derivatives through copper catalyzed C–H amidation reactions. *European Journal of Organic Chemistry*. **2016**, *2016*: 1182-1193.

Chapter 7

Concluding remarks

The main contribution of this PhD thesis is the microscopic approach to efficiently design and engineer self-sufficient heterogeneous biocatalysts mimicking the internal architecture of living cells. The design of immobilized multi-enzyme systems integrating cofactors in the solid phase together the exploitation of single-particle studies have opened new opportunities for applied biocatalysis. Ultimately, these self-sufficient heterogeneous biocatalysts have proven their efficiency in continuous flow reactions, getting a step closer to industrial biocatalysis in a more cost-effective and sustainable fashion.

The major findings of the work conducted during this PhD thesis are summarized as follows:

- The innovative strategy for the synthesis and immobilization of proteins in one pot (CFPS-i) was applied to quickly test the immobilization of different proteins onto several types of materials functionalized with different reactive groups. A set of plasmids encoding the target protein fused to a battery of polypeptide tags was combined with CFPS-i to drive the protein immobilization. This mix-and-go strategy was applied for the synthesis of protein-based biomaterials saving time and costs in comparison with traditional expression and immobilization strategies.
- The immobilization of phosphorylated cofactors onto aminated surfaces by electrostatic interactions was successfully applied during the engineering process of heterogeneous biocatalysts. NADPH, NAD^+, NADH, FAD^+ and PLP were some examples of the broad range of applicability of this technique. PEI-coating has been revealed as the best strategy to establish an association-dissociation equilibrium that allows the intraparticle availability of the cofactors but avoids their lixiviation to the reaction bulk.

- The spatial distribution of immobilized enzymes was demonstrated to be a key parameter to maximize the performance of the heterogeneous biocatalyst. This fact was even more relevant for oxidases whose activity is strongly affected by both oxygen and cofactor mass transport issues.

- Rational co-immobilization of different enzymes and cofactors onto solid carriers was achieved to build artificial metabolic cells, based on the molecular organization and crowding found in living cells. A repertoire of cofactor-dependent enzymes (dehydrogenases, ketoreductases, oxidases and transaminases) from different organisms was successfully tested for the co-

immobilization with their corresponding cofactor to fabricate cell-free artificial metabolic systems. Different structural organizations and micro-architectures were studied to find the most advantageous assembly of molecules.

- Single-particle analysis has demonstrated to be paramount for the functional characterization of immobilized enzymes and cofactors. The application of real-time spectroscopic techniques with spatio-temporal resolution could decipher the kinetics of enzymes at intraparticle scale.

- Highly-demanded chiral alcohols and amines were synthesized reaching maximum of 100% yield and 99% *ee* by using these artificial metabolic cells.

- The integration of self-sufficient heterogeneous biocatalysts into flow-systems for process intensification was addressed responding to industrial demands (> 90% of conversion for several reaction cycles). A packed-bed reactor was operated for the synthesis of amines at the high flow-rate (1.45 mL x min^{-1}) ever reported for co-immobilized enzyme and cofactor.

- The high cost of cofactor-dependent processes at industry could be overcome due to the recycling and reuse of enzymes, cofactors and carriers (accumulated TTN values until 1076 and 19980 for the cofactor and enzyme, respectively).

- These promising results are the first step towards more complex multi-enzyme systems which can be more easily assembled and analyzed by using the strategies developed in this PhD thesis. Although a quite unexplored road lies ahead, we envision the fabrication of artificial metabolic cells to make an important contribution to the development of the of biocatalytic systems of the future.

"The best is yet to come…"

LIST OF ABBREVIATIONS

AG-Co	Agarose microbeads activated with cobalt chelates groups
AG-Co/S	Agarose microbeads activated with both cobalt-chelates and disulfide groups
AG-DEAE	Agarose microbeads activated with tertiary amine groups
AG-DEAE/G	Agarose microbeads activated with glyoxyl and tertiary amine groups
AG-DVS	Agarose microbeads activated with vinyl groups
AG-DVS/PEI25	Agarose microbeads activated with vinyl groups and coated with polyethileneimine 25 kDa
A_e	Specific activity of an enzyme
AG-G/PEI25	Agarose microbeads activated with glyoxyl groups and coated with polyethileneimine 25 kDa
AG-Oct	Agarose microbeads activated with cyclooctyne groups
AG-PEI600	Agarose microbeads coated with polyethileneimine 600-1000 kDa
AG-TEA	Agarose microbeads activated with triethylamine
AN	1-acetonaphtone
AP-IgG-Rh	Inmunoglobulin G chemically conjugated with both rhodamine B and alkaline phosphatase
AuNRs	Gold nanorods
BDE	1,4-butanediol diglycidyl ether
Cb-FDH	Formate dehydrogenase from *Candida boidinii*
CFPS	Cell-free protein synthesis
CFPS-i	Cell-free protein synthesis and immobilization
CLSM	Confocal laser scanning microscopy
$CoCl_2$	Cobalt (II) chloride hexahydrate salt

Cv-ωTA	ω-transaminase from *Chromobacterium violaceum* tagged with poly-(6X)His
Cys-sGFP	sGFP tagged with poly-(6x)Cys
DTNB	5,5'-Dithiobis(2-nitrobenzoic acid) or Ellman´s Reagent
DTT	1,4-Dithiothreitol
EC-Co^{2+}	Sepabeads EC-EP/S microbeads activated with cobalt chelates
EC-Co^{2+}/eA	Sepabeads EC-EP/S microbeads activated with both cobalt chelates and ethanolamine
EC-Co^{2+}/PEI60	Sepabeads EC-EP/S microbeads activated with cobalt chelates and coated with polyethileneimine 60 kDa
EDTA	2-2'-2''-2'''-(ethane-1,2-diyldinitrilo)tetraacetic acid
ee	Enantioselectivity
FAD^{+}	Flavin-adenine-dinucleotide sodium salt
FITC	Fluorescein isothiocyanate
He-ωTA	ω-transaminase from *Halomonas elongata* tagged with poly-(6X)His
His-BsADH	Alcohol dehydrogenase from *Bacillus stearothermophilus* tagged with poly-(6X)His
His-ProA	Protein A tagged with poly-(6X)His
His-sGFP	sGFP tagged with poly-(6X)His
HRP	Horseradish peroxidase
IDA	Iminodiacetic acid
IgG	Inmunoglobulin G
IPA	Isopropanol
IPTG	1-thio-β-d-galactopyranoside
K_{cat}	Catalytic constant

K_d	Dissociation constant
K_M	Michaleis-Menten constant
KRED P1-A04	Ketoreductase from *Lactobacillus kefiri* mutant P1-A04
KRED P2-D11	Ketoreductase from *Lactobacillus kefiri* mutant P2-D11
L-AHA	L-azidohomoalanine
Lys-sGFP	sGFP tagged with poly-(6x)Lys
NAD^+	Nicotinamide-adenine-dinucleotide sodium salt
NADH	Nicotinamide-adenine-dinucleotide reduced sodium salt
NADPH	Nicotinamide-adenine-dinucleotide-phosphate reduced sodium salt
Na_2S	Sodium sulfide
PBR	Packed-bed reactors
PEI	Polyethyleneimine
Pf-ωTA	ω-transaminase from *Pseudomonas fluorescens* tagged with poly-(6X)His
PLP	Pyridoxal 5´-phosphate
pNPP	*p*-nitrophenyl phosphate
Pu-Co^{2+}	Purolite microbeads activated with cobalt chelates
Pu-Co^{2+}/eA	Purolite microbeads activated with both cobalt chelates and ethanolamine
Pu-Co^{2+}/hA	Purolite microbeads activated with both cobalt chelates and hydroxylamine
Pu-DEAE/E	Purolite microbeads activated with epoxy and tertiary amine groups
Pu-E	Purolite microbeads activated with epoxy groups
Pu-G	Purolite microbeads activated with glyoxyl groups

Pu-G/PEI25	Purolite microbeads activated with glyoxyl groups and coated with polyethileneimine 25 kDa
sGFP	superfolded Green Fluorescent Protein
***S*-MBA**	S-(α)-methylbenzylamine
SiO_2NPs	Silica nanoparticles
STY	Space-Time Yied
TEA	Triethylamine
TFA	Trifluoroacetic acid
TFAF	2,2,2-trifluoroacetophenone
TOF	Turnover Frequency
Tt-ADH	Alcohol dehydrogenase from *Thermus thermophilus* tagged with poly-(6X)His
TTN	Total Turnover Number
Tt-NOX	NADH oxidase from *Thermus thermophilus*
V_{max}	Maximun initial velocity of the enzyme-catalyzed reaction
ωTAs	ω-transaminases

ACKNOWLEDGMENTS

First and foremost, I would like to thank my supervisor, mentor and guide Dr. Fernando López Gallego. My experience as your PhD student has been even better that I could ever imagine. Thank you for encouraging me everyday, for your wise advices and for the best environment at work. I am also very grateful for your constant efforts to boost my early-stage career. Professionally and personally, I can just say thank you!

I am thankful with Prof. Luis M. Liz Marzán, head of CIC biomaGUNE, for giving me the opportunity to develop my PhD thesis in this center of international excellence. I want to thank Dr. Irantzu LLarena from the optical spectroscopy platform that kindly helped and taught me about microscopy techniques.

I feel very grateful to Prof. Selin Kara and Dr. Juan Manuel Bolivar for the gentle review of this manuscript to support my PhD thesis as international doctorate. Likewise, thanks to Dr. Javier Rocha Martín, David Roura Padrosa and Dr. Susana Velasco Lozano for your revisions and comments.

Thank you to the evaluation committee composed of Prof. Robert Kourist, Dr. Begoña Sanz Echeverría and Prof. Eduardo García Junceda.

I am pleased for the two travelling fellowships I received during my PhD thesis to visit research laboratories abroad. Thanks to Prof. Francesca Paradisi (Nottingham, UK) and people from her group, Martina, Eimear, Lidia, David and all others for kindly hosting me in your group during the 6 incredible weeks I spent with you. I learnt about the interesting flow biocatalysis field and I also found the beginning of new projects. Thanks to Prof. Sheref Mansy (Trento, Italy) and the guys Noel, Ross, Simone and anyone else for all I have learnt about the origins of life and synthetic biology while in your lab. Grazie mille ragazzi for the amazing italian experience!

Thanks to the group of Prof. Aitziber López Cortajarena for adopting me as a member of your team during the last year.

I should mention people who encouraged me to start this journey as PhD student. I want to thank Dr. Sandra Gavaldá (jefa) and Dr. Leandro López (doble A) for all I learnt about molecular biology and for believing in me when I was ‘bequi chica’. Thanks to Anita (bequi senior) who taught me at lab and shared amazing experiences with me. Moreover, thanks to my colleagues, Antonio, Laura, Maca, Andrés, Javi Robot, Inma, Vero, Claudio, Juanma, Ana chunga, Sol, Pablo, Lopera, Jaime, Luci, Ana Pla, Loli and all others for

teaching me about research in a company, but more important for the friendship after work. I wish to say special thanks to Javi Rocha who supported me to find this project and for your help and friendship before, during and I hope after the PhD thesis.

Once I started my thesis, I met my twin friend Susana (Pili). Thank you for being the best postdoc around the world and for the exchange of chemistry-biology knowledge. But upon the lab, thank you for being a friend. To my almost sister, Bei. We started the PhD trip together and we will finish it together. Thank you for your unconditional help, support and love everyday. To my friends in San Sebastián. Specially, Elena for your love, all the moments in the student´s and outside, and for the half of your bed; the most recent and sweet Verin; the chocolate lover and happy Dani; the basque (but andalusian-like) Idoia; Juan, Antonio, and Alex, the best gift I got from this beautiful city. Thank you for the unforgettable basque moments we lived during these 3 years, and the further experiences we have still to live. Eskerrik asko!

To the former labmates Javi, Ruta, Eunice, Grajalitos, Sindy, Jurgita and specially Laura, for your help and the wonderful moments at lab. Thanks to my former colleagues in CICbiomaGUNE, Manu, Silvia, María, Ane and people from the student´s room. To Ainhoa, María and Christina, the undergraduate students who helped me during my thesis work.

A mi familia. Gracias mamá y papá por darme todo en la vida y ayudarme en cada paso. Al pilar de mi vida, mi abuela, porque me has enseñado a crecer y todo lo que soy es gracias a ti. Gracias Fina y Talía por apoyarme y cuidarme siempre. A tu, David, moltes gràcies per haver aparegut en aquest camí i estar al meu costat sempre.

PERSONAL INFORMATION

Ana Isabel Benítez Mateos

+34 675 055 924

anabel.benitez.mateos@gmail.com

WORK EXPERIENCE

01/2019 – 04/2019	**Graduate researcher** University of Zaragoza-ISQCH (Zaragoza, Spain)
03/2016 – 12/2018	**Graduate researcher** CIC biomaGUNE (San Sebastián, Spain)
08/2015 – 12/2015	**Research technician** Abengoa Research S.L. – Biópolis S.L. (Seville, Spain)
07/2014 – 07/2015	**Research assistant** Abengoa Bioenergy New Technologies S.L. (Seville, Spain)

EDUCATION AND TRAINING

10/2016 – At present	**PhD student in Synthetic and Industrial Chemistry** University of the Basque Country (San Sebastián, Spain)
11/2015 – 07/2016	**M. S. in Molecular Genetics and Biotechnology** University of Seville (Seville, Spain)
09/2009 – 07/2013	**B. S. Biology** University of Seville (Seville, Spain)

COMPLEMENTARY FORMATION

01/2014 – 04/2014	**Internships** Centro Andaluz de Biología del Desarrollo. CSIC. (Seville, Spain)
09/2013 – 12/2013	**Internships** Puleva Food S.L. (Alcalá de Guadaíra, Spain)

LANGUAGE SKILLS

- Mother language **Spanish**
- Other languages **English** (Level C1 CEFR)

FELLOWSHIPS AND GRANTS

09/2018	**Travelling fellowship for a short-stay at CIBIO - UniTrento** The Company of Biologists - Journal of Cell Science (Trento, Italy)
08/2018	**Registration grant for "9th International Congress on Biocatalysis"** Organization of BIOCAT18 (Hamburg, Germany)
10/2017	**Travelling fellowship for a short-stay at University of Nottingham** COST Action "Systems Biocatalysis" CM1303 (Nottingham, UK)
04/2016	**Registration grant for "COST training school: Systems Biocatalysis"** COST Action "Systems Biocatalysis" CM1303 (Siena, Italy)

CONTRIBUTIONS TO CONFERENCES

09/2018	Poster presentation: "*Self-sufficient heterogeneous biocatalysts as artificial metabolic cells for chemical manufacturing*" **EMBO Workshop. Enzymes, Biocatalysis and Chemical Biology** (Pavia, Italy)
08/2018	Oral presentation: "*Self-sufficient biocatalysts co-immobilizing PLP-dependent ω-transaminases and cofactor for flow-biocatalysis*" **BIOCAT18. 9th International Congress on Biocatalysis** (Hamburg, Germany)
06/2018	Poster presentation: "*Understanding the effects of spatial distribution on immobilized enzyme kinetics*" **JEB18. II Jornadas Españolas en Biocatálisis** (Oviedo, Spain)
07/2017	Poster presentation: "*Single-bead kinetics of immobilized enzymes*" **BIOTRANS17. 13th International Symposium on Biocatalysis and Biotransformations** (Budapest, Hungary)
06/2017	Oral presentation: *"Expanding on-demand fabrication of biomaterials by coupling cell-free protein synthesis and immobilization in one-pot"* **BIOTEC17. National Congress on Biotechnology** (Murcia, Spain)
04/2017	Oral presentation: *"On-demand fabrication of biomaterials by coupling cell-free protein synthesis and immobilization in one-pot"* **BIOMAPP17. 2nd Workshop on Biomaterials and Applications** (Santiago de Compostela, Spain)

SCIENTIFIC PUBLICATIONS

- **Benítez-Mateos AI**, Contente ML, Velasco-Lozano S, Paradisi F, López-Gallego F (2018) *ACS Sustain. Chem. Eng.* 6: 13151-13159.
- **Benítez-Mateos AI**, Llarena I, Sánchez-Iglesias A, López-Gallego F (2018) *ACS Synth. Biol.* 7: 875-884.
- Marx L, Ríos-Lombardía N, Farnberger J, Kroutil W, **Benítez-Mateos AI**, López-Gallego F, Morís F, González-Sabín J, Berglund P (2018) *Adv. Synth. Catal.* 360: 1-10.
- **Benítez-Mateos AI**, Nidetzky B, Bolivar JM, López-Gallego F (2017) *ChemCatChem* 10: 654-665.
- **Benítez-Mateos AI**, San Sebastian E, Ríos-Lombardía N, Morís F, González-Sabín J, López-Gallego F (2017) *Chem. Eur. J*. 23: 16843-16852.
- Velasco-Lozano S, **Benítez-Mateos AI**, López-Gallego F (2017) *Angew. Chem. Int. Ed*. 56: 771-775.